

Newcastle University

Investigating The Evolution Of Dexamethasone Resistance In Acute Lymphoblastic Leukaemia

Katherine Louise Dormon

Doctor of Philosophy

Northern Institute for Cancer Research

April 2017

The evolution of ALL from presentation to relapse is often accompanied by the emergence of resistance to commonly used chemotherapeutics, including dexamethasone (Dex), a synthetic glucocorticoid that has been the backbone of ALL treatment since the 1950s. In order to investigate the evolution of drug resistance we focused on the L707 cells, a matched Dex-sensitive presentation and Dex-resistant relapse pair from a patient with t(17;19) B ALL. A major genetic difference between presentation and relapse is a 5q deletion spanning 6 genes, including NR3C1, the glucocorticoid receptor and the site of action for Dex. It was found previously that the L707 presentation engrafts and proliferates faster than the relapse cells in the NSG mouse model. The loss of NR3C1 was hypothesised as the cause for reduced fitness of the relapse. This thesis investigated this, and the mechanisms behind the Dex resistance in the L707 relapse. Using shRNA approaches to look at the function of the genes in the relapse 5q deletion identified NR3C1 as the major driver of resistance but did not provide evidence that loss resulted in reduced fitness. Further in depth analysis of the L707 cells using microarrays has shown that the differences between presentation and relapse extend past the genetic differences, including alterations in transcriptional programmes. To identify further novel drivers of resistance, a whole genome *in vivo* CRISPR screen was carried out, implicating several genes in leukaemic fitness and Dex resistance as well as being a proof of concept for the use of these screens in primary material. Finally, an incidental finding that 697 pre B leukaemic cell line was Dex resistant *in vivo*, but not *in vitro*, and examination of these cells using RNA sequencing resulted in the finding that alterations in transcription induced by the murine microenvironment may be responsible for this change.

Acknowledgements

There are many people who have helped me with this PhD, and a few without whom it would not have been completed.

Firstly, I would like to thank my supervisors, in particular Olaf for teaching me the techniques and analytical thinking required to become a research scientist.

I would also like to thank Helen Blair, who taught me all of the *in vivo* protocols and helped whenever I was unsure.

All of the FISH protocols were kindly and patiently taught by Lisa Jones, and I would like to thank her for that as well as scoring thousands of cells for me as a second scorer.

For the bioinformatics I have to thank Matt Bashton, Matt Selby, Sirintra Nakjang and Ben Allen, who have given me so much help and advice throughout this PhD. Without their help none of the microarrays, RNA sequencing or whole genome sequencing would have been analysed with any finesse or proper statistical methods.

The most thanks however, go to Alex Elder for reading this entire thesis with only the promise of minstrels as reward, answering all and any questions, and doing all the work for the L707 relapse breakpoint PCRs.

Thanks also go to Natalie and Sarah, who have provided me with the will to carry on these last few months with plenty of tea breaks and much needed talk about things other than science.

Lastly, my thanks to George for supporting me, being a shoulder to cry on when things went wrong and agreeing to marry me.

Contents

List of figures.....	x
List of Tables.....	xvii
List of abbreviations.....	xix
List of genes.....	xxiii
Chapter 1: Introduction.....	1
1.1 The Haematopoietic System	1
1.2 Development of the Haematopoietic system	1
1.3 Transcriptional control of HSC	7
1.4 B lymphoid haematopoiesis.....	8
1.5 Paediatric B cell ALL.....	9
1.6 Biology of ALL	10
1.6.1 Genetic translocations	12
1.6.2 Leukaemic transformation	15
1.7 Prognostic factors.....	17
1.7.1 E2A/HLF	19
1.8 Treatment.....	20
1.9 Relapse	22
1.10 Leukaemic stem cells and clonal evolution.....	24
1.11 Recurrent genetic alterations at relapse.....	26
1.12 Glucocorticoids in ALL	27
1.13 Glucocorticoid resistance	29
1.14 NR3C1.....	30
1.15 CRISPR	35
1.16 Genetic Screening	41
1.17 Previous work.....	45
Chapter 2: Materials.....	48
2.1 Chemicals	48
2.2 Equipment.....	48
2.3 Lab ware	49
2.4 Buffers	49
2.5 Kits.....	53
2.6 Cloning enzymes.....	53
2.7 Tissue culture reagents	54

2.8	Antibodies.....	55
2.9	Oligonucleotides and primers	56
2.10	Cells.....	57
2.11	Competent bacteria.....	58
2.12	In vivo model	58
	Chapter 3: Methods.....	59
3.1	Cell culture.....	59
3.1.1	Counting cells	60
3.1.2	Culture of suspension cells	61
3.1.3	Culture of adherent cells	61
3.1.4	Co-culture of leukaemic cells and feeder cells	62
3.1.5	Thawing cells	63
3.1.6	Freezing cells	63
3.2	Flow Cytometry	63
3.3	Cytotoxicity testing.....	64
3.3.1	WST-1 assay.....	65
3.3.2	Luciferase assay	65
3.4	Harvesting cell pellets.....	66
3.5	RNA extraction.....	66
3.5.1	Qiagen RNeasy kit.....	66
3.5.2	mirVana kit	67
3.6	DNA extraction	68
3.7	Protein extraction.....	68
3.7.1	BCA assay.....	69
3.8	Production of cDNA	69
3.9	Real-time PCR	70
3.10	Agarose gel electrophoresis	72
3.11	QIAquick Gel Extraction Kit.....	73
3.12	QIAquick PCR Purification Kit	73
3.13	Western blotting.....	74
3.14	In vivo work	75
3.14.1	Animal husbandry.....	75
3.14.2	Intrafemoral injection.....	75
3.14.3	Dosing	76
3.14.4	IVIS imaging	77

3.14.5	Venepuncture of tail	77
3.14.6	Cardiac puncture	78
3.14.7	Collection of samples from mice.....	78
3.14.8	Histological analysis of samples	79
3.14.9	Ficoll separation of cells	79
3.15	Production of competent bacteria.....	80
3.16	Bacterial transformation	80
3.16.1	Chemically competent cells.....	80
3.16.2	Mix and Go	81
3.17	Production of LB agar plates	81
3.18	Streaking bacteria	81
3.19	Plasmid purification from bacteria.....	82
3.19.1	Miniprep	82
3.19.2	Maxiprep	83
3.19.3	NucleoBond Xtra midi	84
3.20	Transfection of 293T cells	84
3.21	Collection and concentration of lentivirus.....	85
3.22	Transduction of leukaemic cells.....	85
3.23	FISH.....	86
3.23.1	Nick translation	86
3.23.2	Slide preparation	87
3.23.3	Hybridisation	88
3.23.4	Capture and scoring of cells	88
3.24	Microarray analysis	89
3.24.1	GenomeStudio and Excel	89
3.24.2	R packages.....	90
3.25	GATK whole genome sequencing analysis	92
3.26	RNA sequencing analysis.....	93
3.27	CRISPR screen specific methods.....	95
3.27.1	Transduction of electrocompetent bacteria and plasmid collection	95
3.27.2	Transfection of 293T cells and collection of lentivirus.....	96
3.27.3	Transduction and selection of L707 presentation cells.....	96
3.28	Production of amplicon library for lentiCRISPR screen.....	97
3.29	Data Analysis of lentiCRISPR screen	101
3.30	Cloning CRISPR plasmids	102

..... Chapter 4: Investigation of mechanism of relapse using paired presentation and relapse ALL: The L707 cells	105
4.1 Introduction.....	105
4.2 Differential gene expression profile between presentation and relapse in the L707 cells.	107
4.2.1 Analysis using genome studio and excel	108
4.2.2 Microarray analysis using R	115
4.3 Whole genome sequencing: Genetic differences between presentation and relapse.....	120
4.3.1 Relapse specific SNP	121
4.3.2 Relapse specific indels	122
4.3.3 SNPs and indels in both L707 presentation and relapse	124
4.4 Emergence of resistance in the L707 cells.....	129
4.4.1 Previous work	130
4.5 Summary.....	132
Chapter 5: Role of NR3C1 in proliferation and engraftment of ALL cells.....	135
5.1 Introduction.....	135
5.1.1 shRNA constructs.....	137
5.2 Induced NR3C1 targeting shRNA are enriched only in the presence of Dex.....	142
5.2.1 NR3C1 targeting shRNA are enriched when cells are treated with Dex and Dox	143
5.2.2 Survival of mice is not affected by induction of shRNA constructs.....	147
5.2.3 The in vivo screen shows no correlation with treatment group and expression of NR3C1 expressing shRNA constructs.....	148
5.2.4 Mifepristone acts as a partial agonist at NR3C1 in the 697 cells	152
5.2.5 Microarray analysis.....	160
5.2.6 L707 Presentation; control vs Dex treatment	167
5.2.7 Control vs Mifepristone treatment	170
5.3 Summary.....	172
Chapter 6: In vivo lentiCRISPR whole genome screen to determine genes implicated in dexamethasone treatment and the emergence of relapse	176
6.1 Introduction.....	176
6.2 Transduction pilot.....	178
6.3 in vivo screen.....	179
6.3.1 Sample preparation	183
6.3.2 Analysis	184
6.3.3 Functional validation of targets.....	201
6.4 Summary.....	207
Chapter 7: Dexamethasone resistance in Acute Lymphoblastic Leukaemia cell lines	210

7.1	Introduction	210
7.2	The 697 cells show dexamethasone resistance in vivo: An incidental finding	211
7.2.1	697 cell dexamethasone resistance is not mediated by adhesion in vitro	213
7.2.2	Growth of 697 in vivo does not result in resistance when cells are tested in vitro.....	218
7.2.3	No changes in histology are seen in mice from different treatment groups.....	223
7.3	Dexamethasone pharmacokinetics.....	227
7.4	RNA sequencing	229
7.4.1	in vitro control vs in vivo control.....	235
7.4.2	Dexamethasone in vitro vs dexamethasone in vivo.....	244
7.4.3	Control vs Dexamethasone	249
7.4.4	Control vs dexamethasone in vivo	255
7.5	Summary	265
	Chapter 8: Discussion	272
8.1	Paired primary presentation and relapse cells	272
8.2	Role of NR3C1 in ALL	273
8.3	lentiCRISPR screen.....	274
8.4	Dex resistance in an ALL cell line.....	275

List of figures

<i>Figure 1: Primitive haematopoiesis and definitive haematopoiesis</i>	2
<i>Figure 2: The development of HSC from the haemogenic endothelium in the dorsal wall of the aortic endothelium.....</i>	3
<i>Figure 3: Lymphoid differentiation from the multipotent HSC to the terminally differentiated mature B cells that defines definitive haematopoiesis.</i>	6
<i>Figure 4: The correlation of B ALL subtype with stages in B lymphoid differentiation.....</i>	12
<i>Figure 5: The t(17;19) translocation that results in the E2A/HLF fusion proteins</i>	20
<i>Figure 6: The scheme shows the intra-disease heterogeneity.....</i>	27
<i>Figure 7: The structure of NR3C1 from DNA to protein</i>	31
<i>Figure 8: A simplified schematic showing the mechanism of NR3C1 modulated transcription via a classical response element</i>	33
<i>Figure 9: Schematic detailing the several different mechanisms by which NR3C1 can induce alterations in transcription including activation of genes and repression of genes.....</i>	34
<i>Figure 10: Mechanism of CRISPR-Cas mediated bacterial acquired immunity.....</i>	37
<i>Figure 11: Structure of the lentiCRISPRv2 plasmid</i>	39
<i>Figure 12: Mechanism of CRISPR-Cas9 mediated double strand breaks (DSB) using the lentiCRISPRv2 plasmid.....</i>	40
<i>Figure 13: The basic premise of positive and negative genetic screens</i>	44
<i>Figure 14: A circos plot showing the copy number gains and losses compared to normal copy number in the L707 Relapse.....</i>	45
<i>Figure 15: Survival of mice engrafted with 1x10⁵ L707 presentation or L707 relapse</i>	46
<i>Figure 16: Survival of mice engrafted with ratios of L707 presentation and relapse</i>	46
<i>Figure 17: PCR cycling conditions used for real-time PCR run on the ABI 7900HT Sequence Detection system.....</i>	71
<i>Figure 18: The workflow used for analysis of microarray data using the Lumi and Limma method.</i>	91
<i>Figure 19: The workflow for GATK processing of whole genome sequencing data. Yellow boxes indicate input and output files; green boxes indicate data manipulation. Workflow obtained from the GATK best practices, available on the Broad Institute website (Van der Auwera et al. 2013; DePristo et al. 2011; McKenna et al. 2010).....</i>	93
<i>Figure 20: Workflow used for the analysis of RNA sequencing using the Cufflinks suite. Blue boxes denote programmes and yellow boxes are input and output files.</i>	94

<i>Figure 21: The GeneAmp 9700 Thermo Cycler settings for both the first and second step PCR reactions used in the preparation of the lentiCRISPR amplicon library.....</i>	98
<i>Figure 22: Scheme showing steps in the 2 step PCR process to produce amplicons used for next generation sequencing.</i>	100
<i>Figure 23: Analytical gel of amplified DNA with the adaptors and barcodes added</i>	101
<i>Figure 24: Workflow of data analysis used for the lentiCRISPR screen.....</i>	102
<i>Figure 25: Plot showing the comparison of the average probe intensity signals between 2 L707 samples sent for microarray analysis</i>	109
<i>Figure 26: The 4 different assessments made between primary and secondary L707 presentation and L707 relapse samples in excel to generate a list of significant genes to investigate further.</i>	110
<i>Figure 27: Venn Diagram showing the crossover of genes in each of the 4 lists from the multiple comparisons of the primary and secondary engraftment samples for L707 presentation and relapse.....</i>	110
<i>Figure 28: Ranked list of 117 genes for which GSEA allocated a score with the gene name, average probe binding for the presentation and relapse and the average fold increase or decrease.....</i>	112
<i>Figure 29: Scatter plot showing the probe binding for the differentially expressed probes. .</i>	113
<i>Figure 30: Probe binding (as a surrogate for mRNA expression) of the 6 genes in the relapse specific 5q deletion at presentation and relapse.....</i>	114
<i>Figure 31: Intensity box plots for each of the 12 microarray samples before normalisation and after robust spline normalisation.</i>	117
<i>Figure 32: Principal component analysis of the microarray samples after quantile normalisation.....</i>	118
<i>Figure 33: Charts showing the predicted consequences of SNPs unique to the L707 relapse.</i>	121
<i>Figure 34: Charts showing the predicted consequences of indels unique to the L707 relapse.</i>	123
<i>Figure 35: Coding consequences of the SNPs shared between presentation and relapse.</i>	125
<i>Figure 36: Coding consequences of indels shared between L707 presentation and relapse with more than 10 supporting reads and predicted high impact.....</i>	127
<i>Figure 37: Breakpoints in the 5q deletion present in the L707 relapse</i>	128
<i>Figure 38: Representative images of the FISH carried out on the L707 presentation cells from mice treated with Dex or saline.....</i>	132

<i>Figure 39: Sequence of pTRIPZ plasmid.</i>	138
<i>Figure 40: Puromycin kill curve for the 697 cells used to determine the lowest concentration of puromycin required to kill all non transduced cells</i>	139
<i>Figure 41: Cell survival of 697 and 697 pTRIPZ pool cells with and without Dox treatment (2 µg/ml) in response to Dex treatment.....</i>	141
<i>Figure 42: NR3C1 mRNA expression in 697 cells transduced with NR3C1 targeting shRNA, with and without Dox (2 mg/ml).....</i>	142
<i>Figure 43: Fold change of the shRNA count number in the 697 cells transduced with pTRIPZ constructs when treated with Dex/Dox combinations over a 13 day period.....</i>	144
<i>Figure 44: Fold change of the shRNA count number for the 5 separate NR3C1 targeting shRNA constructs and the 3 control shRNA in 697 cells over a 13-day period with combinations of Dex and Dox</i>	145
<i>Figure 45: Fold change of the count number for all constructs for the second in vitro run including 3 concentrations of Dex.....</i>	146
<i>Figure 46: Fold change in the count number for the 5 separate NR3C1 targeting shRNA and the 3 control shRNA in 697 cells treated over a 13-day period with combinations of Dex and Dox for the second run of the experiment.</i>	147
<i>Figure 47: Survival of mice in the 4 different treatment groups.....</i>	148
<i>Figure 48: Fold change of shRNA counts from 697 cells engrafted into NSG mice.....</i>	149
<i>Figure 49: Fold change of shRNA counts from 697 cells engrafted into NSG mice.</i>	150
<i>Figure 50: FACS analysis of 697 cells after puromycin selection before injection into mice, and spleen samples after collection from mice.....</i>	151
<i>Figure 51: Response of NR3C1 target genes and NR3C1 to Dex treatment over a 24 hr period in the 697 cells.....</i>	154
<i>Figure 52: Response of NR3C1 target genes and NR3C1 to Mifepristone treatment over a 24 hr period in the 697 cells</i>	155
<i>Figure 53: Weight of mice normalised to weight at the start of the experiment</i>	156
<i>Figure 54: Representative IVIS image of 3 mice showing bioluminescence in the mouse 13 days after injection with L707 presentation pSLIEW cells.</i>	158
<i>Figure 55: Survival of mice engrafted with L707 presentation pSLIEW cells.</i>	158
<i>Figure 56: Two FACS plots showing the levels of CD19-PE and GFP positive cells.....</i>	159
<i>Figure 57: The Density plot of the raw microarray data for the L707 presentation cells treated with Dex, mifepristone or controls before normalisation.</i>	162

<i>Figure 58: The Density plot of the microarray data for the L707 presentation cells treated with Dex, mifepristone or controls after robust spline normalisation (RSN) has been used.....</i>	163
<i>Figure 59: Principal component analysis showing all 10 samples run on the microarray for the L707 samples treated with either Dex, mifepristone or controls.</i>	164
<i>Figure 60: Principal component analysis of the microarray data for the L707 samples treated with either Dex, mifepristone or controls with the two outlying samples, dexamethasone 3 and mifepristone 1 removed.....</i>	165
<i>Figure 61: Heat map for the top 1000 differentially regulated genes in L707 presentation treated with Dex compared to L707 presentation cells treated as controls.</i>	166
<i>Figure 62: Protein interactions between the 14 genes with >2 fold increase in expression in response to Dex treatment in the L707 presentation cells.</i>	168
<i>Figure 63: Protein association of the genes upregulated >1.5 fold in response to mifepristone treatment in the L707 presentation cells</i>	171
<i>Figure 64: The hypothesised reaction of the UBC promoter in response to Dex treatment in ALL cells transduced with the pTIPZ plasmid.</i>	173
<i>Figure 65: Relative Cas9 DNA levels in samples transduced with the lentiCRISPRv2 plasmid at 3 and 5 days post transduction..</i>	179
<i>Figure 66: Survival of mice engrafted with L707 Presentation cells; L707 Presentation (red), L707 Presentation + Dex (15 mg/kg) after 2 weeks engraftment (blue) and L707 Presentation CRISPR + Dex (15 mg/kg, then 10 mg/kg) (green).....</i>	180
<i>Figure 67: Histology of a section of spleen from an NSG mouse engrafted with L707 presentation CRISPR cells treated with Dex</i>	181
<i>Figure 68: Histology from the spine of a mouse engrafted L707 presentation CRISPR cells treated with Dex.</i>	182
<i>Figure 69: Histology from the liver of a mouse engrafted with L707 presentation CRISPR cells treated with Dex.</i>	183
<i>Figure 70: The number of reads for the top 10 highest reads for KD93 spleen in the contaminated analysis before removal of NR3C1 and NTC reads (red) and after these reads were removed (green).</i>	185
<i>Figure 71: The reads per sample in the raw sequencing data returned from the HiSeq2500 sequencing run from AROS.</i>	186
<i>Figure 72: The reduction in the number of sgRNA found in the original GeCKO library</i>	187

<i>Figure 73: The reduction in sgRNA coverage in the organs of 4 representative mice compared to baseline</i>	188
<i>Figure 74: A comparison of sgRNA in separate organs.....</i>	189
<i>Figure 75: Principal component analysis plot for samples in the screen using the two principal components that contribute most to sample variance.....</i>	190
<i>Figure 76: RRA (Robust rank aggregation) scores for positive selection of sgRNA in mouse samples vs baseline.....</i>	192
<i>Figure 77: Sequence homology, as determined using the NCBI blast online database.....</i>	192
<i>Figure 78: Plot showing the increase in sgRNA reads between the baseline to the endpoint samples (Dex) for all of the genes with significantly ($p<0.05$) upregulated sgRNA calculated using the robust rank aggregation (RRA) score in the MAGECK analysis pipeline</i>	194
<i>Figure 79: Genes with enriched sgRNA and NR31 binding at the transcription start site as determined by ChIP-seq.</i>	195
<i>Figure 80: Genes with enriched sgRNA but no NR3C1 binding as determined by ChIP-seq data</i>	196
<i>Figure 81: RRA scores for depletion of sgRNA in mouse samples vs baseline</i>	198
<i>Figure 82: Traces for the genes with depleted sgRNA that have ChIP-seq peaks at the transcription start site.....</i>	199
<i>Figure 83: Survival of L707 presentation cells grown on an MSC feeder layer when treated with Dex over a 96 hr time period.....</i>	202
<i>Figure 84: The percentage cell survival, assessed by the trypan blue exclusion method in L707 Presentation, L707 Relapse and L707 presentation CRISPR-NR3C1 and L707 presentation CRISPR-NTC (non targeting control) cells</i>	203
<i>Figure 85: NR3C1 mRNA levels in the L707 presentation and L707 presentation cells transduced with a lentiCRISPR pool targeting NR3C1 cells</i>	203
<i>Figure 86: Percentage cell survival of L707 presentation cells with gRNA targeting PLXND1, SEMA3E, PAQR7 B4GALNT4 and NTC with 25nM Dex treatment.</i>	205
<i>Figure 87: Proliferation of L707 Presentation cells and L707 Presentation cells transduced with several different pools of sgRNA over a 25-30 day period.....</i>	206
<i>Figure 88: The decrease in NR3C1 mRNA in cells transduced with NR3C1 sgRNA is not significant.....</i>	207
<i>Figure 89: Survival of mice from first test of 697 engraftment in NSG mice.</i>	212

<i>Figure 90: Survival of mice engrafted with 697 transduced with pTRIPZ shRNA pool treated with either saline or Dex (10 mg/kg)</i>	212
<i>Figure 91: In vitro Dex sensitivity of the 697 cells</i>	213
<i>Figure 92: GFP expression in 697 pSLIEW cells after sorting compared to 697 control cells without transduction</i>	214
<i>Figure 93: Dex cytotoxicity of 697 pSLIEW cells on a feeder layer of MS5 cells.</i>	216
<i>Figure 94: Dex cytotoxicity of 697 pSLIEW cells on a feeder layer of M210B4 cells.....</i>	217
<i>Figure 95: Dex cytotoxicity of 697 pSLIEW cells on a feeder layer of MSC cells.</i>	218
<i>Figure 96: Total flux (photons/s²) emitted from the mice in the two of the treatment groups after dosing with luciferin and imaging using the IVIS.....</i>	219
<i>Figure 97: The survival of mice engrafted with 10⁴ 697 pSLIEW cells</i>	220
<i>Figure 98: Dex sensitivity of 697pSLIEW cells collected from the BM of engrafted mice compared to 697pSLIEW that were not grown in vivo.....</i>	221
<i>Figure 99: Dex sensitivity of 697pSLIEW cells collected from the spleens of engrafted mice compared to 697pSLIEW cells that were not grown in vivo.</i>	222
<i>Figure 100: Dex sensitivity of the 697pSLIEW cells collected from the livers of engrafted mice compared to 697pSLIEW cells not grown in vivo.....</i>	223
<i>Figure 101: H&E, CD45 and CD19 staining of liver from an NSG mouse injected intra-femorally with 10⁴ 697 pSLIEW cells.....</i>	224
<i>Figure 102: Liver and spleen samples from a control mouse that received saline injections after injection with 10⁴ 697 pSLIEW cells intra-femorally.</i>	225
<i>Figure 103: Liver and spleen samples from a mouse that received Dex straight after injection with 10⁴ 697 pSLIEW cells intra-femorally.....</i>	226
<i>Figure 104: Liver and spleen samples from a mouse that received Dex 14 days after injection with 10⁴ 697 pSLIEW cells intra-femorally.....</i>	227
<i>Figure 105: Concentration of Dex (ng/ml) in the peripheral blood of mice</i>	228
<i>Figure 106: Bioanalyser traces for 4 of the representative mouse samples sent for RNA sequencing</i>	230
<i>Figure 107: Quality score across the bases in the RNA sequencing reads for a representative FASTQ file.....</i>	232
<i>Figure 108: The 5 comparisons that were run using the 697 RNA sequencing data in order to determine which genes might be important for the differences between in vitro and in vivo Dex response.....</i>	233

<i>Figure 109: Dispersion plot for the RNA sequencing data of the 697 control TC samples and Control mouse samples</i>	234
<i>Figure 110: Density of the log₁₀ (FPKM) values for the 697 cell TC and mouse control sample data from the RNA sequencing analysis</i>	235
<i>Figure 111: Dendrogram showing the 2 697 cell TC and 2 697 cell mouse control samples cluster separately from each other, but together with the treatment replicates</i>	236
<i>Figure 112: Volcano plot showing the spread of log₂(fold change) of FPKM values for genes between control mouse samples compared to control TC samples</i>	237
<i>Figure 113: Interactions between the top 10 protein coding genes upregulated in mouse control samples compared to TC control samples</i>	239
<i>Figure 114: Differences in FPKM between control TC samples and control mouse samples for the 3 most differentially regulated genes in the control mouse samples.....</i>	240
<i>Figure 115: Differences in FPKM in the 697 cells between TC control samples and Mouse control samples for FOSB in the RNA sequencing data.....</i>	241
<i>Figure 116: Snapshot from genes down regulated >2 log₂(fold change) in control mouse vs control TC, genes in red are those involved in the biosynthesis of small molecules.....</i>	243
<i>Figure 117: Dendrogram showing clustering of 697 cell TC and mouse samples with Dex treatment</i>	244
<i>Figure 118: The top 3 upregulated genes in the 697 cells for TC Dex vs mouse Dex samples; FOS, EGR1 and MS4A1.</i>	246
<i>Figure 120: The overlap between the downregulated genes (with gene IDs only) in the 697 cells when control samples were compared to Dex treated samples for both the <i>in vitro</i> and <i>in vivo</i> conditions.....</i>	248
<i>Figure 121: Changes in RASD1 FPKM in four of the analyses</i>	249
<i>Figure 122: Dendrogram produced using the normalised read counts from the 697 RNA sequencing data</i>	250
<i>Figure 123: Log₂ fold change in FPKM in the 697 cells between control and Dex treated samples <i>in vitro</i></i>	251
<i>Figure 124: GRE consensus sequences indicated by the green lines in the genomic sequence of UBA7 and FKBP5</i>	252
<i>Figure 125: Increase in the FPKM of PLS3 seen in the 697 Dex TC samples compared to control TC samples.</i>	253

<i>Figure 126: Plots showing the reduction in FPKM for 2 of the most significant genes down regulated in the 697 Dex TC samples compared to the 697 control TC samples</i>	254
<i>Figure 127: Dendrogram showing the clustering of mouse control and mouse Dex treated 697 samples</i>	256
<i>Figure 128: PCA plot for the in vivo samples, the control samples are separated from the Dex samples based on principle component M1, and from each other on M2. Two of the Dex samples cluster tightly whilst the other has more differences based on component M2. The Dex treated outlier is one of the female Dex treated mice, indicating the difference in expression was not due to sex differences.</i>	257
<i>Figure 129: Log2 fold change in FPKM in the 697 cells between control and Dex treated samples in vivo. Red points indicate significant genes ($p<0.01$), data points to the left of centre indicate down regulated genes and points to the right indicate upregulated genes. Data points on the edge of the plot are those for which the log2(fold change) is inferred due to one of the conditions having an FPKM value of 0. Significance was calculated and the plot generated using the R package CummRBund, which is designed for the analysis and visualisation of CuffDiff RNA sequencing data.</i>	258
<i>Figure 130: Venn diagram showing the crossover between genes upregulated in the 697 cells control vs Dex for the in vivo and in vitro conditions.</i>	260
<i>Figure 131: Plots showing the reduction in FPKM for the top three down regulated genes in the 697 cells when the control samples are compared to the Dex treated samples in vivo ..</i>	261
<i>Figure 132: Dendrogram showing clustering of all 697 samples</i>	263
<i>Figure 133: The change in expression of the isoforms of FKBP5 in the 697 cells control vs Dex treatment.....</i>	264
<i>Figure 134: Transcripts of TP53INP1</i>	265
<i>Figure 135: Schematic detailing the deregulation of FOS, JUN and EGR genes in the 697 cells in vitro and in vivo.,</i>	268
<i>Figure 136: The known protein interactions between the JUN, FOS and EGR genes found differentially expressed in the analysis of Dex and control 697 samples both in vivo and in vitro.....</i>	268

List of tables

<i>Table 1: Frequency, prognosis, relapse rates and 5-year survival for some of the different subsets of paediatric ALL.....</i>	14
<i>Table 2: Summary of the 3 main stages in the treatment of paediatric ALL.....</i>	22
<i>Table 3: Comparison of the advantages and disadvantages of CRISPR and RNAi screening methods.....</i>	42
<i>Table 4: Patient information and treatment details for patient L707</i>	47
<i>Table 5: Equipment used during the PhD, the manufacturer and if applicable the software ..</i>	49
<i>Table 6: Antibodies used for FACS analysis of peripheral blood and organs collected from mice engrafted with ALL cells.....</i>	55
<i>Table 7: Antibodies used for western blotting</i>	55
<i>Table 8: Primer pairs used for real-time PCR using cDNA made from mRNA as the template</i>	56
<i>Table 9: Primer pairs used for real-time PCR using genomic DNA as the template</i>	56
<i>Table 10: Primers used in the production of the lentiCRISPR amplicon library used for next generation sequencing.....</i>	56
<i>Table 11: Information on culture of all cell lines used including disease type, cell type and the culture conditions required.</i>	59
<i>Table 12: Information on culture of primary human and primary derived cells including disease type, cell type and the culture conditions required.....</i>	60
<i>Table 13: Reagents used for the first step of cDNA synthesis.....</i>	70
<i>Table 14: Reagents used for the reverse transcription PCR master mix.....</i>	70
<i>Table 15: Reagents per well for quantitative real-time PCR.....</i>	71
<i>Table 16: Percentage of cells with any abnormal cells (not 2R2G) in healthy control cells as determined by FISH. Percentages are the average of 2 scores by different people.</i>	89
<i>Table 17: Calculations for cut-off for positivity.....</i>	89
<i>Table 18: Reagents and volumes required for the first step amplification PCR for the lentiCRISPR samples</i>	97
<i>Table 19: Reagents and volumes required for the second step PCR.....</i>	99
<i>Table 20: Reagents and volumes required for BsmBI digestion of lentiCRISPRv2 plasmid.....</i>	103
<i>Table 21: Reagents and volumes required for annealing the sense and antisense sgRNA oligos</i>	104

<i>Table 22: Reagents and volumes required for the ligation of the annealed sgRNA oligos into the digested lentiCRISPRv2 plasmid.</i>	104
<i>Table 23: karyotype at presentation and relapse, work carried out by NHS cytogenetics services as part of normal treatment protocols.</i>	106
<i>Table 24: Array Location, sample type, mouse and labels used for analysis for samples used for microarray analysis of L707 presentation and relapse.</i>	108
<i>Table 25: Top 5 gene ontology hits for list of 2122 differentially expressed genes between presentation and relapse.</i>	115
<i>Table 26: Known variants from the list of SNP with predicted moderate or high impact unique to the L707 relapse, the affected gene and the associated disease.</i>	122
<i>Table 27: Known variants from the list of indels with predicted moderate or high impact, unique to the L707 relapse and the gene affected.</i>	123
<i>Table 28: Selected SNP predicted as high consequence shared between presentation and relapse that have been associated with cancer</i>	126
<i>Table 29: Sequences of the breakpoints in the relapse specific 5q deletion.</i>	129
<i>Table 30: Percentage of cells with heterozygous deletion of NR3C1 in all L707 presentation samples tested.</i>	131
<i>Table 31: Treatment groups used in the testing of the pTRIPZ transduced 697 cells.</i>	143
<i>Table 32: The cell and FBS concentrations used for the four different conditions for testing 697pSLIEW cells on different supporting stromal cells.</i>	216
<i>Table 33: Samples used for the 697 Dex resistance RNA sequencing.</i>	231

List of Abbreviations

AGM	Aorta-gonad-mesonephros
ALL	Acute lymphoblastic leukaemia
AML	Acute myeloid leukaemia
β -ME	B-mercaptoethanol
BAC	Bacterial artificial chromosome
BCA	Bicinchoninic acid
BCR	B cell receptor
bHLH	Basic helix loop helix
BLAST	Basic Local Alignment Search Tool
BM	Bone marrow
BSA	Bovine serum albumin
BWA-mem	Barrows-Wheeler alignment
bZIP	Basic leucine zipper
Cascade	CRISPR associated complex for anti-viral defence
CLP	Common lymphoid progenitor
CNA	Copy number alteration
COSMIC	Catalogue of somatic mutations in cancer
CpG	cytosine-phosphate-guanine
CRISPR	Clustered regularly interspaced short palindromic repeats
Ct	Cycle threshold
CV ₂	Coefficient of variation
DAB	3,3'-diaminobenzidine tetrahydrochloride
DBD	DNA binding domain
$\Delta\Delta Ct$	Delta-delta Ct
Dex	Dexamethasone
DI	De-ionised
DNA	Deoxyribonucleic acid
Dox	Doxycycline
DSB	Double strand break
DTT	Dithiothreitol
EDTA	Ethylenediaminetetraacetic acid

EFS	Event free survival
FACS	Fluorescence activated cell sorting
FDR	False discovery rate
FISH	Fluorescent <i>in situ</i> hybridisation
FPKM	Fragments per kb of transcript per million mapped reads
GATK	Genome Analysis Toolkit
GC	Glucocorticoid
GFP	Green fluorescent protein
GRE	Glucocorticoid response element
GSEA	Gene set enrichment analysis
GTC	Cluster reference information files
H&E	Haematoxylin/eosin
HDAC	Histone deacetylase
HR	Homologous recombination
HRP	Horseradish peroxidase
HSC	Haematopoietic stem cell
IDAT	Intensity data files
IgG	Immunoglobulin
IP	Intra peritoneal
IRES	internal ribosome entry site
IVIS	In Vivo Imaging System
LBD	ligand binding domain
LT-HSC	Long term HSC
LTR	Long terminal repeats
MAGECK	Model based analysis of genome wide CRISPR/Cas9 knockout
MPP	Multipotent progenitor
MRD	Minimal residual disease
MSC	Mesenchymal stem cell
NHEJ	Non homologous end joining
NSG	NOD/SCID/IL2Ry null
NTC	Non targeting control
OS	Overall survival

PAM	Protospacer adjacent motif
PAR	Proline and amino rich domain
PBS	Phosphate buffered saline
PCA	Principal component analysis
PCR	Polymerase chain reaction
PK	Pharmacokinetic
PNK	T4 Polynucleotide Kinase
polyA	Polyadenylated
pre-BCR	Pre B cell receptor
RIN	RNA Integrity Number
RISC	RNA induced silencing complex
RNA	Ribonucleic acid
RNAi	RNA interference
RRA	Robust rank aggregation
RSN	Robust spline normalisation
rtTA3	Reverse tetracycline transactivator 3
sgRNA	Short guide RNA
shRNA	Short hairpin RNA
siRNA	Short interfering RNA
SNP	Single nucleotide polymorphism
ST-HSC	Short term HSC
STRING	Functional protein association network
TAD	Transactivation domain
TALENs	Transcription activator like effector nuclease
TET	Tetracycline
tRFP	Turbo red fluorescent protein
UDG	Uracil DNA glycosylate
UTRs	Untranslated region
VEP	Variant effect predictor
VST	Variance stabilisation transformation
WGS	Whole genome sequencing
WGS	Whole genome sequencing

List of gene names

ABCC3	ATP binding cassette subfamily C member 3
AGO	Argonaute
AKT1	V-Akt Murine Thymoma Viral Oncogene Homolog 1
AP-1	Activator protein 1
ARHGAP26	Rho GTPase activating protein 26
ASNS	Asparagine Synthetase (Glutamine-Hydrolyzing)
ASS1	Argininosuccinate synthase 1
ATP10A	ATPase phospholipid transporting 10A
ATR	ATR Serine/Threonine Kinase
BCL2	B cell CLL/lymphoma 2
BCL2L1	BCL2 like 1
BIM	BCL211, BCL2 like 11
BRCA2	Breast cancer 2
CD	Cluster of differentiation
CDKN2A	Cyclin-dependent kinase inhibitor 2A
CEBP α	CCAAT/Enhancer Binding Protein Alpha
CEPB β	CCAAT/ Enhancer Binding Protein Beta
CHEK1	Checkpoint Kinase 1
CLEC1A	C-type lectin domain family member 1A
CNTN5	Contactin 5
DICER1	Dicer 1, Ribonuclease III
DKK1	Dickkopf 1
EBF	Early B-Cell Factor
EED	Embryonic ectoderm development
EGR1	Early growth response 1
FGF1	Fibroblast growth factor 1
FKBP	FK506 binding protein
FKBP5	FK506 binding protein 5
FOS	Fos proto-oncogene
FOSB	FosB proto oncogene
GAS1	Growth arrest specific

GATA2	GATA Binding Protein 2
GFI1	Growth Factor Independent 1 Transcription Repressor
GILZ	Glucocorticoid induced leucine zipper
GILZ	Glucocorticoid induced leucine zipper
GLI3	GLI family zinc finger 3
GSTT1	Glutathione S-transferase Theta 1
HAT	Histone acetyl transferase
HLF	Hepatic leukaemia factor
HMHB1	Histocompatibility (minor) HB-1
HSP70	Heat shock protein 70
HSp90	Heat shock protein 90
HSPA1A	Heat shock protein 1A
HSPA1B	Heat shock protein 1B
IGF1R	Insulin like growth factor
IKZF1	Ikaros
IL6ST	Interleukin 6 signal transducer
INHBE	Inhibin Beta E
ITGB7	Integrin subunit Beta 7
JAK2	Janus kinase 2
JUN	Jun proto-oncogene
JUNB	JunB proto-oncogene
JUND	JunD proto-oncogene
KCTD16	Potassium channel tetramerization containing 16
KRAS	Kirsten Rat sarcoma viral oncogene homolog
LDLR	Low density lipoprotein receptor
LILRB4	Leukocyte immunoglobulin like receptor B4
MAP4K4	Mitogen-Activated Protein Kinase
MAPKBP1	Mitogen-Activated Protein Kinase Binding Protein 1
MCL1	Myeloid cell leukaemia 1
MDM2	Mouse double minute 2 homolog
MEK2	Mitogen activated protein kinase 2
MEK4	Mitogen activated protein kinase 4

MLL	Mixed lineage leukaemia
MRAS	Muscle Ras oncogene homolog
MS4A6E	Membrane spanning 4-domains A6E
MSH6	MutS homolog 6
MSL1	Male specific lethal 1
MSRB2	Methionine Sulfoxide Reductase B2
NDUFB11	NADH:Ubiquinone oxidoreductase subunit B11
NFKBIA	NFKB inhibitor alpha
NFKBIA	NFKB inhibitor alpha
NHEJ1	Non-Homologous End Joining Factor 1
NR2E1	Nuclear receptor subfamily 2, group member E
NR3C1	Nuclear receptor subfamily 3, group C member 1
NR4A1	Nuclear receptor family 4, member 1
NRAS	Neuroblastoma RRAS viral oncogene homolog
p23/PTGES3	Prostaglandin E synthase 3
PAX5	Paired box 5
PEG3	Paternally expressed 3
PIK3R1	Phosphoinositide-3-Kinase Regulatory Subunit 1
PLS3	Plastin 3
PLXNA1	Plexin A1
PLXNB1	Plexin B1
PLXND1	Plexin D1
PROM1	Promonin 1
PTPN11	Protein tyrosine phosphatase, non-receptor type 11
PTPRN2	Protein tyrosine phosphatase, receptor type N2
RAG1/2	Recombination activating gene 1/2
RASD1	Ras related Dex induced 1
RCAN1	Regulator of calcineurin 1
RNF20	Histone H2B E3 ubiquitin ligase ring finger protein 20
RRBP1	Ribosome binding protein 1
RUNX1	Runt Related Transcription Factor 1
S100A8	S100 Calcium binding protein A8

S100A9	S100 Calcium binding protein A9
SCD	Stearoyl-CoA Desaturase(Delta-9-Desaturase)
SEMA3E	Semaphorin 3E
SIAH11A	Seven in absentia 1A
SLAMF6	Slam family member 6
SNAI2	Snail family zinc finger 2
SNORA79	Small nucleolar RNA, H/ACA Box 79
STAT5	Signal transducer and activator of transcription 5
STN	Striatin
TBL1XR1	Transducin (Beta)-Like 1 X-Linked Receptor 1
TBP	TATA-Box binding protein
TCEA3	Transcription elongation factor A3
TCF3	Transcription Factor 3
TMEM182	Transmembrane protein 182
TP53	Tumour protein p53
TP53BP1	TP53 binding protein 1
TP53INP1	Tumour protein P53 inducible nuclear protein 1
TP53RK	TP53 regulating kinase
TRRAP	Transformation/transcription domain associated protein
UBA7	Ubiquitin Like Modifier Activating Enzyme 7
UBC	Ubiquitin C
VPREB1	Pre-B lymphocyte 1
YIPF5	Yip 1 domain family member 5

Chapter 1: Introduction

1.1 The Haematopoietic System

The haematopoietic system is essential for the production of the immune system, as well as the cells responsible for the transport of oxygen around the body. The system is a hierarchy, with a stepwise progression from the multipotent haematopoietic stem cell (HSC) through several intermediates to fully differentiated mature immune cells. HSCs have the capacity to produce every cell of the immune system, and in mice, the injection of a single HSC ($CD34^{\text{low/neg}}$, c-kit $^+$, Sca-1 $^+$, Lin $^-$) into a sub lethally irradiated recipient results in the production of the entire range of immune cells (Osawa et al. 1996; LeBien 2000; Welner, Pelayo, and Kincade 2008). Differentiation and commitment to each of these immune cell lineages is determined by several complex transcriptional programmes that alter the pattern of gene expression within the cells.

1.2 Development of the Haematopoietic system

The production of the complex multi-lineage haematopoietic system starts pre-natally, in the yolk sac. The commencement of haematopoiesis occurs with the development of haemangioblasts, precursor cells with both endothelial and haematopoietic potential (Kennedy et al. 2007). Haemangioblasts initiate the first stage of haematopoiesis, primitive haematopoiesis. This occurs at embryonic day 7 (E7) in the mouse and between days 16-19 in human gestation in blood islands in the mesodermal layer of the yolk sac. These blood islands consist of immature erythroid cells surrounded by endothelial cells (Palis et al. 1999). The first wave of haematopoiesis results in the production of primitive erythroid cells to enable oxygenation of the embryo.

After primitive haematopoiesis there is a transient wave of definitive haematopoiesis that also occurs in the yolk sac, and results in the production of erythroid and myeloid progenitors. This second wave occurs at E8.25 in the mouse, and with the start of circulation at E8.5 the foetal liver is colonised. Mature erythrocytes produced from this transient wave

are detectable in circulation shortly after, at E11.5 (Cumano and Godin 2007; Godin and Cumano 2005; Palis et al. 1999; Jagannathan-Bogdan and Zon 2013; Kennedy et al. 2007).

The second phase of definitive haematopoiesis, which initiates the production of HSC occurs in the aorta-gonad-mesonephros (AGM) region, specifically the ventral wall of the dorsal aorta (Moore 2009; Ivanovs et al. 2011), where haematopoietic clusters form. This is thought to occur through the haematopoietic transition of endothelial cells. This mechanism has been shown experimentally in both zebrafish and mice, and is the most likely route of formation for human HSC as well (Bertrand et al. 2010; Kanz et al. 2016). The exact mechanism is still unclear though as pre-HSC have been found in the sub-endothelial layer of the AGM, whereas the mature HSC are found in the endothelial layer of the aortic wall. It is not known if these pre-HSC incorporate into the haemogenic endothelium or migrate directly to the lumen of the aorta (Figure 2). The haemogenic endothelial cells of the AGM, from mid-gestation are the first cells to show HSC engraftment potential in mouse models (Müller et al. 1994; Medvinsky et al. 1993).

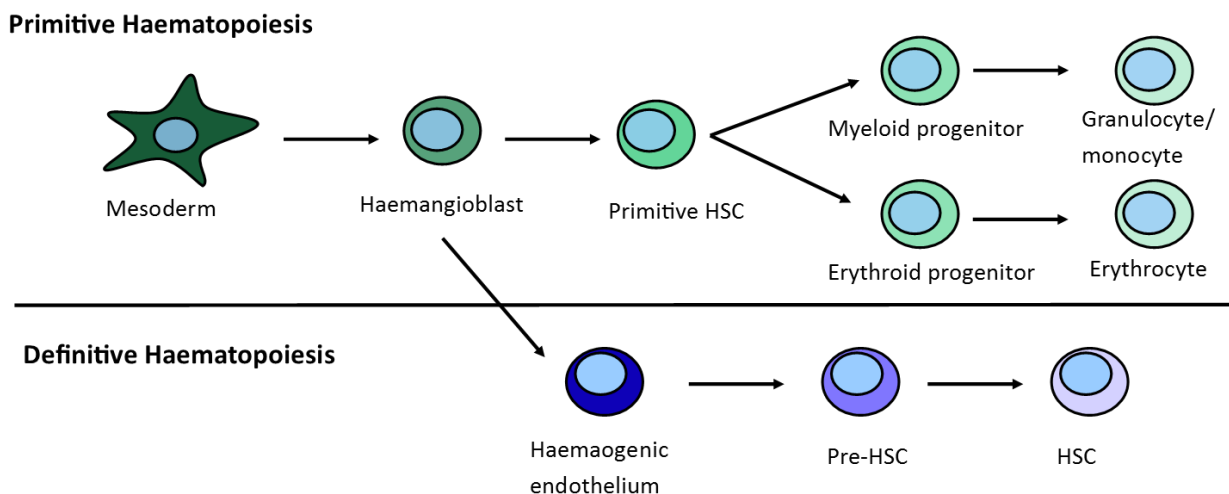


Figure 1: Primitive haematopoiesis and definitive haematopoiesis. The schematic shows the two routes of haematopoiesis in the foetus, with a progression from the pluripotent mesoderm down one of the two pathways. The primitive HSC has no self-renewal capacity and can only produce the myeloid and erythroid cells of primitive haematopoiesis. Definitive haematopoiesis and the production of the classical HSC comes later by way of the haemogenic endothelium. This is the route by which the entire complement of blood and immune cells is produced in both the foetus and adult (Jagannathan-Bogdan and Zon 2013; Ivanovs et al. 2011; Kennedy et al. 2007; Cumano and Godin 2007; Godin and Cumano 2005).

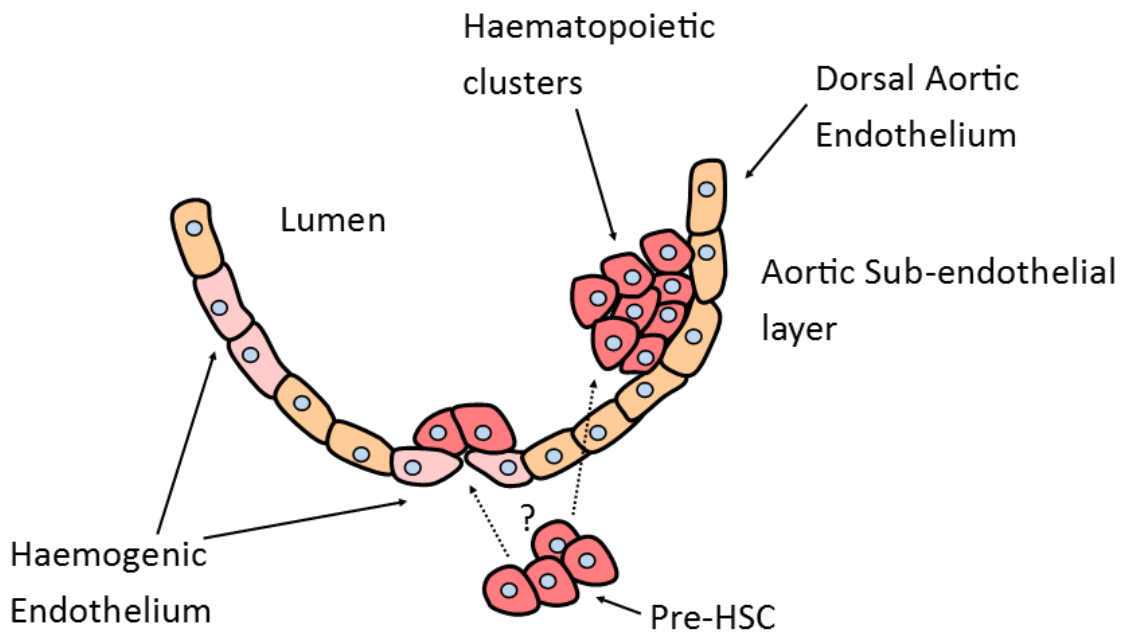


Figure 2: The development of HSC from the haemogenic endothelium in the dorsal wall of the aortic endothelium. The haemogenic endothelium differentiate into haematopoietic clusters which contain HSC and are located on the wall of the dorsal aorta. Pre-HSC have also been found in the sub-endothelial layers and it is not known whether these pre-HSC are incorporated into the haemogenic endothelia or head straight to the haematopoietic clusters (dotted lines) (Ivanovs et al. 2011; Kennedy et al. 2007; Costa, Kouskoff, and Lacaud 2012).

HSC produced by the haematopoietic clusters of the AGM colonise the foetal liver at E14.5 in mice, and by 2-4 days post-natally foetal liver haematopoiesis has finished and the HSC have homed to, and colonised the BM (Bone Marrow) (Sasaki and Sonoda 2000). In humans foetal liver haematopoiesis occurs slightly differently with 2 waves of hepatic colonisation, the first at day 23, when primitive erythromyeloid cells are found in the liver, and the second a week later at day 30 when the first CD34⁺ precursor cells can be detected in foetal liver (Tavian and Péault 2005).

It is not just the liver where foetal haematopoiesis occurs, After HSC have colonised the foetal liver they also spread to other sites of extramedullary haematopoiesis, the thymus and the spleen. The thymus in the embryonic mouse is seeded with haematopoietic cells at E11. The thymus, unlike the other extramedullary haematopoietic organs, is derived from the endoderm rather than the mesoderm. It has a complex spongiform structure and it is the interplay between developing haematopoietic cells and the thymic endothelial cells that

promotes the development of this structure (Dzierzak and Speck 2008; van Ewijk et al. 2000). The foetal spleen starts forming at E11.5 in mice and is seeded with HSC from circulation, presumably from the foetal liver, between E12.5-E13. The foetal spleen does not have the same levels of HSC seen in the foetal liver and equivalent to 4 foetal spleens are needed to reconstitute the entire haematopoietic system in recipient mice compared to just one foetal liver (Bertrand et al. 2006).

Haematopoiesis in the BM initiated by HSC born in the AGM region and expanded in the foetal liver is a late occurring event; E18.5 in mice and 10.5 weeks post-natally in humans (Baron, Isern, and Fraser 2012; Babovic and Eaves 2014; Jagannathan-Bogdan and Zon 2013). Limited haematopoiesis in the marrow can be detected earlier, in mesodermal structures (E17 in mice and week 11 in humans). This is thought to be the maturation of pre committed progenitors seeded from other sites with HSC in the developing embryo (Tavian and Péault 2005; Blazsek, Chagraoui, and Péault 2000). Once the HSC have colonised the BM they retain the characteristics of foetal HSC for a short period before switching to a quiescent adult phenotype. In both humans and mice foetal HSC are proliferative, human foetal HSC proliferate around 10x faster than adult HSC, once every 3.5-4 weeks vs 40 weeks respectively (Ivanovs et al. 2011; Catlin et al. 2011). This switch occurs 1-2 years after birth as inferred from a dramatic reduction in the rate of telomere shortening in leukocytes, which is used as a surrogate for measuring proliferation (Rufer et al. 1999).

The switch in proliferative capacity of HSC is accompanied by a change in the transcriptional landscape. Using murine foetal HSC to investigate the transcriptional differences between foetal and adult HSC reveals increased expression of CEBPa (CCAAT/enhancer-binding protein alpha) as a key factor in the switch. Indeed knockout of *CEBPa* in adult murine HSC reverts them to a proliferative state with characteristics of HSC found in the foetal liver (Ye et al. 2013).

Even before the switch to an adult HSC phenotype there is already heterogeneity in the HSC compartment, as both foetal and adult HSC contain different subtypes which have different clonal differentiation potential. Three subtypes of HSC have been described, α , β and γ . α HSC have reduced lymphoid potential compared to β and γ HSC but the number of these in foetal liver is very low (2/43 measured). In the adult mouse (10 months) this is increased to 45% (Benz et al. 2012). This increase in lymphoid deficient α HSC is mirrored by the

downregulation of lymphoid specific and upregulation of myeloid specific transcriptional programmes in HSC from old mice (Rossi et al. 2005; Cho, Sieburg, and Muller-Sieburg 2008). This reduction in lymphoid progenitor cells is mirrored in humans with increasing age, and assuming a similar picture for the subtypes of HSC could account for the increase in myeloid malignancies in adults, as there are less lymphoid competent HSC (Benz et al. 2012). Conversely the increased number of HSC that can form lymphoid cells in the young could account for the tendency towards lymphoid leukaemia in children (Babovic and Eaves 2014). The development of the haematopoietic system from these HSC follows a hierarchy, Figure 3 outlines the process of haematopoiesis in the adult, starting from the mature HSC with a focus on B lymphoid development.

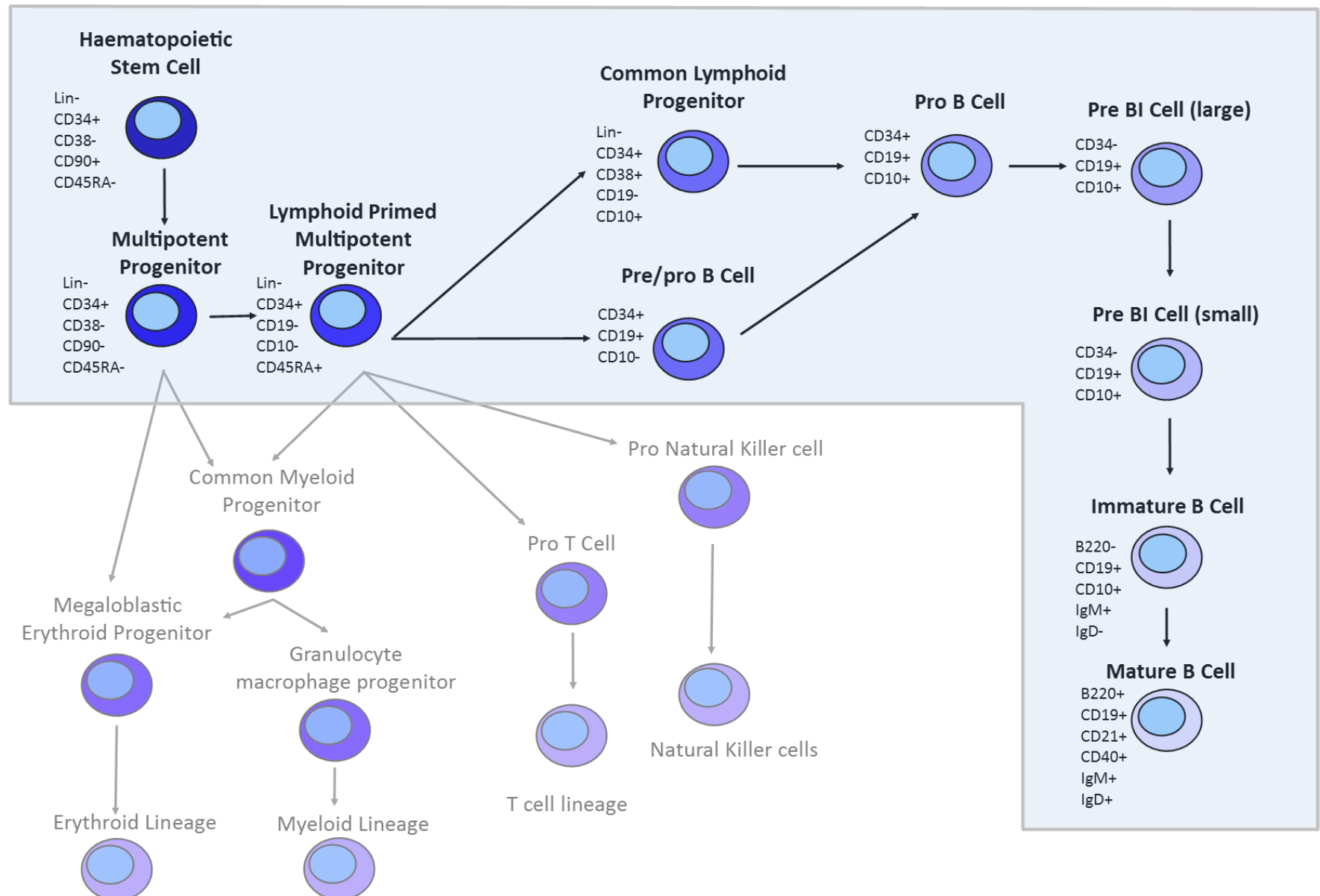


Figure 3: Lymphoid differentiation from the multipotent HSC to the terminally differentiated mature B cells that defines definitive haematopoiesis. The schematic includes immunophenotype for B cells which shows the progressive loss of stem cell markers such as CD34 and acquisition of lineage specific markers such as CD19 and CD10. This process takes place entirely in the bone marrow (after birth). Greyed out cells are haematopoietic cells not in the B lymphoid lineage (Carroll et al. 2009; LeBien 2000; Sanz et al. 2010; Welner, Pelayo, and Kincade 2008; Rieger and Schroeder 2012).

1.3 Transcriptional control of HSC

The differentiation stages in haematopoiesis are tightly controlled by specific transcriptional programmes, driven by key transcription factors. At the earliest stages of haematopoiesis transcription factors are required for HSC maintenance. Two important examples are *GATA2* (GATA binding protein 2) and *RUNX1* (Runt-related transcription factor 1). *GATA2* is expressed in the precursor cells that give rise to HSC and marks them as haematopoietic cells (Minegishi et al. 1999). Without *GATA2* expression mice die at embryonic day 10/11 with severe anaemia. *In vitro*, *GATA2* null progenitor cells do not proliferate well, and the colonies that are formed are small with a high percentage of dead cells (Tsai and Orkin 1997). *RUNX1* is another gene that is an essential HSC factor required for haematopoiesis. Mice lacking *RUNX1* die at E12.5 with no definitive haematopoietic cells, just primitive erythropoiesis (Okuda et al. 1996). These are just two of the genes with vital functions in the regulation of HSC and haematopoiesis. For example the loss of *GFI1* (Growth factor 1 independent transcriptional repressor) expression results in a cascade of changes that causes HSC to enter cell cycle more often, resulting in reduced long term repopulating efficiency (Muench et al. 2015). E2A, encoded by the *TCF3* gene (transcription factor 3) is another protein that controls cell cycle within the HSC, and loss results in increased cell cycle.; E2A null mice have a reduced HSC pool, as well as a reduction in myeloid and lymphoid progenitors in the BM, a direct result of increased cell cycling and reduced long term self-renewal (Semerad et al. 2009).

Even small changes in the expression of transcriptional modulators can have drastic effects on HSC. In a study looking at the transcriptional differences between long term-HSC (LT-HSC) and short-term HSC (ST-HSC) just 210 genes were found to be differentially expressed. However, it appears this is sufficient for the loss of long term repopulating potential (Zhong et al. 2005). This switch from LT-HSC to ST-HSC, and the associated change in gene expression is also accompanied by a change in phenotype. 75% of HSC have cell surface markers that denote long term repopulation potential has been lost, either the expression of CD38 or CD34 (Zhong et al. 2005; Morrison and Weissman 1994). These ST-HSC have more colony forming units *in vitro* as a result of being in cell cycle more often, but have a reduced capacity for self-renewal (Morrison and Weissman 1994). The ST-HSC give rise to multi-potent progenitor cells (MPP), the last cells able to generate all cells of the haematopoietic

system. The MPP pool is heterogeneous and among other cell types gives rise to the common lymphoid progenitor (CLP) (Adolfsson et al. 2005).

1.4 B lymphoid haematopoiesis

Once the HSC have passed through the ST-HSC and MPP stages, those cells that will become B lymphocytes become committed to the lymphoid lineage by differentiating into CLP. This is marked by the expression of several genes defined as lymphoid lineage commitment factors such as E2A, EBF (Early B cell factor) and PAX5 (Paired box 5), which are each heavily implicated in the development of B lymphocytes. Each of these drives specific transcriptional programmes that bring about the changes needed within the cell for further differentiation. This change in transcription and commitment marks the start of B lymphoid haematopoiesis, the result of which is the 2×10^{12} lymphocytes in a healthy human. Each of these mature cells is the end product of clonal selection with several steps and checkpoints and are important in the ability to mount an immune response upon exposure to foreign antigens.

Passage through these checkpoints is determined by the expression of appropriate factors, and levels of immunoglobulin (IgG) recombination, a process that increases as the cells move further down the B lymphoid pathway. This rearrangement, which involves 3 variable regions of the Ig gene is mediated through the recombinase activating genes (RAG) *RAG1* and *RAG2*, which in turn are modulated by transcription factors. Three regions of the IgG gene are involved in this rearrangement; variable (V), diverse (D) and joining (J), and it is the juxtaposition of different segments of each region to produce a novel transcript that constitutes recombination. It is a tightly controlled and ordered process with D-J recombination first, followed by V-DJ recombination, rearrangement of heavy chains precedes light chains (Sigaux 1994; González et al. 2003).

Progression of CLP into the B lymphoid pathway is controlled by the transcription factor E2A, encoded by the *TCF3* gene. The gene codes for 2 basic helix loop helix (bHLH) proteins, E47 and E12 made by alternate splicing of the exon encoding the DNA binding region in E2A. The interaction of E12 and E47 with immunoglobulin genes is how this gene exerts control over differentiation. In E2A null mice there is no RAG1 expression, resulting in the absence of DJ recombination, and thus lack of progression past the earliest lymphoid development checkpoints. As a result, E2A null mice have no mature B cells, and the progenitors do not

progress past the CLP stage (Bain et al. 1994; Zhuang, Soriano, and Weintraub 1994) EBF is expressed in B lymphocytes from the pro B stage to mature B cells, but not in mature plasma cells, it is important for B cell development at a similar time point as E2A. EBF knockout mice have a block in differentiation early in B cell development, prior to any VD recombination. Mice with heterozygous loss of one EBF allele on the other hand do have pro B cells but at a reduced frequency, indicating a dose response for EBF (O'Riordan and Grosschedl 1999). Interestingly, the block in differentiation and resultant lack of cells past the pre/pro B cell stage caused by E2A knockout can be reduced *in vitro* by the addition of EBF and E2A related proteins to E2A null cells (Seet, Brumbaugh, and Kee 2004) indicating that there is a cooperating role for these two proteins. Mice with double knockout of both alleles of E2A and EBF have a differentiation block of B cells earlier in lymphobopoiesis than mice with heterozygous E2A and EBF knockout (O'Riordan and Grosschedl 1999).

PAX5 is a transcription factor exclusively expressed in B cells, and is an early irreversible B cell commitment factor. PAX5 expression is repressed in HSC through histone modifications, but upon entry to the B cell pathway these are lost and PAX5 expression increased (Weishaupt, Sigvardsson, and Attema 2010). Pro B cells without expression of PAX5 are not committed B cells and they are still able to produce cells of the myeloid lineage. This is the result of deregulation of lineage commitment genes, and the expression of non B lineage markers in these cells belies the underlying expression of myeloid associated genes; genes that under normal circumstances are repressed by the expression of PAX5 (Nutt et al. 1999). PAX5 null progenitor cells show DJ rearrangement, but not VDJ rearrangement indicating a later role than E2A and EBF in B lymphoid haematopoiesis (Nutt et al. 1997).

1.5 Paediatric B cell ALL

Understanding the normal biology of haematopoiesis is important for the study of acute lymphoblastic leukaemia (ALL) because they are inextricably linked. There are two main subtypes of ALL, B cell and T cell, dependent on the immunophenotype and morphology of the leukaemic blasts, which can be correlated with stages in normal haematopoiesis. Of the acute leukaemias, B cell ALL is the most common, accounting for approximately 85% of all cases (Carroll et al. 2009).

B cell ALL is a disseminated haematological malignancy characterised by the uncontrolled proliferation of differentiation arrested immature B lymphocytes. As is the name suggests, the disease has an acute presentation with a swift disease progression in the absence of medical intervention. The overproduction of leukaemic blasts results in changes in the BM that lead to the failure of normal haematopoiesis. As well as BM failure, leukaemic blasts infiltrate other organs and patients often present with splenomegaly or hepatomegaly (Reiter et al. 1994; Marwaha et al. 2010).

Although B cell ALL has an excellent prognosis with current treatment regimens in developed countries, around 85%, those patients that suffer a relapse have a significantly worse outcome with survival rates falling to less than 50% (le Viseur, Hotfilder, Bomken, Wilson, Rottgers, et al. 2008; Rivera et al. 2005; Nguyen et al. 2008). The incidence of ALL has a marked distribution, with a peak in children less than 4 years with an average of 122 male and 101 female patients presenting in the UK each year, an average of 6 and 5.2 cases per 100,000 per year respectively. This rate decreases as age increases, and by age 20 is around 0.8 cases per 100,000 (Tobergte and Curtis 2013). The upper age limit for patients to be described as paediatric ALL is not clear cut, but it is generally accepted that paediatric ALL includes adolescents up to age 20. It has been shown for this group of older children and adolescents (age 15-20) that treatment on a paediatric regime results in better outcomes compared to those treated with adult protocols (Boissel et al. 2003). Interestingly, there have also been studies in which a paediatric regimen was used for the treatment of adults and it was found that intensive treatment was beneficial up to the age of 55 (Huguet et al. 2016).

1.6 Biology of ALL

ALL is characterised by leukaemic fusion genes, which are the result of chromosomal translocations. These fusion genes are in most cases the driving force behind the aetiology of ALL, but the factors that cause the chromosomal translocation responsible for the production of fusion proteins is less well known. Only 5% of ALL cases are associated with predisposing factors such as ionizing radiation and Downs syndrome (Pui and Robison 2008). Several other factors have been hypothesised including household chemicals (Freedman et

al. 2001), paternal exposure to ionizing radiation (McKinney et al. 1991) and electromagnetic fields (Linet et al. 1997), but these have mostly been found to be unfounded or only weakly associated.

One of the prevailing theories about the development of paediatric ALL is the hygiene hypothesis. First described by Strachan in 1989, the hypothesis was described after a study linked hay fever to family size. It was theorised that “unhygienic contact” with older siblings and family members was protective against the development of hay fever (Strachan 1989). Greaves was the first to link this hypothesis to the development of paediatric ALL in 1997. He postulated that the reduced exposure to infection of children, as a result of lower numbers of women breast feeding and cleaner environments, results in the abnormal programming of the immune system. This mis-priming of the immune system means that later infections result in an aberrant immune response and increased risk for ALL (Greaves 1997). This has been expanded on since then and is now thought of as the delayed infection hypothesis. In support of this theory, it has been found that there is a reduced risk of paediatric ALL in children who received their childhood immunisations on time. The childhood immunisations could be described as the early insult to the immune system, which is possibly enough to modulate the immune system so that later infections do not result in aberrant immune response and increased risk of ALL (MacArthur et al. 2008).

However, in refutation of this, another study done in the 1990s in Canada found that being born 2nd or later and having older siblings increased the risk of paediatric ALL which would suggest that older siblings do not result in a protective effect as initially postulated with the hygiene hypothesis. The same study did find that attendance at nursery and breast feeding reduced the risk of paediatric ALL. This does indicate a role for childhood infections in the development of ALL, but also serves as a reminder that it is a complex association and it is still not fully understood (Infante-Rivard, Fortier, and Olson 2000).

A meta-analysis published in 2013 found that 16 out of 21 studies investigating the effect of maternal infection on the risk of leukaemia development found them to be positively correlated. The remaining 5 studies found no significant correlation. Again the picture is not clear regarding the effect of childhood infections on the development of ALL. 5 of the studies investigated found that childhood infections lowered the risk of ALL development, whereas 2 found the opposite, a remaining 5 studies that looked at the risk from childhood infections

found that some increased risk and others decreased the risk (Maia and Wünsch 2013). This unclear picture reinforces the need for meta-analysis of large scale epidemiology studies as they can present with very different results.

The cells characteristic of B ALL are malignant B lymphoid progenitor cells with an arrest in differentiation. These malignant cells can often be correlated with a step in normal B lymphoid haematopoiesis, dependent on the stage of differentiation the blasts are arrested (Figure 4). However, there is overlap between the different subtypes and in up to 30% of pre B ALL cases there is also the expression of myeloid markers, so this relationship between ALL subtype and differentiation stage may not be as simple as it first seems (Cobaleda and Sánchez-García 2009).

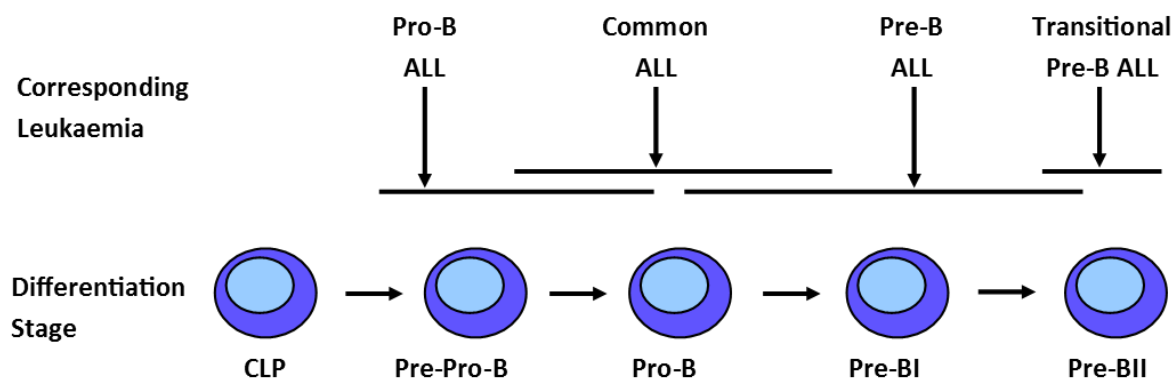


Figure 4: The correlation of B ALL subtype with stages in B lymphoid differentiation. The subtypes are not fully correlated and there is crossover as leukaemic transformation can result in aberrant expression of surface markers used for discrimination of differentiation stages (Cobaleda and Sánchez-García 2009).

1.6.1 Genetic translocations

Genetic translocations involve the juxtaposition of separate genes at the DNA level, they can involve a small part or the whole gene and often result in the production of chimeric fusion proteins. These proteins are the hallmark of many haematological malignancies including ALL. The link between cytogenetics and prognosis in ALL was first demonstrated in the 1970s, when it was found that hyper-diploid patients had an increase in the length of

remission compared to other subtypes (Secker-Walker, Lawler, and Hardisty 1978). Since then there has been an expansion of research and the differential prognosis conferred by the recurrent subtypes is known (Table 1). Thanks to the advent of gene expression profiling subtypes can be grouped according to the expression profile of leukaemic blasts. Different cytogenetic subgroups cluster together indicating similar transcriptional programmes are active in the cells (Yeoh et al. 2002). One subtype for which this has been important is the BCR/ABL like cases. This subtype of ALL is characterised by similar gene expression profile as the t(9;22), BCR/ABL positive cases but without the BCR/ABL translocation. As these cases have a similarly poor prognosis as cases with t(9;22) they benefit from intensified chemotherapy, which without transcriptional stratification of the subtype might not have happened (Den Boer et al. 2009).

Some of the genetic translocations are associated with particular subtypes of B ALL. For example, 25% of Pre-B ALL cases are t(1;19), compared to around 5% in all B precursor ALL (Raimondi et al. 1990). Hyperdiploid ALL, (>50 chromosomes) is also seen more frequently in pre pro B ALL, and t(12;21) translocations, which are more common in paediatric ALL than adult, have a skew towards pre-pro B ALL and pre B ALL (Yeoh et al. 2002). Another interesting finding is that CRLF2 translocations are found in 50% of Downs syndrome ALL (Mullighan 2012). MLL (Mixed lineage leukaemia) rearranged ALL cases have low levels of CD24 and CD79b, a phenotype associated with pro B cells in normal haematopoiesis (De Braekeleer et al. 2010).

Chromosomal abnormality	Frequency	Genes involved	Prognosis	Relapse (%)	5-year survival (%)
t(9;22)	2	BCR/ABL	Poor unless imatinib used	42	80
t(12;21)	20-25	ETV/RUNX1	Very good	13	80-95
t(1;19)	3-5	E2A/PBX	intermediate	21	80-85
t(14;various)	2-5	IGH@/several partner genes	intermediate		
t(8;14)	2	IGH@/MYC	intermediate		
t(17;19)	<1	E2A/HLF	Very poor	100	0
t(4;11)	1-2	MLL/AF4	Very poor	43	30-40
t(11;various)	4	MLL/Several partner genes	Variable/poor		30-50
iAMP21	3-5	RUNX1 amplification	Very poor, increased risk of relapse	76	30-40
Various	10-15	BCR/ABL like	Very poor	50	57
high hyperdiploidy (>50 chromosomes)	25-35	-	good	15	85-93
near haploidy (<30 chromosomes)	1	-	Very poor	60	35-40

Table 1: Some of the genetic translocations that are seen in several subsets of paediatric B ALL including the frequency at which they are seen, the genes involved in the fusion protein, the associated prognosis, rates of relapse and the overall survival. As can be seen, those subtypes with a higher risk of relapse are also associated with a poorer prognosis, for example iAMP21, t(17;19). (Den Boer et al. 2009; Harrison 2009; Moorman et al. 2010; CH Pui et al. 2011; Ching Hon Pui et al. 2012).

1.6.2 Leukaemic transformation

The first step in leukaemogenesis is frequently the genetic translocation and resulting oncogenic fusion protein which characterises ALL. This first step is thought to primarily be a pre-natal event. The MLL/AF4 translocation can be found in neonatal blood spots (Gale et al. 1997). Despite this being a pre-natal event not all babies with a translocation develop ALL. For example, the AML1/ETO fusion gene is found at 100x higher frequency in cord blood than the incidence of ALL, and concordance of ALL is only around 5% in monozygotic twins. This demonstrates the need for post-natal secondary events to drive leukaemogenesis (Mori et al. 2002). The presence of a genetic translocation may pre-dispose cells to further secondary hits, for example by the down regulation of DNA repair genes or stem cell maintenance (Alcalay et al. 2003; Forster et al. 2015).

As outlined in previous sections, haematopoiesis is a tightly controlled process with an ordered progression from progenitor to differentiated cells. Cells that fail any of the several differentiation check points are induced to apoptosis. In ALL however, cells are able to evade apoptosis as well as blocking differentiation, forming the pathophysiological basis of the disease. There are several mechanisms by which leukaemogenesis occurs, and the mechanisms can differ between the subgroups, but there are a few genes and pathways that are frequently affected across several ALL subtypes.

Several B cell differentiation factors have been implicated in leukaemogenesis (Mullighan et al. 2007) and considering the differentiation block seen in ALL this is unsurprising. For example, *PAX5*, the B cell commitment factor essential for B cell development. Loss of *PAX5* results in cells arrested at the pro B stage (Nutt et al. 1999). *PAX5* loss of function mutations are found in one third of ALL cases and can be considered the mechanism of differentiation block in these cases (Mullighan et al. 2008). Furthermore, *PAX5* also functions as a tumour suppressor, as re-expression of *PAX5* in established disease results in ALL regression (Liu et al. 2014).

Another important player in B cell differentiation, the pre-B cell receptor (pre-BCR) is also implicated in leukaemogenesis. The pre-BCR is a membrane bound immunoglobulin composed of both heavy chains and light chains that acts as a marker for differentiation checkpoints during B lymphoid haematopoiesis as well as a tumour suppressor (Klein et al.

2004). Without the correct arrangement of the pre-BCR as a result of VDJ recombination pro B cells are not able to transition to the pre B stage (LeBien 2000). In the majority of ALL leukaemic blasts do not express the pre-BCR, but in the 13% that do re-expression of the receptor results in loss of leukaemic growth (Klein et al. 2004; Geng et al. 2015).

Downstream of the pre-BCR is Ikaros (*IKZF1*), and this gene is mutated or deleted in 15% of ALL cases, it is especially prevalent in ALL with the translocation t(9;22) (BCR/ABL), where it is present in 80% of cases. *IKZF1* modulates gene expression by chromatin remodelling, and is also a tumour suppressor. Forced expression of *IKZF1* can reverse the differentiation block in blasts, providing a mechanism for this gene in leukaemogenesis (Trageser et al. 2009; Payne 2011).

As well as genes associated with B cell differentiation such as *PAX5* and *IKZF1*, genes associated with a wide range of other pathways can be mutated in ALL. One important spectrum of mutations in genes not considered B cell factors are seen in the RAS pathway. RAS pathway activating mutations are common in ALL, and 35% of B ALL cases have mutations in RAS pathway genes such as *NRAS* (Neuroblastoma RAS viral oncogene homolog) and *KRAS* (Kirsten Rat Sarcoma viral oncogene homolog) and *PTPN11* (protein tyrosine phosphatase, non-receptor type 11). The majority of mutations in this pathway result in constitutive activation, which in turn activates expression of RAS pathway target genes. Importantly in ALL the RAS pathway is involved in the regulation of apoptosis by the *BCL-2* proteins as well as interactions with the PI3K pathway, a pathway integral for cell growth and survival signalling (Yamamoto et al. 2006; Case et al. 2008; Paulsson et al. 2008; Balmanno and Cook 2009; Mendoza, Er, and Blenis 2011; Julie Irving et al. 2014).

Despite recurrent mutations being seen frequently in ALL, the overall picture is one of genetic stability as somatic copy number variations in ALL are not found very frequently. There is an average of just 6.4 genetic alterations per case, which when compared to the median of 39 per case in solid cancers is significantly less (Mullighan et al. 2007; Zack et al. 2013).

1.7 Prognostic factors

Several of the recurrent genetic alterations can also be linked to prognosis. For example, ALL with IKZF1 deletions have a higher frequency of relapse (24% vs 13%) and a reduced 5 year event free survival (EFS) (Palmi et al. 2013). RAS pathway mutations, especially KRAS mutations are associated with reduced overall survival in ALL (Julie Irving et al. 2014). Mutations in the Janus Kinase (JAK) genes which are seen in 2-5% of ALL also confer a poorer prognosis in ALL, with patients having a reduced 5 year EFS of around 60% (Mullighan et al. 2009).

Not all prognostic factors denote poorer outcome; patients with trisomies of chromosomes 4 and 10 have increased prognosis, with a 5 year EFS of between 85-90%, these are found in almost a quarter of ALL cases (20-25%) (Salzer et al. 2010).

Age at diagnosis is an important indicator of prognosis, and infants (<1 year) fare much worse than children aged 1-9. This is partly because 80% of infant leukaemia have MLL rearranged translocations and these leukaemias have a particularly poor prognosis. The 4 year EFS is between 30-50%. When these patients are further split according to prednisone response, those with a poor response have a 4 year EFS of just 18% (Pieters et al. 2007). The prognosis for older adolescents was historically worse with 5 year EFS of 34-60% compared to 72-81% for younger children. This is partly due to the increased frequency of the poor prognostic translocation t(9;22) coupled with reduced frequency the good prognostic translocation t(12;21) (C H Pui et al. 2011). This poor prognosis for adolescents can be alleviated by intensive treatment. In one study adolescents (16-20yrs) who were treated with a paediatric regimen had overall survival (OS) of 67% compared to 46% for those treated on adult protocols (Stock et al. 2008). By giving adolescents intensive chemotherapy, which includes intrathecal triple therapy, intensive dexamethasone (Dex), vincristine and asparaginase treatment the 5 year EFS can be increased to 86% in the newest protocols, which is more in line with younger paediatric patients (C H Pui et al. 2011).

Another stratification of risk is white blood cell count at presentation. Patients with $<10 \times 10^3$ blasts/ μl at presentation have a 5-year OS of around 90%. However, as the levels of blasts in the blood at presentation increase OS decreases, and those patients with $>10 \times 10^3$ blasts/ μl have a lower survival of 66% (Salzer et al. 2010). The presence of blasts in the CNS is another

predictive risk factor, and as could be expected those patients with CNS disease at presentation have a poorer outcome compared to negative patients (OS 69% vs 86% respectively) (Salzer et al. 2010). As well as the number of blasts and their location at presentation, the properties of the blasts themselves has prognostic importance. The DNA index is the ratio of DNA in leukaemic cells in G₀/G₁ phases of the cell cycle compared to normal cells in G₀/G₁. In ALL a DNA index of between 1.16 and 1.6 is considered indicative of good prognosis whereas a DNA index <1.16 confers a worse prognosis (Salzer et al. 2010).

Race is another factor that has implications for prognosis. The frequency of ALL in children of African descent may be reduced compared to patients of European descent but so too is the 5 year EFS (61%). The differences in prognosis are thought to be a result of different risk of relapse between different ethnic backgrounds. Native American heritage increases the risk of relapse significantly, even when adjusted for other relapse risk factors (Lim et al. 2014). Sex of the patient is another factor in prognosis, with males having a worse prognosis compared to females, 84.7% 5-year OS vs 87.9% respectively (Salzer et al. 2010) . This difference can be attributed to several factors including a higher frequency of CNS relapses in males compared to females (Silverman et al. 2010), increased likelihood of males having an unfavourable DNA index (<1.16), a higher white cell count at diagnosis and a poor initial response to treatment (C H Pui et al. 1999).

All of these factors are taken into account and patients are stratified into a risk group to determine treatment, with lower risk patients receiving less intensive therapy in order to reduce the side effects of a lengthy dosing regimen. Even with increased treatment compared to standard risk groups very high risk patients still fare worse with a 4 year EFS probability of just 46% (Schultz et al. 2007).

Despite these poor prognosis factors it should be taken into account that there has been a steady increase in survival since the 1950s when ALL was first treated. The improvement of treatment regimens and personalised treatment means that for a lot of the subtypes with poor prognostic factors survival is increasing.

1.7.1 E2A/HLF

Of the factors that are indicative of prognosis, the t(17;19) translocation is one of the poorest. t(17;19) (q22/q23;p13) is a rare event found in <1% of paediatric ALL, but ALL with t(17;19) is invariably fatal and there are no reports of survivors in the literature (Moorman 2012). The translocation occurs between the amino terminus of E2A on chromosome 19 and the carboxyl terminus of HLF (Hepatic leukaemia factor) on chromosome 17. This joins 2 transactivation domains (TAD) from E2A and the basic leucine zipper DNA binding region of HLF (Figure 5), which is important for DNA binding and protein dimerization (Hunger et al. 1994). It is thought that the E2A/HLF translocation occurs in lymphoid committed progenitor cells (Fischer et al. 2015).

There are two subsets of t(17;19) translocation dependent on which exon of E2A is involved in the translocation. Type 1 has a breakpoint in exon 13 of E2A and type 2 has a breakpoint in exon 12, both are fused to exon 3 of HLF. These subsets have slightly different clinical features with type 1 being associated with disseminated intravascular coagulation and type 2 with hypercalcaemia, both confer an equally dismal prognosis (Yeung et al. 2006).

As detailed previously, E2A is vital for early B cell differentiation. The translocation partner gene HLF encodes a transcription factor that is part of the proline and acidic rich (PAR) subtype of basic leucine zipper proteins. Wild-type HLF binds to DNA as either a homodimer or as a heterodimer with other members of the PAR subtype to induce transcriptional alterations (Hunger et al. 1992). These transcriptional changes are associated with the inhibition of apoptosis, both via the up-regulation of anti-apoptotic genes and the down regulation of pro-apoptotic genes (Waters, Sontag, and Weber 2013). Interestingly, under normal conditions HLF is not expressed in haematopoietic cells, but in the liver lung and kidneys. It is only when HLF is involved in the E2A translocation that it is expressed in lymphoid cells (Hunger et al. 1992).

E2A/HLF is a transcriptional activator and experiments with mutated E2A/HLF reveal a possible double mechanism for oncogenesis, firstly the interaction between the TAD1 region and the bZIP (basic leucine zipper) to block apoptosis, and secondly the interaction of the amino terminal of E2A/HLF with other proteins to repress expression of apoptosis regulating genes (Inukai et al. 1998; Yeung et al. 2004). E2A/HLF dysregulates several other genes

thought to mediate the leukaemic phenotype of ALL cells such as the ‘haematopoietic master regulator’ RUNX1 and the zinc finger transcription factor SNAI2 (snail family zinc finger 2), which has anti-apoptotic activity when expressed as a result of E2A/HLF (Takeshi Inukai et al. 1999; Dang et al. 2001). Patients that have the E2A/HLF fusion protein as a result of the t(17;19) translocation also have recurrent mutations in VPREB1 (Pre B lymphocyte 1), part of the pre-BCR. Mutations are also frequently seen in PAX5 and BTG1 (B cell translocation gene 1), an anti-proliferative protein (Fischer et al. 2015), providing further mechanisms for leukaemogenesis in this subtype.

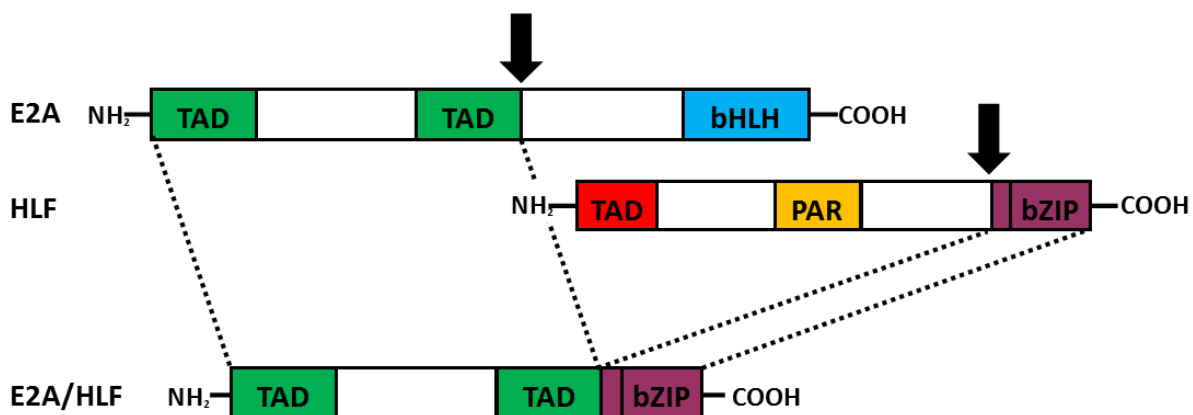


Figure 5: The t(17;19) translocation that results in the E2A/HLF fusion proteins. The E2A gene is located on chromosome 19 and HLF is on chromosome 17. The translocation juxtaposes the two transactivation domains (TAD) from the N terminus of E2A with the basic leucine zipper domain (bZIP) region at the C terminus of HLF to produce a highly oncogenic protein that increases cell survival by inhibition of apoptosis. Black arrows indicate breakpoints and dotted lines indicate the new location of the gene fragments (Latif 2012).

1.8 Treatment

Treatment for paediatric patients diagnosed with ALL is a lengthy process lasting 3-4 years. There are several stages to treatment, and each is a combination of different cytotoxic drugs for varied durations. Each stage of treatment is essential for ALL treatment, but the drug regimens differ depending on the risk grouping of the patient. Patients classed as high risk receive a more aggressive treatment style than those in standard risk subgroups. In general treatment for ALL follows the plan outlined in Table 2. Induction therapy, the first step in

treatment of ALL aims to induce a remission, and in over 95% of patients it is successful (Cooper and Brown 2015). The drugs used for induction therapy include a synthetic glucocorticoid (Dex or prednisone), vincristine, asparaginase and an anthracycline (doxorubicin or daunorubicin). In low risk patients the anthracyclines are removed to try and limit the toxic side effects of induction therapy (Cooper and Brown 2015). Dex is the glucocorticoid of choice in the treatment of most patients due to its increased CNS penetration and longer half-life. In the minority for whom induction therapy is not successful allogenic bone marrow transplants are an option. Transplants can slightly improve outcome in patients with induction failure in T-ALL but for B-ALL patients the results are mixed and seem to be dependent on subtype. For example; in patients less than 6 years old with non MLL rearranged leukaemia and induction failure, treatment with chemotherapy has a better prognosis than chemotherapy combined with a transplant. However, patients over 6 years did benefit from transplants, but only if the transplant was from a matched, related donor (Schrappe et al. 2012). The 10 year survival in patients with induction failure is around 32%.

The second phase of treatment, consolidation aims to remove the residual disease and allow the restoration of normal haematopoiesis. The drugs used for consolidation are often the same as those used for induction phases, with the addition of others to increase efficacy such as mercaptopurine, thioguanine, cyclophosphamide and etoposide (Cooper and Brown 2015). In high risk patients such as those with a slow early response to induction this phase includes an intensification of treatment which can significantly improve outcome (Seibel et al. 2008; C.-H. Pui and Robison 2008). During both induction and consolidation phases of treatment CNS directed treatment is also given. Intra-thecal administration of chemotherapy agents is used rather than CNS irradiation due to the toxic side effects of the latter (Pui and Robison 2008).

The final stage of treatment, maintenance is far less intensive than the previous two stages and has been shown to reduce the risk of relapses. This phase lasts 2-3 years, (boys receive longer treatment) and involves treatment with mercaptopurine and methotrexate on a daily basis (Pui and Robison 2008).

Treatment stage	Duration	Drugs commonly used ⁶
Induction	3-8 weeks	Dexamethasone Vincristine Asparaginase Anthracycline
Consolidation/Intensification	20-30 weeks	Methotrexate Mercaptopurine Vincristine Asparaginase Dexamethasone
Maintenance	2-3 years	Mercaptopurine Methotrexate

Table 2: Table 2 details a brief summary of the 3 main stages in the treatment of paediatric B ALL. Induction is the shortest treatment period followed by consolidation or intensification and lastly the longest phase, maintenance which is used to prevent leukaemic relapse. The drugs used in each phase of treatment are often shared but the doses and change between them. Induction is the most aggressive phase of treatment and is designed to induce a remission. The drugs listed are a selection of the commonly used ones but are not exhaustive, subgroup specific treatments are not included (Pui and Evans 2006; Pui and Robison 2008).

1.9 Relapse

Despite high survival rates with modern regimens, treatment failure and relapse still remains a problem in ALL. Between 15-20% of patients will relapse at some point during or after treatment. Around 70% of these patients will go into a second remission but failure to re-induce remission or a second relapse reduces prognosis significantly and 5 year EFS after a second relapse is just 27% (Bhojwani and Pui 2013).

The strongest prognostic factor for relapse is minimal residual disease (MRD), where the amount of blasts still present in the BM is measured. The presence of MRD after induction treatment is inversely correlated with prognosis; patients with MRD 0.01-0.1% have a better prognosis than those with MRD >0.1% MRD (5 year EFS - 74% vs 60% respectively) but both

are worse than the prognosis for those patients who are MRD negative after induction (~ 90% 5yr EFS). Intensive treatment of MRD positive patients does not prevent relapses, but there is a delay of approximately 1 year for those patients (Borowitz et al. 2015; van Dongen et al. 2015).

An analysis of 10 ALL trials from 1988-2002 retrospectively looked in a large cohort (n=1,961) of relapsed patients to determine factors that influenced survival after relapse. There was a clear correlation between the location of relapse and the duration of the first remission with survival. Relapse in the BM was a poor prognostic factor, with isolated BM relapses faring the worst (24% 5yr EFS) compared to combined BM and extramedullary (39%) or isolated extramedullary (59%). Shorter durations of remission were also associated with poor prognosis, and a combination of the two factors resulted in just 11.5% 5yr EFS for patients with early, isolated BM relapse. The duration of remission being a prognostic factor is not a surprising statistic, as relapse whilst the patient is still on treatment would indicate a highly resistant disease. The study failed to find any significant increase in the prognosis for relapsed ALL in these trials compared to trials carried out from 1983-1989 (Nguyen et al. 2008b).

There are multiple theories for the origins of relapse in ALL, with clonal evolution being the most prevalent. Using genomic analysis, it has been shown that between 78-94% of relapsed ALL cases arise from either a pre-diagnosis (52%) or a diagnosis clone (32%). The emergence of the same diagnosis clone, without clonal evolution or the emergence of a distinct leukaemia being much rarer events (8% and 6% respectively) (Mullighan et al. 2008). The difference between ALL presentation and relapse has been studied in depth. Interestingly it has been found that there is no significant difference in clonal diversity or mutation burden between presentation and relapse, but there is enrichment of certain mutations in relapsed ALL (Ma et al. 2015). The lack of difference in clonal diversity may be attributed to the loss of presentation specific subclones and the gain, or expansion of relapse specific subclones as a result of treatment. It has been found that when investigated using lesion specific PCR relapse specific subclones can be detected in 70% of presentation cases, indicating that treatment might cause enough of an evolutionary bottle neck for minor subclones to become dominant at relapse (Mullighan et al. 2008). The development of relapse in which the major subclone has the same CNA as the presentation is a rare event but does still occur. In relapses that happen early it was found in that the predominant clone at relapse was the

same as the diagnosis clone, but for many of these cases there were also some additional CNA indicating clonal evolution between the two timepoints (Yamashita et al. 2015). The cases for which relapse from the presentation subclone does occur without clonal evolution may indicate induction therapy that has failed to fully eliminate the predominant clone at presentation, which then proliferates to become the major subclone at relapse. Or the possibility of the presentation subclone being drug resistant before treatment has started.

1.10 Leukaemic stem cells and clonal evolution

When thinking about relapse in ALL, the leukaemic stem cells which are responsible for disease propagation should be considered. Their subsequent clonal evolution results in a heterogeneous pool of cells that might have different genetic alterations or treatment responses. Whether the leukaemia stem cells were a small subset, a large population, or whether they even existed was contested for many years. Leukaemic stem cells were first demonstrated experimentally in acute myeloid leukaemia (AML) in 1994 using the transplantation of leukaemic cells into immune compromised mice. These leukaemia initiating cells were able to home to the BM and repopulate the leukaemia in a similar manner to the original disease. This seminal work demonstrated the cells responsible for leukaemia in the murine model were the same as those responsible for disease in the patient(Lapidot et al. 1994). The finding that one cell in every 250,000 malignant blast cells had leukaemia initiating capabilities does not hold true for ALL. Although it was originally thought that just a small proportion of ALL cells had leukaemia initiating properties (Cox et al. 2004) it has now become apparent that there is a much wider range of cells with the potential to initiate leukaemia in ALL. In fact, a diverse range of leukaemic blasts have the ability to engraft and recapitulate the original ALL in the NOD/SCID/IL2R γ null (NSG) mouse model. CD19 $^+$ cells with any of CD10 $^{\text{high/low}}$, CD20 $^{\text{high/low}}$ or CD34 $^{\text{high/low}}$ result in engraftment in up to tertiary mice, interestingly, the injection of both sorted and unsorted cells will still recapitulate the entire phenotype of the original leukaemia (le Viseur, Hotfilder, Bomken, Wilson, Rottgers, Schrauder, Rosemann, Irving, Stam, Shultz, Harbott, Jurg, et al. 2008; Rehe et al. 2013). The frequency of leukaemia stem cells in B ALL has been shown to be as much as 1 in 40 for primary engraftment into NSG mice, increasing to 1 in 6 for secondary and tertiary engraftment (Rehe et al. 2013).

The high proportion of cells with leukaemia repopulating ability is especially relevant for the emergence of relapse. As almost all blasts in ALL are able to reconstitute the leukaemia, the genetics of the stem cell pool can be diverse. This genetic variation within the population provides the ‘units’ for development of the disease through clonal evolution. Clonal evolution, which has been demonstrated as the prevalent origin for relapse is a Darwinian process in which inter-clonal heterogeneity is the substrate that drives change. The clonal architecture in ALL can be linear or branching and is a dynamic process with deletions and copy number alterations (CNA) acquired independently in separate subclones in no particular order (Anderson et al. 2011; Notta et al. 2011; Waanders et al. 2012). Convergent evolution has also been found in ALL samples, with subclones from the same patient having different mutations of the same gene (Waanders et al. 2012). Samples with fewer CNA tend to have linear evolution compared to samples with increased CNA having a more complex clonal architecture. A more complex branching evolution is also associated with relapse in ALL. However, in both linear and branching clonal architecture the terminal clone does not always represent the major subclone, in fact there are branches that are evolutionary dead ends due to deleterious genetic alterations (Anderson et al. 2011; Landau et al. 2014). Experimental evidence for the variegated genetics of leukaemia initiating cells comes from murine engraftment experiments, as serial transplantation with a single ALL sample and multiple xenografts of a single primary ALL results in different clones engrafting, an indication of the many subclones in ALL that are capable of initiating leukaemia (Anderson et al. 2011; Notta et al. 2011).

If variegated genetics provides the units for evolution of ALL, chemotherapy represents the evolutionary driver for relapse. Treatment represents an evolutionary bottleneck in clonal evolution with the death of the majority of subclones. Survival of the fittest means that only those clones with a genetic alteration which grants them increased fitness allowing them to evade chemotherapy will survive to expand and cause a relapse (Figure 6). These relapse initiating subclones may be part of the initial diagnosis or even a pre-leukaemic clone (Mullighan et al. 2008). Wherever the relapse originates from, high inter-clonal heterogeneity increases the chance for one of the subclones to harbour a mutation that increases the risk that relapse will occur.

1.11 Recurrent genetic alterations at relapse

Analysis of paired diagnosis and relapse samples represents an excellent way to determine which mutations are driving relapse. These pairs have been used to determine a specific signature of genes which are significantly up or down regulated at relapse. This signature includes genes involved in cell cycle, apoptosis, DNA repair, metabolism, B cell development and drug resistance genes (Beesley et al. 2005; Bhojwani et al. 2006; Staal et al. 2010; Kuster et al. 2011). Interestingly, this signature is different when comparing early or late relapse (Hogan et al. 2011).

Changes to the epigenetic landscape have also been implicated in the emergence of relapse. The methylation of cytosine-phosphate-guanine (CpG) sites in the genome is increased in relapsed ALL compared to presentation, indicating dysregulation at an epigenetic level has a role in the emergence of relapse (Hogan et al. 2011). In fact, treatment of ALL cell lines and patient samples either with a DNA Methyltransferase inhibitor or a histone deacetylase inhibitor can alter the relapse specific gene signature, reversing it to a diagnosis like signature, as well as acting synergistically with chemotherapy or restoring drug sensitivity (Bhatla et al. 2012). These drugs might represent a useful addition to treatment protocols for relapsed ALL as there is increased drug resistance at relapse, which is increased further with subsequent relapses (Styczynski et al. 2015).

As well as epigenetic alterations throughout the genome there are also recurrent somatic mutations associated with relapse. Relapse specific deletions in the DNA mismatch repair gene MSH6 (Muts homolog 6) have been found recurrently in ALL. MSH6 is not only a DNA repair gene but has also been implicated in drug resistance to mecaptoperines and steroids (Hogan et al. 2011). Other recurrent deletions that affect drug resistance have been found in BTG1, a co-activator of *NR3C1* (Nuclear receptor subfamily 3 group C member 1), and *TBL1XR1* (Transducin (Beta)-like 1 X linked receptor 1), which is also involved in glucocorticoid (GC) signalling at rates of 10-14%. BTG1 and TBL1X1R mutations do not occur together. Which indicates that loss of just one is enough to result in GC resistance (Bhatla et al. 2014).

Not only can chemotherapy select for clones that will cause a relapse, such as subclones with a mutations resulting in drug resistance, but due to the nature of the drugs used for

treatment, some of the commonly used drugs can induce mutations that could drive relapse or even second cancers (Godley and Larson 2008).

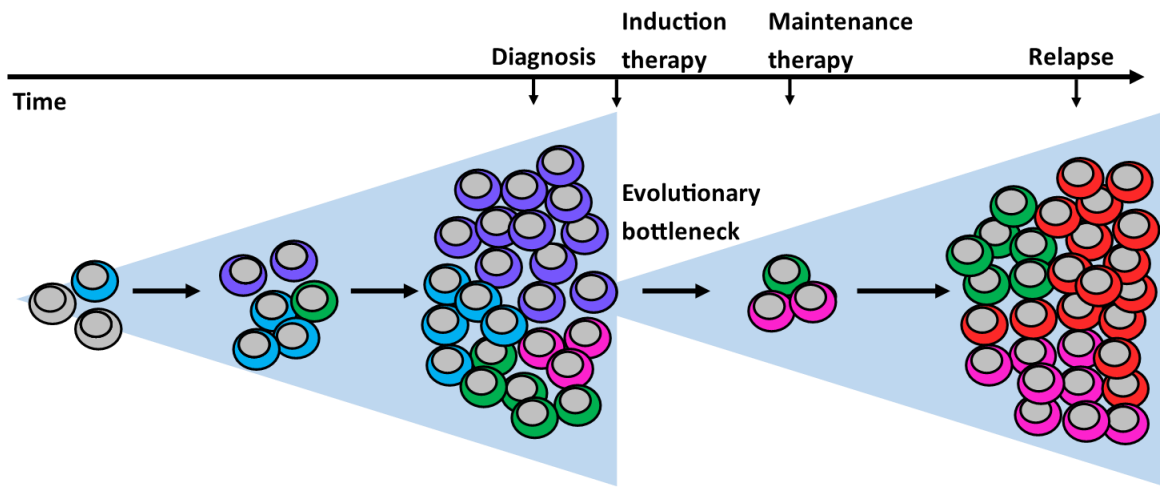


Figure 6: The scheme shows the intra-disease heterogeneity of ALL. The disease at diagnosis is already heterogenous having developed clonally from the leukaemia initiating cell over an unknown period of time. The use of treatment acts as an evolutionary bottleneck where only cells able to evade chemotherapy survive. These cells then act as the initiating cells for clonal evolution and the relapse is often the re-emergence of these cells or subclones derived from these with the acquisition of further mutations (Landau et al. 2014; Mullighan et al. 2008).

1.12 Glucocorticoids in ALL

The pro-apoptotic action of synthetic GC on lymphoid tissues has been exploited for the treatment of leukaemia since the late 1950s (Pearson and Eleil 1950). In 1959 prednisone, a synthetic GC, was used to induce remission before treatment with 6-mercaptopurine. This was the first trial to use synthetic GC in combination with other drugs for the treatment of ALL and 67% of patients had induction of remission by prednisone, and although the median length of remission was only 29 weeks this represented a major step in the treatment of ALL (Freireich et al. 1963). Over the following years treatment protocols were improved and prednisone became part of the backbone of ALL treatment. Dex, another synthetic GC was first compared to prednisone in the 1970s, it was found that with Dex treatment there was a lower incidence of CNS disease (14.3% vs 25.6%) (B. Jones et al. 1991). As well as better CNS treatment, Dex has a longer half-life than prednisone and a higher cytotoxicity in patient cells than prednisolone (the active metabolite of prednisone) (IC_{50} 0.2 μ M vs 3.5 μ M). Dex

has become the main GC used for ALL treatment. This increase in efficacy is linked to an increase in the side effects such as osteonecrosis, mood effects and infections compared to prednisone (Inaba and Pui 2010). Not only are synthetic GC indispensable in the treatment of ALL, sensitivity to GC is a major prognostic factor, with patients classed as GC poor responders having a 5 year EFS of just 55% compared to >80% for the good responders (Moricke et al. 2008).

The anti-apoptotic effects that make synthetic glucocorticoids so useful in ALL are mediated through NR3C1, the GC receptor, by a complex process. Both transcriptional modulation and cytoplasmic protein: protein interactions are required for the initiation of the apoptosis cascade. De novo RNA and protein production appears to be a requirement for GC induced apoptosis, cells treated with actinomycin D (transcriptional inhibitor) do not have a GC induced increase in cytosolic Ca^{2+} and the downstream apoptosis pathway (McConkey et al. 1989). Blockage of several steps can result in inhibition of apoptosis, for example caspase activation, aSMase (Acid sphingomyelinase) activity and phospholipase C indicating that the process from GC treatment to apoptosis is a multi-stepped process (Cifone et al. 1999; Marchetti et al. 2003). The NR3C1 target gene BIM (BCL2L1, BCL2 like 11), which is up-regulated by GC treatment is essential for GC induced apoptosis. siRNA (small interfering RNA) knockdown of this gene results in GC resistance in lymphoid cells, likely because loss of the BIM expression results in lack of antagonism of the anti-apoptotic proteins BCL2 (B cell CLL/lymphoma 2), BCL2L1 (BCL2 like 1) and MCL1 (Myeloid cell leukaemia 1) (Abrams et al. 2004; Schmidt, Rainer, et al. 2006; Bachmann et al. 2005; Jing et al. 2015).

Interestingly, glucocorticoids have an anti-apoptotic effect in some cells such as granulosa cells and liver fibroblasts (Costas et al. 2000; Evans-Storms and Cidlowski 2000; Sasson, Tajima, and Amsterdam 2001). This is likely due to differences in the genes activated and activity of the different α isoforms of NR3C1.

1.13 Glucocorticoid resistance

Although synthetic GC are efficient at the induction of apoptosis in lymphocytes, a number of patients become GC resistant after prolonged treatment. The mechanisms of this resistance are not well understood but the number of patients developing resistance is disparate to resistance to other drugs, with >24-fold increased resistance to GC at relapse compared to presentation. With only 0.8-1.9 fold increases at relapse for other commonly used drugs (Klumper et al. 1995; Bachmann et al. 2005).

In cell lines GC resistance may be mediated by deletions or somatic mutations that alter ligand binding to NR3C1, NR3C1 translocation to the nucleus or NR3C1 dimer binding to the glucocorticoid response element (GRE) sequences. This resistance is dose dependent to the levels of NR3C1 expression and can be restored by the re-expression of wild type NR3C1 (Helmberg et al. 1995; Schmidt, Irving, et al. 2006; Bachmann et al. 2007; Gruber et al. 2009).

This is not the case for primary ALL samples, which even at relapse only have approximately 5% frequency of NR3C1 deletions or mutations (Mullighan et al. 2007). In a small study of patient derived xenografts none were found to have deficient nuclear translocation of activated NR3C1, and the receptor was transcriptionally active. In selected patient-derived xenografts resistance could also be reversed pharmacologically (Bachmann et al. 2007), these different mechanisms for resistance in primary derived samples and cell lines highlights the need for the use of appropriate models when investigating drug resistance in ALL.

Although deletions are relatively rare in ALL, in blastic plasmacytoid dendritic cell neoplasm (BPDCN), an aggressive leukaemia it is much more common, with 28% of cases having monoallelic deletion on NR3C1 (Emadali et al. 2016). The high percentage of monoallelic rather than homozygous deletions in BPDCN along with the rarity of NR3C1 deletions in ALL points to the requirement of NR3C1 for cell viability. This is supported by the fact that NR3C1 knockout mice die at birth as a result of respiratory failure, showing poor lung development as well as lack of adrenaline synthesis, and reduced erythropoiesis and gluconeogenesis (Manwani et al. 2010).

Changes in the transcriptional activity of NR3C1 are the likely cause for GC resistance. The inability of NR3C1 to induce transcription of BIM has been found as a mechanism for GC resistance at relapse, due to both increased methylation of BIM and also reduced histone modifications, this can be reversed by treatment with the HDAC (histone deacetylase) inhibitor vorinostat (Bachmann et al. 2010). Deletion of IKZF1, which is correlated with an increased risk of relapse, also alters the transcriptional response of cells to GC. IKZF1 increases NR3C1 transcription and knockdown in GC sensitive cell lines results in gain of resistance (Klumper et al. 1995; Marke et al. 2015).

GC resistance at diagnosis is also an issue. The 10% of paediatric patients that are classed as GC poor responders have reduced survival (Moricke et al. 2008). Analysis of the genetics of GC poor responders has identified several genes that confer risk, including the expression of ABCC3 (ATP binding cassette subfamily C member 3) and GSTT1 (Glutathione S-transferase Theta 1)(Anderer et al. 2000; Steinbach et al. 2003). The local chromatin environment of NR3C1 target genes is also implicated in GC resistance, GC poor responders were found to have significantly reduced H3K9 acetylation of BIM, a gene essential for GC induced apoptosis (Bachmann et al. 2010). Interestingly polymorphisms in NR3C1 have not been associated with an increase in GC resistance in leukaemia or other diseases, but levels of NR3C1 expression are associated with changes in GC sensitivity (Koper et al. 1997; Niu et al. 2014; Kaspers et al. 1994).

1.14 NR3C1

The nuclear receptor subfamily 3, group C, member 1 protein (NR3C1) is the GC receptor which is located on the q arm of chromosome 5 at q31.3. The endogenous GC cortisol binds to this receptor and has numerous biological functions.

There are 9 known alternative first exons, each of which is controlled by a separate promoter (Turner and Muller 2005), resulting in a variable 5' untranslated region (UTR). These different 5' UTRs have been shown to have several implications for NR3C1, including changes to the secondary structure of RNA, the half-life of transcripts and the levels of NR3C1 protein expressed (Turner et al. 2014).

There are two main isoforms of the glucocorticoid receptor (GR), alpha(α) and beta (β), the exon and protein structure of these two isoforms is shown in Figure 7. The β isoform was originally thought just to be a dominant negative regulator of the α form, but more recently it has been found to have transcriptional activity of its own (Lewis-Tuffin et al. 2007; Kelly et al. 2008). The α form is transcriptionally active and has many isoforms as a result of the alternate first exons. The α isoforms are all able to translocate to the nucleus upon ligand activation but have different transcriptional activity and regulate a different set of genes. Less than 10% of glucocorticoid modulated genes are regulated by all of the α isoforms of NR3C1 (Lu and Cidlowski 2005).

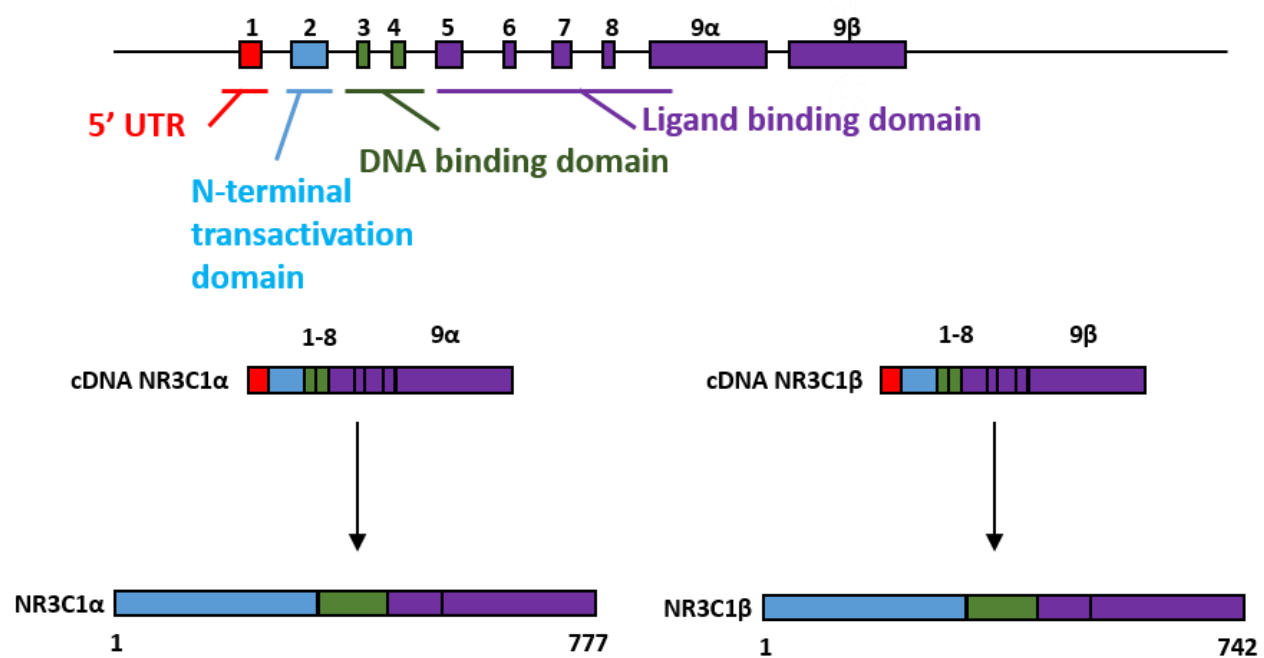


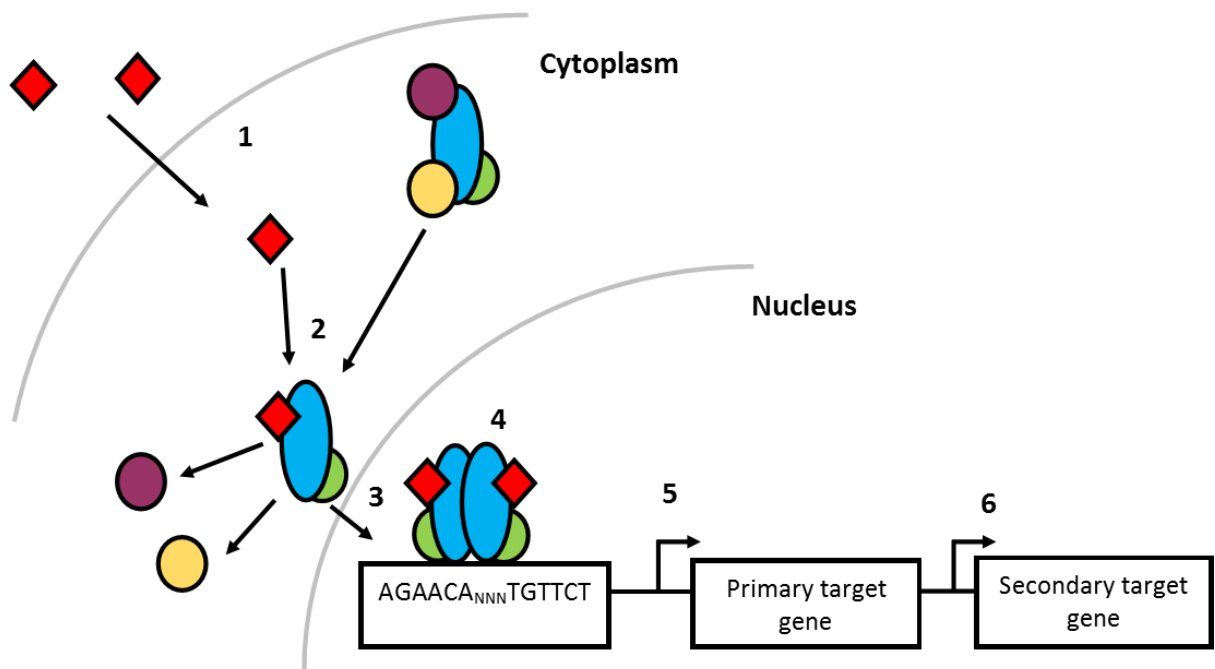
Figure 7: The structure of NR3C1 from DNA to protein. Top – the exon structure of NR3C1, including both exon 9 α and β . Middle – the cDNA sequences of the two main isoforms of NR3C1, α and β . Bottom – the protein sequence of the same two isoforms showing nucleotide length of the final protein. The colours used correspond to the regions of the gene and protein, red indicates the 5' untranslated region (UTR) in which there are many possible splice variants. Blue indicates the N terminal transactivation domain, Green shows the DNA binding domain and the purple regions denote the exons that make up the ligand binding domain where glucocorticoids bind.

The alternative exons are expressed differently in different tissues and only the hippocampus expresses all of the known isoforms. CD19 positive B cells express all isoforms except 1D, and only very low levels of 1E, whereas the liver only expresses exons 1G and 1B (Turner and Muller 2005). These differences in tissue expression and the modulation of different genes by different isoforms could be the basis for the differential effect of GC in different tissues, notably the induction of apoptosis in lymphoid cells.

As well as a variable N terminal domain, the protein also consists of two other main regions. The DNA binding domain (DBD), which contains a zinc finger, is required not only for the receptor to bind specific DNA sequences but also for homodimerisation and interaction with co-factors. The ligand binding domain (LBD) is where glucocorticoids bind with the receptor as well as chaperone and co-regulatory proteins (Zhou and Cidlowski 2005). NR3C1 protein is found in the cytoplasm as part of a large complex with several chaperone proteins including HSP90, HSP70 (heat shock protein 70/90), p23 (PTGES3, Prostaglandin E synthase 3), and several immunophilins including FKBP proteins (Pratt and Toft 1997; Morishima et al. 2003). Upon the passive diffusion of glucocorticoids into the cytoplasm they bind with NR3C1 and the complex disassembles and NR3C1 translocates to the nucleus. Not all of the chaperone proteins are disassociated from NR3C1 upon ligand binding. HSP70 does not disassociate and it is thought that it is involved in the DNA binding or transcriptional activity of NR3C1 (Srinivasan, Patel, and Thompson 1994).

Translocation of ligand bound NR3C1 to the nucleus occurs within minutes, and the most rapidly modulated genes have an increase in mRNA after just 15 minutes (Ringold et al. 1977). Most genes however take a couple of hours for alterations in mRNA levels to be seen. The classical view of NR3C1 gene activation occurs by homodimers of NR3C1 binding to specific sequences in promoters called glucocorticoid response elements (GRE) to induce transcription of target genes. The classical GRE consist of 2 mirrored short sequences joined by 3 nucleotides. Each is an inverted repeat of the other (Scheidereit et al. 1983). The transcriptional response is influenced by the number of GRE in a promoter (Freedman and Luisi 1993). As well as the transcription inducing GRE there are also negative GRE (nGRE) that repress transcription. The repressive action of nGRE has been shown to result from the unique binding of NR3C1 at the sites which inhibits receptor homodimerization, resulting in monomers of NR3C1 bound at negative response elements in the DNA (Ratman et al. 2013). Binding of NR3C1 monomers at these sites results in the recruitment of a repressor complex

that inhibits transcription (Sakai et al. 1988; Surjit et al. 2011). Figure 8 outlines the process of glucocorticoid regulation on transcription via the GRE.



1. GC enter the cell by passive diffusion
2. GC binds to NR3C1, some chaperone proteins disassociate
3. Activated NR3C1 is translocated to the nucleus
4. Homodimers of activated NR3C1 bind GRE
5. Transcriptional modulation of primary gene targets
6. Transcriptional modulation of secondary gene targets

Figure 8: A simplified schematic showing the mechanism of NR3C1 modulated transcription via a classical response element. Briefly, GC (glucocorticoids) enter the cell by passive diffusion, once in the cytoplasm GC bind to NR3C1 and most chaperone proteins disassociate. Once the chaperone proteins have disassociated NR3C1 translocates to the nucleus where it homodimerizes with other GC:NR3C1 complexes. NR3C1 homodimers bind to GRE (glucocorticoid response element) sequences and modulate transcription. The DNA interaction show is via a classical GRE sequence, several other interactions also occur.

Adapted from (Bhadri, Trahair, and Lock 2012; Little and Storb 2002).

It has also become apparent that homodimers of NR3C1 binding to the consensus GRE sequence is not the only mechanism by which it exerts its effects on gene expression. NR3C1 also acts via direct protein interactions and with other transcription factors (Yang-Yen et al.

1990). There are several mechanisms by which NR3C1 can result in transactivation and transrepression of genes, both by direct interactions with the DNA sequence, and by protein interactions with other transcription factors (Figure 9). NR3C1 not only induces changes in gene expression of its direct target genes but also acts with several other transcription factors including AP-1, STAT1-3 and CEBPB (Ratman et al. 2013; Latchoumanin et al. 2007; Wu and Bresnick 2007)

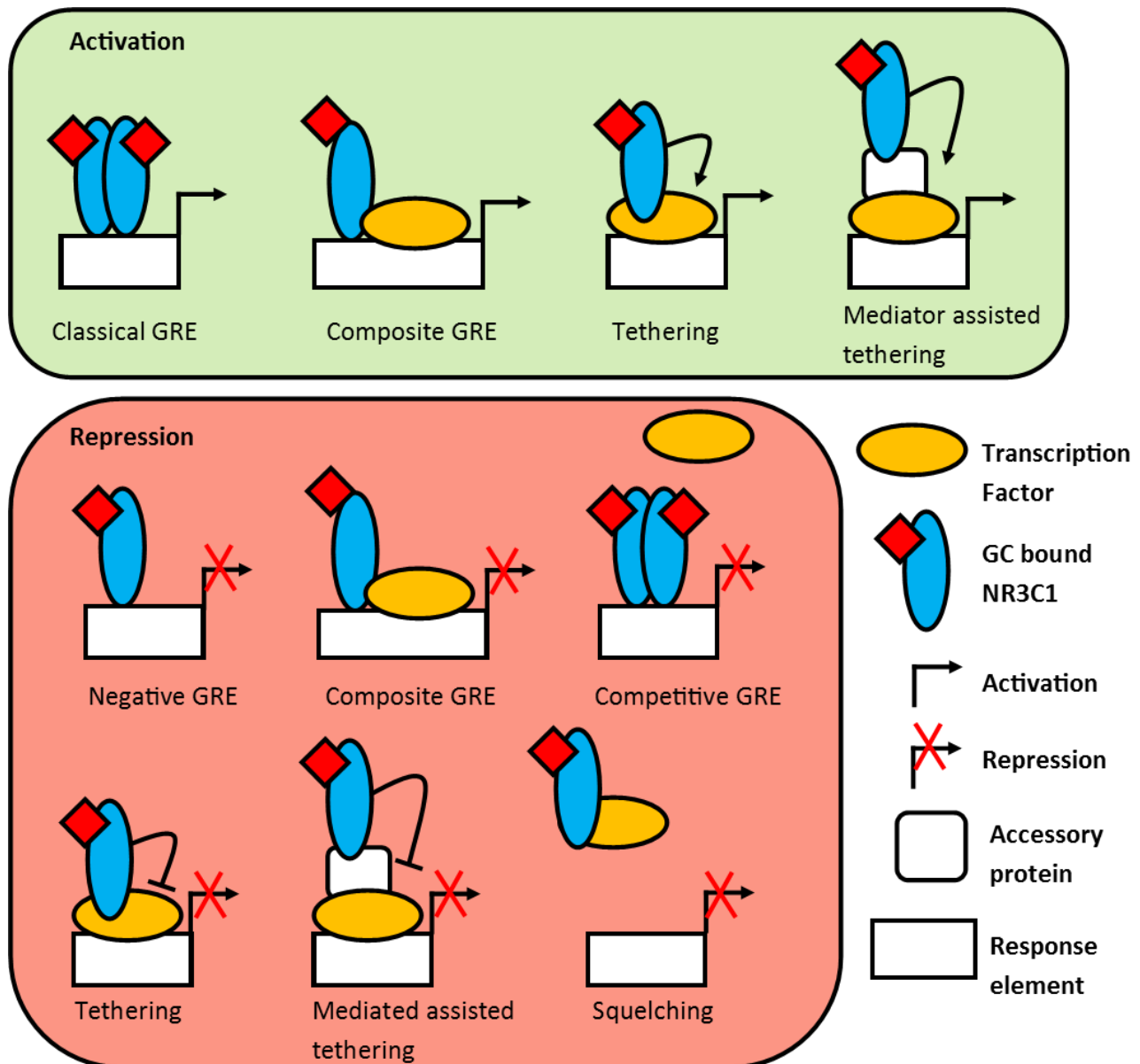


Figure 9: Schematic detailing the several different mechanisms by which NR3C1 can induce alterations in transcription including activation of genes (top) and repression of genes (bottom). The NR3C1:GC complex interacts with both DNA and other transcription factors in at least 10 different ways (shown above) to result in either transactivation or transrepression of NR3C1 target genes. Adapted from (Ratman et al. 2013).

1.15 CRISPR

The use of clustered regularly interspaced short palindromic repeats (CRISPR) technologies is rapidly becoming an important technique in genome editing, it is relatively new, only having come to the forefront in the past few years.

Repeats of DNA that would later go on to be determined as CRISPR loci were first found in 1987 as a coincidental finding whilst sequencing a gene in *Escherichia coli* (Ishino et al. 1987). It was not until 2005 that the idea that these repeated elements might have a role in immunity was postulated when three different groups independently found that the sequences between the spacers were from foreign DNA (Bolotin et al. 2005; Mojica et al. 2005; Pourcel, Salvignol, and Vergnaud 2005). This role was experimentally proven a few years later when after phage exposure, resistant *Streptococcus thermophilus* were found to have integration of phage DNA into novel CRISPR spacers (Barrangou et al. 2007). This immunity is dependent on previously encountered DNA and so can be thought of as similar to the adaptive immunity in humans. There are three types of CRISPR-Cas immune systems in archaea and bacteria, type I, II and III. 90% of archaea and 40% of bacteria have been found to have CRISPR-Cas systems and of those a further 44% have Cas genes associated with more than one of these systems. So far 65 Cas proteins have been identified (Makarova et al. 2011).

Type I systems are characterised by the presence of Cas3 proteins. This system uses the cascade (CRISPR associated complex for anti-viral defence) complex for DNA targeting, and the Cas3 enzyme for DNA degradation (Huo et al. 2014). In type III CRISPR-Cas systems the associated protein is Cas10 and they have a targeting system similar to the cascade complex of type I. Type III systems have also been implicated in RNA cleavage, and may have a similar function to RNA interference (RNAi) systems in eukaryotes. Type II CRISPR systems have so far only been found in bacteria whereas type I and type III systems have also been found in archaea (Rath et al. 2015).

It is the type II CRISPR-Cas systems that have been exploited for genome engineering because of the system's reliance on just one Cas protein for cleavage rather than several as in type I and III. The Cas9 endonuclease cleaves DNA, targeted by short RNA sequences to guide Cas9 to the complementary DNA sequence. The Cas9 proteins are large proteins that

vary across bacteria with type II systems, which is around 10% of all bacteria (Makarova et al. 2011). There are three subtypes of Cas9 proteins, A B and C, which are composed of between 1100 and 1400 amino acids that form a 2 lobed secondary structure. There are two active sites, the HNH site that cleaves the complementary DNA strand, and the RuvC domain that cleaves the non-complementary DNA strand, resulting in double strand breaks (DSB) in the DNA. These active sites are in highly positively charged DNA binding grooves to facilitate binding of the negatively charged DNA. When Cas9 is not in a complex with crRNA to guide I, the protein adopts an auto-inhibitory conformation which abrogates nuclease activity (Garrett, Vestergaard, and Shah 2011; Gaj, Gersbach, and Barbas 2013; Jinek et al. 2014). All Cas proteins need a protospacer adjacent motif (PAM) sequence at the end of the targeting RNA and this differs between the different types of Cas proteins. This results in a vast array of targeting options, especially in bacteria that have been found to have more than one CRISPR-Cas system.

There are three main steps in CRISPR-Cas immunity. Firstly the integration of new sequences into the CRISPR locus, then the processing of this locus to give crRNA sequences and finally targeting by the crRNA to foreign DNA and cleavage by Cas endonucleases. Briefly, foreign DNA enters the cell and is targeted by Cas1 and Cas2. These proteins mediate the production of novel spacers of around 30bp that are integrated into the CRISPR locus in the genome. They are highly conserved across all bacteria and are found in conjunction with all of the different Cas systems, mutations that result in disrupted Cas1-Cas2 complexes cause loss of spacer acquisition activity (Nuñez et al. 2014). The CRISPR locus is then transcribed with the new spacers into the pre-crRNA transcript, which is further modified resulting in short crRNA transcripts. These assemble with Cas proteins and upon the entry of the same foreign DNA into the bacteria the Cas-crRNA complex is targeted to the DNA by the crRNA and the DNA is cleaved (Figure 10).

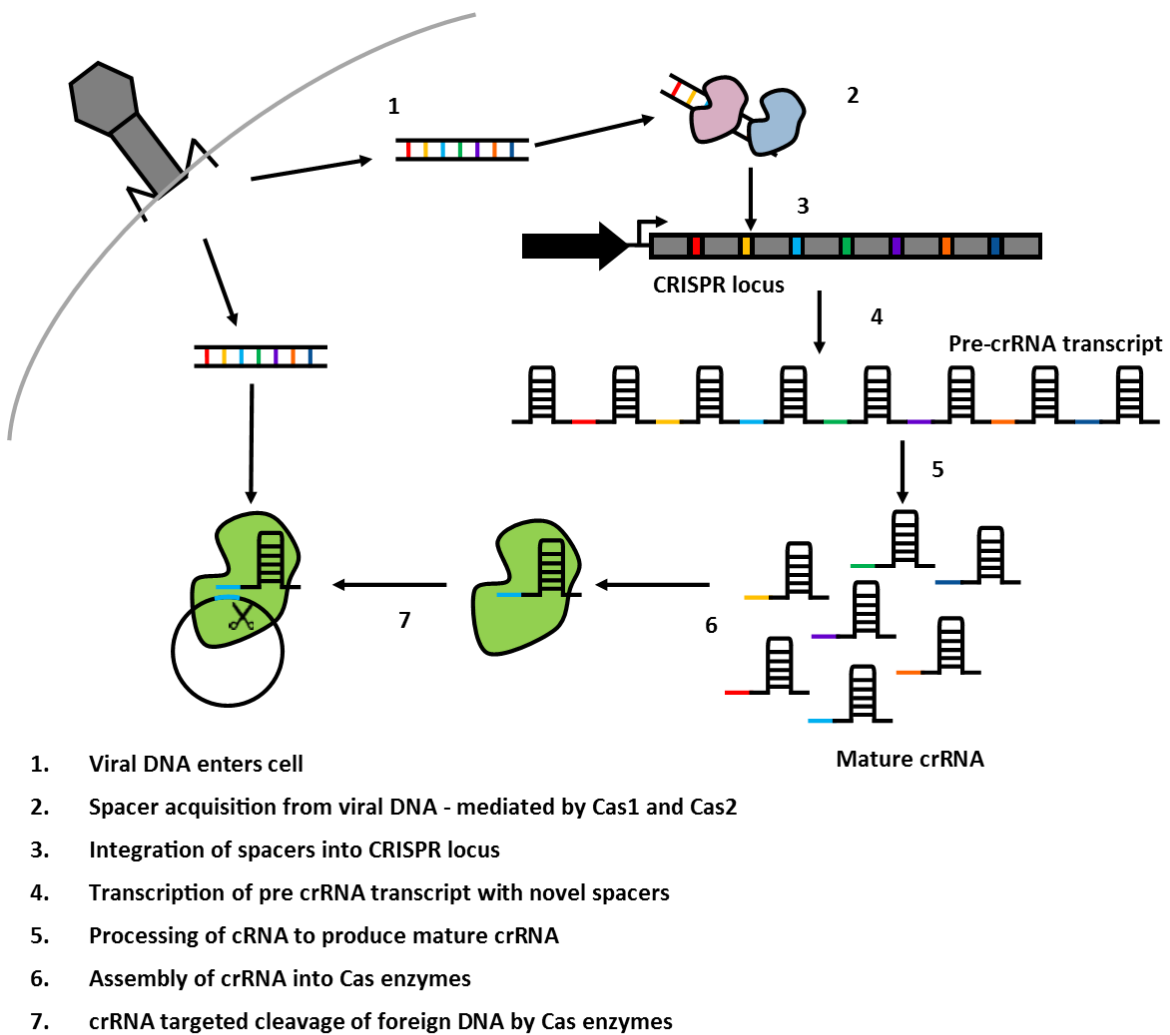


Figure 10: Mechanism of CRISPR-Cas mediated bacterial acquired immunity. Viral DNA enters the cell and is targeted by a complex of Cas1 and Cas2 endonucleases. This results in the fragmentation of viral DNA and insertion into the CRISPR locus, with short repeat sequences known as spacers between viral DNA sequences. This locus is then transcribed by the endogenous bacterial transcriptional machinery and cleaved resulting in mature crRNA that forms complexes with the Cas enzymes. These crRNA:Cas complexes are then guide the targeting of foreign DNA complementary to the spacer in the complex (Makarova et al. 2011; Bondy-Denomy and Davidson 2014; Nuñez et al. 2014; Gaj, Gersbach, and Barbas 2013).

The lentiCRISPRv2 CRISPR-Cas system which has been developed for genome engineering uses the Cas9 from *Streptococcus pyogenes*, a type II A Cas9, with around 1400 amino acids. The mechanism by which CRISPR-Cas technology has been harnessed for genome engineering by the lentiCRISPRv2 plasmid (Figure 11) is outlined in Figure 12 (Jinek et al.

2012; Shalem et al. 2014). Briefly, cells are transduced with plasmids carrying the short guide RNA (sgRNA), which is the targeting molecule like the crRNA in the bacterial system. The plasmid is integrated into the host genome and the Cas9 and sgRNA are transcribed under the control of two separate promoters, the U6 and EFS promoters. The sgRNA and Cas9 assemble into a complex and are targeted to the complementary sequence in repaired using the cellular machinery for non-homologous end joining (NHEJ) or homologous recombination (HR), the two main DNA repair pathways in cells.

HR is the less error prone of the two systems, and uses a homologous DNA sequence to guide repair. Often this will be the sister chromatid, but this system is being utilised with short donor guide sequences in CRISPR-Cas systems for site directed mutagenesis (Collonnier et al. 2016). HR is active mainly during the S and G2 phases of cell cycle (Grzegorz et al. 2004). Conversely, NHEJ is active throughout the cell cycle and is more active than HR, meaning it is the main pathway by which DSB are repaired. NHEJ re-ligates DSB without a guide sequence and has a high frequency of errors. These errors are small, often between 1 and 10bp but these indels are enough to result in frame shifts or stop codons that would result in loss of protein function. The acquisition of indels after NHEJ does not occur at a very high rate, only around 5%, but if the target sequence is repaired faithfully the Cas9-sgRNA complex can target the sequence again, resulting in an increase in target sites with indels over a period of time (Chiruvella, Liang, and Wilson 2013; Jasin and Rothstein 2013; David Wyatt 2015). By the introduction of indels CRISPR-Cas9 systems offer gene knockout rather than gene knockdown as with the previous generation of genome engineering tools that utilised RNAi and shRNA to reduce gene expression. This will be especially useful for the investigation of genes in which only a complete loss of protein results in a phenotype.

The Cas9 from *Streptococcus pyogenes* has the PAM sequence of 3'-NGG, and assuming the frequency of CG of 5.2% in the genome there would be 1.6×10^8 predicted NGG sites in the genome. This results in the possibility of targeting almost every gene in the genome.

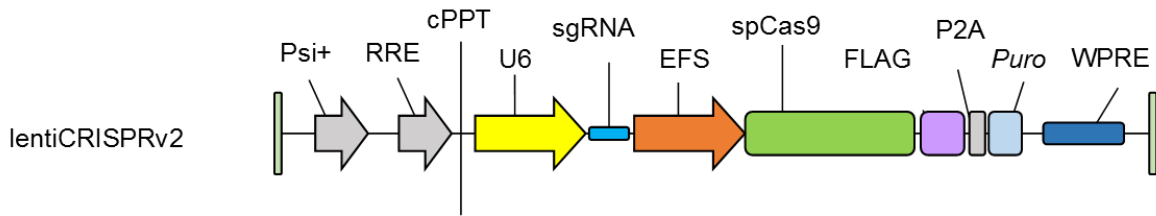
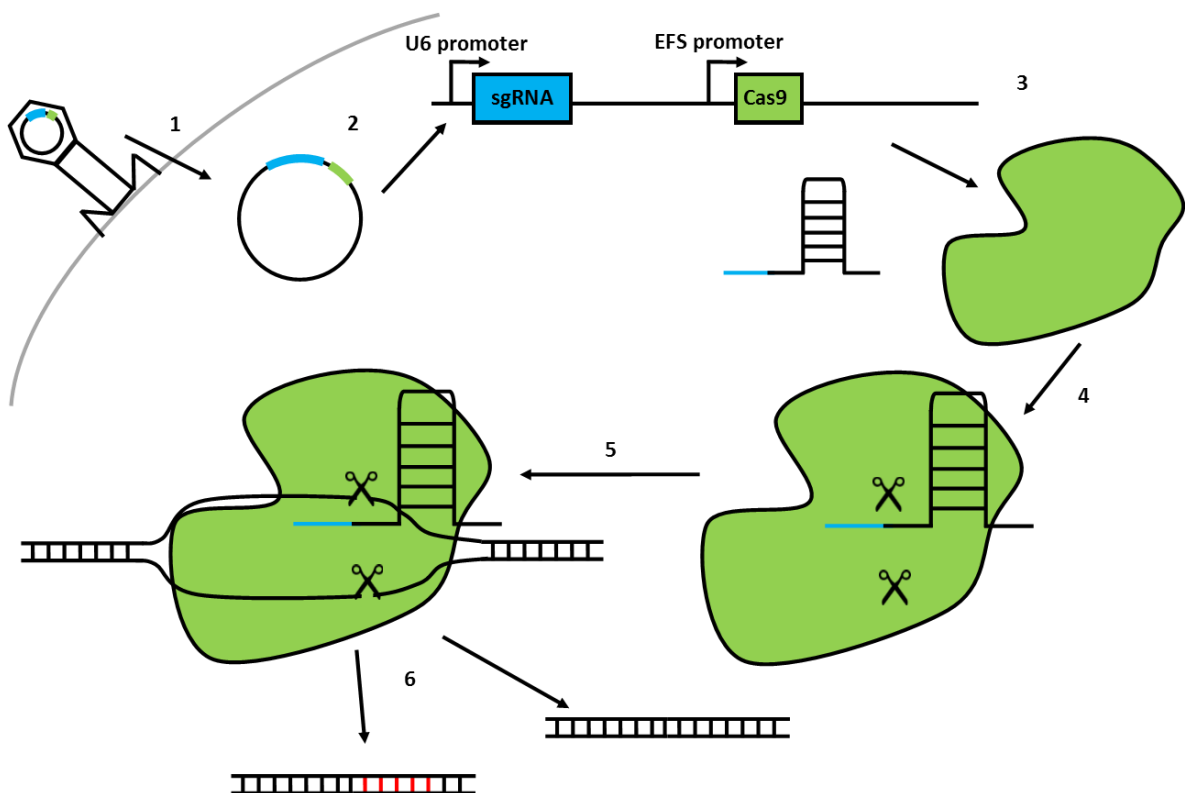


Figure 11: Structure of the lentiCRISPRv2 plasmid showing the genes required for lentiviral production such as Psi+ (Psi packaging element), RRE (Rev response element), cPPT (central polypurine tract) and WPRE (Woodchuck hepatitis virus posttranscriptional regulatory element) and then elements specific to the lentiCRISPRv2 plasmid such as the U6 (U6 promoter), sgRNA (short guide RNA), spCas9 (Streptococcus pyogenes Cas9), FLAG (FLAG tag) and Puro (puromycin resistance gene) (Sanjana, Shalem, and Zhang 2014; Shalem et al. 2014).



1. Cells are transfected with CRISPR lentivirus
2. Lentiviral DNA is integrated into genome
3. sgRNA and Cas9 transcription
4. Assembly of sgRNA-Cas9 complex
5. Cas9 is targeted to DNA by complementary sgRNA—active sites cleave DNA
6. Repair of DNA double strand

Figure 12: Mechanism of CRISPR-Cas9 mediated double strand breaks (DSB) using the lentiCRISPRv2 plasmid. Lentivirus produced using the lentiCRISPRv2 plasmid and packaging and envelope plasmids are used to transfect target cells. The lentiCRISPRv2 plasmid DNA is incorporated into the host genome. sgRNA and Cas9 transcribed under control of the U6 and EFS promoters which are constitutively active. Once transcribed and translated the Cas9 and sgRNA form a complex which is then guided to the complementary DNA sequences in the host genome. The Cas9:sgRNA complex binds to the DNA and the DNA is cleaved at the two active sites in Cas9 resulting in DSB. DSB are repaired by non homologous end joining(NHEJ) or less frequently homologous recombination (HR) resulting in the acquisition of indels, or the re-formation of the intact targeting sequence (Jinek et al. 2014; Shalem et al. 2014; Sanjana, Shalem, and Zhang 2014).

1.16 Genetic Screening

Genome editing using CRISPR or any of the other available techniques such as RNAi, Zinc fingers, TALENs (Transcription activator like effector nuclease) or transposon directed mutagenesis all represent a way to interrogate the function of genes in both normal and pathological conditions. CRISPR and RNAi are the most widely used, and each has advantages and disadvantages (Table 3), but for all loss of function techniques screening works in broadly the same way. There are two main types of screen, positive or negative and each looks for a different endpoint (Figure 13). Positive screens are designed to look for constructs which are enriched in the sample compared to the baseline (or control), which will be targeting genes harmful to cancer propagation. For example, positive screens have identified GAS1, (Growth arrest specific 1) a metastasis suppressor CDKN2A (Cyclin-dependent kinase inhibitor 2A) which is a cell cycle control gene, and genes involved in drug resistance such as MEK2/4 (Mitogen activated protein kinase 2/4) (Gobeil et al. 2008; C. L. Jones et al. 2015; Wallace et al. 2016). Negative screens on the other hand look for which constructs are lost from the baseline as these constructs cannot be tolerated in the cell, so the genes they are targeting may be important for leukaemic growth, such as STAT5 (Signal transducer and activator of transcription 5), or anti-apoptotic genes such as BCL2 (Wallace et al. 2016).

Screening technique	Advantages	Disadvantages
CRISPR	<ul style="list-style-type: none"> • Easy to target • Less Expensive for library • Can target specific exons • Complete knockout • Less off target effects due to requirement of PAM 	<ul style="list-style-type: none"> • Off target effects of Cas9 • Possible haploinsufficiency • In frame mutations/null mutations • Requires intact DNA repair pathways • Closed chromatin may affect targeting
RNAi	<ul style="list-style-type: none"> • Easy to target • Expensive to buy library • Identify genes with dose/phenotype relationship • Reversible 	<ul style="list-style-type: none"> • Incomplete mRNA knockdown • May affect endogenous RNAi pathway • Nuclear transcripts harder to target • Binding with mismatches causing off target effects • Prone to silencing

Table 3: Comparison of the advantages and disadvantages of CRISPR and RNAi screening methods. Both methods have positive and negative features which makes selection of the right choice important when designing experiments (Housden and Perrimon 2016; Boettcher and McManus 2015; Kuscu et al. 2014)

There are several factors that should be taken into account when designing screens in order to have high statistical power, and to be sure that hits are not false positives. Reproducibility between screens can be used to determine the relative statistical power of each screen. Statistical power is the chance of calling correctly whether a found difference is actually statistically significant. A power of 80 % is considered necessary for genome wide screens (Cohen 1988; Stombaugh et al. 2015). Increased coverage of targeting constructs in screens results in more overlap between repeats and better reproducibility. As well as coverage, optimisation of the PCR (polymerase chain reaction) steps is also important in ensuring reproducibility and in turn statistical power of screens. PCR needs to maintain the coverage of the DNA pool as well as keeping amplification steps in the exponential phase (Strezoska et al. 2012).

As the PCR steps are essential for maintenance of the pool complexity a large number of reactions can be required. Considering one molecule of DNA can be synthesised into millions of copies in just 30 cycles of amplification, even a tiny contamination can skew results. An aerosol from a PCR product can contain as many as 1×10^6 copies of DNA (Persing 1991) which can contaminate the PCR area. Furthermore as dried DNA is less susceptible to ultraviolet light, as are short sequences, it can be very difficult to clean an area once contaminated (Sarkar and Sommer 1990).

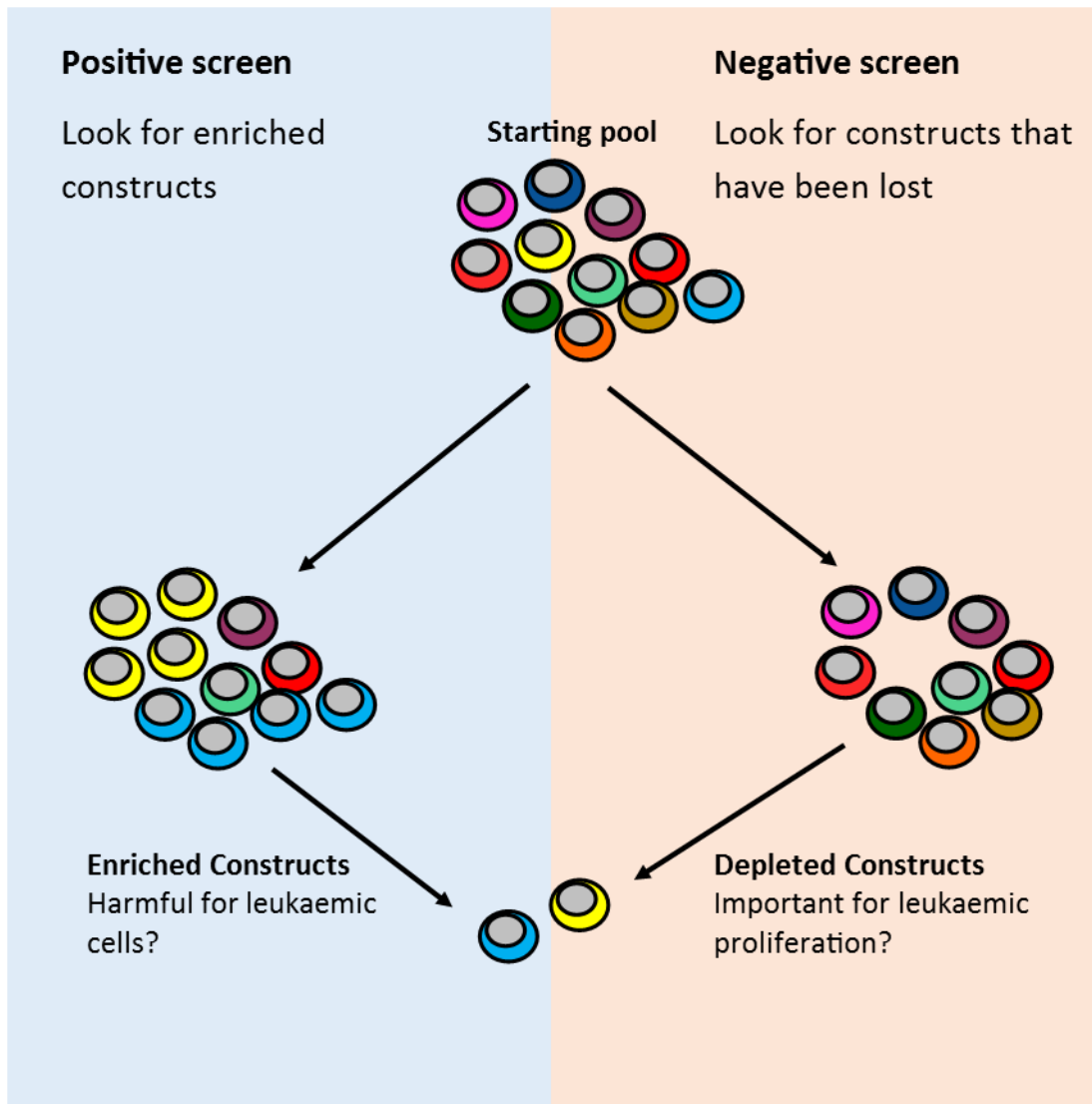


Figure 13: The basic premise of positive and negative genetic screens. Both types of screen start with a pool of cells transduced with many different constructs. The treatment of the cells throughout the screen may also be the same for a positive and negative screen, the main difference is when it comes to analysis. A positive screen is designed to identify constructs which are enriched at the end, and negative screens are designed to determine both the enriched constructs and the depleted constructs. The major reason why a positive screen would be chosen instead of a negative screen is the levels of coverage generally accepted to be required for a negative screen, which is 1000x coverage. If a whole genome screen is being used then the numbers of cells needed rapidly gets unmanageable in vivo. Different coloured cells indicate different targeting constructs in each cell.

1.17 Previous work

Previous work was carried out in the lab by Dr. Elda Latif (Latif 2012) on paired presentation and relapse samples from a case of t(17;19) B cell progenitor ALL; the L707 cells (Table 4).

The samples were chosen as in the relapse there is a homozygous deletion on the q arm of chromosome 5 spanning 6 genes; *NR3C1*, *HMHB1*, *YIPF5*, *ARHGAP26*, and *KCTD16* that was identified by Affymetrix SNP6 sequencing (Figure 14). Comparison of the SNP6 data between the original patient sample and engrafted samples showed there were no major differences between them, indicating the mouse model to be representative of the patient samples.

L707 presentation cells were found to engraft faster than relapse cells except in the presence of Dex treatment, when survival of mice was significantly increased. The relapse cells were unaffected by Dex treatment (Figure 15).

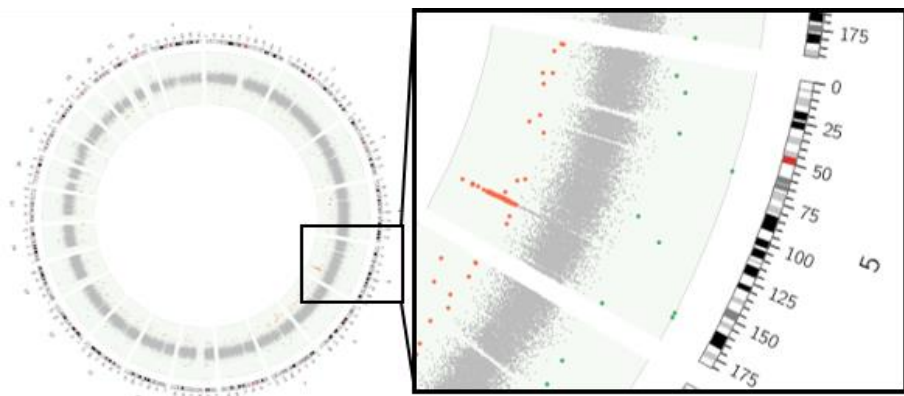


Figure 14: A circos plot showing the copy number gains (green dots radiating outwards) and losses (red dots radiating inwards) compared to normal (grey dots in the centre) in the L707 Relapse, shown on the left. Constructed using the SNP6 data for the L707 relapse. Data produced by Elda Latif and Vikki Rand and circus plot produced by Sirintra Nakjang. The expanded section shows the region of the circus plot showing chromosome 5, with chromosomal location shown to the right of the SNP6 data. The 5q deletion can be seen in this expanded section as the thicker line of red dots on the lower half of the chromosome (the q arm) towards the centre of the plot.

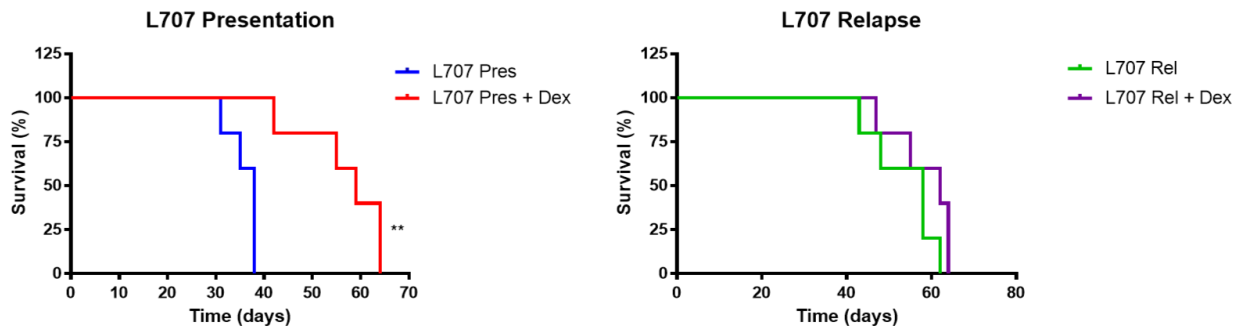


Figure 15: Survival of mice engrafted with 1×10^5 L707 presentation (left) or L707 relapse (right), cells were injected intra-femorally. Mice were treated with either I.P. Dex (15 mg/kg) on weekdays, or saline controls. Treatment was started 2 weeks after intra-femoral injection of leukaemic cells. Treatment was continued until mice reached license endpoints and were humanely killed. Data produced by Elda Latif (Latif 2012).

To investigate this difference in engraftment time between the presentation and relapse L707 cells were injected into NSG mice in a competitive setting. Different ratios of presentation: relapse cells were used and it was found that the presentation cells engrafted and repopulated faster than the relapse cells at all ratios, which resulted in mice succumbing to the disease sooner. This was not the case when Dex treatment was given and the sensitivity of the L707 presentation to Dex closed the gap between presentation and relapse (Figure 16).

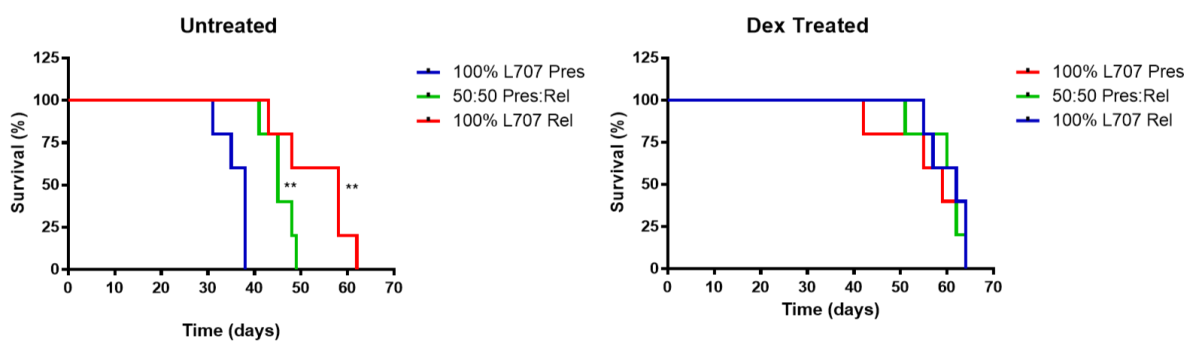


Figure 16: Survival of mice engrafted with ratios of L707 presentation and relapse, 1×10^5 cells/mouse. 2 weeks after intra-femoral injection of leukaemic cells treatment was started, saline I.P. on weekdays (left) or 15 mg/kg Dex I.P. on weekdays (right). Treatment was continued until mice reached license endpoints and were humanely killed. Data produced by Elda Latif (Latif 2012).

Age	16 years
Sex	Female
Presentation karyotype	46,XX,der(19)t(17;19)(q2?;p13)[12]/46,idem,fra(10)(q25)[17] /46,XX[1].ishder(19)t(17;19)(19ptel-,wcp17+,wcp19+,19qtel+)
Relapse karyotype	46,XX,der(19)t(17;19)(q2?;p13)[5]
Treatment protocol	Regimen B, ALL2003
MRD day 28	Negative
Relapse	<5 months
Relapse treatment	R3 FLAG
Current	Patient died shortly after relapse from intracranial bleed

Table 4: All available patient information and treatment details for patient L707 including age, sex, karyotype of both presentation and relapse. The treatment protocol used at diagnosis and the treatments used for the relapse. The patient was negative for MRD at day 28 but had an early relapse and no second remission was induced. The patient died shortly after the second relapse due to an intracranial bleed.

Chapter 2: Materials

2.1 Chemicals

Standard chemicals and reagents used were purchased from Sigma-Aldrich unless stated otherwise.

2.2 Equipment

Instrument	Manufacturer	Software
1000 electroporator	Stratgene, USA	---
ABI 7900HT Sequence Detection system	Applied Biosystems, USA	SDS
Avanti J-26 XP centrifuge	Beckman Coulter, UK	---
Centrifuge 5424	Eppendorf, Germany	---
Centrifuge 5424R	Eppendorf, Germany	---
Class II microbiological safety cabinet	Medical Air Technology Ltd., UK	---
CP 225D Balance	Sartorius, Germany	---
CytoVision Automated Cytogenetics Platform	Leica, UK	CytoVision 7.2
FACS Aria III	Beckton Dickinson, UK	FACS Diva
FACS Calibur	Beckton Dickinson, UK	Cell Quest Pro, Flowing Software
FACS Canto II	Beckton Dickinson	FACS Diva
FLUOstar Omega	BMG labtech, Germany	MARS Data Analysis Software
GelDoc Imager	BioRad, UK	Quantity One
IVIS	Caliper Ltd., USA	Living Image®
MCO-18AC-PE CO2 Incubator	Panasonic, Japan	---
Mediphot937 X-ray film developer	Colenta Labortechnik, Austria	---
Mini-PROTEAN Tetra Cell 2-gell system	BioRad, UK	---

Mini-sub Cell GT	BioRad, UK	---
Multipette stream®	Eppendorf, Germany	---
Multitron Pro, bacterial orbital shaker	Infors, UK	---
Nanodrop 1000 spectrophotometer	Thermo Fisher Scientific, UK	Nanodrop 1000
Optima L-100 XP ultracentrifuge	Beckman Coulter, UK	---
Perkin Elmer GeneAmp 9700 Thermo Cycler	Perkin Elmer, USA	---
ThermoBrite StatSpin®	Abbott Molecular, USA	---

Table 5: The equipment used during the PhD, the manufacturer and if applicable the software used with the equipment.

2.3 Lab ware

Standard lab ware was used throughout the project, separate consumables required for specific work are listed below.

polyallomer Konical™ (Beckman Coulter, USA)

0.45 µm Acrodisc® syringe filter (Sigma Aldrich, UK)

Illustra MicroSpin G-50 columns (GE Healthcare Life Sciences, UK)

1mm electroporation cuvettes (Peqlab, Germany)

2.4 Buffers

Luria-Bertani (LB) broth (1)

- 25g LB broth powder

Contains: 10g/l Tryptone

10g/L NaCl

5 g/l Yeast extract

- 1L DI H₂O

Autoclave to sterilise

SOB Media (1l)

- 20g Tryptone
- 5g Yeast extract
- 0.5g NaCl
- 186 mg KCl
- 1g MgCl₂
- 2.4g MgSO₄
- 1l DI H₂O

Autoclave to sterilise

LB agar (1l)

- 25g LB broth powder
- 12.5g Bacto agar
- 1L DI H₂O

Autoclave to sterilise

10x TBE (1l)

- 108g Trizma (TRIS base)
- 55g Boric acid
- 40 ml 500mM EDTA solution
- Make up to 1l with DI H₂O

0.5x TBE (1l)

- 50 ml 10X TBE
- 950 ml DI H₂O

500mM EDTA (500 ml)

- 84.05g Ethylenediaminetetraacetic acid (EDTA)
- Make up to 500 ml with DI H₂O

RIPA Buffer

- 197 mg Tris-HCl

- 219.1 mg NaCl
- 25 mg SDS
- 0.25 ml Triton-X
- 5.18 mg Sodium deoxycholate
- 1 x cOmplete™ EDTA-free protease inhibitor cocktail tablet (Roche, UK)
- 25 ml DI H₂O

Lammeli Buffer (25 ml)

- 2.5 g SDS
- 1.97 mg Tris-HCl
- 12.5 ml DI H₂O
- 11.5 ml Glycerol

10% Milk (100 ml)

- 10 g Milk powder
- 100 ml PBS

10X TST (1l)

- 12.114 g Tris
- 87.66 g NaCl
- 10 ml Tween 20

HeBS 2X Buffer (1 l)

- 16.36 g NaCl
- 11.9 g HEPES
- 0.123 g Na₂HPO₄
- 1 l DI H₂O
- Required pH = 7
- Filter sterilise (0.2 µm) before use

Special H₂O (50 ml)

- 29.8 g HEPES
- 50 ml DI H₂O

- Filter sterilise (0.2 µm) before use

Polybrene (8 mg/ml, 10 ml)

- 80 mg hexadimethrine bromide
- 10 ml DI H₂O
- Filter sterilise (0.2 µm) before use

Tris-Glycine Buffer (1 l)

- 30 g Tris
- 144 g Glycine
- 1 l DI H₂O

Electrophoresis Buffer (1 l)

- 100 ml Tris-Glycine buffer
- 10 ml 10% SDS (1g SDS)
- 890 ml DI H₂O

Transfer Buffer

- 100 ml Tris-Glycine Buffer
- 10 ml methanol
- 890 ml DI H₂O

Fixative

- 30 ml Methanol
- 10 ml Acetic acid

SOC (super optimal broth with catabolite repression) media (Sigma Aldrich, UK)

20X SSC (Thermo Fisher Scientific, UK)

- Diluted 1:10 before use

Wash Buffer 1

- 2 ml 20X SSC
- 300 µl IGEPAL

- Make up to 1 l with DI H₂O

Wash Buffer 2

- 10 ml 20X SC
- 1 ml IGEPAL
- Make up to 1 l with DI H₂O

2.5 Kits

NucleoBond Xtra (Macherey Nagel, Germany)

Nick Translation kit (Abbott Molecular, USA)

*mirVana*TM miRNA Isolation Kit, with phenol (Ambion, Thermo Fisher Scientific, UK)

BCA Protein Assay Kit (Santa Cruz Biotech, USA)

RevertAidTMH Minus First Strand cDNA Synthesis Kit (Fermentas, Thermo Fisher Scientific, UK)

Phusion[®] High-Fidelity PCR Master Mix with HF Buffer (NEB, USA)

Platinum[®] SYBR[®] Green qPCR SuperMix-UDG w/ROX (Fermentas, Thermo Fisher Scientific, UK)

Mix & Go *E. Coli* Transformation Kit & Buffer Set (Zymo Research, USA)

NucleoBond Xtra mini kit (Clontech, Japan)

The following kits were purchased from Qiagen:

QIAquick PCR Purification Kit, QIAquick Gel Extraction Kit, Miniprep Plasmid Isolation Kit

Maxiprep Endofree Plasmid Isolation Kit, DNeasy Blood and Tissue Kit, RNeasy Mini Kit

2.6 Cloning enzymes

T4 DNA ligase 5 u/μl (Fermentas, Thermo Fisher Scientific, UK)

FastAP Thermosensitive Alkaline Phosphatase (10 U/μl) (Fermentas, Thermo Fisher Scientific, UK)

T4 Polynucleotide Kinase (10 U/μl) (Fermentas, Thermo Fisher Scientific, UK)

Esp3I (BsmBI) (10 U/μl) (Fermentas, Thermo Fisher Scientific, UK)

2.7 Tissue culture reagents

RPMI 1640 (R8758) (Sigma Aldrich, UK)

DMEM (D5671) (Sigma Aldrich, UK)

low glucose DMEM (D6046) (Sigma Aldrich, UK)

StemSpan™ SFEM II (Stemcell technologies, Canada)

GIBCO™ Foetal calf serum (Thermo Fisher Scientific, UK)

L-Glutamine (Sigma Aldrich, UK)

Penicillin-streptomycin (Sigma Aldrich, UK)

GIBCO™ basic fibroblast growth factor (bFGF) (Thermo Fisher Scientific, UK)

recombinant IL-3 (R&D Systems, UK)

recombinant IL7 (R&D Systems, UK)

Trypsin-EDTA 10X solution (Sigma Aldrich, UK)

Sodium-pyruvate (Sigma Aldrich, UK)

VivoGlo™ Luciferin (Promega, USA)

2.8 Antibodies

Antibody	Fluorophore conjugated	Clone	Supplier	Volume per 10 ⁶ cells (μl)
CD19	PE	SJ25C1	BD Biosciences, USA	10
Mouse CD45	PE-Cy7	2.5	BD Biosciences, USA	2.5
Mouse Ter119	PE-Cy7	TER-119	BD Biosciences, USA	2.5

Table 6: Antibodies used for FACS analysis of peripheral blood and organs collected from mice engrafted with ALL cells.

Antibody	Source	Clone	Supplier	Dilution
Anti-α-Tubulin	Mouse monoclonal	B-5-1-2	Sigma Aldrich, UK	1:200000
NR3C1	Rabbit polyclonal	E-20	Santa Cruz Biotechnology, USA	1:500
PLXND1	Rabbit polyclonal	ab96313	Abcam, UK	1:1000
Anti-mouse IgG-HRP	Goat polyclonal	P0447	DAKO, Denmark	1:10000
Anti-rabbit IgG-HRP	Goat polyclonal	P0448	DAKO, Denmark	1:10000

Table 7: Antibodies used for western blotting analysis of protein extracted from both cultured cells and samples collected from mice engrafted with ALL.

2.9 Oligonucleotides and primers

All oligonucleotides were ordered from Sigma Aldrich

Gene	Forward 5'-3'	Reverse 5'-3'
TBP	CTGGCCCATA GTGATCTTGC	TCAATT CCTGGTTATCTTCACA
NR3C1	AGGACGCCACCCATTG	TGTCTGAAGGGTCCCAGTTG
PLXND1	CTCTTAGCTTGT CGGGTCA	ACAGTTGTGGAGGAGAGAGC
GILZ	CATGGAGGTGGCGGTCTA	TTACACCTCATACCACCAT
NFKBIA	GAAGTGTGGGGCTGATGTCA	TGGCCTCAAACACACAGT
FKBP5	CATTATCCGGAGAACCAAC	AATTGGAATGTCGTGGTCTT

Table 8: Primer pairs used for real-time PCR using cDNA reverse transcribed from mRNA.

Gene	Forward 5'-3'	Reverse 5'-3'
ATP10A	AGCCCCATGGTGAGTGTACAG	GTAGGATTAAATATAGACACCTTCCATGAG
NR3C1	AGGACGCCACCCATTG	TGTCTGAAGGGTCCCAGTTG
Cas9	AGCTGATCCGGGAAGTGAAA	GATTT CCTGCTCGCTCTTGG

Table 9: Primer pairs used for real-time PCR using genomic DNA as the template

Primer	Primer 5'-3'
CRISPR amplification forward	ACACTGACGACATGGTTCTACACTGTGGAAAGGACGAAACACC
CRISPR amplification reverse	TACGGTAGCAGAGACTTGGTCTGTTGATAACGGACTAGCCTTA
CRISPR adaptor addition forward	AATGATA CGCGACCACCGAGATCTACACTCTTCCCTACACGACGCTC TTCCGATCTTGTGGAAAGGACGAAACACCG
CRISPR adaptor addition reverse	CAAGCAGAAGACGGCATACGAGATNNNNNGT GACTGGAGTT CAGA CGTGTGCTCTCCGATCTGTTGATAACGGACTAGCCTTA

Table 10: Primers used in the production of the lentiCRISPR amplicon library before next generation sequencing was carried out.

2.10 Cells

697

Pre B ALL cell line derived from the BM of a 12yr old male at relapse. The patient had null cell ALL (non B, non T) ALL at presentation but cells cultured at relapse had a pre-B phenotype. Carry the t(1;19) translocation (Findley et al. 1982).

293T

Cell line derived from embryonic kidney fibroblasts, contains the SV40 T antigen. These cells are highly transfectable, which is why they are used in the production of lentiviral particles (Pear et al. 1993).

MS-5

Murine bone marrow stromal cell line, derived by irradiation of adherent cells from the long term culture of C3H/HeNSIc mouse marrow samples. Capable of supporting growth of haematopoietic stem cells for more than 2 months (Itoh et al. 1989).

M210B4

Murine bone marrow stromal cell line, derived from a C57BL/6J X C3H/HeJ F1 mouse. This cell line produces pre-B stimulatory factors and are able to support the proliferation of pre-B cells in long term culture (Lemoine et al. 1988).

L707

Primary derived cells obtained at presentation and relapse from a 16-year-old female with B ALL, passaged through several xenografts.

MSC

Primary human mesenchymal stem cells. Collected from the hip of mostly hip replacement patients. Collection and purification by Dr. Deepali Pal.

2.11 Competent bacteria

STBL3

E. coli strain with the recA13 mutation that results in reduced recombination of cloned DNA, which is required for propagation of lentiviral plasmids.

E. Cloni 10G

Specific cloning strain of *E. coli* with high transformation efficiency. Have the recA1 mutation, which causes reduced recombination of cloned DNA.

2.12 *In vivo* model

NSG (NOD.Cg-*Prkdc*^{scid} *Il2rg*^{tm1Wjl}/SzJ)

The NSG (NOD scid gamma) mice are a transgenic line established from the NOD/ShiLtj mice with the addition of a scid (severe combined immunodeficiency) mutation and an IL2 receptor gamma chain deficiency. The resulting mouse is highly immunodeficient, lacking in mature B, T and NK cells with deficient cytokine signalling. The NSG mice have 6x higher engraftment efficiency than the NOD-Scid mice without the IL2Rgamma chain mutation (Shultz et al. 2005). These mice were bred in house, with additional mice purchased from Charles River (USA) when additional animals were required.

RAG2 (BALB/c *Rag2*^{-/-} *gamma c*^{-/-})

The RAG2 mice are another immune deficient strain. These mice lack the ability to undergo VDJ rearrangement and so mice have no mature B or T cells. The loss of the gamma chain, which is part of the IL2,4,7,9 and 15 receptors results in a loss of natural killer cells (Colucci et al. 1999). These mice were bred in house.

CD1® IGS

The CD-1 IGS mouse is an outbred mouse used as a multi-purpose model with no harmful genetic phenotype. These mice were purchased from Charles River (USA)

Chapter 3: Methods

3.1 Cell culture

All tissue culture was carried out in a type II fume hood to maintain sterility. Cells lines were passaged 3 times a week and primary cells passaged as needed.

Cell line	Disease/model	type	Media	density
697	pre B ALL	suspension	RPMI 1640 10% FBS	0.5x10 ⁶ /ml
SEM	pre B ALL	suspension	RPMI 1640 10% FBS	0.5x10 ⁶ /ml
HAL-01	pre B ALL	suspension	RPMI 1640 10% FBS	0.5x10 ⁶ /ml
293T	Human embryonic kidney	adherent	DMEM 10% FBS 1% L-glutamine 1% Sodium pyruvate	2.5x10 ⁵ /ml
MS-5	murine BM stromal	adherent	RPMI 1640 10% FBS	2.5x10 ⁵ /ml
M210B4	murine BM stromal	adherent	RPMI 1640 10% FBS	2.5x10 ⁵ /ml

Table 11: Information on culture of all cell lines used including disease type, cell type and the culture conditions required including the media used, the concentration of supplements including FBS and the density that cells were seeded at when split.

Cell	Disease	type	Media	density
L707	Pre B ALL	suspension	SFEM 20% FBS 20 ng/ml IL-3 10 ng/ml IL-7 1% pen/strep	0.5-1x10 ⁶ /ml
MSC	healthy	stromal	DMEM 20% FBS bFGF 1% L-glutamine 1% pen/strep	6000- 10000cells/cm ²

Table 12: Information on culture of primary human and primary derived cells including disease type, cell type and the culture conditions required.

3.1.1 Counting cells

Cells were counted using the trypan blue exclusion method. 10 µl of trypan blue and 10 µl cells were mixed and pipetted onto a haemocytometer for counting. This method uses the ability of viable cells to keep trypan blue out of the cell as a measure of viability. The disrupted membrane allows the trypan blue into the cells, showing them as blue, whereas live cells stay white. Haemocytometers have 4 squares, each comprised of 16 smaller squares; any cells in these 4 large squares were counted and used to determine the concentration of cells in the sample, with the following equation:

$$\text{Conc} = n \times df \times cf = \text{cells/ml}$$

Conc = concentration of cells in solution

n = sum of cells counted

df = dilution factor

cf = chamber factor = (desired final volume/counting square unit volume)

An alternative method was used for cells collected from mouse organs, especially spleen and liver. This used methylene blue, at the same 1:1 ratio as trypan blue. Methylene blue causes red cells to lyse, making counting of lymphocytes easier in spleen and liver samples as these samples had high levels of red cells in. Methylene blue does not distinguish living from dead cells, and so trypan blue counting was also required for these samples.

3.1.2 *Culture of suspension cells*

All of the leukaemic cells used during the course of this PhD were suspension cells. These cells do not need to adhere to a tissue culture flask but grow in a suspension in media. To culture suspension cell lines, cells were mixed by shaking the flask and a small aliquot taken from the flask using a 5 ml stripette. This was pipetted onto Parafilm and 10 µl taken from this and added to 10 µl trypan blue. Using a sterile stripette reduces the risk of infection from using a pipette in the flask. Cells were counted using the trypan blue exclusion method (3.1.1). Cell number/ml was calculated and cells split to the required density using media pre-warmed in a water bath at 37°C. Mycoplasma testing was carried out periodically to ensure cells were uninfected, this test was done by Liz Matheson.

3.1.3 *Culture of adherent cells*

Adherent cells were used as feeder layers and in the production of lentivirus. The culture of these cells is different to suspension cells due to them attaching to the surface of the tissue culture flasks. To culture adherent cells, old media was removed from flasks using an aspirator and glass Pasteur pipette before 10 ml of pre-warmed PBS was added and the flask gently swirled to wash cells. This was then removed using a fresh Pasteur pipette and 3 ml 1x trypsin-EDTA (0.05% trypsin, 0.02% EDTA) added before incubation at 37°C for 3-5 minutes. Once cells were detached 7 ml fresh media was added to the cells in order to inactivate the trypsin before 10 µl was taken for counting (3.1.1)

3.1.4 Co-culture of leukaemic cells and feeder cells

3.1.4.1 Growth on murine stromal cell line feeder layers

In order to culture leukaemic cells in a manner that mimics the *in vivo* niche or to support growth *ex vivo*, feeder layers were used. These cells produce the necessary cytokines required to support growth of cell lines at low FBS concentrations, or primary derived cells that would usually not proliferate *in vitro*.

The MS5 and M210B4 murine BM stromal cell lines were used as feeder layer to support growth of 697 cells. As adherent cell lines they were passaged 3 times a week (3.1.3) and re seeded in a new 75cm² tissue culture flask or 96 well plates. If cells were to be used for cytotoxicity assays with the 697 cells, they were seeded at 4.5x10⁴/ml the day before use in a 96 well plate.

3.1.4.2 Growth on MSC feeder layer

The MSC cells are primary cells, these were obtained from hips removed for hip replacement surgeries as a result of osteoarthritis. Dr. Deepali Pal received the hips and did all the processing. Cells were retrieved, purified and cultured according to the method in Pal et al 2016. Briefly, BM was removed from the femoral head and cells were separated using Lymphoprep™ (1.077 g/ml). The mononuclear cells remaining after separation were collected and washed before culture. MSC adhered to the flask, and after a wash using MSC wash buffer 24h later the cells were cultured by Dr. Pal until ready to be split. At which point cells were kindly given to me for use. MSC were cultured in the same way as the other adherent cell lines used, although with less frequent cell passages required due to slower proliferation. MSC were seeded at 6000-10000 cells per cm² 3-5 days prior to use in plates or flasks as needed. Once the MSC had reached optimal confluence the cells were gently washed with PBS and the leukaemic cells added at a concentration of 0.5x10⁴/ml -1x10⁶/ml depending on when they are to be split again or the testing to be done.

3.1.5 *Thawing cells*

Cells were thawed from storage in liquid nitrogen or -80°C by heating cells in a water bath at 37°C until one ice crystal remained, cells were then pipetted into 10 ml of pre-warmed media and centrifuged at 300g for 5 minutes. The supernatant was removed by inversion of the tube and cells re-suspended in 5 ml of fresh pre-warmed media. Cells were then counted and seeded at a suitable concentration.

3.1.6 *Freezing cells*

In order to cryopreserve cells, they were split the day before freezing to ensure they were in log phase growth when frozen. On the day of freezing cells were counted and centrifuged at 300g for 5 minutes. The supernatant was discarded and an appropriate volume of freezing media (FBS +10% DMSO) added (1 ml per 1×10^6 cells). Once freezing media was added, cells were kept on ice and aliquoted into labelled cryovials. Vials were then transferred to polystyrene boxes filled with cotton wool and stored at -80°C. This is to ensure the cells freeze slowly and so maintain viability when thawed. After 24 hours at -80°C cells were moved to liquid nitrogen for long term storage.

3.2 Flow Cytometry

Flow cytometry was used to determine levels of transduction with fluorescent tagged plasmids, determine engraftment in the peripheral blood of mice and sort cells.

Determination of transduction was done using the FACS Calibur. 500 µl of cells was taken from the culture and put into polystyrene FACS tubes (BD). The FACS machine was set up before use by filling the sheath tank 2/3 full with FACS flow (BD) and emptying the waste tank before putting 100 ml FACS Clean (BD) in. The sheath tank was pressurised and bubbles removed from the sheath tubing before the machine was primed twice. After priming, water was run through the machine on a high flow rate before samples were run. GFP (Green

fluorescent protein) positive samples were measured on FL1 of the FACS machine, and tRFP samples on FL2. If the sample was positive for both, compensation was carried out using singly positive samples before-hand to compensate for the bleed through of each fluorophore into the other filters. Samples were always run with a negative control so the threshold could be set for positivity, this was set as the top 0.3% of the negative control.

Analysis of engraftment in the peripheral blood of mice was done using the FACS Canto with Dr. Helen Blair. After collection of blood from mice by tail vein venepuncture or cardiac puncture antibodies were added to 50 µl of blood. 10 µl of CD19-PE, 2.5 µl mouse CD45-PECy7 and 2.5 µl Mouse Ter119-PECy7 were added to the sample before mixing and incubation for 20 minutes in the dark. 1.2 ml of 1x ammonium chloride solution was used to lyse red cells, sample was mixed by inversion and incubated for 5 minutes before centrifugation at 400g for 2 minutes. Pellet was washed twice with 1% PBSA (0.2% BSA in PBS) before being re-suspended in 500 µl PBSA in a polystyrene FACS tube for analysis. Samples were run on the FACS Canto and as no negative control was run when the samples were, the same parameters were used each time.

Cell sorting was done by Hesta McNeill using the FACS Aria. Cells were counted and re-suspended in PBSA at a concentration up to 10^7 cells/ml in polypropylene FACS tubes (BD). Cells were gated on GFP positivity for sorting and were sorted into 15 ml falcon tubes. After sorting cells were counted and re-suspended in an appropriate volume of pre warmed media before culture as usual, with the addition of 1% pen/strep to the media for 1 week to ensure cells remained un-infected after sorting.

3.3 Cytotoxicity testing

Cytotoxicity testing of cells was used to determine the sensitivity to drugs. Cells were counted and seeded in a 96 well plate. The compound being tested was added to wells and cells were incubated for 96hrs before analysis. For both WST-1 and luciferase assays only the internal 60 wells were seeded with cells. This was so that any evaporation that occurred to the external wells didn't affect read-out, and for the WST-1 assay, there were control wells.

Cytotoxicity is calculated as the reduction in signal as a percentage of the vehicle treated cells.

3.3.1 WST-1 assay

WST-1 is a tetrazolium salt that when cleaved results in the production of formazan, a dye. The cleavage of WST-1 occurs at the cell surface and is dependent on the glycolytic production of NAD(P)H, which occurs in viable cells. The amount of formazan dye, and thus the colour change from light red to yellow, is directly proportional to the number of cells with active metabolism in the sample. Cell Proliferation Reagent WST-1 (Roche) contains WST-1 and an electron coupling reagent and is a ready to use solution. Cells were cultured in a clear 96 well plate, with the compounds being tested for 96h before the addition of 10 µl of WST-1 reagent was added to each well. The plate was incubated for a further 2 hours at 37°C before the absorbance of the wells was measured using the FLUOstar Omega plate reader at a wavelength of 450nm. Control wells containing WST-1 reagent and media but no cells were measured and then subtracted as background to control for the colour of the cell culture medium.

3.3.2 Luciferase assay

One of the plasmids used throughout much of this PhD is the pSLIEW plasmid. This plasmid when used to produce lentivirus and transduced into target cells, encodes the luciferase enzyme. This enzyme catalyses the oxidation of luciferin to oxyluciferin along with the production of bioluminescence. This bioluminescence can be used in a number of ways including to determine the number of cells transduced using FACS, the levels of engraftment in mice injected with transduced cells, using in vivo imaging and for use in a cytotoxicity assay.

In cell lines transduced with the pSLIEW plasmid, the luciferase assay was used to determine cytotoxicity. Cells were seeded in white walled 96 well plates and treated with drugs for 96h, as with the WST-1 assay. D-Luciferin (VivoGlo, Promega), stored at -20°C was thawed and diluted to a working stock of 7.5% just prior to use in tissue culture media. 10 µl of diluted

luciferin was added to each well and after 3 minutes the bioluminescence measured using the FLUOstar Omega late reader. Bioluminescence is a by-product of the oxidation of D-luciferin to oxyluciferin by the luciferase enzyme, which is encoded by the pSLIEW plasmid (Bomken et al. 2013). The amount of bioluminescence produced is proportional to the amount of luciferase enzyme in the cell culture, and thus is an indirect read-out of the number of cells in the well. The luciferase assay is useful for when cells are being cultured with a feeder layer as the assay is not affected by different amounts of cells that are not transduced with pSLIEW.

3.4 Harvesting cell pellets

Cell pellets for the extraction of RNA, DNA or protein were collected after counting cells. An appropriate volume of cells was pipetted into a 1.5 ml collection tubes and centrifuged at 500g for 5 minutes. Cells were washed once with PBS before removal of supernatant and addition of buffers or storage at -20°C depending on downstream use.

3.5 RNA extraction

3.5.1 *Qiagen RNeasy kit*

RNA extraction with the RNeasy kit (Qiagen) was done according to the protocol. Cells were collected and washed in PBS by centrifugation at 500g for 5 minutes. 350 µl buffer RLT with β mercaptoethanol added (β-ME) (1:1000) was then added to cells (up to 3.5×10^6 cells) before storage at -20°C or use straight away. Upon thawing the samples were passed through a QIAshredder column by centrifugation for 2 minutes at full speed (16,000g), this homogenises the sample. DNA was precipitated by the addition of 350 µl 70% ethanol before being pipetted into and RNeasy spin column. Centrifugation for 15 seconds at >8000g ensured the sample passed through the membrane, where the RNA binds. The flow through was discarded and the column washed with 700 µl buffer RW1. Centrifugation for another 15 seconds washes the column before addition of 500 µl buffer RPE and centrifugation twice to wash the column. The column was put in a new collection tube before an extended

centrifugation to remove any remaining liquid to dry the column and ensure the eluted fraction was not contaminated. The dry column was placed in a 1.5 ml collection tube and 50 µl buffer EB pipetted directly onto the membrane. This was left for 5 minutes before centrifugation to elute the RNA. Sample concentration was measured using the Nanodrop 2000 spectrophotometer and samples stored at -20°C.

3.5.2 *mirVana kit*

The *mirVana* kit (Ambion, Fisher Scientific) allows extraction of RNA without loss of microRNA, making it ideal for RNA extractions to be used for microarray analysis. The kit uses glass fibre filters instead of the silica membranes used for the RNeasy kit. Samples were first washed in PBS with centrifugation at 500g for 5 minutes before being disrupted with 300 µl lysis/binding buffer. Vigorous vortexing was used to lyse the cells. 30 µl (1/10 volume) of miRNA homogenate additive was added to the samples before mixing by vortexing and incubation on ice for 10 minutes. 300 µl Acid-phenol-chloroform was added to the sample followed by further vortexing for 1 minute. This step was to extract the RNA from the lysate, and after centrifugation at 10,000g for 5 minutes at room temperature the aqueous and organic phases were separated. The aqueous phase, containing the RNA was removed and 1.25 volumes of 100% ethanol added to precipitate the RNA. The sample was then passed through the filter cartridge by centrifugation for 15 seconds at 10,000g. After centrifugation the flow through no longer contains the RNA as it has bound to the column and was discarded. The column was next washed with 700 µl miRNA wash solution 1, and then 500 µl wash solution 2/3. After the last wash the column was centrifuged in a fresh collection tube to ensure there was no residual buffer left. RNA was eluted with the addition of 100 µl Nuclease-free water pre-heated to 95°C. The column was incubated for 5 minutes before elution to maximise yield. RNA concentration was determined using the Nanodrop 2000 spectrophotometer before samples were stored at -20°C.

3.6 DNA extraction

Extraction of genomic DNA was done using the DNeasy blood and tissue kit (Qiagen). This kit works with the same silica based technology as the RNeasy kit. Cells were collected and washed in PBS by centrifugation at 500g for 5 minutes. PBS was removed from samples and they were stored at -20°C before use. When needed, samples were thawed and 200 µl fresh PBS was added, 20 µl proteinase K was added to the sample before the addition of 200 µl buffer AL. Samples were mixed by vortexing before incubating at 56°C for 10 minutes. For mouse samples, with a lot of cells this incubation was increased to 1 hour to ensure full lysis of samples. After incubation DNA was precipitated by the addition of 200 µl of 100% ethanol. The sample was pipetted onto a DNeasy spin column and centrifuged at >6000g for 1 minute. The DNA was then bound to the column, and so the flow through discarded. The column was washed with 500 µl buffer AW1 then AW2 before centrifugation for 3 minutes to remove residual buffer. DNA was eluted using 200 µl buffer AE that was incubated on the column for 5 minutes before centrifugation. Concentration was determined using the Nanodrop 2000 spectrophotometer before storage at -20°C.

3.7 Protein extraction

Protein was extracted from cells using the RIPA buffer to lyse cells and collect protein. Samples that had been washed in PBS after collection and frozen at -20°C were thawed and 100 µl ice cold RIPA buffer was added. Samples were vortexed before incubation on ice for 30 minutes with regular vortexing to aid in lysis of the cells. Samples were then centrifuged at 14,000g for 15 minutes in a pre-cooled centrifuge at 4°C. This resulted in pelleting of the cell debris, leaving the protein in the supernatant. The supernatant was removed and kept on ice whilst protein concentration estimation was done.

3.7.1 BCA assay

The bicinchoninic acid (BCA) protein estimation assay uses the measurement of a colour change from green to purple in the presence of protein to determine the concentration. This change is a result of the reduction of Cu²⁺ to Cu⁺ by the peptide bonds present in protein. The amount of protein in the solution is proportionate to the amount of reduction. These reduced Cu⁺ ions are then chelated by the bicinchoninic acid to form the purple complex that is measured by spectroscopy (Smith et al. 1985).

A standard is included on each plate in order to quantify the samples, this was made from bovine serum albumin (BSA) at concentrations of 125-2000 µg/ml. 10 µl of each of the concentrations was pipetted into a clear 96 well plate in triplicate along with 10 µl triplicates of each sample, pre diluted 1:10 in H₂O. The BCA assay reagents were then mixed at a ratio of 1:50 reagent A: reagent B, before 190 µl of the mixture was then added to each well. The plate was shaken for 30 seconds before incubation at 37°C for 30 minutes. After incubation changes in colour, as measured by absorbance at 560nM was determined using the FLUOstar Omega plate reader. The concentration of protein in samples was quantified by comparison to the BSA standard.

After protein concentration estimation, samples were diluted to a concentration of 1 µg/ml with Laemmli buffer, and β-ME and bromophenol blue added at a final concentration of 5% each.

3.8 Production of cDNA

Reverse-transcriptase polymerase chain reaction (PCR) was used to produce cDNA from mRNA using the RevertAid H Minus First Strand cDNA synthesis kit (Thermo Fisher Scientific). This kit uses the RevertAid H Minus M-MuLV Reverse transcriptase enzyme, which contains a point mutation that removes RNase H activity of the enzyme, resulting in reduced RNA degradation, and thus better cDNA yield from long template RNA. The RiboLock RNase inhibitor binds RNases thus protecting RNA from degradation at temperatures below 55°C.

Random hexamers were added to RNA and RNase free H₂O (Table 13) before incubation at 70°C for 5 minutes in a GeneAmp 9700 Thermo Cycler PCR machine. This step allows for the random hexamers to bind to the RNA. After 5 minutes, with the thermo cycler set at 4°C, 8 µl of PCR master mix (Table 14) was added to each sample. The thermo cycler was then run at 25°C for 10 minutes, 42°C for 60 minutes and 70°C for a further 10 minutes before samples were removed and 30 µl RNase free H₂O added to each before storage at -20°C until use.

Reagent	Volume (µl)
RNA (500 ng-1µg)	X
Random hexamers (100 µM)	1
RNase free H ₂ O	X
Total	12

Table 13: Reagents used for the first step of cDNA synthesis, the binding of the random hexamers to the RNA.

Reagent	Volume per reaction (µl)
Buffer (5X)	4
dNTP mix (10mM)	2
RiboLock inhibitor	1
RevertAid H Minus M-MuLV Reverse Transcriptase (200 u/µl)	1

Table 14: Reagents used for the second step of reverse transcription, including the reverse transcriptase enzyme, dNTPs and Ribolock to inhibit RNases.

3.9 Real-time PCR

To determine the expression of genes real-time PCR was used. This allows for quantification of cDNA or genomic DNA in a sample. This was done using a 384 well plate, with 8 µl of

PCR master mix (Table 15) per well. This was done with an Eppendorf Multipette stream multistepper pipette (Eppendorf). To each well, 2 µl of sample was added in triplicate for each primer pair. The plates were centrifuged before use to ensure sample was at the bottom of the well and there were no bubbles before being run on the ABI 7900HT Sequence Detection system (Figure 17).

Reagent	Volume per reaction (µl)
SYBrGreen (2X)	5
Primer Mix (10 µM)	0.3
RNase free H ₂ O	2.7
Total	8

Table 15: Reagents and volumes per reaction for quantitative real-time PCR. Reagents were pipetted with a multi-stepper pipette before the addition of cDNA.

The first step of the PCR run results in denaturing of cDNA, UDG (Uracil DNA glycosylate) inactivation and enzyme activation, this consisted of 2 minutes at 50°C and 10 minutes at 95°C. The second step was 40 cycles of denaturing and hybridisation/amplification steps at 95°C for 15 seconds and 30 seconds at 60°C, this is when the detector records signal amplification as SYBR Green is incorporated into double strand cDNA. The final step of the PCR programme is the amplicon disassociation step when the dissociation curve is recorded. This consists of 95 for 15°C seconds followed by 1 minute at 60°C.

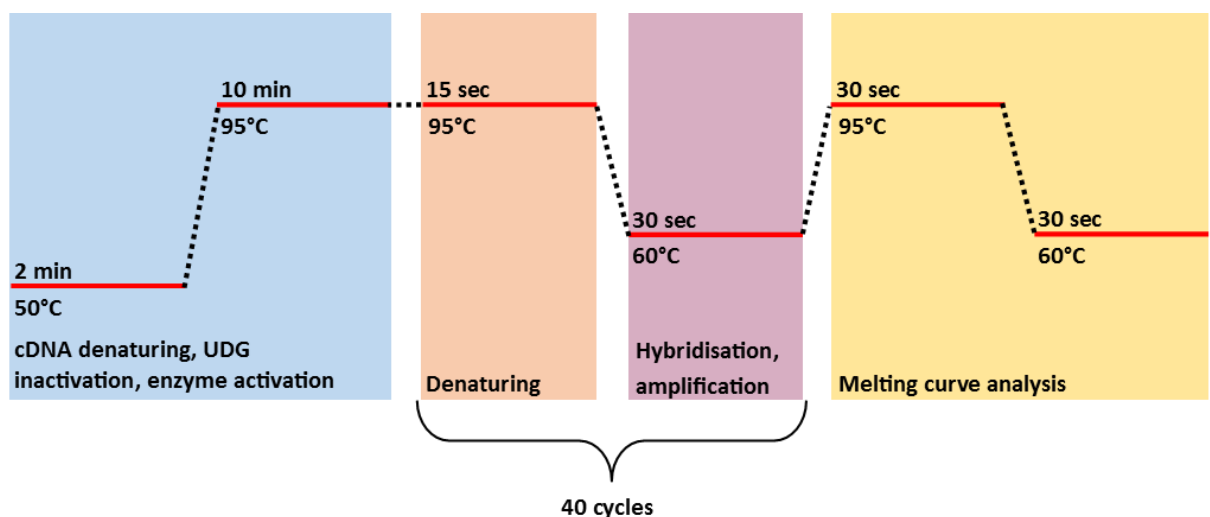


Figure 17: PCR cycling conditions used for real-time PCR run on the ABI 7900HT Sequence Detection system.

Data is collected from the PCR machine and analysed using SDS2.3. The Ct (cycle threshold) value, which is the cycles needed for the fluorescent signal from incorporated SYBR green to exceed a threshold. This threshold was set by the machine, but in analysis could be changed if it was too low/high. The Ct values are used with the delta-delta Ct method ($\Delta\Delta Ct$) method to determine the expression compared to a control sample.

This method has 3 steps, first the Ct values of the gene of interest was normalised to the Ct of the housekeeping gene. These values are then normalised to the $-\Delta Ct$ of an untreated control sample, resulting in $-\Delta\Delta Ct$ values. Each Ct unit represents a 2-fold change in expression, so to obtain a relative RNA expression value the inverse of the $-\Delta\Delta Ct$ values are found. These steps are outlined in the formulas below.

$$Ct_{sample} - Ct_{housekeeping} = -\Delta Ct_{sample}$$

$$-\Delta Ct_{sample} - \Delta Ct_{control} = -\Delta\Delta Ct_{sample}$$

$$2^{-(-\Delta\Delta Ct_{sample})} = \text{Relative RNA expression}$$

3.10 Agarose gel electrophoresis

Agarose gel electrophoresis was used to visualise bands of DNA after PCR amplification or restriction digest. Agarose was melted in 60 ml 1x TBE buffer using a microwave before adding 6 μ l gel red (1:10000), the solution was then poured into a Mini-Sub cell gel tray with a gel casting gate with either 8 or 14 wells and left to set. The amount of agarose used was dependent on the size of the band to be visualised. Bands 500-10000bp were run on a 1% gel, whereas for smaller bands 200-3000 a 1.5% gel was used.

The gel was loaded onto a Mini-Sub GT cell (BioRad) and submersed in 0.5x TBE. Samples were mixed with 5x gel loading dye before being loaded into the gel. A PowerPac™ basic power supply (BioRad) was connected to the cell and used to run electricity through the gel, between 60-80V. Once binding buffer reached far enough down the gel the bands were visualised using a GelDoc™ XR+ Gel Documentation system.

3.11 QIAquick Gel Extraction Kit

To extract DNA bands from agarose gels, the bands were visualised using UV light, a clean scalpel was then used to cut out the band, which was put into a 1.5 ml collection tube. These tubes were weighed and 3 volumes of buffer QG were added to 1 volume of gel (100 mg gel ~ 100 µl buffer QG). Samples were then incubated at 50°C for 10 minutes to dissolve the gel. Incubation time was increased if the gel was not dissolved in 10 minutes. After the gel has dissolved, 1 volume isopropanol was added and the sample mixed by vortexing. This was then pipetted into a QIAquick spin column in a collection tube. This was centrifuged for 1 minute at 17,900g to pass the sample through the column and allow the DNA to bind to the membrane. The flow through was discarded and the column washed by centrifugation with 500 µl Buffer QG and then 750 µl Buffer PE. After the second wash the column was centrifuged for 2 minutes (17,900g) to dry the membrane and ensure all buffer was removed. The column was then transferred to a clean 1.5 ml collection tube and 30 µl Buffer EB added to the membrane. This was left for 5 minutes before elution of the sample with 30s centrifugation. DNA was quantified using the Nanodrop and stored at -20°C until needed.

3.12 QIAquick PCR Purification Kit

The QIAquick PCR Purification kit was used for the concentration of several DNA samples as well as the clean-up of PCR reactions. It works in a very similar way to the QIAquick Gel Extraction kit but. To the PCR products, or DNA to be concentrated 5 volumes of Buffer PB were added. This was then pipetted into a QIAquick column and centrifuged to pass the sample through the column (1 min, 17,900g). The flow through was discarded and the column washed by centrifugation with 750 µl Buffer PE before an extended centrifuge to dry the column. 50 µl Buffer EB was used to elute samples after a 5-minute incubation on the membrane. Samples were quantified using the Nanodrop and stored at -20°C until needed.

3.13 Western blotting

Western blotting was used to visualise protein expression in samples. The pre-cast 4-20% Mini-PROTEAN® TGX™ gels (BioRad) were loaded into the Mini-PROTEAN® Tetra Cell tank (BioRad), which was then filled with electrophoresis buffer before 15 µg of protein sample in Laemmli buffer was pipetted into each well. 5µ Spectra™ Multicolour Broad Range Protein Ladder (Thermo Fisher Scientific) was added in order to determine the size of bands. The gel was run at 100V for approximately 1h, or until the bands reached the bottom of the gel. Following electrophoresis, the gel was removed and put into a tank of ice cold blotting buffer whilst the transfer cassette was prepared. This consisted of the cassette, a sponge, a piece of blotting paper and the PDVF membrane, which had been submerged in methanol before use. The gel, once removed from the plastic case was placed on top of the membrane, before another piece blotting paper and a second sponge were placed on top. Bubbles were removed from the cassette to ensure an even transfer. This cassette was put into the Mini Trans-Blot® Cell (BioRad) with an ice pack and a magnetic stirrer to keep the solution cool. Transfer was done at 100V for 1h on a magnetic stirrer plate.

After transfer the membrane was carefully removed from the cassette and blocked in 10% milk for 1h to reduce background signal. After blocking, the membrane was cut if required, and incubated with primary antibody in 5% milk for 1hr. Following incubation, the membrane was washed in 1X TST for 3 10 minute periods. Incubation with the secondary antibody in 5% milk, at a concentration of 1:1000 followed this before another step of 3 1X TST washes for 10 minutes each. During the final wash the ECL reagents were prepared in a 1:1 solution. This was pipetted onto the membrane once removed from the wash and left to incubate for a further 5 minutes before x-ray films were used to detect chemiluminescence produced by the oxidation of substrates by the horse radish peroxidase (HRP), which is conjugated to the secondary antibody. X-ray films were developed using the Mediphot937 X-ray film developer (Colenta Labortechnik).

3.14 *In vivo* work

All *in vivo* work was carried under home office personal license F3AC40BF, under the project number PPL60/4552. Procedures were checked and signed off by either Helen Blair or Chris Huggins before being carried out without supervision.

3.14.1 Animal husbandry

Animal husbandry such as weighing and checking for signs of ill health was carried out at least once a week after animals had been injected with leukaemic samples. Once mice were on dosing regimens this was increased to everyday, and for mice engrafted with the 697 cells this increased to monitoring at least twice a day every day past 21 days of engraftment as this was seen to be a very aggressive leukaemia with effects being very swift. End points, as defined on the Home Office license were >20% weight loss or >10% weight loss maintained for 72h (compared to heaviest weight), tumours >10mm in any direction, (15mm if on treatment). As well as these defined endpoints, the health of animals was taken into account such as piloerection, anaemia or poor circulation indicated by paleness of the feet ears and tail, a starey coat with porphyrin staining around the nose/eyes, loss of skin tone, laboured breathing, inability to maintain upright position, reduced movement and as was often seen in the case of the L707 cells, hind limb paralysis. Mice were killed by cervical dislocation, a schedule one method.

3.14.2 Intrafemoral injection

The intrafemoral injection was used to engraft ALL cells in NSG mice. The entire procedure was carried out in a category II laminar flow hood to maintain sterility and an isoflurane anaesthetics trolley was used to administer anaesthetic. Mice were anaesthetised in an induction box with 5% isoflurane before being moved to a face mask for maintenance at a surgical depth of anaesthesia (~3% isoflurane) throughout the procedure. Mice were weighed and 5 mg/kg Carprofen (Rimadyl, small animal injection) was given for analgesia at

the start of the procedure. The leg was shaved and sterilised using Hydrex Derma Pink Spray before a 29G insulin needle was used to drill through the kneecap and into the femur. A new needle was then used to inject 20 µl of the sample in SFEM II media, into the femur. Mice were returned to the home cage and monitored until recovery from anaesthesia. Ear notching was used to differentiate mice in a single cage, this was done whilst animals were under anaesthetic.

3.14.3 Dosing

3.14.3.1 Intra peritoneal

Intra peritoneal (I.P.) dosing was used for the administration of both Dex and D-luciferin. It was done using a 29G insulin needle. The mouse was restrained by grasping the scruff and the skin down the back of the body. In order to reduce stress and possible accident a firm hold was needed. The needle is then inserted at approximately a 45° angle, bevel upwards into the peritoneal area of the mouse. For female mice this was the lower part of the abdomen, and for males slightly higher to avoid injecting the testicles. If dosing was done every day, then the location of injection was switched sides to avoid excessive bruising and discomfort.

3.14.3.2 Oral

Oral dosing was used for the administration of Dex and Mifepristone. This was chosen on the advice of the head technician, who believed that for long periods of dosing oral gavage was less stressful for the mice. Oral dosing of drugs was done with a round tipped gavage needle. The mouse was restrained in a firm grip and the needle inserted into the mouth, the head was gently pushed back and the needle allowed to drop down the oesophagus into the stomach. At no time was the needle pushed as this could rupture the oesophagus and cause serious injury or death of the mouse. Once the needle had dropped into the stomach the drug was given slowly and smoothly before removal of the needle.

3.14.3.3 Sub cutaneous

Sub cutaneous dosing of mice was only used for the administration of Carprofen during the intrafemoral injection. Mice were anaesthetised at the time, and a 29G insulin needle used to inject into tented skin on the scruff.

3.14.4 IVIS imaging

In order to measure bioluminescence of pSLIEW transduced leukaemic cells in mice the IVIS (*in vivo* imaging system) (Caliper) was used. Mice were injected with 100 µl of D-luciferin (VivoGlo, Promega) I.P. After 5 minutes, mice were anaesthetised with isoflurane in an induction box (4-5% isoflurane). This timing was kept regular to avoid differences in bioluminescence due to changes in blood flow of anaesthetised animals. Once under anaesthetic, mice were moved to the IVIS imaging chamber and placed onto the block heated at 37°C, in a face mask to continue the delivery of anaesthetic (3% isoflurane). After a total of 10 minutes from D-luciferin injection, imaging was started. Length of exposure was determined by the IVIS software, Living Image and ranged between 1 second and 5 minutes. Once imaging was finished mice were returned to the home cage and monitored until they woke from anaesthetic.

3.14.5 Venepuncture of tail

In order to measure leukaemic blasts or drug levels in peripheral blood, venepuncture of the tail vein and collection of blood was used. Mice were placed into a restraint tube and a scalpel blade was used to nick the tail vein. Heparin coated blood collection tubes were filled from the droplet of blood that formed on the tail by capillary action. Once blood was collected pressure was applied above the cut to stop bleeding and the mouse released from restraint and placed back in the home cage. Mice were checked several times to ensure bleeding had stopped. On a single occasion <10% total circulating blood volume was taken,

up to 3 times a week. <20% could be taken once in a 28-day period, but 50 µl (<10%) was sufficient for FACS analysis.

3.14.6 Cardiac puncture

To get larger volumes of blood cardiac punctures were performed. This procedure is done under terminal anaesthetic. Mice were anaesthetised with isoflurane and were at a surgical plane of anaesthetic throughout the procedure, which was checked by testing the foot withdrawal reflex. A 1 ml syringe with 100 µl heparin (2.5 U/µl) with a 19G needle attached was used to withdraw blood. This was done by insertion of the needle between the ribs. Upon pulling the plunger back, blood was drawn out of the heart. Once 1 ml had been taken, cervical dislocation was used to confirm death. For drug testing the blood was then put into a 1.5 ml collection tube and centrifuged at 14000 rpm for 5 minutes. After centrifugation, serum was removed from the cell pellet with a pipette and put into a fresh 1.5 ml collection tube before being frozen at -20°C. For FACS analysis, 50 µl of whole blood was used for antibody staining as previously described.

3.14.7 Collection of samples from mice

Once mice reached endpoints defined in the license they were killed by cervical dislocation and organs removed for analysis. The spleen livers BM from femurs were regularly collected. The spleen and liver were extracted and weighed before being homogenised using the plunger of a 1 ml syringe and passed through a cell sieve with sterile PBS in order to achieve a single cell suspension. Cells were then counted using trypan blue and methylene blue (3.1.1) before freezing and storage at -80°C. The BM was collected by removing the femurs, and breaking off the kneecap (breaking was used rather than cutting with scissors due to reduced frequency of bone shattering using this method). The bone was then flushed with PBS using a 19G needle in order to remove the marrow.

3.14.8 Histological analysis of samples

When samples were collected from mice, some organs were fixed in formalin and sent for staining with haematoxylin/eosin (H&E) and human CD19 to determine morphology and engraftment of human cells. All of the work was performed by Anna Long in the histology department of the Royal Victoria Infirmary. Samples were decalcified if required using EDTA and x-ray of the samples before being set in paraffin wax, sectioned and mounted on slides. These slides were then used for staining. H&E works by the binding of 2 dyes to positively or negatively charged components in the cell. Haematoxylin is a violet dye, and binds to negatively charged molecules such as DNA and RNA as the stain is positively charged. Eosin is negatively charged and so binds to positively charged amino acids and stains them pink. The L707 presentation cells express CD19 on the cell surface, so organs were stained with an anti-CD19 antibody to determine engraftment. Staining was carried out using a Ventana BenchMark Ultra machine (Ventana, Roche), and the detection kit used was the Ultraview Universal DAB Detection kit. The secondary antibodies in this kit are conjugated to an Ultraview HRP multimer. Which catalyses the oxidisation reaction of the DAB (3,3'-diaminobenzidine tetrahydrochloride) chromogen to produce a brown stain.

3.14.9 Ficoll separation of cells

When cells were collected from the livers of NSG engrafted with 697 cells they were separated from the murine cells using Ficoll-Paque Premium (GE Healthcare) which has a density of 1.077 g/ml and has been optimised for isolating human mononuclear cells from peripheral blood. Livers homogenised by passing through a cell sieve in falcon tubes were topped up to 40 ml with PBS and centrifuged for 5 minutes at 500g. Media was removed and cells re-suspended in 5-10 ml PBS. Ficoll was extracted from the bottle using a needle and added to a 20 ml universal tube, Ficoll was used at a ratio of 4:3 to cells in PBS. The cell suspension was then carefully pipetted onto the Ficoll. The difference in the density between PBS and Ficoll means that the layers do not mix. Samples were centrifuged for 40 minutes at 400g, deceleration was done without a break resulting in a gentle deceleration, to avoid mixing of the separated layers. A glass Pasteur pipette was used to carefully

remove the buffy layer, which contained the lymphoblasts. PBS was added to the sample before centrifugation at 500g for 5 minutes to pellet cells. PBS was removed and the cells re-suspended in 2-5 ml media depending on pellet size. Cells were then counted and used for downstream applications.

3.15 Production of competent bacteria

The mix and go *E. coli* transformation Kit (Zymo Research) is a relatively new method of making competent cells that does not require a heat shock step in order to transform cells. STBL3 bacteria were grown from a stock in a starter culture of 5 ml SOB media for approximately 5h before being used to inoculate 500 ml SOB media. The culture was incubated overnight in a bacterial shaker (200rpm) at 22°C. Optical density was measured the following morning, and once bacteria reached OD_{600nm} of between 0.4-0.6, incubation was stopped. Directly after incubation, the culture was placed on ice to cool for 10 minutes, and all following steps were done on ice. Bacteria were then pelleted by centrifugation at 3000rpm for 10 minutes at 4°C. The supernatant was removed and the cells re-suspended in 5 ml ice cold 1x Wash Buffer. The cells were centrifuged again, the supernatant was removed and the cells re-suspended in 5 ml ice cold Competent Buffer. The culture was kept on ice whilst bacteria were aliquoted in 100-200 µl aliquots in pre-cooled 1.5 ml collection tubes, before storage at -80°C.

3.16 Bacterial transformation

3.16.1 *Chemically competent cells*

Transformation of DNA into bacteria that had been made competent using the traditional chemical method was done as follows. Cells were thawed on ice briefly and mixed by swirling with a pipette tip before 1-10 ng of DNA was added to 50 µl bacteria per transformation reaction and the mix incubated on ice for 30 minutes. The bacteria were heat shocked by incubation at 42°C for 20 seconds, before being returned to the ice for a further two minutes. 950 µl SOC media, without antibiotics was added to the bacteria and the

sample was incubated at 37°C for 1 hour in a heat block with shaking at 300rpm. After 1 hour, 50 µl of the transformed bacteria were spread onto agar plates with the required antibiotics and incubated at 37°C overnight. To maintain competency bacteria were kept on ice at all times.

3.16.2 Mix and Go

To transform using the Mix & Go bacteria, cells were thawed on ice briefly and 1-10 ng DNA added. Bacteria and DNA were left on ice for a further 5 minutes before 50 µl were plated directly onto agar plates with ampicillin (100 µg/ml). Plates were then incubated at 37° overnight.

3.17 Production of LB agar plates

LB agar plates were used to grow colonies of bacteria, which were then used to inoculate larger volumes of LB. They were made by adding 25 g of LB powder and 12.5 g of Bacto agar to a 1 l Duran bottle along with 1 l of DI H₂O. This was then autoclaved to sterilise and melt the agar. This was cooled to around 50°C before the addition of ampicillin (100 µg/ml) and then pouring into 10 cm petri dishes. Pouring was done near a Bunsen burner flame to keep the plates sterile. Poured plates were left for 1-2 hr to set before being dried, inverted in an incubator at 37°C. Plates refrigerated for up to 1 month, and were warmed to 37°C before use.

3.18 Streaking bacteria

Transformed bacteria and bacterial stocks were streaked on an LB plate in order to pick a single colony to expand. This was done by a Bunsen burner flame to keep the LB agar plates sterile. 100 µl of transformed bacteria, or 10 µl bacterial stock was pipetted onto the agar. This was then spread using glass spreader, sterilised in ethanol and then passed through the Bunsen burner flame. Once done, agar plates were incubated inverted at 37°C

3.19 Plasmid purification from bacteria

3.19.1 *Miniprep*

If small quantities of plasmid were required for cloning or sequencing, then the Miniprep kit (Qiagen) was used. This kit is not endotoxin free and so is not suitable for use for plasmids that will be used in tissue culture. 5 ml of LB broth (ampicillin 100 µg/ml) was inoculated with a single colony from an LB plate and grown overnight in an orbital shaker, 200rpm, 37°C. The following morning, 1.6 ml of this culture was pipetted into a 1.5 ml collection tube and centrifuged for 3 minutes at 6800g to pellet bacteria. After removal of the supernatant, 250 µl Buffer P1 containing lyse blue and RNase A (each at 1:1000) was used to re-suspend the pellet. 250 µl of Buffer P2 was added and the solution mixed by inversion 4-6 times. At this point the solution went blue due to the presence of Lyse Blue in Buffer P1, once the colour change had occurred mixing was stopped to avoid the risk of shearing the genomic DNA. 350 µl Buffer N3 was added to the solution before mixing by inversion 4-6 times. The solution went colourless at this point, indicating the SDS had been precipitated. Centrifugation for 10 minutes at 17,900g resulted in a compact white pellet, which contained the cell debris. The supernatant from this was added to a QIAprep 2.0 spin column before centrifugation for 30s at 17,900g to draw the solution through the filter and allow the DNA to bind. All following centrifugation steps were also carried out at 17,900g. The flow through was discarded and the column washed using 500 µl of Buffer PB and centrifugation. After discarding the flow through the column was washed again with 750 µl Buffer PE. The flow through was discarded and the column centrifuged for another minute to fully dry the column. The column was then placed in a clean 1.5 ml collection tube before addition of 50 µl Buffer EB. The columns were left for 5 minutes before centrifugation to elute DNA. DNA concentration was quantified using the Nanodrop before storage at 4°C or -20°C as required.

3.19.2 Maxiprep

The Endofree Plasmid Maxi Kit (Qiagen) works on the same principles as the Miniprep but with an additional endotoxin removal step so that the plasmids can be used in tissue culture. From a single colony a starter culture in 5 ml LB was grown for 8h (200rpm, 37°C) before being used to inoculate 500 ml LB for overnight growth with the same conditions. This culture was then collected the following morning and centrifuged at 6000g for 15 minutes at 4°C using the Avanti J-26 XP centrifuge. The supernatant was discarded and the bacterial pellets re-suspended in 10 ml Buffer P1 with LyseBlue and RNase A by vortexing. 10 ml Buffer P2 was then added to the solution and the tube inverted 4-6 times before incubating at room temperature for 5 minutes. At this point the solution turns blue. During the 5-minute incubation the QIAfilter Cartridge is prepared. 10 ml chilled Buffer P3 is added to the solution next, and after mixing by inversion 4-6 times the solution turns colourless. The solution is then poured into the barrel of the QIAfilter Cartridge before incubating at room temperature for 10 minutes. The cell lysate was passed through the filter by insertion of the plunger and removal of the cap, approximately 25 ml of lysate was recovered. 2.5 ml of Buffer ER was added after filtering and the solution mixed before incubation on ice for 30 minutes. This is the endotoxin removal step. During this time the QIAGEN-tip 500 was equilibrated by the addition of 10 ml Buffer QBT. The filtered lysate was then added to the QIAGENtip 500 and allowed to drip through, at this point the plasmid DNA binds to the resin in the tip. The flow-through was removed and the column washed with 30 ml of Buffer QC twice. After washing, the DNA was eluted with 15 ml of Buffer QN. This was collected and the DNA precipitated by the addition of 10.5 ml isopropanol. This was then centrifuged at 600g for 1h at 4°C. After this centrifugation the supernatant was carefully removed and the pellet re-suspended in 5 ml endotoxin free 70% ethanol before centrifugation at 6000g for 1h at 4°C. The supernatant was carefully removed and the pellet allowed to dry at room temperature before the addition of 500 µl endotoxin free Buffer TE. Plasmids were quantified using the Nanodrop before storage at 4°C.

3.19.3 NucleoBond Xtra midi

For the extraction of DNA to be used in nick hybridisation to make FISH probes the NucleoBond Xtra midi kit (Clontech). This kit is suitable for the extraction of large constructs such as the BAC clones that are used in the production of FISH probes.

500 ml of LB broth was inoculated with a 5 ml starter culture grown from a single colony, picked from an LB agar plate streaked from the bacterial stock. This was grown overnight at 37°C with shaking at 200rpm in an orbital shaker. The following morning bacterial was collected and centrifuged at 6000g for 15 minutes at 4°C in the Avanti J-26 XP centrifuge. The supernatant was removed and the bacterial re-suspended in 12 ml Buffer RES. Bacteria were lysed with the addition of 12 ml Buffer LYS, and the tube inverted 5 times to mix before 5 minutes incubation at room temperature. During this incubation the column filter was inserted into the NucleoBond ® Xtra column and then equilibrated with 25 ml of Buffer EQU. Neutralisation of the lysed bacteria was done by addition of 12 ml Buffer NEU and inversion of the tube 3 times. This lysate was then poured into the column and allowed to flow through. After the lysate had filtered through the column it was washed with 15 ml Buffer EQU before removal of the filter from the column. The column, without filter was then washed with 25 ml Buffer WASH before elution with 15 ml Buffer ELU pre-heated to 50°C. DNA was precipitated from the solution with the addition of 15 ml isopropanol. This solution was then centrifuged at 1000g for 30minutes at 4°C. After centrifugation the supernatant was removed and 4 ml 70% ethanol used to re-suspend the pellet. This was then centrifuged again at 1000g for 5 minutes at room temperature. The supernatant was removed and the pellet allowed to air dry before resuspension in 500 µl buffer TE. Samples were analysed using the Nanodrop before storage at -20°C before use.

3.20 Transfection of 293T cells

Once plasmids were extracted using the Maxiprep kit they were used to make lentivirus by transfection of 293T cells. The protocol used was described in Bomken et al 2013. 293T cells were seeded the day before use at 1.5×10^5 cells/ml in 10cm tissue culture plates. The following day 15 µg transfer plasmid, 20 µg pCMVΔR8.91 packaging plasmid and 5 µg pMD2.G envelope plasmid were mixed and made up to 250 µl by the addition of special H₂O.

To this, 250 µl of 0.5M CaCl₂ was added and samples were mixed vigorously. This solution was then added to 500 µl 2X HeBS dropwise with bubbling to mix before incubation in the CAT II tissue culture hood for 30 minutes. This incubation time allows a precipitate of CaPO₄/DNA to form. If the incubation is too short this will not form, and if it is too long then the precipitate will be too coarse which will result in a less efficient transfection. This solution was then gently added to the 293T cells, which were then returned to the incubator overnight. The following morning the media was carefully removed and the cells washed with 10 ml pre-warmed PBS and removed, before the addition of 10 ml pre-warmed fresh media. Plates were returned to the incubator for a further 3 days, before collection of the supernatant into 50 ml falcon tubes after this time.

3.21 Collection and concentration of lentivirus

The supernatant from the transfected 293T cells was centrifuged at 3000rpm, 4°C for 15 minutes to pellet cell debris before being passed through a 0.45 µm Acrodisc® syringe filter to remove cell debris too small to be pelleted by centrifugation at 3000rpm. 30 ml of the filtered supernatant was then added to ethanol sterilised thickwall-style (open-top) polyallomer Konical™ (Beckman Coulter) tubes. Which were then put into the SW28 swinging bucket rotor tubes (Beckman Coulter) with Derlin™ PKGED'1 adaptors (Beckman Coulter). The use of adaptors stops the tubes from collapsing during centrifugation. The tubes containing the samples were weighed to ensure the centrifuge was balanced before centrifugation for 2hr at 26000rpm, 4°C in an Optima™ XL-100K (class S) preparative ultracentrifuge (Beckman Coulter). After centrifugation the supernatant was discarded by gentle inversion and the tubes allowed to dry. The lentivirus was re-suspended in an appropriate volume of media dependent on the cells in use further downstream.

3.22 Transduction of leukaemic cells

Transduction of cells was carried out using spinfection with polybrene as a transduction agent. Cells were counted and split to 1x10⁶ cells/ml and 1 µl 8 µg/ml polybrene was added per ml. 500 µl of cells were pipetted into the wells of a 48 well plate and lentivirus added to

each well. Unless primary material was being transduced then several volumes of lentivirus were used (1-30 µl). PBS was added to wells around the edge of the plate and plates were sealed with Parafilm to avoid evaporation of media. Spinfection was carried out by centrifugation at 900g for 50 minutes at 34° C. After centrifugation Parafilm was removed and the cells returned to the incubator overnight. The following morning ~350 µl media was removed and 500-800 µl of fresh pre-warmed media added. After a further 3 days incubation cells were ready for FACS analysis or puromycin selection.

The protocol with the primary derived L707 cells differed a little from that for the cell lines used, mainly in the concentration of cells used for the transduction (up to 5×10^6 /well of a 48 well plate) and the volume of lentivirus used. The primary derived cells were centrifuged at 350g for 5 minutes and then re-suspended in lentivirus in order to maximise transduction levels.

3.23 FISH

All FISH (Fluorescent *in situ* hybridisation) protocols were kindly taught by Lisa Jones and Lisa Russell, they also provided the reagents for nick translation and FISH that were not included in the nick translation kit such as the spectrum red labelled dUTP and sephadex columns.

3.23.1 Nick translation

Nick translation is the method by which Bacterial artificial chromosome (BAC) clone DNA is tagged with fluorescently labelled nucleotides for the visualisation of binding of the probe to genomic DNA for FISH. This was done with DNA extracted using the NucleoBond Xtra kit (Macherey Nagel).

0.5 ml collection tubes were chilled on ice before use, to these tubes 10 µl dNTP, 5 µl dTTP and 5 µl nick translation buffer were added. 2.5 µl of dUTP labelled with spectrum red was also added and the sample was mixed by vortexing before centrifugation to remove reagents from the sides of the tubes. 17.5 µl of DNA was added to this before gentle mixing using a

pipette. 10 µl nick translation enzyme was added to this before incubation at 15°C overnight. The following morning, 3 µl of 0.5 M EDTA was added to the samples and left to incubate whilst the Sephadex columns were prepared. This was done by removal of the bottom of the tube before it was put in a 1.5 ml collection tube before centrifugation for 1 minute at 4000rpm. The flow through was discarded and the column placed in a 1.5 ml collection tube. The entire sample was then pipetted into the centre of the column and spun for a further 2 minutes at 4000rpm. The column was discarded and to the flow through 10 µl of human cot-1 DNA, 6 µl of 3 M sodium acetate and 160 µl of ice cold ethanol was added. This was then incubated at -80°C for 2 hours before centrifugation at 13000rpm for 30 minutes at 4°C to pellet the probe. The supernatant was carefully discarded and the pellet allowed to air dry in the dark before resuspension in 14 µl hybridisation buffer. 6 µl of nuclease free H₂O was added to this before allowing the probes to dissolve at room temperature in the dark. Once probes were dissolved they were stored at -20°C until use.

3.23.2 *Slide preparation*

Samples were thawed using the method described previously (3.1.5) before being centrifuged at 1200rpm for 5 minutes. The supernatant was discarded and 10 ml 0.075M potassium chloride was added. This was incubated for 10 minutes at 37 °C before centrifugation at 1200rpm for a further 5 minutes. The supernatant was discarded and the pellet disrupted by vortexing. 1 ml of fixative (3:1 methanol:acetic acid) was added dropwise to the pellet whilst vortexing. This was done to avoid clumping of the cells. A further 4 ml of fix was added before centrifugation at 1200rpm for 5 minutes to pellet fixed cells. After removal of the supernatant 1 ml of fresh fixative was added and cells were stored at -20°C. The addition of potassium chloride before fixing causes the cells to swell, which results in the plasma membrane erupting when they are dropped onto the slide. This makes probe binding more efficient.

Before use fixed cells were centrifuged at 1300rpm for 2 minutes and 1 ml of fresh fixative added. 2.5-3 µl of cells were then dropped onto a pre labelled slide, washed with fixative. Slides were allowed to air dry on a damp piece of blue roll and cell density was checked with

a microscope. If cells were not dense enough, then the process was repeated. Once the desired amount of cells were on the slide it was dried on a hot plate at 60°C for 10 minutes.

3.23.3 Hybridisation

Once cells were made hybridisation was used to mark the DNA with fluorescent probes. Homemade probes were mixed to make a working stock of the 3 spectrum red labelled NR3C1 probes at a 1:1:1 ratio. This was then used to make a master s containing 1 µl Green 5p telomere probe (Cytocell), 2 µl pooled Red NR3C1 probe and 1 µl hybridisation buffer for each slide. This was then applied to a 22 mm coverslip and the slide gently lowered onto this. Bubbles were removed by gently pressing with a pipette tip and the coverslip sealed with rubber cement. Slides were transferred to a HiBrite (Abbott Molecular) and hybridised at 72°C for 5 minutes and 37°C overnight.

The following morning the rubber cement was removed from the slide before they were immersed in a pot of 2X SSC (sodium citrate and sodium chloride) (Thermo Fisher Scientific) to allow the coverslip to soak off. Once the coverslip had detached, the slides were submerged in pre-heated (72°C) buffer 1 for 2 minutes. After 2 minutes, slides were removed and put into buffer 2 for a further 2 minutes. DAPI was dropped onto cover slides and the slide, once excess buffer 2 was blotted off was lowered onto this, bubbles were removed using a pipette tip to gently press the bubbles out. Slides were cleaned using ethanol and a lint free tissue before being mounted onto the microscope platform.

3.23.4 Capture and scoring of cells

Slides were mounted onto the microscope platform for capture using a GSL-120 slide loading fluorescence microscope (Leica) with an 8 bay motorised stage. This microscope is part of the Leica CytoVision platform and is able to automatically scan and capture FISH slides. All slides were scanned using a 10x objective to determine cell location, before being captured using a x60 objective. The scores allocated by the CytoVision 7.2 software were reviewed by myself and Lisa Jones, and the average of our findings used for further analysis.

Several healthy controls, kindly given by the Leukaemia Research Cytogenetics Group from their pool of controls were run alongside the samples in order to determine a lower cut-off for positivity (Table 16). The standard cut-off, as used by the Leukaemia Cytogenetics Research Group was the average of 3 controls + 3 standard deviations, which for this set of experiments was 5.96% (Table 17).

Control	Percentage Abnormal cells
Control M	5.6
Control C	5.5
Control 141701	5.7

Table 16: Percentage of cells with any abnormal cells (not 2R2G) in healthy control samples as determined by FISH. Percentages are the average of 2 scores by different people, approximately 1000 cells were scored for each sample.

Average	5.6
1 standard deviation	0.125
3 standard deviation	0.377
Average + 3 standard deviation	5.96

Table 17: Calculations used to determine the cut-off for heterozygosity in L707 presentation samples treated with Dex in vivo.

3.24 Microarray analysis

3.24.1 GenomeStudio and Excel

Data returned from oxford Genomics in the form of encrypted IDAT (intensity data files) files, with a file for each the red and green probes. These were imported into GenomeStudio, an Illumina software for the analysis of microarrays. Data was normalised using quantile and the background was subtracted. Illumina recommended statistics applied to the data before comparisons were run between primary and secondary presentation vs primary and secondary relapse. The resulting data, with p.values for both probe binding and

differential expression were exported to Excel for further manipulation. In Excel, the sort function was used to select probes dependent on several parameters; p.value <0.01, fold change >2 in either direction and probe binding of at least 1 sample >100. This resulted in a list of genes with differential expression that were expressed well above background in at least one condition and were significantly different between presentation and relapse. No further statistics were applied to the data after the Illumina recommended stats in GenomeStudio, meaning the data had no corrections for multiple testing

3.24.2 R packages

Microarray data was analysed by myself after completion of the 5-day R and Bioconductor course provided by the bioinformatics support unit. Scripts that were adapted for use with this data were provided in the hand out from this course (Produced by Dr. Simon Cockell).

The workflow for microarray analysis is outlined in Figure 18. Raw data in the form of IDAT files were imported into R using the read function of the Illumina microarray specific programme, Lumi. Data was transformed using variance stabilisation transformation (VST) before being normalised using robust spline normalisation (RSN). VST takes advantage of the large number of technical repeats in the Illumina microarrays to stabilise variances between the bead replicates within a single bead chip (Lin et al. 2008). RSN normalises the data between chips, it does this using both quantile and loess normalisation (Du, Kibbe, and Lin 2016). Quality control and filtering resulted in any probes that failed to meet the detection call thresholds applied by Lumi being discarded. This filtered data was used with Limma to determine which of the remaining probes were significantly different between conditions and a ranked gene list produced. Limma used t-statistics to determine significance, and the Benjamini-Hochberg method to correct data and produce a false discovery rate statistic. This list was then used for gene ontology statistics to determine which pathways were significantly upregulated in the samples.

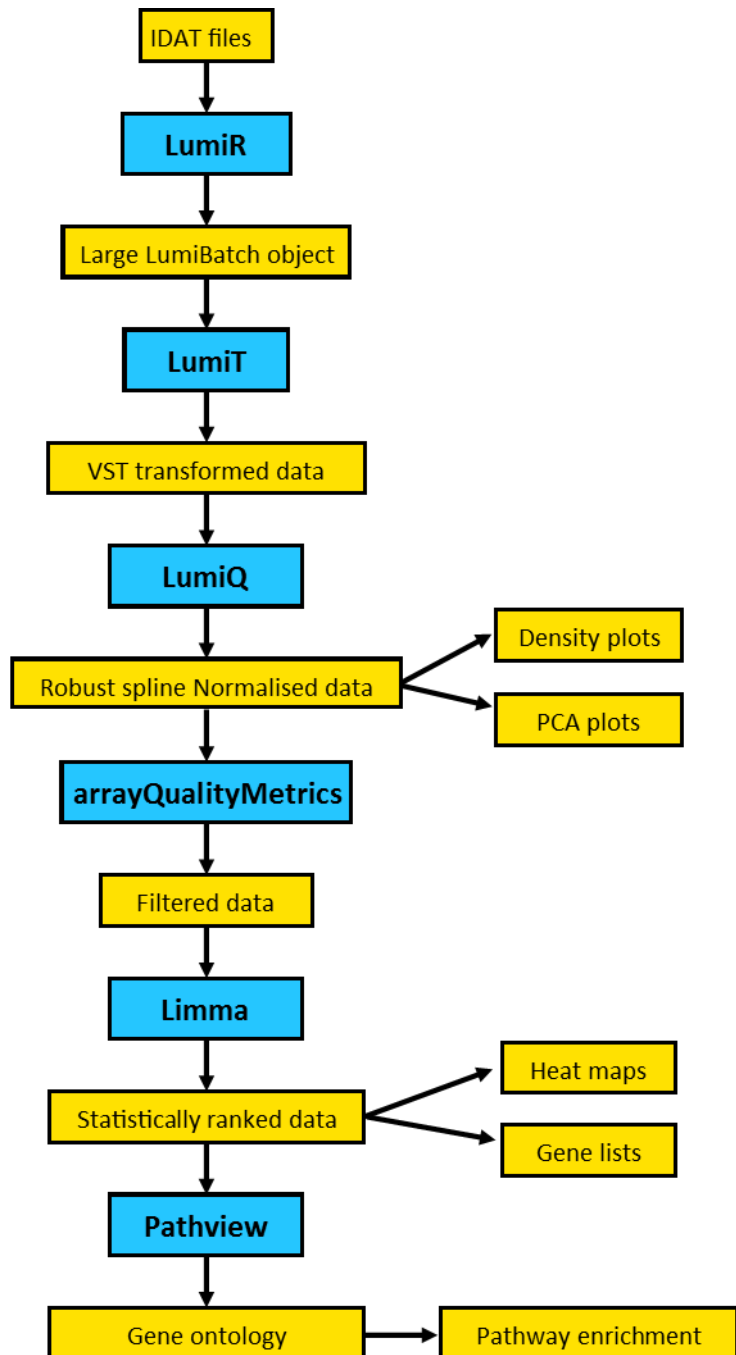


Figure 18: The workflow used for analysis of microarray data using the Lumi and Limma method. Input and output files are in yellow boxes whereas the programmes used are in blue boxes. The workflow is the gold standard for analysis of microarray data.

3.25 GATK whole genome sequencing analysis

The Genome Analysis Toolkit (GATK) is a suite of programmes produced by the Broad Institute for the analysis of whole genome sequencing data (McKenna et al. 2010; DePristo et al. 2011; Van der Auwera et al. 2013). It is widely considered the gold standard for whole genome data variant analysis (Figure 19).

GATK comprises three main steps;

1. **Pre-processing**; this is the process that transforms a raw FASTQ file into an aligned BAM file. The alignment used is Barrows Wheeler Alignment (BWA). Duplicates are marked and the samples are sorted.
2. **Variant discovery**; this is the main step and uses the aligned BAM file to produce a list of variants, this is done by looking at regions with genetic variation in order to call variants resulting in the production of a VCF call set file
3. **Call set refinement**; variants in the form of VCF files are refined, annotated and evaluated, this is done using the Variant effect predictor (VEP) programme from Ensembl for all variants with more than 10 supporting reads.

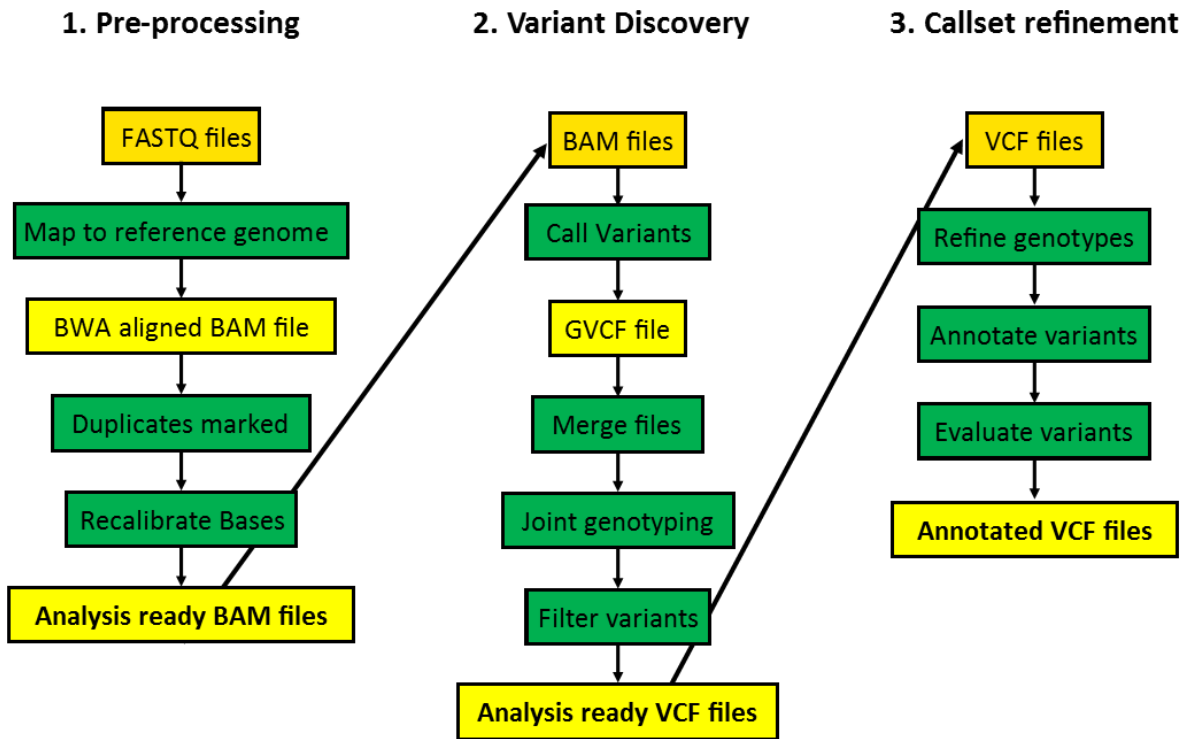


Figure 19: The workflow for GATK processing of whole genome sequencing data. Yellow boxes indicate input and output files; green boxes indicate data manipulation. Workflow obtained from the GATK best practices, available on the Broad Institute website (Van der Auwera et al. 2013; DePristo et al. 2011; McKenna et al. 2010)

3.26 RNA sequencing analysis

Raw data was returned from AROS in the form of FASTQ files. Quality control was run on these files and the parameters needed for further analysis such as the median insert size, standard deviation and pair orientation were determined using the Picard metrics tool. Once files had passed quality control, analysis was done using the Cufflinks suite of programmes, which was done by myself with significant help from Ben Allen at the bioinformatics support unit. The workflow is outlined in Figure 20. Briefly, the reads were mapped to a bowtie2 generated genome index (hg19) using the programme Tophat. These reads were then assembled into transcripts using Cufflinks and the final transcript assembly was done with Cuffmerge. To determine differentially expressed transcripts Cuffdiff was used. The output from this is a list of differentially expressed transcripts which can be used with CummeRbund to generate plots in R as well as for gene ontology.

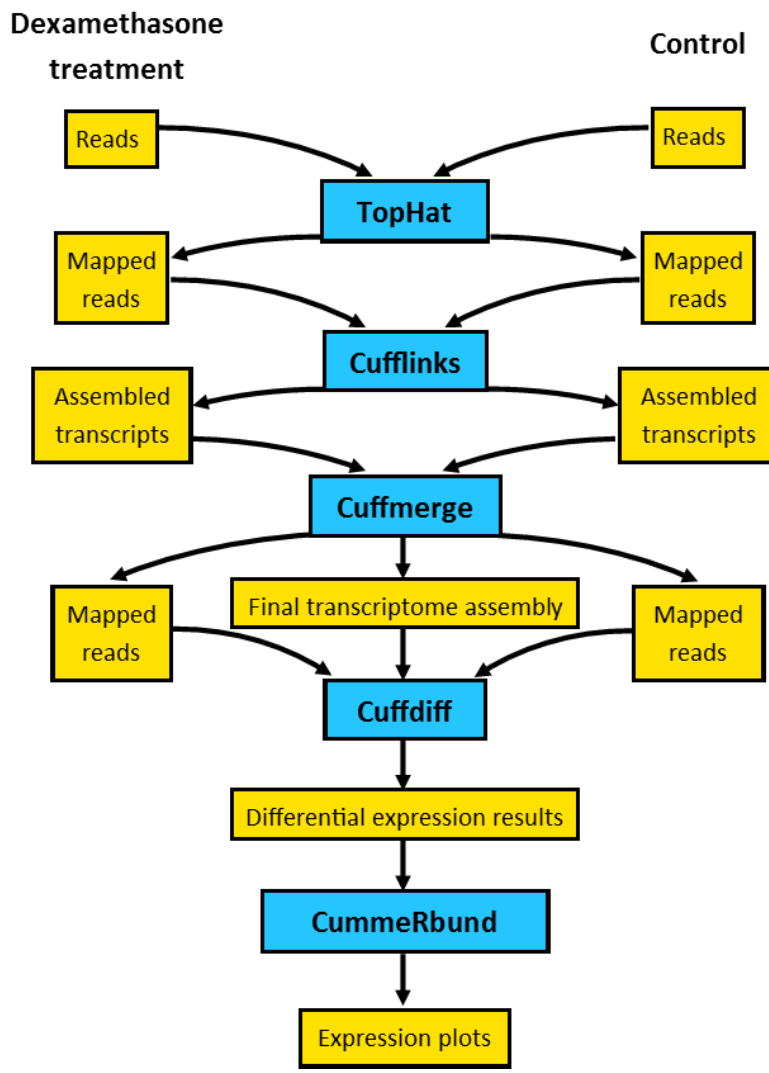


Figure 20: Workflow used for the analysis of RNA sequencing using the Cufflinks suite. Blue boxes denote programmes and yellow boxes are input and output files.

3.27 CRISPR screen specific methods

3.27.1 Transduction of electrocompetent bacteria and plasmid collection

The lentiCRISPRv2 GeCKO library is a plasmid library that contains over 122000 sgRNA targeting the whole genome. There are 6 sgRNA for each gene and 4 for each miRNA in the library, it comes as two separate half libraries, A and B with each library containing half of the sgRNA for each target. The plasmid library was designed and used in the papers from the Zhang lab at MIT (Shalem et al. 2014; Sanjana, Shalem, and Zhang 2014). The library was purchased from Addgene, was transformed into electrocompetent cells as per the library protocol (Sanjana, Shalem, and Zhang 2014; Shalem et al. 2014). The E. cloni 10G SUPREME Electrocompetent *E. coli* cells (Lucigen) were used for this. Cells were thawed on ice and the entire 25 µl transferred to 1mm electroporation cuvettes (PeqLab), with 75 µl sterile RNase free H₂O to increase volume to 100 µl. 2µl of the GeCKO lentiCRISPRv2 library DNA (50 ng/µl) was added followed by 20 minutes incubation on ice before electroporation at 2500V using a Stratgene 1000 electroporator. To recover cells from the cuvette, 900 µl SOC media (pre-warmed to 37°C) was added. A further 1 ml of pre warmed SOC media was also added. The samples were incubated for 1hr at 37°C with shaking at 250rpm without antibiotic. For each library a total of 4 electroporations were done.

After 1hr incubation the samples were pooled into the two libraries (8 ml each). 400 µl of the transformation mix was pipetted onto LB agar plates containing ampicillin (100 µg/ml) and spread. 20 plates were used for each library, resulting in 40 plates in total. As well as these 40 plates a dilution plate was made for each library to determine the coverage of the library. 10 µl transformation mix was added to 1 ml of SOC media, and 20 µl of this pipetted onto an LB agar plate and spread. The colonies on this plate represented a 40,000-fold dilution of the un diluted plates. If the colonies on this plate, when multiplied by 40,000 was more than 3x10⁶ library coverage would be at least 50X.

All plates were grown inverted for 14h overnight at 34°C. The lower incubation temperature results in reduced recombination within the lentiviral LTR (long terminal repeats). The following morning bacteria were recovered from the plates by adding 500 µl LB broth to each plate and scraping colonies off before pipetting into a 50 ml falcon tube. The plates were washed to ensure maximum colony collection with a further 500 µl of LB broth. All

plates were collected and tubes were centrifuged at 6000g for 10 minutes at 4°C to pellet bacteria. The supernatant was removed before weighing of pellets and freezing at -20°C for use later.

The dilution plates each had >1500 colonies, which equates to 6×10^7 colonies total for each of the libraries. This represents approximately 490x coverage of the plasmid library.

Plasmids were extracted from bacterial pellets using the Maxiprep kit (3.19.2), with 14 and 13 Maxipreps used for library A and B respectively.

3.27.2 Transfection of 293T cells and collection of lentivirus

The lentiCRISPR library was transfected into 293T cells using the protocol described previously (3.20). However, it was done on a much larger scale, with 48 100cm tissue culture dishes seeded with 293T cells used. These larger TC plates roughly equate to 3 100mm plates each, and hold 30 ml of media. The transfection was scaled up to accommodate this.

Lentivirus was collected as per the original protocol (3.21) and a total of 8 ultracentrifuge spins were used over 2 days to concentrate it. The final lentivirus was re-suspended in a total of 4.5 ml SFEM II media with 20% FBS.

3.27.3 Transduction and selection of L707 presentation cells

On the day of transduction 3 vials of L707 presentation cells were thawed, after washing in pre-warmed SFEM II media and counting, 4.7×10^7 cells were re-suspended in the 4.5 ml lentivirus and a further 11.5 ml media containing 1% pen/strep, 20% FBS with 20 ng/ml IL-3 and 10 ng/ml IL-7. 15 µl, 8 µg/ml polybrene was added to this to aid transduction. Cells were then pipetted into 30 wells of 2 48 well plates, approximately 1.5×10^6 cells/well. Plates were wrapped in Parafilm before centrifugation for 50 mins at 900g, 34°C. After centrifugation the Parafilm was removed and cells placed in an incubator at 37°C overnight.

The following morning, ~350 µl media was removed and 500 µl fresh media added. Cells were transferred to 24 well plates and returned to the incubator for 72h.

After 72h growth to allow the expression of the plasmid, cells were selected with puromycin. 0.25 µg/ml was added to cells for 48 hr before being increased to 0.5 µg/ml for a further 24 hr. At this point cells were counted and washed twice in PBS, counted and re-suspended in SFEM II media for intrafemoral injection into 15 NSG mice (10^5 cells/mouse). After puromycin selection there were approximately 45% viable cells in the sample.

3.28 Production of amplicon library for lentiCRISPR screen

After DNA was extracted from samples from mice engrafted with L707 presentation CRISPR cells it was used in a two-step PCR process to create an amplicon library that was used for next generation sequencing. To 0.5 ml PCR tubes 825 ng DNA was added along with 1 µl primer mix (50 µM) and 12.5 µl of Phusion® High-Fidelity PCR Master Mix with HF Buffer (Table 18). RNase free H₂O was used to make this volume up to 25 µl before samples were centrifuged and according to the temperatures in Figure 21. A total of 5 reactions was done for each sample. This was chosen after discussion about coverage with a bioinformatician, 5 was determined to give enough coverage without increasing the number of PCR reactions too much.

Reagent	Volume(µl)
DNA	825 ng
50 µM Primer Mix	1
2x Phusion® High-Fidelity PCR Master Mix with HF Buffer	12.5
H ₂ O	Up to 11
Total	26

Table 18: Reagents and volumes of each required for the first step amplification PCR of genomic DNA for the lentiCRISPR samples before the addition of the barcodes and illumina adaptors required for sequencing on the HiSeq.

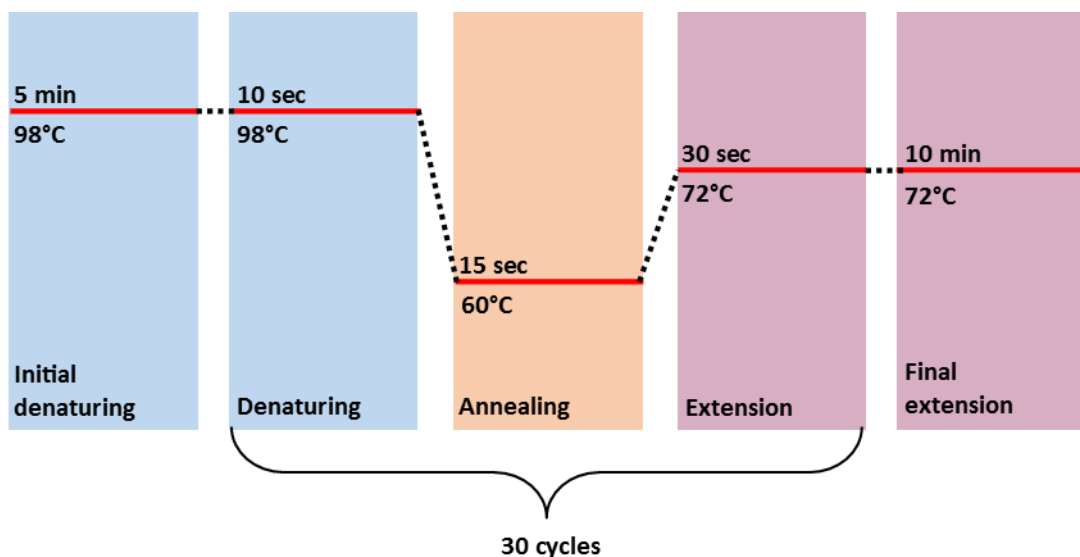


Figure 21: The GeneAmp 9700 Thermo Cycler settings for both the first and second step PCR reactions used in the preparation of the lentiCRISPR amplicon library.

Due to problems with previous sequencing runs some samples were amplified from pre-amplified material where there was no DNA left. Each pre-amplified sample was the result of 5 PCR reactions that were pooled, and where there wasn't enough genomic DNA left, 1 µl of these pooled samples was used for each PCR. The resulting 5 PCR reactions (from genomic or pre-amplified DNA) were pooled and concentrated using the QIAquick PCR clean-up kit (Qiagen) and eluted in 20 µl of EB buffer and used for the second step PCR to add the Illumina adaptors. The second PCR was done in a 0.5 ml PCR tube and all the reagents were added before centrifugation and then running on a thermocycler. This PCR used a universal forward primer (50 µM), and a barcoded reverse primer (50 µM) so that samples could be de-multiplexed after the sequencing run. 1 µl DNA from the pooled first step PCR reactions was used (Table 19). The same temperatures were used for the second PCR as for the first (Figure 21).

Reagent	Volume(µl)
Pooled, concentrated DNA	1
Universal forward primer (50 µM)	0.5
Barcoded reverse primer (50 µM)	0.5
2x Phusion® High-Fidelity PCR Master Mix with HF Buffer	12.5
RNase H ₂ O	10
Total	26

Table 19: Reagents and volumes required for the second step PCR in which amplified DNA has adaptors and a barcode added.

DNA was amplified using primers located close to the sgRNA region but the amplicon from this reaction was less than 100bp, which is the smallest recommended amplicon for retrieval using the PCR clean up kit (Qiagen). In order to avoid this issue, the forward and reverse primers also had CS1/2 sequences. These sequences were originally designed so that the samples could be used with the Fluidigm system, but after this did not work they were kept to increase amplicon size. The PCR clean up kit was used to concentrate and purify products before the second step of PCR. The second round of PCR added the adaptors and barcodes required for multiplexing and sequencing on the Illumina HiSeq2500 (Figure 22).

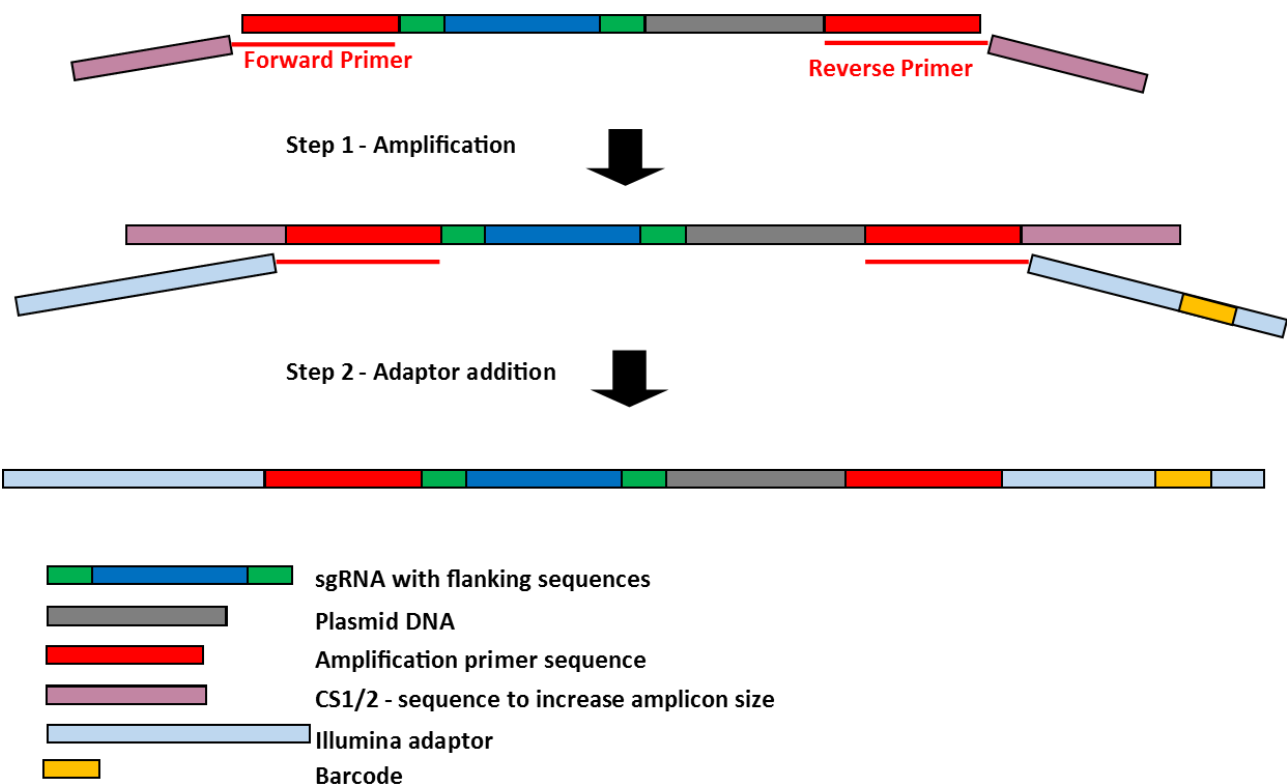


Figure 22: Scheme showing steps in the 2 step PCR process to produce amplicons used for next generation sequencing. Genomic DNA is extracted and the 1st step PCR used to amplify material. Amplification primers had the addition of CS1/2 sequences in order to ensure the amplicon was more than 100bp and so could be used with PCR clean up columns. The 2nd step PCR replaces these sequences with the standard Illumina adaptors with a barcode.

Before being sequenced, samples were run on a large 1.5% agarose gel at 70V for 1.5hr and the band at 216bp extracted (Figure 23). This was purified using the QIAQuick Gel extraction kit (Qiagen), samples were quantified using the Nanodrop and pooled into 7 samples before being sent for sequencing by AROS using an Illumina HiSeq2500 with v4 chemistry.

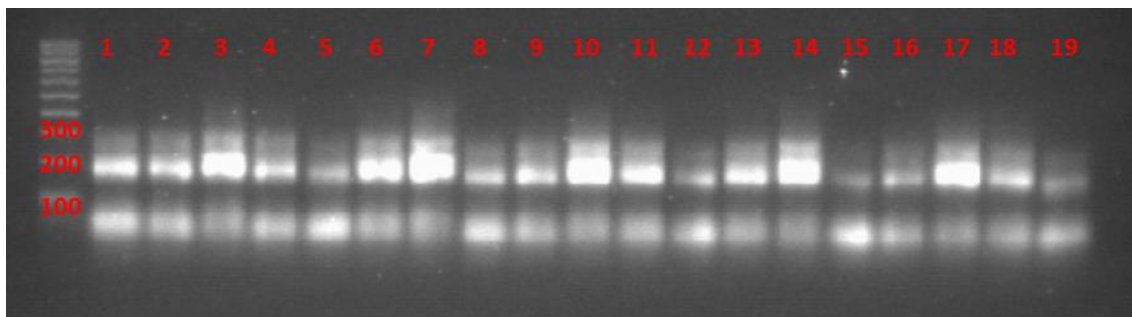


Figure 23: Analytical gel of amplified DNA with the adaptors and barcodes added. First 19 samples are shown. The expected amplicon is 216bp which is reflected by the higher band, the lower band reflects primer dimers. The gel shows smeared bands due to the high levels of DNA loaded in each well, a consequence of the high concentrations after several amplifications and PCR concentration.

3.29 Data Analysis of lentiCRISPR screen

All of the analysis of the raw FASTQ files and MAGeCK (Model based analysis of genome wide CRISPR/Cas9 knockout) analysis was done by Dr Matt Bashton. First reads were trimmed down from the 50bp read output from the HiSeq2500 to the 20bp sgRNA sequence. For trimming the sequence of the CACCG adaptor was used to ensure the sgRNA was selected rather than using hard coded bp position, this avoided loss of reads through artefacts that resulted in shifts in reads. Once reads were trimmed, a false genome of the sgRNA in the screen was created using Bowtie2 and reads were aligned to this. Read counting was done using the count function of MAGeCK, before normalisation by mean variance.

The workflow of data analysis is outlined in Figure 24. Once reads had been trimmed, aligned and counted they were normalised using median normalisation. Significance calculations and ranking is done using mean-variance modelling and modified robust rank aggregation (RRA), which utilises an algorithm that assumes sgRNA with no effect will be evenly distributed throughout the sample, comparison of actual sgRNA frequency to the model can then be used to find which sgRNA have an effect. Genes are also ranked using RRA, dependent on the location of the sgRNA for that gene in the list of ranked sgRNA (Li et al. 2014).

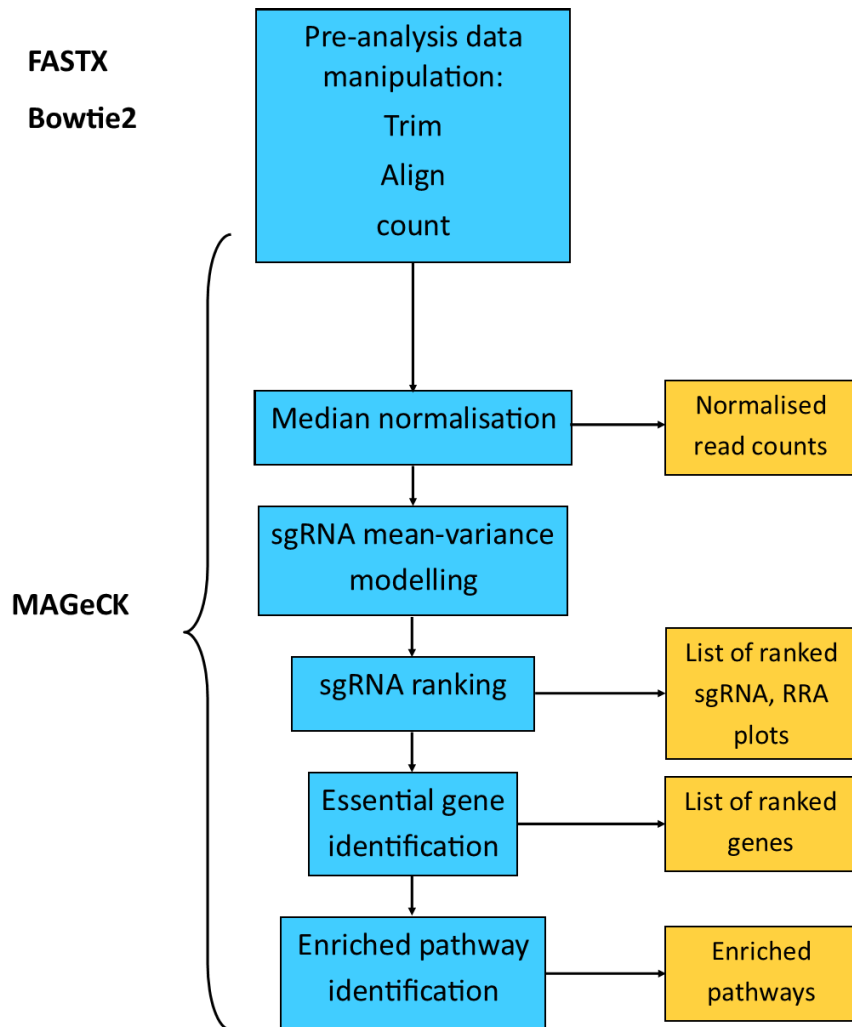


Figure 24: Workflow of data analysis used for the lentiCRISPR screen. The programme MAGeCK is a purpose designed software for whole genome screens using lentiCRISPR plasmids. Blue boxes indicate functions and yellow boxes indicate output files. Programmes used are indicated to the left.

3.30 Cloning CRISPR plasmids

sgRNA constructs were inserted into the lentiCRISPRv2 plasmid using the protocol published by the Zhang lab, who created the plasmid (Sanjana, Shalem, and Zhang 2014; Shalem et al. 2014). In a sterile 0.5 ml tube 1 µg lentiCRISPRv2 plasmid was added to 0.5 µl BsmBI (10 U/µl), 0.5 µl FastAP (10 U/µl), 1 µl 20 mM DTT (Dithiotheritol), 2 µl 10X Tango Buffer and made up to 20 µl with RNase free H₂O (Table 20). This was centrifuged to bring the reagents to the bottom of the tube before being placed in the GeneAmp 9700 Thermo Cycler for 1hr

at 37°C. After restriction, 5 µl loading dye was added and the whole sample run on a 1% agarose gel at 70V for 1.5hr. After visualisation using UV two bands were visible at 12.8kbp and 2kb. The larger of these two was cut out and extracted from the gel using the QIAquick Gel Extraction kit (Qiagen) and stored at -20°C before use. FastAP was used to de-phosphorylate the restricted ends of the plasmid which aids in ligation with a phosphorylated insert.

Reagent	Volume(µl)
lentiCRISPRv2 plasmid (1 µg/µl)	1
BsmBI (10 U/µl)	0.5
FASTAP	0.5
20 mM DTT	1
Tango Buffer	2
RNase free H2O	15

Table 20: Reagents and the volumes required of each for BsmBI digestion of the lentiCRISPRv2 plasmid.

Before the oligos could be ligated into the restricted plasmid the sense and antisense strands were annealed. 1 µl of both the sense and antisense oligos were added to a 0.5 ml collection tube along with 1 µl T4 DNA ligase buffer (10X) and 1 µl T4 Polynucleotide Kinase (10 U/µl) (Table 21). This was made up to 10 µl with RNase free H2O and after centrifugation and annealed using the following temperature profile; 37°C for 30 minutes, 95°C for 5 minutes, 70°C for 10 minutes, 25°C for >2hrs. Samples were then taken out of the GeneAmp 9700 Thermo Cycler and left on the bench overnight. Phosphorylation of the sgRNA was done at the same time by the addition of T4 Polynucleotide Kinase (PNK) (10 U/µl), this aids ligation into the de-phosphorylated plasmid.

Reagent	Volume(µl)
Sense oligo (100 µM)	1
Anti-sense oligo (100 µM)	1
T4 DNA ligase buffer (10X)	1
T4 Polynucleotide Kinase (10 U/µl)	0.5
RNase free H ₂ O	6.5

Table 21: Reagents and the volumes required of each to anneal the sense and antisense sgRNA oligos before cloning into the restricted lentiCRISPRv2 plasmid.

Annealed oligos were diluted 1:200 in RNase free H₂O before ligation into the restricted lentiCRISPRv2 plasmid. Ligation was done at approximately a 1:10 molar ratio, with 50 ng restricted lentiCRISPRv2 plasmid, 1 µl of the diluted annealed oligos, T4 DNA ligase (10 U/µl), T4 DNA ligase buffer (10X) and RNase free H₂O, to make a total volume of 10 µl (Table 22). Ligation was carried out on the bench at room temperature overnight. The following day ligation products were transformed into stbl3 according to 3.16.2. Bacteria were spread on agar plates containing ampicillin (100 µg/ml) and incubated overnight, colonies were picked the next morning and used to inoculate 5 ml of LB broth, which was grown for 8h at 37°C with shaking at 200rpm. Bacteria was collected and the plasmid DNA extracted using a Miniprep kit (3.19.1) Plasmid DNA was sent for Sanger sequencing (Source Bioscience, UK) to check the correct insertion of sgRNA before being expanded and a maxiprep (3.19.2) done to get DNA for transfection of 293T cells. All single gene knockouts were done with a pool of 6 sgRNA targeting one gene.

Reagent	Volume(µl)
BsmBI digested plasmid (25 ng/µl)	2
Diluted oligo complex	1
T4 DNA ligase (10 U/µl)	0.5
T4 DNA ligase buffer (10X)	1
RNase free H ₂ O	5.5

Table 22: Reagents and the volumes required of each for the ligation of the annealed sgRNA oligos into the digested lentiCRISPRv2 plasmid.

Chapter 4: Investigation of mechanism of relapse using paired presentation and relapse ALL: The L707 cells

4.1 Introduction

The investigation of the emergence of relapse and the acquisition of drug resistance in ALL is an important area of study, as relapse and the often associated loss of chemosensitivity represent a significant number of deaths in paediatric ALL cases. The use of matched presentation and relapse samples represent an excellent model that has been used for several studies including the determination of the origin of relapses in ALL (Mullighan et al. 2008), comparison of the immunophenotypic characteristics of presentation and relapse in ALL (Eveillard et al. 2013) and investigations into the genesis of therapy resistance (Buijs et al. 2014). The use of matched pairs generally relies on the sequencing of DNA from samples rather than the culture of primary material. This is partly because the culture of primary material is more troublesome than cell lines due to issues with viability and proliferation *in vitro*. The engraftment of primary ALL samples in immunocompromised mice has proven to be invaluable for the evaluation of the disease. This technique has allowed for investigation of leukaemic stem cells in ALL (le Viseur, Hotfilder, Bomken, Wilson, Rottgers, Schrauder, Rosemann, Irving, Stam, Shultz, Harbott, J??rgens, et al. 2008), drug testing (Leclerc et al. 2016; Tomkinson et al. 2003) and the expansion of cells for *ex vivo* manipulation. Several studies have been undertaken to evaluate the correlation between primary samples and xenograft samples and the results are encouraging for research using these models. The rate of engraftment of relapse samples has been found to be correlated to the length of remission, indicating preservation of disease aggressiveness. These rates were stable for at least 6 engraftment passages and the immunophenotype was often maintained over several passages, as were rearrangements of antigen receptor genes (Lock et al. 2002). Importantly for the investigation of the acquisition of resistance, the drug sensitivity profile of xenograft cells has been shown to be stable over several xenograft passages (Liem et al. 2004; Lock et al. 2002). It should be noted that xenograft models have not been so favourably reported for other diseases however. Murine models of hepatocellular carcinoma show very different microarray profiles compared to primary tumours even when injected orthotopically (W. Wang et al. 2015). The reported success of ALL xenografts could be due to the nature of ALL,

being a haematological malignancy it might be better able to engraft in a way that mirrors the original disease. It could also be that there is lesser impact on the cells of the differences between the human and murine BM niche.

The L707 patient samples are a matched presentation and relapse from a patient with pre B-ALL carrying the t(17;19) translocation. The patient was a 16-year-old female who presented with a dexamethasone (Dex) sensitive t(17;19) pre B ALL. The patient was treated according to regimen B of ALL 2003 and was MRD negative at day 28. However, the patient suffered a relapse within 5 months and despite further treatment (R3 and then FLAG), re-induction of remission was not possible. The patient developed encephalopathy and died from an intra-cranial bleed 2 months after relapse. Cytogenetics for presentation and relapse are detailed in Table 23.

The L707 presentation and relapse cells were investigated by Dr. Elda Latif and all the initial data on engraftment and Dex resistance were obtained during her PhD. The percentage of leukaemic blasts in the primary patient BM was found to be 99% and 97% for the presentation and relapse respectively, and the cells were found to be CD10⁺, CD19⁺, CD20^{lo/negative}, CD34^{negative} at both presentation and relapse. The intra-femoral injection of the primary samples into NSG mice resulted in rapid engraftment, with splenomegaly as well as some mice exhibiting ovarian tumours, leg tumours, engraftment of the gastric lining and brain stem engraftment (Latif 2012).

Time-point	Karyotype
Presentation	46,XX,der(19)t(17;19)(q2?;p13)[12]/46,idem,fra(10)(q25)[17]/46,XX[1].ishder(19)t(17;19)(19ptel-,wcp17+,wcp19+,19qtel+)
Relapse	46,XX,der(19)t(17;19)(q2?;p13)[5]

Table 23: The karyotype of the L707 cells at presentation and relapse, work carried out by NHS cytogenetics services as part of normal treatment protocols (Latif 2012).

Genetic characterisation of the L707 presentation and relapse using the Affymetrix 500k array and SNP6 array revealed that there was a 5q deletion at 5q31.3-q32. This deletion was present in the relapse and maintained in the relapse xenograft samples with the same

breakpoints indicating little change between primary and xenograft samples. The 5q deletion spans 6 genes; NR3C1, FGF1, ARHGAP26, HMHB1, YIPF5 and KCTD16 (Latif 2012).

The aims of this work were to investigate the mechanisms of relapse and Dex resistance in ALL. The use of paired presentation and relapse samples represents an excellent way to determine the driver genes behind the emergence of relapse in ALL. To complement this, the Dex sensitivity of the presentation, and the resistance in the relapse makes this case a useful tool for the investigation of the acquisition of Dex resistance in ALL.

4.2 Differential gene expression profile between presentation and relapse in the L707 cells

In order to augment the data obtained during Elda's PhD, and look further into differences in the gene expression profile between the presentation and relapse samples, microarray analysis was carried out. Samples were collected from mouse spleens and the Ambion MirVana total RNA kit was used to extract RNA under instruction from Oxford Genomics, the company that carried out the microarray. Samples were originally going to be sorted prior to RNA extraction but FACS analysis revealed that the engrafted spleens were ~98% human cells, so this was not necessary. 12 samples were sent for analysis, 6 presentation and 6 relapse representing both earlier primograft and later secondary engraftments of the L707 cells into NSG mice, these samples were labelled primary and secondary respectively (Table 24).

Array Location	Sample	Mouse	Label
K1	L707 Presentation primograft	F4033 LN	Primary
K2	L707 Presentation primograft	F4033 NN	
K3	L707 Presentation primograft	F4033 NN	
K4	L707 Relapse primograft	F3887 LN	
K5	L707 Relapse primograft	F3887 RN	
K6	L707 Relapse primograft	F3887 RN	
K7	L707 Presentation secondary xenograft	G6766 LN	Secondary
K8	L707 Presentation secondary xenograft	G6766 LN	
K9	L707 Presentation secondary xenograft	G6766 LN	
K10	L707 Relapse secondary xenograft	G6766 NN	
K11	L707 Relapse secondary xenograft	G6766 NN	
K12	L707 Relapse secondary xenograft	G6766 NN	

Table 24: Array Location, sample type, mouse and labels used for analysis for samples used for microarray analysis of L707 presentation and relapse.

4.2.1 Analysis using genome studio and excel

Data was returned from Oxford Genomics in the form of IDAT and GTC files (cluster reference information files). These were loaded into GenomeStudio, which was then used to run statistics to produce p values for probes. Quantile normalisation was applied to the data, the background subtracted and the standard Illumina statistics used (3.24.1)

The average signals of each sample were compared to check for discrepancies (Figure 25) before data was used for further analysis. Samples were found to have similar intensities throughout.

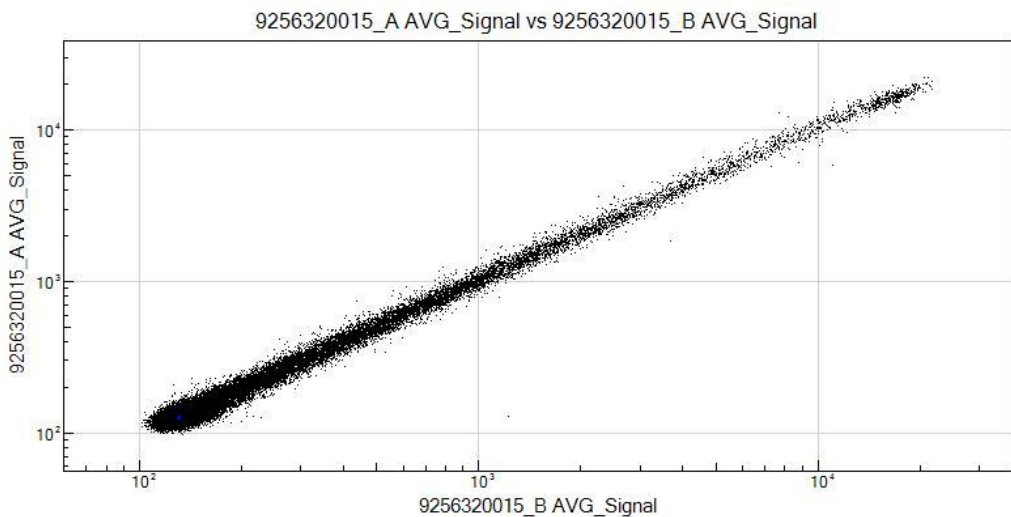


Figure 25: Plot showing the comparison of the average probe intensity signals between 2 L707 samples sent for microarray analysis, A and B which correspond to two L707 presentation samples. The alignment of samples indicates that arrays have similar intensity and so do not have significantly different levels of probe binding between them that could affect analysis of data. Comparison of 2 samples is shown as a representative, no differences were seen in any of the multiple comparisons.

Once statistics and normalisation had been done in GenomeStudio, data was exported to Excel for further manipulation. In order to create a stringent list several parameters were applied to the data in order to determine which genes were significantly altered. Firstly, a cut-off for differential p values of less than 0.01 was applied, then a fold change of more than 2 in either direction. Lastly the probe binding (intensity) in one or both of the samples had to be over 100 for the probe to be accepted. This set of parameters was applied to the four permutations of comparison (Figure 26) and thus 4 lists of genes differentially expressed between presentation and relapse were generated. Comparison of these 4 lists showed an overlap of 124 probes common to all lists (Figure 27), from these 124 probes 117 had gene names.

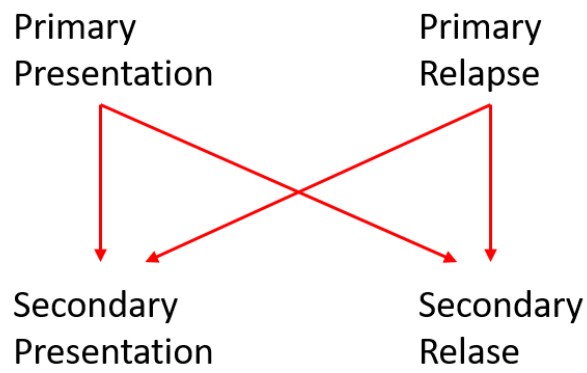


Figure 26: The 4 different assessments made between primary and secondary L707 presentation and L707 relapse samples in excel to generate a list of significant genes to investigate further. Red arrows indicate which samples were compared to one another, resulting in a total of 4 lists of genes.

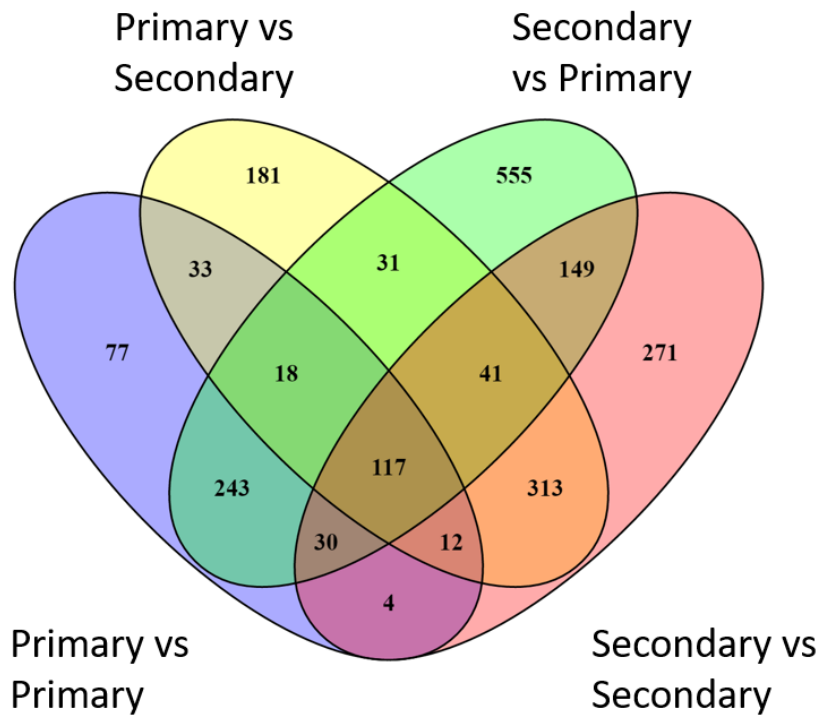


Figure 27: Venn Diagram showing the crossover of genes in each of the 4 lists from the multiple comparisons of the primary and secondary engraftment samples for L707 presentation and relapse. Only probes that had a p value of <0.01, binding of >100 in either condition and a 2-fold change in either direction were included in lists, and only probes that had associated gene symbols were used for final lists used to produce venn diagram. The labels indicate the two lists compared.

The resulting list of 117 genes was then used for gene set enrichment analysis (GSEA) to rank the genes and determine which pathways were significantly enriched (Figure 28). Analysis was carried out with weighted enrichment statistics and genes were ranked using the log2 ratio of classes. The levels of binding for each of the differentially expressed probes was also plotted to determine if there were large differences between the primary and secondary samples, which was not found (Figure 29).

4.2.1.1 *Genes downregulated at relapse*

Of the 37 genes for which expression is decreased at relapse the top 2 as ranked by GSEA are NR3C1 and HMHB1 (Figure 28), which is unsurprising due to their deletion in the relapse. None of the other genes in the 5q deletion are in the list because the other 4 are not expressed at any significant amount in the presentation (Figure 30). As well as NR3C1 and HMHB1 downregulation at relapse, there are several genes that are potentially interesting. DKK1 (Dickkopf 1) expression is significantly reduced in the relapse. This protein is known to be an antagonist of WNT signalling, a pathway activated in many chronic lymphocytic leukaemia cases which is thought to contribute to oncogenesis (Filipovich et al. 2010; D. Lu et al. 2004). PEG3 (paternally expressed 3), another potentially interesting gene has reduced expression at relapse. This gene is a mediator of apoptosis, and in the absence of TP53 is able to induce apoptosis in cooperation with the p53-inducible gene SIAH1A (*seven in absentia 1A*). Loss of PEG3 expression inhibits TP53 induced apoptosis (Relaix et al. 2000), indicating a possible reason for loss of this gene at relapse.

Gene	Presentation binding	Relapse binding	Fold change	Gene	Presentation binding	Relapse binding	Fold change
NR3C1	658	7	159.71	HSPA1A	2001	5227	2.63
HMHB1	697	6	185.64	VTRNA1-1	186	505	2.73
ZNF135	113	3	47.89	HIST2H2AA4	95	266	2.80
HOPX	727	16	224.70	IDS	65	194	2.82
NAV2	380	24	17.90	FOXA2	70	211	3.23
LPAR1	282	26	11.25	GCAT	37	117	3.13
LARP6	174	1	245.93	HIST2H2BF	74	246	3.19
KHDRBS3	693	70	85.49	HIST1H2AD	173	572	3.32
DKK1	445	61	8.56	HOMER2	128	431	3.37
CLDN10	138	19	7.24	DFNA5	54	183	3.57
BEX4	487	69	7.30	PDE4DIP	474	1629	3.39
DUSP23	141	23	6.13	NPY	441	1833	3.81
CTGF	2775	466	7.30	HIST2H2AA3	747	2803	4.18
BEX1	983	175	5.80	OVGP1	47	171	3.62
CEBPB	1469	269	5.63	RNU11	1145	4301	4.14
PEG3	1557	292	5.54	HIST2H2AB	115	439	3.85
KCNK12	5184	997	5.21	DBNDD2	30	115	3.87
EML1	112	22	5.28	EFNB2	37	150	4.09
CTDSPL	183	37	6.15	MF12	42	180	4.67
SCHIP1	111	24	5.43	LOC468164	27	118	6.14
KLF9	631	141	4.49	HIST1H2AM	97	434	4.49
BNIP3	448	136	3.82	HIST1H2AC	209	969	4.64
IGF2BP2	264	59	4.80	HIST1H2BD	297	1412	5.11
DSCR6	370	86	5.12	HIST1H3B	64	315	4.95
LOC144481	144	34	5.31	RNU2-1	216	1085	5.06
S100A9	260	63	4.24	NUAK2	33	167	5.09
PROM1	1866	485	4.21	HIST1H4H	147	773	5.28
PPP2R3B	165	46	3.86	RNU12	129	703	6.24
XIST	1055	308	3.56	KIAA1666	84	463	5.54
PLCXD1	503	152	3.31	HLA-DQA1	91	511	5.62
SNRPN	616	201	3.32	HIST1H3D	45	259	6.52
ARPP-21	719	244	2.95	HIST1H2BF	129	769	6.76
GIMAP4	1182	426	2.87	LOC653610	91	556	6.40
AFAP1L2	202	77	2.67	LOC10013367	132	847	7.06
TMEM71	188	72	2.63	RNU1-5	2463	15866	7.96
UBAP2L	668	259	2.58	EPCAM	31	207	6.76
MDK	661	259	2.59	RNU1A3	1945	13678	8.22
TPAN9	835	327	2.59	HIST1H2BG	150	1099	7.35
PCYOX1L	172	68	2.58	RNU1-3	2037	15043	8.88
CNN3	2459	986	2.50	HIST1H2AE	51	381	7.90
GSN	140	56	2.49	LOC10013142	18	136	7.62
LGR5	205	83	2.46	RNU5A	172	1326	7.79
FBN2	739	300	2.48	RNU1G2	1871	14769	9.91
AIF1	638	266	2.43	SNORD3A	705	5804	8.33
FYN	132	57	2.31	PTK2	95	873	9.21
HUWE1	224	102	2.20	LOC10013386	22	215	10.24
MAN1A1	247	116	2.13	HIST1H2BJ	61	592	9.84
TIRI	175	226	2.52	RNU1F1	903	8957	12.01
MTL5	95	214	2.27	HIST1H2BB	33	332	10.81
PHC3	92	215	2.34	SNORD3D	1031	10899	10.58
LY86	254	607	2.39	LOC643031	20	219	10.88
RNY4	300	743	2.48	MAST4	237	2809	17.87
SPAG1	115	292	2.54	SNORD3C	35	440	12.29
IRAK2	167	425	2.58	TACSTD1	61	817	13.19
NCRNA00152	67	174	2.63	HIST1H4B	15	417	14.34
TMEM107	246	646	2.63	HIST1H4A	302	3008	31.78

Figure 28: Ranked list of 117 genes for which GSEA allocated a score with the gene name, average probe binding for the presentation and relapse and the average fold increase or decrease (average of the 4 permutations of data analysis previously used to generate the list input into GSEA. Fold changes for several genes are the averages of several probes for the same gene that scored as significant). Genes and values shown in green indicate genes for which expression is higher in the presentation than the relapse. Genes and values in red indicate genes for which expression is higher in the relapse than the presentation. Genes are ranked in order, i.e. NR3C1 is the most significant of the lost genes and HIST1H4A is the most significant of the increased genes.

Binding for differentially expressed probes

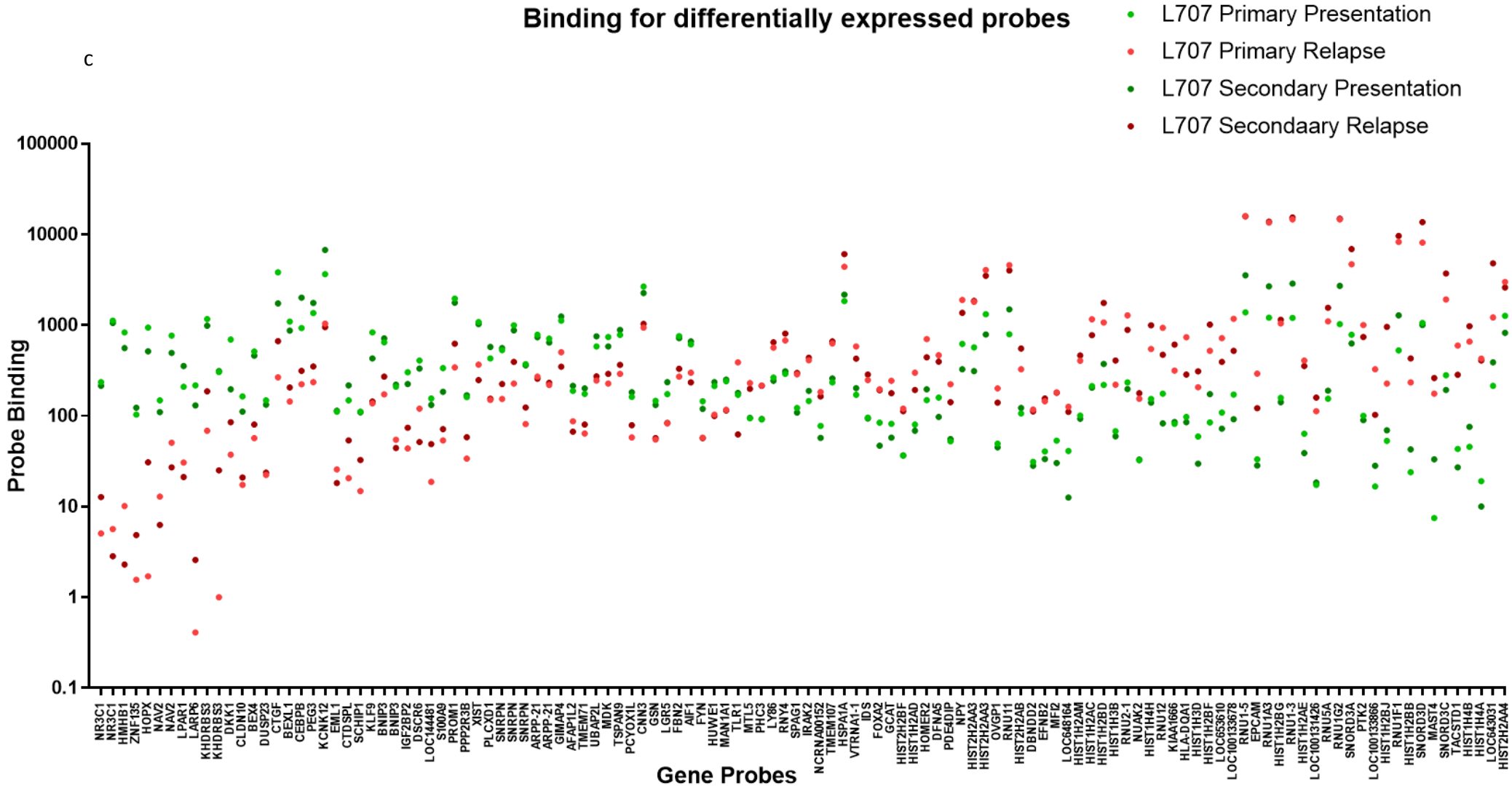


Figure 29: Scatter plot showing the probe binding for the differentially expressed probes as determined using the protocol described ($p<0.01$, >2 fold difference, probe binding >100 in either presentation or relapse. Present in all 4 lists). Presentation samples are shown in green and relapse in red. For both, the lighter shade represents the primary timepoint and the darker shade the secondary.

Expression of deleted genes in the L707 presentation and relapse

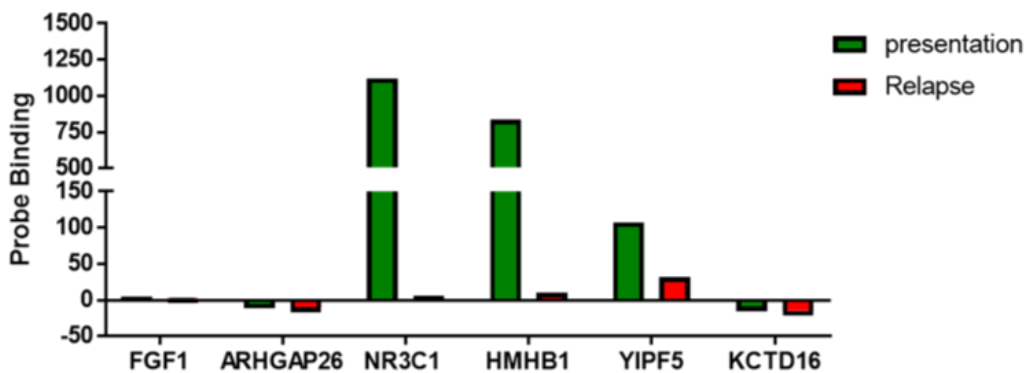


Figure 30: Probe binding (as a surrogate for mRNA expression) of the 6 genes in the relapse specific 5q deletion at presentation and relapse. Only NR3C1, HMHB1 and YIPF5 are expressed in the presentation, with YIPF5 expression levels still very low compared to NR3C1 and HMHB1. Gene expression in L707 Presentation is shown in green and expression in L707 relapse in red.

4.2.1.2 Genes upregulated at relapse

In the genes upregulated at relapse there is a large proportion of histone genes, which were all replication dependent (Marzluff et al. 2002) rather than the histone genes which are not cell cycle regulated. This indicates that the L707 may have altered cell cycle, and although the increase in histones might indicate that there is an increase in cell cycling, the fact that it has been found by others in our lab that the L707 relapse, when in culture on a MSC feeder layer *in vitro* has an increased number of cells in G0 and has slower proliferation (Pal et al. 2016), this would indicate that the increased histones somehow result in the opposite; reduced proliferation.

Gene ontology analysis of the genes down regulated at relapse shows several significantly enriched gene sets, including DNA methylation, (FDR=0.000381), the nucleosome (FDR=1.67e-17) and chromatin (FDR=7.53e-9), all of which suggest an altered transcriptional profile in the L707 relapse. These gene sets are all enriched due to the presence of a number of histones in the genes upregulated at relapse.

Running gene ontology on both the upregulated and downregulated genes similar pathways are enriched as for the downregulated genes alone. These include the nucleosome core (FDR=2e-14) and the histone core (FDR=2.3e-14), somewhat interestingly systemic lupus erythematosus is also highly enriched for in the gene list (FDR=2.6e-12), an autoimmune disease which does have an increased risk of haematopoietic malignancies, in particular lymphoma associated with it (Sultan, Ioannou, and Isenberg 2000; Abu-Shakra, Gladman, and Urowitz 1996)

When gene ontology analysis is run again with the larger list of all genes differentially expressed in any of the 4 lists (2122 genes) rather than the shortened list, the categories are very similar (

Table 25).

Term	p Value	Benjamini score
Nucleus	9.90E-22	6.20E-19
Phosphoprotein	4.50E-19	1.40E-16
Protein-DNA complex	5.30E-12	6.00E-14
Nucleosome	1.50E-16	2.90E-11
Nucleosome assembly	1.10E-11	2.70E-08

Table 25: Top 5 gene ontology hits when all genes are used to generate the input data for GSEA to determine enriched pathways between the L707 presentation and L707 relapse rather than the 4 lists generated through excel analysis. Table shows the gene ontology term as well as the p value and Benjamini score (corrected p value), Hits are ranked by p value.

4.2.2 Microarray analysis using R

Analysis using excel produces a list of genes that are differentially expressed between two conditions. This however has no corrections for multiple testing, and relies on the user creating several lists and then comparing those. Analysis using statistical programmes provides a better option. This is because the significance determined using statistical programmes will take into account all biological and technical repeats, as well as correcting

for multiple testing. Data was re-analysed using the R programmes Lumi and Limma (3.24.2). These programmes are just some of the vast array available for this type of analysis but are the most commonly used analysis programmes (Eijssen et al. 2015)

Raw IDAT files were imported into R using the Illumina microarray specific programme, Lumi. Data was analysed in the standard way for microarray, with the VST method of transformation and RSN normalisation (Figure 31). At this point, 7 probes were excluded due to low bead numbers in one or more of the samples. 61% of probes then failed to meet the detection call threshold applied after normalisation. This is lower than would have been expected but there was enough data remaining to continue with analysis.

Principal component analysis (PCA) (Figure 32) shows the presentation samples cluster, with the primary and secondary samples clustering closest. There is more variance between the primary and secondary samples in the relapse.

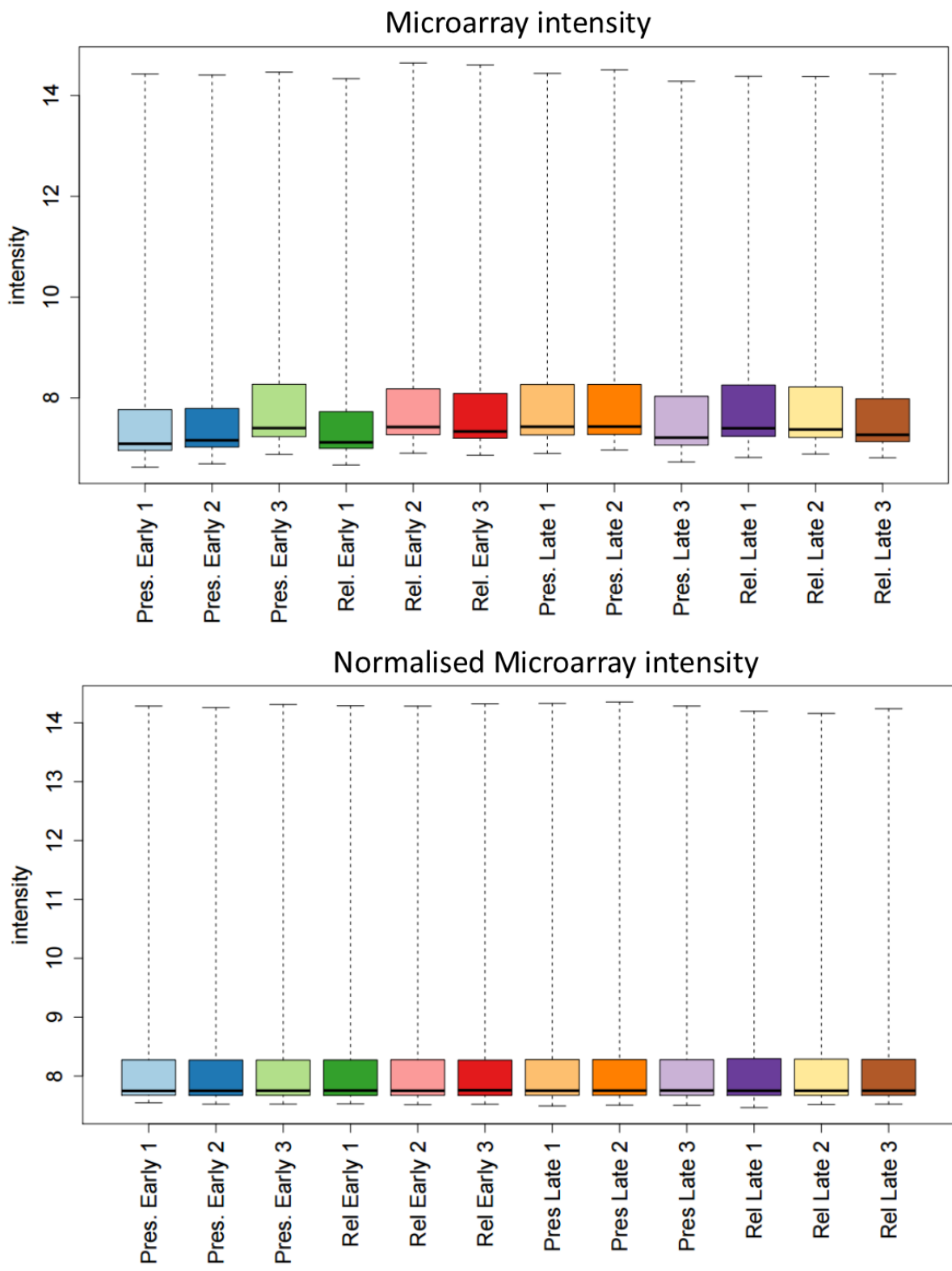


Figure 31: Intensity box plots for each of the 12 microarray samples before normalisation (top) and after robust spline normalisation (bottom). Plots show the median intensity (bold line) as well as the upper and lower quartiles (top and bottom of box) for probe intensity for each sample. The error bars represent the extremes at the upper and lower ends. As can be seen, robust spline normalisation results in more evenly distributed probe intensity between samples.

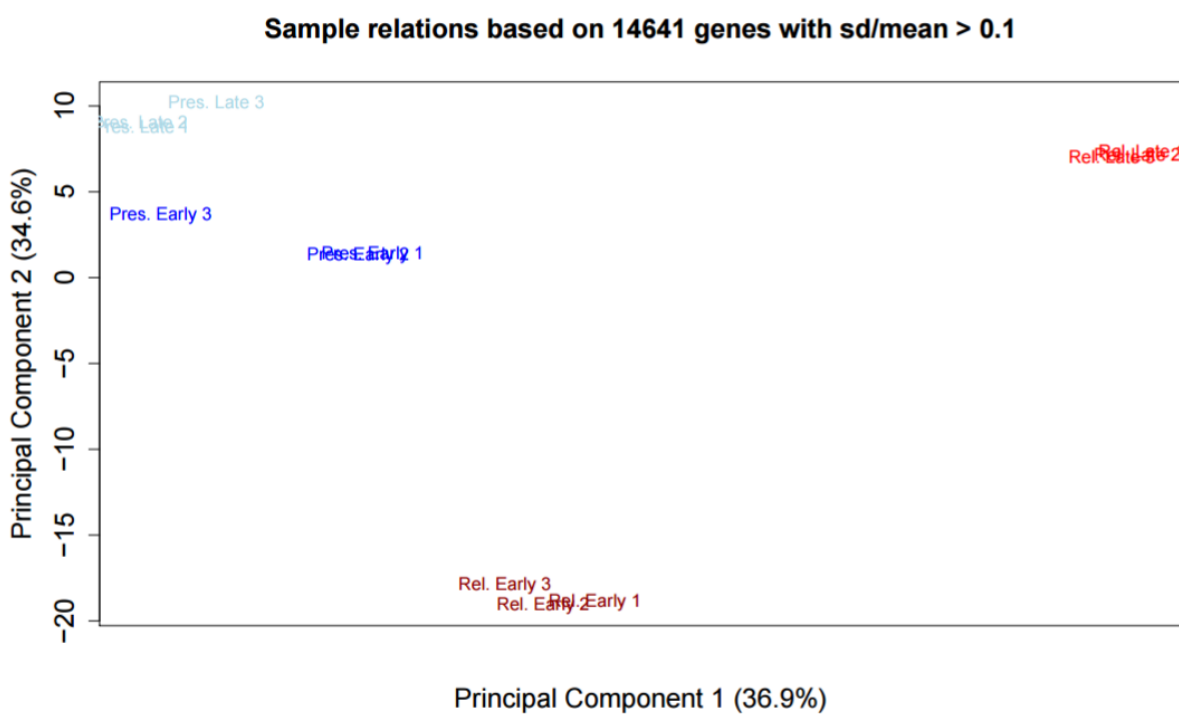


Figure 32: Principal component analysis of the microarray samples after quantile normalisation. Presentation samples are shown in blue and relapse samples in red with the darker shade representing the primary time point samples (labelled early) and the lighter shade representing the secondary timepoint samples (labelled late). The two principal components contributing the most to the total variance between samples are shown on the x and y axis, with the percentage contribution to the differences shown.

4.2.2.1 **Genes down-regulated at relapse**

Expression of 4825 genes are significantly different ($p<0.01$) between the presentation and relapse when analysed . The most significant of these genes is TCEA3 (Transcription elongation factor A3) with an adjusted p. value of 9.05e-14. TCEA3 has been found to be significantly enriched in mouse embryonic stem cells and is implicated in differentiation, although it appeared to have no effect on proliferation in these cells (Park et al. 2013). TCEA3 has also been found to be repressed upon treatment with Dex in breast cancer cells (Kinyamu et al. 2008).

NR3C1, the most significant using the genome studio and excel analysis is the 16th ranked gene, the 3rd most significant of genes lost at relapse with an adjusted p. value of 2.8e-11. This is still highly significant but highlights the differences when analysis data using Excel or the statistical programmes designed specifically for analysis of microarray data. Another gene of interest that is lost in the relapse includes CEBPB (CCAAT/enhancer binding protein beta) (adj. p.value = 4.93e-8). CEBPB has been implicated in ALL with an IGH translocation, but is usually found to be upregulated in these cases (Akasaka et al. 2007). PEG3 and DKK1 are both still significantly down regulated at relapse, but using this method of analysis are further down the ranked list (position 25 and 103 respectively), again highlighting the differences in the analysis compared to using Excel.

4.2.2.2 *Genes up regulated at relapse*

The 3 most significant genes upregulated at relapse are SNORD3D, 3A and 3C. These are all small nucleolar RNA, they are non-coding RNA that have vital roles in the processing of ribosomal RNA. Although not a lot is known about them, these RNA are highly conserved across eukaryotes indicating an important function (Scott and Ono 2011). These RNA molecules have been found to associate with AGO (Argonaute) and may have RNAi capabilities (Ender et al. 2008).

Similar to the Excel analysed data a large proportion of the highly significant genes are histones including genes from the HIST1 and HIST2 loci. These genes are replication dependent histones, which are unusual genes in so much as the mRNA does not have a polyA (polyadenylated) tail but a stem-loop and the genes are encoded by exons without introns (Marzluff et al. 2002). These proteins are increased 35 fold when the cells enter S phase, thus gaining the name replication dependent histones. The histones that are not regulated with the cell cycle are more classical as they do have a polyA tail. How an increase in these histones results in a phenotypic change in the L707 relapse is not known, but the fact that all of the significantly upregulated histones are replication dependent, and the fact that so many are high in the ranked list indicates that they play some role. One option is that the L707 relapse cells were in a different phase of cell cycle when they were collected, but this is unlikely as there were 3 replicates for each presentation and relapse.

Of the 1459 gene ontology biological process IDs tested, 142 were returned as significant ($p<0.01$), and after multiple testing correction using an FDR of 0.05, 91 were left. The top enriched gene ontology term is chromatin silencing, followed by nucleosome assembly and chromatin assembly. These terms are similar to the results from the upregulated genes at relapse in the excel analysis. The similarity between the analysis results indicates that the excel analysed data, which was used throughout most of the PhD is a good indicator of the gene expression profile differences between the L707 presentation and relapse.

What can be taken from this microarray analysis, either the genome studio and excel or the R method is that the L707 relapse shows an alteration in the gene expression profile consistent with an altered chromatin landscape, and it is likely that this alters the transcriptional profile. How this change in gene expression results in relapse is harder to pinpoint , and although one mechanism for Dex resistance is the loss of NR3C1 in the relapse, it is possible that there are other mechanisms, as well as mechanisms that drive the emergence of relapse.

4.3 Whole genome sequencing: Genetic differences between presentation and relapse

Whole genome sequencing was carried out on the L707 presentation and relapse cells by Dr. Lisa Russell in conjunction with Illumina. Bam files and output from mutation analysis were returned. However, the alignment did not appear to be good quality so the files were re-analysed by Dr. Matt Bashton. Briefly, this involved extracting FASTQ files from the BAM files and, sorting and re-running the alignment protocol. The type of alignment used was Barrows-Wheeler alignment (BWA-mem) and hg19 was the reference genome. Aligned BAM files were then used with the GATK method of analysis (3.25), which was run using scripts from Dr. Sirintra Nakjang. Variant discovery was used to produce a list of variants, which are then refine, annotated and evaluated using the online Variant effect predictor (VEP) programme from Ensembl (McLaren et al. 2016). The average read depth of the sequencing for both the L707 presentation and L707 relapse was approximately 35X.

Due to the lack of germline material for patient L707, variants that are disease specific cannot be determined. However, looking at those that are relapse-specific could elucidate

possible mechanisms of relapse and drug resistance, and looking overall may give clues to possible oncogenic driver mutations. Without germline material it can also not be determined for all variants whether they are constitutional or somatic variants other than by looking in the literature for those that have been reported before. The variants that have been identified before and that were flagged up by the variant effect predictor have been further investigated using the 1000 Genomes data available on the online database Ensembl (Aken et al. 2016). For the rest this has not been done as it was beyond my limited bioinformatics skill.

4.3.1 Relapse specific SNP

Of the 2355169 single nucleotide polymorphisms (SNP) that were above the thresholds used to remove false positives during analysis, 0.365% (8610) were unique to the L707 relapse, and of these 58% (4999) had >10 reads each. This list of variants was then used with the online VEP programme to annotate and give a predicted effect.

The most frequent effects of SNPs unique to the L707 relapse were intron variants (47%) intergenic variants (16%) and non-coding transcript variants (13%). Of those that were predicted to have coding consequences the majority were missense variants or synonymous variants, 7% were gain of a stop codon (Figure 33). Just 33/4999 of the annotated variants scored moderate or high in the effect predictor, mapping to 9 genes, including 2 genes with existing variants known.

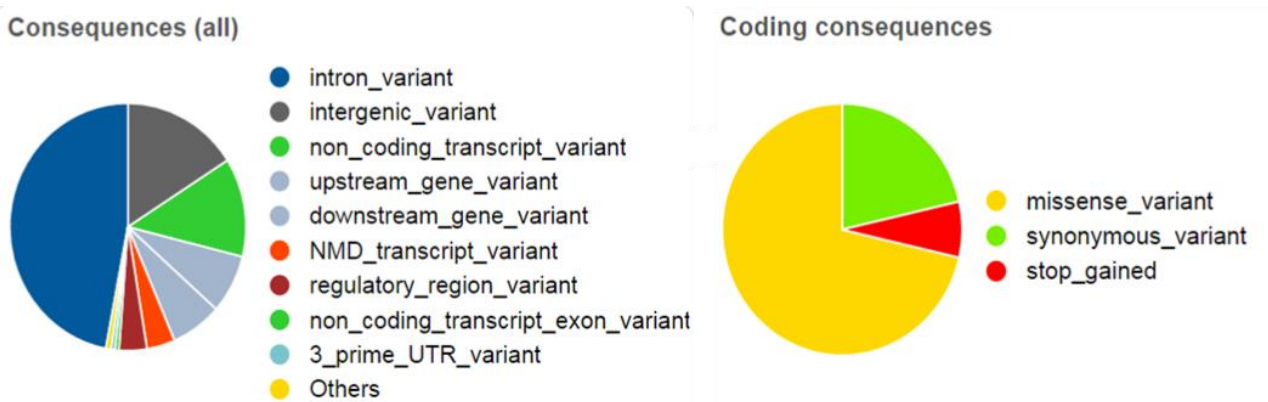


Figure 33: Charts showing the predicted consequences of SNPs unique to the L707 relapse. Consequences were determined using the online tool Variant effect predictor (VEP). The left pie chart shows all consequences; the right chart shows only the consequences predicted to be coding consequences.

In all of the SNPs unique to the L707 relapse there were 4 that were associated with existing variants, affecting 3 genes. The catalogue of somatic mutations in cancer (COSMIC) database was used to look these up and they were all found to be associated with carcinoma (Table 26). These three genes all have roles that could be important in the emergence of relapse in the L707 cells. CLEC1A (C-type lectin domain family member 1A), the SNP in which is associated to invasive breast cancer, is part of the c-type lectin family of genes, these genes have diverse roles in cell adhesion and signalling and the innate immune response (Drickamer 1999). TRRAP (Transformation/transcription domain associated protein) is a part of the histone acetyl transferase (HAT) complex. TRRAP is responsible for the recruitment of HAT to the chromatin (Murr et al. 2007). It is thought that deregulation of this protein contributes to cancer, and this SNP is associated with renal cell carcinoma. The last of the 3 genes with cancer associated SNPs is NDUFB11 (NADH:Ubiquinone oxidoreductase subunit B11), a mitochondrial enzyme. Disruption of metabolism as a result of de-regulation in the mitochondria is associated with cancer and the progression of leukaemia (Basak and Banerjee 2015)

SNP	Gene	Mutation	Consequence	Associated disease
COSM5811821	CLEC1A	c.423G>C	Stop gained	Liver Cancer
COSM485794	TRRAP	c.10339G>C	Missense variant	Renal clear cell carcinoma
COSM485795	TRRAP	c.10426G>C	Missense variant	Renal clear cell carcinoma
COSM1468092	NDUFB11	c.161C>T	Missense variant	Colon adenocarcinoma

Table 26: Known variants in the SNPs with predicted moderate or high impact unique to the L707 relapse. SNPs with associated COSMIC identifiers were found using VEP and the identifier looked up using the COSMIC database. The table shows the SNP identifier from COSMIC, the gene affected, the mutation and the consequence as well as the associated disease.

4.3.2 Relapse specific indels

In the L707 relapse, 254,349 indels were called over thresholds, and of these 3.4% (8656) were unique to the relapse. 31% of these indels (2693) had more than 10 supporting reads

for each variant, the allele frequency for the majority of these was 1 or 0.5. Predictions of the effects of these variants showed similar effects to the unique SNPs with most being intron variants (50%), non-coding transcript variants (15%) and downstream gene variants (8%) (Figure 34). Of these indels, 82 scored high or moderate for impact, with a total of 26 genes affected, and within this list 2 indels were found to be existing variants affecting the genes LILRB4 (Leukocyte immunoglobulin like receptor B4) and STRN (striatin) (

Table 27). LILRB4 is an immunoglobulin like receptor. This gene family encodes cell surface receptors important for the recognition of HLA proteins and modulation of the immune system (Cella et al. 1997) . STRN is a calmodulin binding protein that has roles in oestrogen receptor signalling, a steroid receptor related to NR3C1 (Lu et al. 2004).

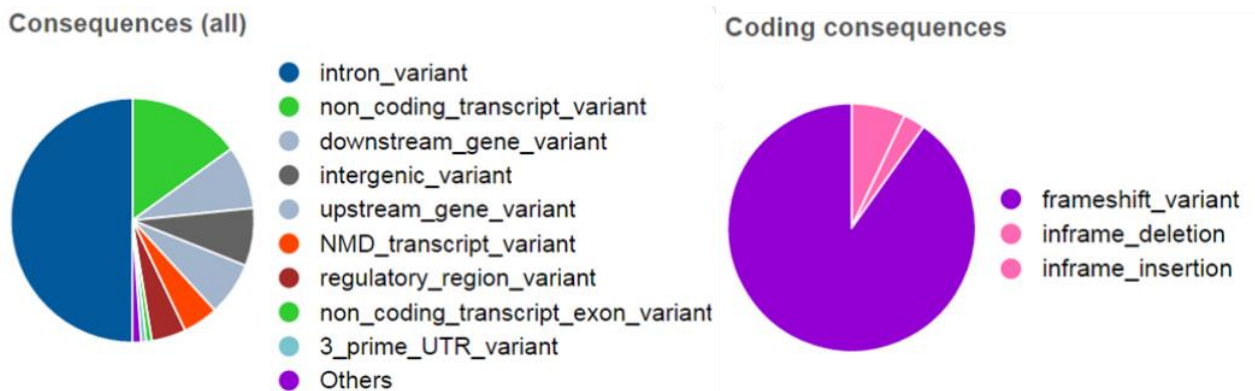


Figure 34: Charts showing the predicted consequences of indels unique to the L707 relapse, determined using VEP. The left pie chart shows all consequences and the right chart shows only consequences predicted as coding consequences.

Variant	Gene	Mutation	Consequence	% in population
rs146936423	LILRB4	G/T	Frameshift variant	1%
rs763151379	STRN	G/A	Frameshift variant	0.9%

Table 27: Known variants found in the list of indels with predicted moderate or high impact, unique to the L707 relapse. Variants were identified using VEP. The table shows the variant identifier, the gene affected, the change in nucleotide sequence, the consequence of the indel and the percentage of the variant present in the population as determined from the 1000 genomes data available on the online Ensembl database (Aken et al. 2016)

4.3.3 SNPs and indels in both L707 presentation and relapse

Although there is no remission or germline sample to compare the presentation and relapse to, some information can be gained from the SNPs and indels that are shared between the two. These majority of these variants will be germline, but some will be oncogenic, and looking at the genes affected may provide a route for carcinogenesis in patient L707.

4.3.3.1 Shared SNP between L707 presentation and relapse

There are 4,646,346 SNP that are found in both presentation and relapse and 99% of these have a least 10 supporting reads. Only the predicted high impact consequences were looked further into due to the large size of the dataset. There were 13586 SNPs with more than 10 supporting reads that were predicted to have a high impact, representing 0.29% of the total SNPs in the sample. Of these SNPs 28% were loss of stop codons and 26% were gain of stops (Figure 35). The 13586 SNPs correspond to 1988 different genes and within this gene list there are several interesting hits that could possibly account for oncogenic transformation (Table 28). One of these interesting hits is BRCA2 (Breast cancer 2), a known tumour suppressor that is important in haematological malignancies as well as ovarian and breast cancer (Friedenson 2007). Protein association and gene ontology analysis reveal that the TP53 signalling pathway is enriched in this set of genes (FDR=0.003).

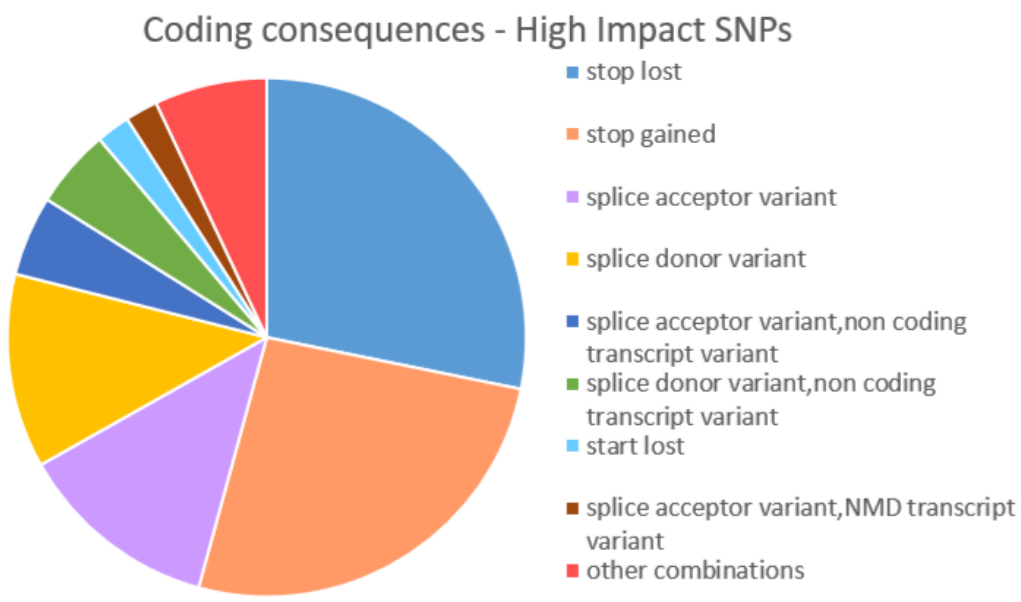


Figure 35: Coding consequences of the SNPs shared between presentation and relapse. Only SNPs with more than 10 supporting reads and predicted high impact are shown. All combinations of impact types with less than 2% of the total are grouped together (other combinations)

Location	Consequence	Gene	Info
15:41821752- 41821752	Splice donor variant	MAPKBP1	MAPK signalling
5:68294662- 68294662	Stop gained	PIK3R1	PI3K-AKT signalling
1:243499744- 243499744	Stop lost	AKT3	PI3K-AKT signalling
3:142507966- 142507966	Stop gained	ATR	Phosphorylates CHEK1, cell cycle arrest
11:125635478- 125635478	Stop lost	CHEK1	checkpoint protein, cell cycle arrest
2:219078116- 219078116	Stop gained	NHEJ1	Non homologous end joining protein
13:32339465- 32339465	Stop lost	BRCA2	tumour suppressor
11:44573235- 44573235	Splice donor variant	CD82	metastasis suppressor gene
2:101887152- 101887152	Stop lost	MAP4K4	MAPK signalling, associated with leukaemia
14:95133457- 95133457	Start lost	DICER1	microRNA processing

Table 28: Selected SNP shared between the L707 presentation and relapse that when input into VEP have predicted high consequence and have been associated with cancer in the literature (Fu et al. 2015; Casazza et al. 2010; Chang et al. 2003; Breaks et al. 2006; Vago et al. 2014; Marjon et al. 2015; Bai et al. 2013; Friedenson 2007)

4.3.3.2 Shared Indels between L707 presentation and relapse

The indels that are shared between the L707 presentation and relapse show a similar distribution of types as the indels that are specific to the relapse with 50% being intron variants. Of those that have coding consequences 79% were frameshift variants (Figure 36). There were 16009 indels with a high predicted impact, which related to 2028 genes. In this list of genes, 116 were known variants and there were several genes that have been associated with cancer and could possibly account for leukaemic transformation of cells. For example, TP53, known as the ‘Guardian of the Genome’ is a tumour suppressor gene and has a shared indel between L707 presentation and relapse. Two TP53 related genes TP53RK (TP53 regulating kinase) and TP53BP1 (TP53 binding protein 1) also have indels with a predicted high impact. MDM2 (Mouse double minute 2 homolog), the negative suppressor of TP53 also has high impact predicted indels. Although it is just speculation, this could imply a role for deregulated TP53 in the oncogenesis of the L707 cells.

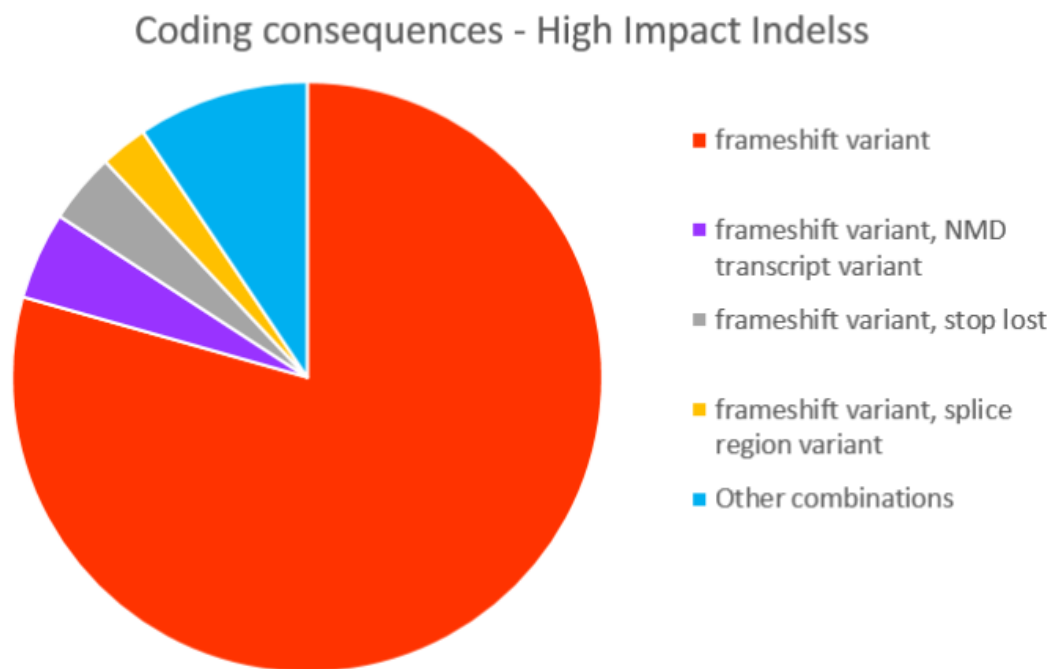


Figure 36: Coding consequences of indels shared between L707 presentation and relapse with more than 10 supporting reads and predicted high impact. Data generated using VEP. All combinations of impact types with less than 2% of the total are grouped together (other combinations).

4.3.3.3 Identification of deletion breakpoints

With the re-aligned BAM files, we were able to run Pindel, a programme designed to analyse paired end reads from WGS (Whole genome sequencing) to determine breakpoints of deletions, insertions inversions and other structural changes in DNA. Once breakpoints had been found using Pindel, Dr. Alex Elder designed primers and used PCR to generate small amplicons for sanger sequencing of the breakpoint. All of the following work on the breakpoints was done by him.

From the PCR analysis of the breakpoints and the reads in the WGS it can be seen there are 2 major products resulting from likely 2 separate deletions (Figure 37). One complex deletion product, with a duplication and inversion as well as the deletion and one a simple product, with just a deletion. At the breakpoints for 2 of these genetic alterations there are small insertions of 2-3bp (Table 29)

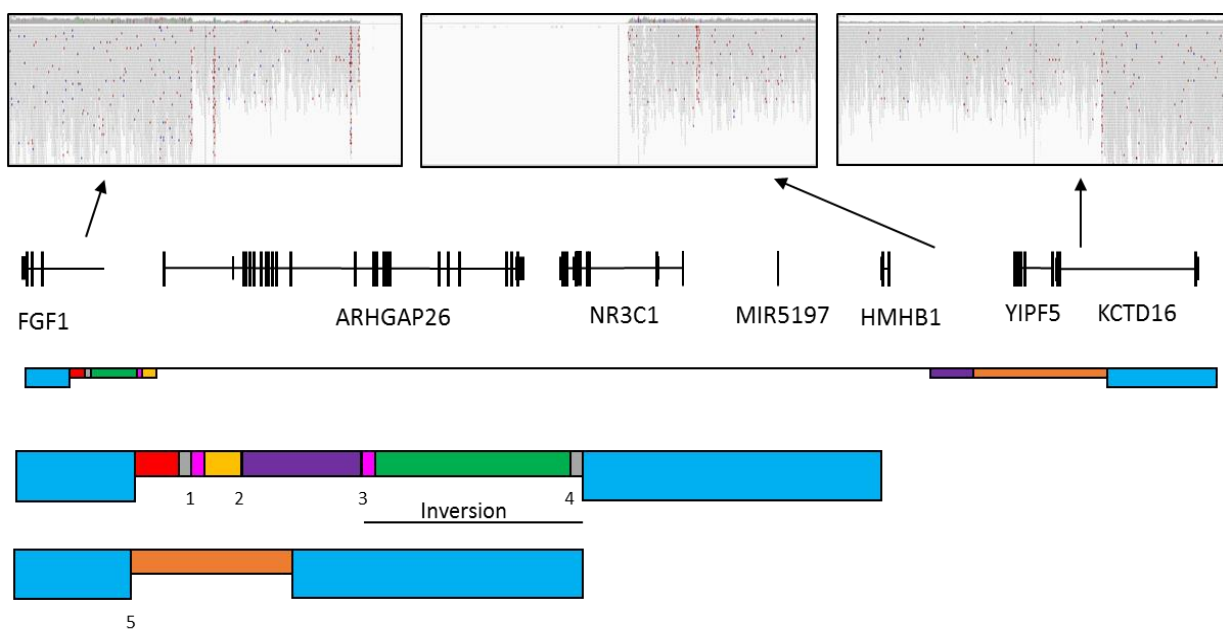


Figure 37: Breakpoints in the 5q deletion present in the L707 relapse; Top - WGS reads of the breakpoint (top) with corresponding genes (below) and sections of heterozygous and homozygous loss (below). Coloured blocks represent regions of DNA that are in a different orientation or location in the L707 relapse compared to the presentation. Two deletion products are made as a result of the deletion.

Breakpoint	Sequence
1	CCCAAGCATAGGGCTTCACAGTGT <ins>CGTAATCAGTTAGTTCTCCATTCTG</ins>
2	<ins>CTGTGAAGCTTCGGCACAGTCTGGACAGGTTGGTTACCCACAAAGGGAAGCCC</ins> <ins>ATCAG</ins>
3	<ins>TTACTGTATCTGTGCCTAAGTACCACTGCTTTAAATGG</ins> <ins>TAATCATTAAAAAA</ins> <ins>GACTGAATTAAAGTATTAA</ins>
4	<ins>GAAGACGTGTCTGGTGTTCCTATTTTATTCA</ins> T GAGATCATCAGCACTCTAATGAA
5	<ins>AAAAGAAGTTATTCTCGG</ins> <ins>GGTAGAAAAAAACTGGACTAGTTAGAAATGGCAA</ins> A

Table 29: Sequences of the breakpoints in the relapse specific 5q deletion. Colours correspond to the schematic of the deletion in Figure 37. Black letters represent small insertions between the breakpoints of the deletion.

4.4 Emergence of resistance in the L707 cells

An interesting question in the field of relapse in ALL is whether the relapse clone already existent in the presentation sample or are the relapse specific molecular alterations induced by chemotherapy. The question remaining after investigation of the L707 presentation and relapse by microarray and whole genome sequencing was where was the relapse clone emerging from. One previous sample of the L707 presentation was found to have a heterozygous deletion of NR3C1 and so this was investigated further to elucidate the genesis of the relapse.

4.4.1 Previous work

Dr. Elda Latif, previous to my starting, carried out experiments whereby L707 presentation cells were engrafted in NSG mice and then treated with Dex (15 mg/kg). These samples were then tested by FISH to determine the effect of Dex dosing. One of these mice was found to have 16% heterozygous deletion of *NR3C1*. As a result of this a larger experiment was carried out to screen for this emergence of the deletion induced by Dex treatment in the L707 presentation.

11 NSG mice were injected with 10^4 L707 presentation cells, either from KD2 (3rd passage xenograft) or KD68 (5th passage xenograft). Mice were left to engraft for 2 weeks before treatment was started with 10 mg/kg Dexamethasone I.P. every weekday. This was continued until mice reached license defined endpoints and were humanely killed. Samples collected from mice were fixed in methanol and acetic acid before being used for fluorescence *in situ* hybridisation (FISH).

The probes used to detect *NR3C1* were made in the lab, using the bacterial artificial clones (BAC) RP11-790H04, RP11-9268O6 and RP11-614D16. These probes were the same probes used for the original study and were designed by Elda Latif and Lisa Russell. A 5p telomere probe (CytoCell) was used as a control.

FISH was carried out according to the protocol detailed previously (3.23). A high number of cells was used to increase the likelihood of finding a very rare clone in the population. The average of three healthy controls + 3 standard deviations was used to determine the cut-off for positivity, which was 5.9%.

After the first experiment was scored some mice were found to have low levels of heterozygous *NR3C1* deletion, although not over the cut-off for positivity determined using the negative controls (Table 30). Despite no samples being overtly positive, 2 samples, KD71 and KD77 were thawed and re-injected. Mice were dosed in the same way as with the first experiment and samples collected for FISH. These samples when tested by FISH were found to have increased levels compared to the initial sample, indicating further selection. However, only one of these samples, KD139 was positive above the cut-off for *NR3C1* heterozygous deletion (Figure 38).

Mouse	Sample	% heterozygous del.
---	Control M	1.5 (5.6 % total abnormal)
---	Control 141702	1.9 (5.7 % total abnormal)
---	Control C	0.9 (5.5 % total abnormal)
KD70	L707 Presentation – from KD2 (3 rd passage xenograft)	4.2
KD71	L707 Presentation – from KD2 (3 rd passage xenograft)	1
KD73	L707 Presentation – from KD2 (3 rd passage xenograft)	1.4
KD74	L707 Presentation – from KD2 (3 rd passage xenograft)	2
KD75	L707 Presentation – from KD68 (5th passage xenograft)	2.6
KD77	L707 Presentation – from KD68 (5th passage xenograft)	3.1
KD78	L707 Presentation – from KD68 (5th passage xenograft)	2.5
KD79	L707 Presentation – from KD68 (5th passage xenograft)	2.95
KD137	L707 Presentation – from KD71 (4 th passage xenograft)	5.1
KD138	L707 Presentation – from KD71 (4 th passage xenograft)	4
KD139	L707 Presentation – from KD77 (6 th passage xenograft)	7.4

Table 30: Percentage of cells with heterozygous deletion of NR3C1 in all L707 presentation samples tested. Mouse number, the sample (passage of L707 presentation injected into mice) and the percentage of cells with heterozygous deletion of NR3C1 as determined by FISH are shown. The 3 control samples used to determine the cut off are also shown, with both the percentage of cells with a heterozygous deletion and the total percentage of abnormal cells that was used to determine the cutoff for positivity, which was the average + 3 standard deviations. All but one case fall below the cutoff for positivity (5.96).

The cut off for positivity was calculated using the standard method employed by the Leukaemia Research Cytogenetics lab at Newcastle under the advice of Dr. Lisa Russel. Despite the majority of samples not passing the cut-off there is the suggestion of a minor clone with heterozygous deletion of NR3C1 and it could be that more rounds of Dex treatment are needed to increase this further and the initial sample with 16% heterozygous deletion was an anomaly. In the cells with the higher percentages of heterozygous deletion, PCR used by Alex Elder to identify the previously defined relapse breakpoints in the samples but none of the breakpoints were present.

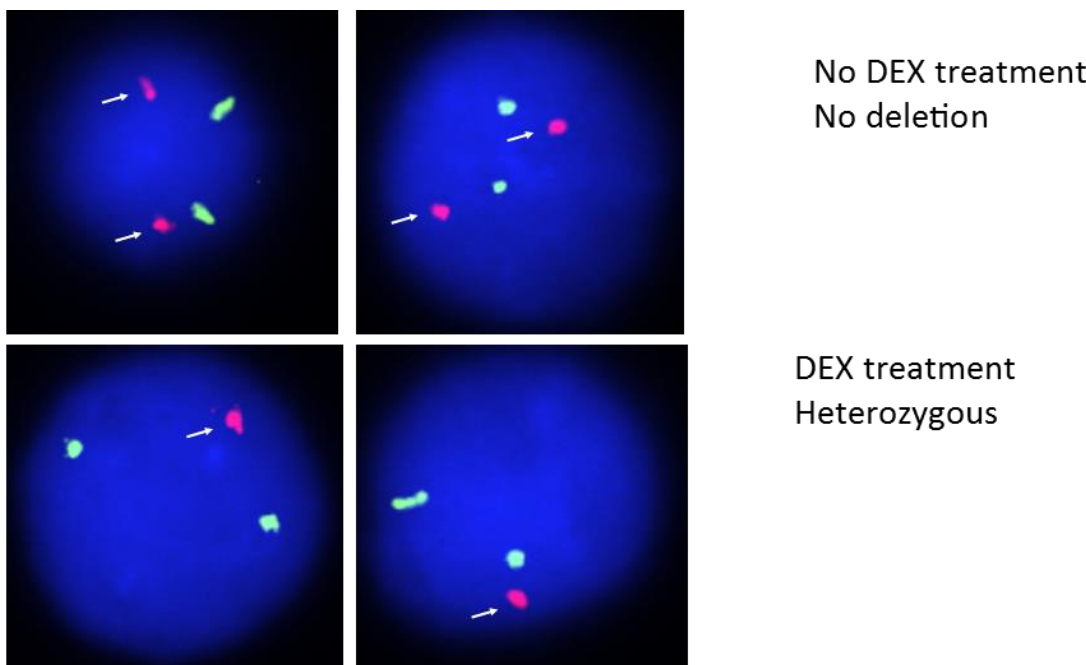


Figure 38: Representative images of the FISH carried out on the L707 presentation cells from mice treated with Dex or saline. Arrows point to NR3C1 probes (red), the control probe used was a 5 telomere probe (green). Images were generated using the CytoVision Automated Cytogenetics Platform and analysed in CytoVisionV7.

4.5 Summary

The L707 cells represent an interesting case to use for the study of acute lymphoblastic leukaemia and the acquisition of dexamethasone resistance at relapse. There are several genes highlighted by the analysis of this data that should be investigated further in my opinion. Firstly, the role of the replication dependent histones in the L707 relapse cells. The fact that so many of these genes are significantly upregulated leads to the hypothesis that they are having an effect and are not just a side effect of other expression profile alterations. It would suggest that these cells are in cell cycle more often, but that does not fit with the reduced proliferation and fitness of these cells *in vivo* compared to the presentation. The down-regulation of TCEA3, the most significant of all downregulated genes may be a result of Dex treatment of these cells (Kinyamu et al. 2008), but whether the downregulation of this gene is a driver event is unknown.

The enrichment of genes associated with chromatin silencing, nucleosome assembly and chromatin assembly may indicate a change in the transcriptional landscape of the L707 relapse and altered epigenetics. Considering NR3C1 is known to interact with proteins that alter the structure of chromatin (Johnson et al. 2008) this change in chromatin associated pathways could be the readout from loss of NR3C1 signalling. It could be a separate entity. Alterations in the epigenetic landscape of ALL at has also been reported, and epigenetic reprogramming using a DNA methyltransferase inhibitor can revert the relapse specific epigenetic landscape to a presentation signature (Bhatla et al. 2012). This change is also accompanied by a reversal in chemo-resistance. Altered epigenetics could be important for the acquisition of resistance (Bhatla et al. 2012). Whether this occurred before or after the 5q deletion that resulted in dexamethasone resistance is not known, but considering the suggestion of the emergence of a heterozygous clone in the L707 presentation with Dex treatment, it could have occurred concurrently or after.

Unfortunately, the drug sensitivity of the L707 to other commonly used chemotherapeutic drugs was not tested. This would be a good experiment to do in order to determine if the alterations in chromatin associated pathways at relapse have an effect on overall drug resistance.

The whole genome sequencing of the L707 cells not only allowed identification of the relapse specific 5q deletion breakpoints but also allowed for investigation into possible oncogenic SNPs and indels, as well as those that could be driving relapse. Unfortunately, without a remission sample to test any oncogenic mutations are purely speculative. The most attention-grabbing SNPs and indels that are present in both the presentation and relapse that could possibly be driver mutations are BRCA2 and TP53, both well known to be involved in various cancers. Of the relapse specific SNPs and indels several have been associated with cancer, for example TRRAP, NDUFB11 and CLEC1A for which the variants are recorded in COSMIC. These are not the only genes that have links to cancer. RNF20 (Histone H2B E3 ubiquitin ligase ring finger protein 20), which has a predicted high impact frameshift variant in the relapse is a regulator of chromatin that has been found to be necessary for leukaemogenesis induced by MLL fusion genes (Wang et al. 2013). PDS5A (precocious dissociation of sisters 5A), another gene with a predicted high impact indel has been found as a novel translocation partner of MLL in AML. This gene is a cell cycle gene and has been associated with several cancers (Put et al. 2012). None of these variants present an obvious

case for the emergence of relapse. However, further investigation using targeted mutagenesis and knockout studies would be helpful to determine if they are actually driver mutations. From the WGS data it would seem likely that NR3C1 deletion appears to be the main driver of relapse in the L707 samples. There are several possible contributing factors too but these are unproven as of yet.

The presence of two breakpoints in the relapse indicate that this deletion likely occurred as a two-step process, which is supported by the emergence, albeit slightly limited, of a heterozygous clone in the presentation. The lack of proof that the heterozygous deletion has the same breakpoints as either of the relapse breakpoints provides an interesting point. If the breakpoints were not the same it could imply that NR3C1 is targeted somehow in this case. NR3C1 deletions being relatively rare, the presence of another deletion occurring, that is not related to the ones seen in the relapse would be very unlikely. In order to investigate this further the clones with the heterozygous deletion would need to be expanded further to allow for genomic sequencing to determine the breakpoint.

The treatment of L707 presentation cells with dexamethasone and the subsequent trend towards an increase in cells with a heterozygous deletion of NR3C1 represents a mechanism for relapse. However, this data is not very convincing as only one of these samples shows a population with a heterozygous deletion over the cut-off. Also, despite knowing the breakpoints in the relapse 5q deletion, these could not be found in the samples with heterozygous deletion. This could be indicative of the levels being too low to test, or that the breakpoints are not the same in these cells as the relapse.

What can be taken from this data is that the L707 presentation are an excellent model of B-cell ALL due to the low variation between the primary and secondary xenograft passages. The L707 relapse do not appear to be so closely related when investigating the expression pattern using PCA. The underlying cause for relapse has not been definitively proven, but the acquisition of Dex resistance with the deletion of NR3C1 is likely a driver, along with altered chromatin assembly and the likely resulting changes in epigenetic programming.

Chapter 5: Role of NR3C1 in proliferation and engraftment of ALL cells

5.1 Introduction

The hyper-activation of NR3C1 by synthetic glucocorticoids and subsequent apoptosis this induces has been used in the treatment of ALL for decades. The role of NR3C1 in the transduction of Dex signalling has been thoroughly investigated. It is known that Dex binds to the receptor and results in homodimerisation, nuclear translocation and activation or repression of target genes via action at GRE sequences (Bhadri, Trahair, and Lock 2012). The pathway by which Dex initiates apoptosis in ALL cells after binding to consensus GRE sequences has several components that are known to be essential for apoptosis, including BIM transcription (Abrams et al. 2004), caspase activation (Cifone et al. 1999) and an increase in cytosolic Ca^{2+} (McConkey et al. 1989). Inhibition of any of the steps in this pathway reduces apoptosis in ALL cells. Altered function of downstream targets of NR3C1, such as the reduced acetylation of BIM are often the source of Dex resistance in ALL (Bachmann et al. 2010). Deletions and mutations that affect NR3C1 are relatively rare in ALL, with a frequency of just 5% even at relapse (Mullighan et al. 2007). When this is compared to the relatively high frequency of GC resistance at relapse (>24 fold compared to presentation), it appears there is a disparate increase in GC resistance compared to other drugs, but a lack of causative mutations in *NR3C1*, the effector of Dex induced apoptosis (Bachmann et al. 2005; Klumper et al. 1995).

As deletions are relatively rare it would imply that they are disadvantageous for ALL cells except in certain situations where the disadvantage is negated by other factors. However, as all ALL patients will be given Dex as part of treatment, the reasons why this deletion is not more common is still unknown. The hypothesis that loss of NR3C1 is a disadvantage to the cells can be investigated using the L707 relapse cells. These relapse cells have a deletion on the q arm of chromosome 5 that results in homozygous loss of NR3C1, as well as 5 other genes. These cells engraft and proliferate slower than the L707 presentation *in vivo* (Latif 2012), which was presumed to be a result of the loss of NR3C1.

The mechanism by which loss of *NR3C1* could result in a reduction of fitness of ALL cells is not fully understood, but as GC signalling is one of the most ubiquitous signalling pathways it

is hypothesised that loss of the gene is not well tolerated. Glucocorticoid signalling via NR3C1 and cortisol, the endogenous ligand, is involved with several key processes including metabolism, the immune system, stress response and learning and memory (Miller, Chen, and Zhou 2007; Sapolsky, Romero, and Munck 2000). It is not hard to see why loss of this gene is a poor evolutionary choice for most cells.

In order to investigate the role of NR3C1 in proliferation and engraftment of ALL cells, and whether loss results in reduced fitness, the inducible shRNA plasmid pTRIPZ was used. This plasmid induces mRNA knockdown of target genes. This is achieved using short hairpin RNA (shRNA) technology, which utilises the RNA interference (RNAi) pathways within the cell to produce degradation of target mRNA and knockdown of expression. shRNA constructs are delivered to cells lentivirally and integrate into the genome where they are transcribed by the endogenous cellular machinery. The pri-miRNA produced by transcription of this sequence is then cleaved by Drosha, which results in a 2 nucleotide 3' overhand, which targets the molecule for export to the cytoplasm. Here it is further processed by Dicer, resulting in the production of mature siRNA that is able to reduce mRNA expression (Silva et al. 2005; Y. Lee et al. 2003). The degradation of mRNA occurs when the mature siRNA is loaded into the RNA induced silencing complex (RISC), which then binds to the complimentary mRNA sequences resulting in cleavage by the AGO family of endonuclease proteins (Taxman et al. 2010).

The pTRIPZ plasmid has several features to increase efficiency including the use of a humanised shRNA backbone in an HIV-1 derived plasmid. By inserting the shRNA sequence into this miR-30 pre-microRNA backbone, delivery of the pre-miRNA precursor was found to be 80% more effective in reduction of the target gene mRNA (Boden et al. 2004). Another feature of the pTRIPZ plasmid that makes it a very useful tool is the use of the rtTA3 (reverse tetracycline transactivator 3), which is a mutant version of the wildtype tetracycline transactivator. This protein has several mutations that increase the transcriptional activity, resulting in increased doxycycline sensitivity, as well as a modifications that result in activity only in the presence of doxycycline, not the absence like the wildtype protein (Das et al. 2004).

Another method by which to reduce NR3C1 signalling is through pharmacological inhibition rather than mRNA knockdown. This was done using mifepristone, an anti-glucocorticoid

compound. Originally developed in 1981 as a synthetic NR3C1 antagonist. Mifepristone was quickly discovered to have anti-progesterone activity and found use as an abortive drug. It is this use for which the drug is well known and is its major use, but its actions as an anti-glucocorticoid have also been used for Cushing's disease (Johanssen and Allolio 2007).

When mifepristone was first synthesised, two other known anti-glucocorticoid drugs, deoxycorticosterone and progesterone had been found to have partial agonist activity against NR3C1 (Rousseau et al. 1973), but mifepristone was found to be much better, with only slight agonist activity reported at concentrations $> 5 \mu\text{M}$ (Bourgeois, Pfahl, and Baulieu 1984). This was put down to contamination with an agonist in the preparation or an off-target effect. The affinity of mifepristone for NR3C1 is 3-4 fold greater than that of Dex, and around 18 fold more than the affinity of cortisol. Mifepristone exerts its actions by inhibiting the dissociation of heat shock proteins from NR3C1, resulting in significantly reduced nuclear translocation and thus transcriptional activation of target genes (Johanssen and Allolio 2007).

The hypothesis that led to this work being carried out was that loss of NR3C1 is infrequently seen in ALL because the gene is required for cellular function. Only in the presence of Dex treatment does loss of this gene become an advantage, and even then it is a rare occurrence. The reduced proliferation of the L707 relapse *in vivo* appeared to support this hypothesis as the relapse specific 5q deletion covers NR3C1, giving a possible cause for this reduced fitness. This led to the idea that reduction of NR3C1 signalling in cells without a deletion, using a GC antagonist such as mifepristone, may result in the L707 presentation having a similar engraftment and proliferation phenotype as the L707 relapse *in vivo*.

The aims of this study were to investigate the effect of knockdown of NR3C1 mRNA *in vitro* and *in vivo* in response to Dex as well as determine if mifepristone treatment had any effect on the survival of mice engrafted with ALL cells.

5.1.1 shRNA constructs

When the PhD project was started only the SNP6 data were available for the L707 and from this it appeared that there were only 5 deleted genes in the 5q deletion of the L707 relapse

not 6. These 5 genes were *FGF1*, *ARHGAP26*, *NR3C1*, *HMHB1* and *YIPF5*, but not *KCTD16*, and so for this reason, *KCTD16* was not investigated as part of these experiments. The hypothesis behind using a pool of shRNA targeting these genes was to determine which were enriched or lost, which would give an indication of which genes were leukaemic driver genes and which were passenger deletions.

All available pTRIPZ constructs (Figure 39) were purchased for *NR3C1*, *HMHB1*, *FGF1*, *ARHGAP26*, and *YIPF5*. Bacterial stocks were amplified and plasmid DNA extracted which was then used for lentiviral production. The 697 cells were used for the pTRIPZ pool as they are a Dex sensitive ALL cell line and the titre of pTRIPZ was not high enough to transduce the primary derived L707 presentation cells. 697 cells were transduced with this pool and puromycin (0.6 µg/ml) used to select transduced cells. This concentration of puromycin was selected based on a puromycin kill curve done with the 697 cells (Figure 40). Selection was continued for approximately 3 weeks, until 697 cells were ~90% RFP positive based on FACS analysis before experiments using the pool were started.

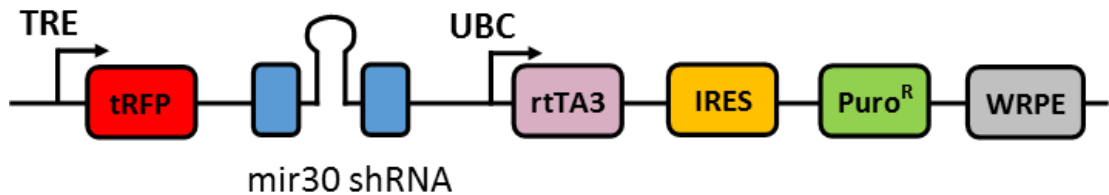


Figure 39: Sequence of pTRIPZ plasmid. Doxycycline, a tetracycline antibiotic, binds to rtTA3 (reverse tetracycline transactivator) which in turns activates the TRE(tetracycline responsive element). The TRE then drives expression of tRFP (turbo red fluorescent protein) and the shRNA construct. The rtTA3, as well as the lentiviral integration, resistance and stabilisation components; IRES (internal ribosome entry site), Puro^R and WPRE (Woodchuck hepatitis virus posttranscriptional regulatory element), are expressed under the drive of the constitutively active UBC promoter.

Puromycin cytotoxicity in the 697 cells

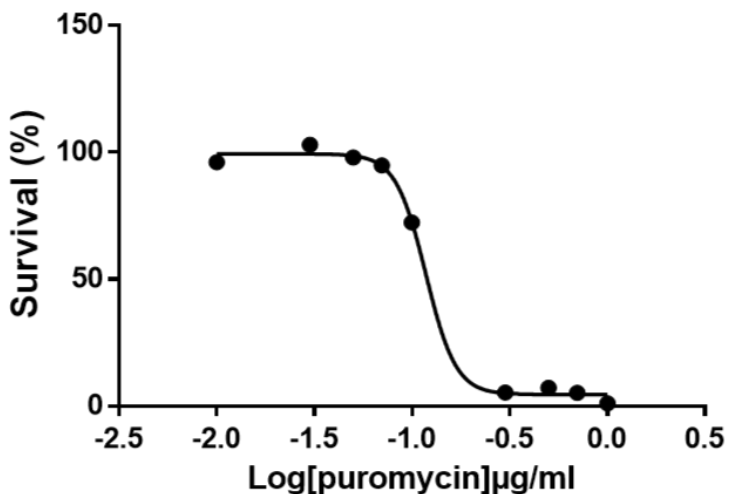


Figure 40: Puromycin kill curve for the 697 cells used to determine the lowest concentration of puromycin required to kill all non transduced cells. Cells were incubated with puromycin for 48h before WST-1 assay, data was analysed using a 4 parameter dose response curve, n=1. -0.5 Log[puromycin]μM is 0.3 μg/ml which was initially used with transduced cells but cells were found to select slowly so the concentration was increased to 0.6 μg/ml for puromycin selection.

5.1.1.1 Pool Validation

The addition of doxycycline to 697 cells transduced with pTRIPZ plasmids will induce shRNA expression and gene knockdown. This is done by the activation of the rtTA3 by doxycycline and subsequent activation of the TRE which drives expression of the shRNA. Before this was tested in a large experiment cytotoxicity assays were carried out to determine the sensitivity of the transduced cells to Dex as well as the levels of NR3C1 mRNA knockdown caused by each single constructs for NR3C1 targeting shRNA. The 697 pTRIPZ cells had no change in Dex sensitivity compared to un-transduced 697, with an IC₅₀ of 18.3nM compared to 20.5nM in the un-transduced cells. This was changed if the cells were treated with Dox (Figure 41). When the individual NR3C1 targeting shRNA were tested separately they did show knockdown of mRNA when treated with doxycycline compared to un treated controls. The untreated controls also showed knockdown in NR3C1 mRNA compared to cells transduced

with pTRIPZ constructs targeting AML1/ETO, which the 697 cells do not have (Figure 42). This implies that the constructs are leaky and expression is driven even in the absence of doxycycline. No effect on proliferation was seen in 697 cells with NR3C1 knockdown (data not shown). The apparent disparity between levels of knockdown and effect on Dex resistance could be attributed to the shRNA affecting the protein more than it does the mRNA.

When the 697 cells transduced with the full pool of pTRIPZ constructs was treated with Dex, the cells treated with doxycycline were resistant. No resistance was seen in cells not treated with doxycycline. The lack of resistance in 697 pTRIPZ cells not treated with doxycycline would indicate that the leakiness of single NR3C1 shRNA seen by qPCR does not affect drug response.

Investigation of the NR3C1 targeting shRNA individually shows that some are more efficient than others with NR3C1-sh1 and sh5 not showing the same level of increase as sh2-4 in the Dex + Dox group, which have around 2 fold increase compared to control (Figure 44).

This disparity between the mRNA levels and the resistance to Dex could be accounted for by an inhibition of protein translation by the shRNA. A decrease in protein expression without an accompanying reduction in mRNA has been found in several studies investigating RNAi (Nottrott, Simard, and Richter 2006; Maroney et al. 2006). For these reasons despite apparent leakiness the 697 pTRIPZ pool cells were used for further experiments.

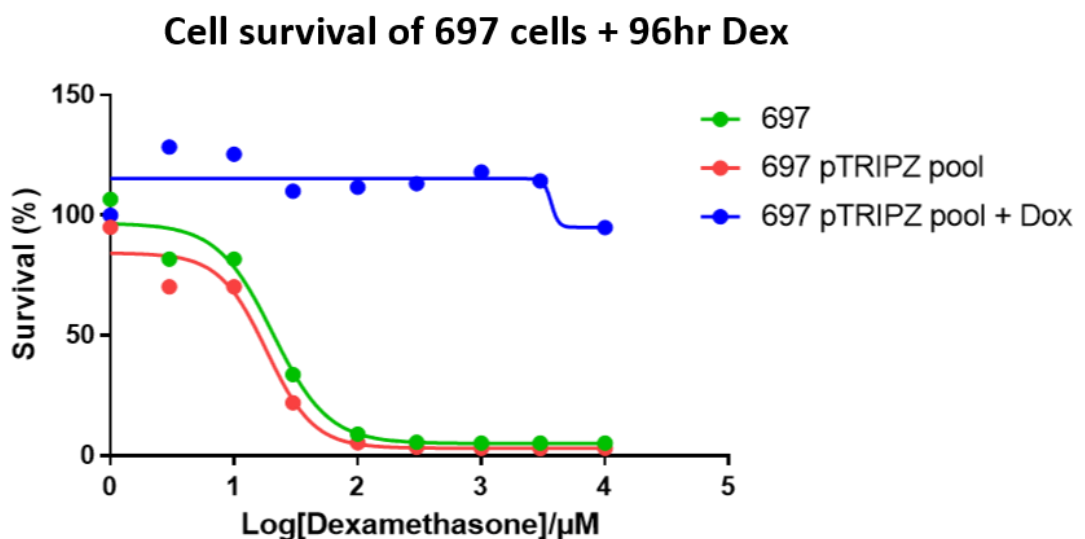


Figure 41: Cell survival of 697 and 697 pTRIPZ pool cells with and without Dox treatment (2 µg/ml) in response to Dex treatment. Viability was measured using WST-1 assay after 96h treatment and data analysed using a 4 parameter dose response curve . 697 pTRIPZ pool cells do not show any increase in Dex compared to the untransduced 697 cells resistance unless they are also treated with Dox, n=1.

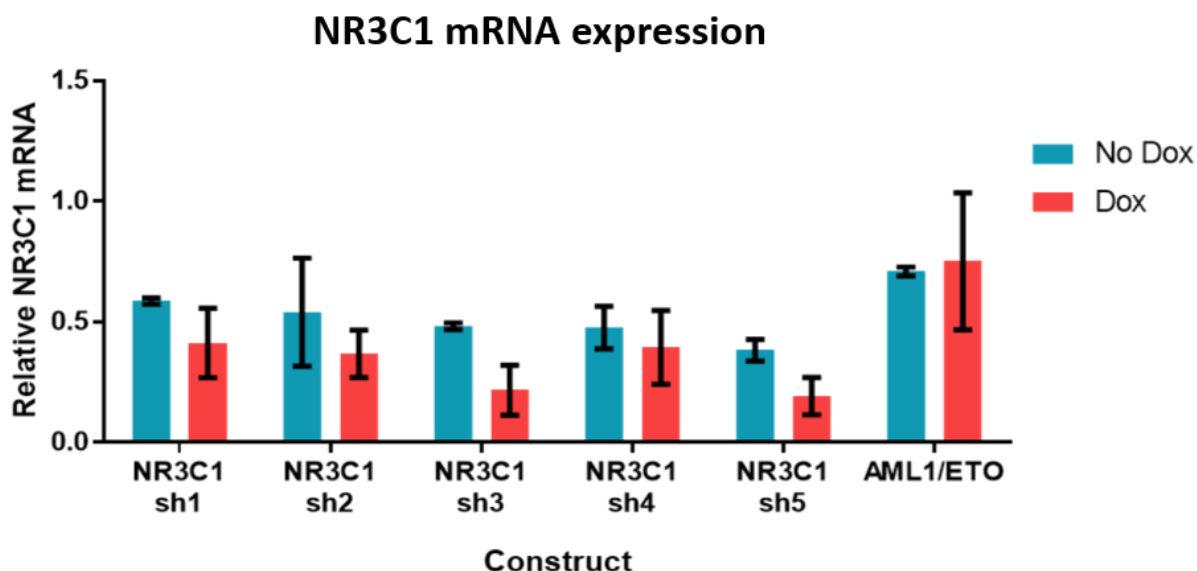


Figure 42: NR3C1 mRNA expression in 697 cells transduced with NR3C1 targeting shRNA, with and without Dox (2 mg/ml). Although the constructs when treated with Dox were not significant compared to the constructs without Dox (due to the leakiness of construct) using one way ANOVA. NR3C1-sh2, sh3 and sh5 had a significant ($p<0.05$) reduction in NR3C1 mRNA with Dox treatment compared to AML1/ETO with Dox treatment (one way ANOVA). The decrease in NR3C1 mRNA in many of the constructs not treated with Dox indicates leakiness of the construct and aberrant expression of the shRNA which resulted in reduced NR3C1 mRNA in the absence of Dox induction, n=3, error bars show mean SEM.

5.2 Induced NR3C1 targeting shRNA are enriched only in the presence of Dex.

In order to determine the contribution of the 5 genes within the 5q deletion seen in the L707 relapse, to Dex resistance, the cells were treated with combinations of Dex and Dox over a short time period. Cells were dosed with Dex for 10 days, and if they were also receiving Dox, a further 3 days before the Dex treatment to induce shRNA expression. Analysis of pool complexity at the end of the 10-day testing period was used to determine which shRNA levels were changed between baseline and the end point. The enrichment or depletion of constructs would indicate loss of gene expression or the incompatibility of reduced expression with survival respectively. Cells were tested using 4 different treatment groups as shown in Table 31

Group	Treatment
Control	0.05% ethanol 3 times a week
Dox	0.6 µg/ml Dox media
Dex and Dox	20 nM Dex 3 times a week, 0.6 µg/ml Dox media
Dex	20 nM Dex 3 times a week

Table 31: Table showing the different treatment groups and the treatments those cells received in the testing of the pTRIPZ transduced 697 transduced cells.

After samples were collected genomic DNA was extracted and a 1 step PCR process to create an amplicon library. The Decode PCR primers provided with the Decode Pooled Lentiviral shRNA Screening library, which are designed to amplify pGIPZ and pTRIPZ constructs were used amplify the region around the shRNA and add the Illumina adaptors and barcodes. Barcoded primers meant that samples could be run together on the Illumina MiSeq and then de-multiplexed to determine changes in pool complexity between samples.

Files were returned in the form of FASTQ files and were de-multiplexed and counted by Dr, Simon Cockell from the Bioinformatics Support Unit. Data in the form of count tables was used for analysis. It was normalised by using the sample count as a percentage of total reads. The fold change between the baseline and experimental samples was calculated, and these values were used to determine which shRNA were enriched and which were depleted.

5.2.1 NR3C1 targeting shRNA are enriched when cells are treated with Dex and Dox

NR3C1 targeting shRNAs are enriched in the Dex + Dox treatment group compared to all other treatment groups, to a much greater extent than the other targeting shRNA (Figure 43-44). There is also a smaller increase in NR3C1 targeting shRNA in the Dex only treatment group. The increase in NR3C1 targeting shRNA in the Dex + Dox group indicates the NR3C1 targeting shRNA are having the expected effect and knockdown of the gene results in increased Dex resistance in these cells. However, as there is no change in the levels of any of the other shRNA constructs, this implies that they have no effect in the 697 cells. As there was only one repeat statistical analysis could not be carried out.

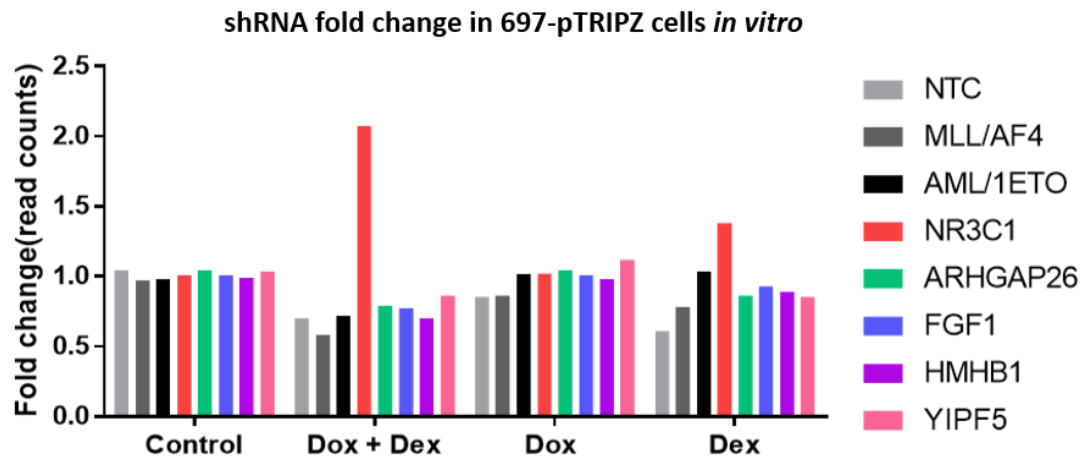


Figure 43: Fold change of the shRNA count number in the 697 cells transduced with pTRIPZ constructs when treated with Dex/Dox combinations over a 13 day period. Separate constructs for the genes with more than one targeting shRNA are shown as an average. Fold change was calculated using the normalised reads in the baseline compared to the normalised reads at the endpoint. NR3C1 targeting constructs are increased in both the Dex + Dox and Dex groups, n=1.

The apparent disparity between the mRNA knockdown of NR3C1 for each shRNA (Figure 42) and the shRNA which are enriched most in the screen in Dex + Dox treated cells (Figure 44) further lends credence to the theory that the mRNA knockdown is not totally indicative of the levels of protein down regulation in the 697 cells. The shRNA with the most enrichment are sh-2-4, wheras the shRNA showing the highest levels of mRNA knock down are sh-3 and sh-5. This contradiction in results could have been better explained if a western blot had been carried out on the 697 transduced with each shRNA.

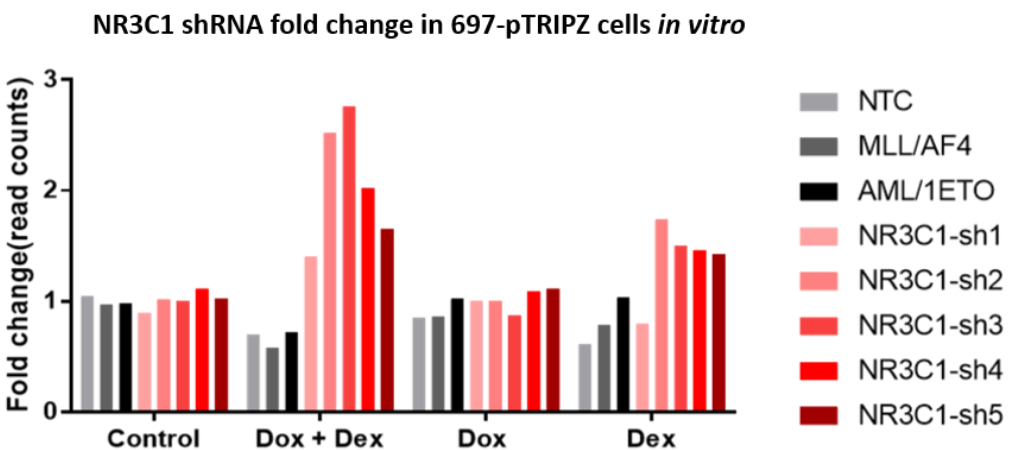


Figure 44: Fold change of the shRNA count number for the 5 separate NR3C1 targeting shRNA constructs and the 3 control shRNA in 697 cells over a 13-day period with combinations of Dex and Dox. Fold change was calculated using the normalised reads in the baseline compared to the normalised reads at the endpoint, n =1.

The screen was run a second time to verify the results as well as determine the effect of varying the dose of Dex. When this was done, three concentrations of Dex were used, 10 nM, 20 nM and 50 nM, equating roughly to the IC₂₅, IC₅₀ and IC₇₅ values. The other treatment conditions were kept the same as the first experiment. There was a substantial increase in NR3C1 targeting shRNA in all 3 groups treated with Dex and Dox but as only one repeat was done statistics could not be done on the data to determine the significance. One thing noted with this experiment is there was also an increase in NR3C1 targeting shRNA in the Dex only groups (Figure 45). Upon further investigation this appears to be a result of the pTRIPZ plasmid containing the UBC (Ubiquitin C) promoter to control expression of rtTA3, which is activated in response to Dex treatment (Marinovic et al. 2002a). It was hypothesised that increased expression of UBC driven rtTA3 may be enough to activate the TRE in the absence of doxycycline. This was not tested however. There also appears to be loss of MLL/AF4 targeting constructs when cells are treated with Dex alone. The cause for this is not known as the 697 cells do not express the MLL/AF4 fusion protein.

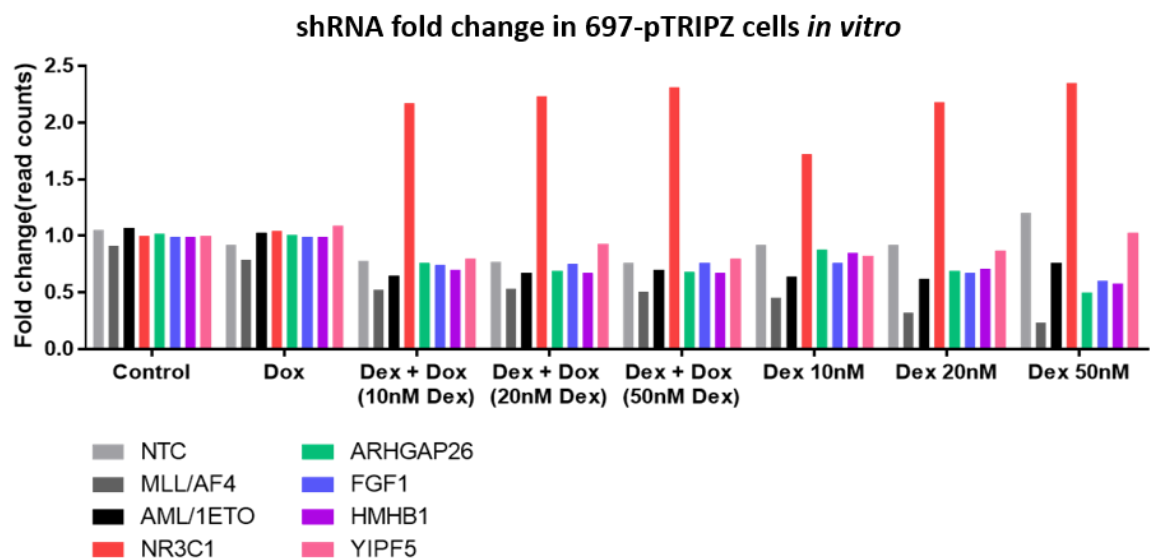


Figure 45: Fold change of the count number for all constructs for the second in vitro run including 3 concentrations of Dex. Dex + Dox, and Dex only treatment groups have increased NR3C1 shRNA expression. Fold change was calculated using the normalised reads in the baseline compared to the normalised reads at the endpoint, n=1.

The same trend seen with first screen was also seen in the second screen, with an increase in NR3C1-targeting shRNA in both Dex and Dox and Dex only treatment groups (Figure 46). The increase corresponds with an increase in Dex concentration. The same pattern of shRNA increases is seen, with levels of sh2-4 being the most increased. This is likely as a result of increased efficiency of those shRNA compared to sh1 and sh5. Indeed, NR3C1-sh3 has the highest level of NR3C1 mRNA knockdown when investigated singly.

NR3C1 shRNA fold change in 697-pTRIPZ cells *in vitro*

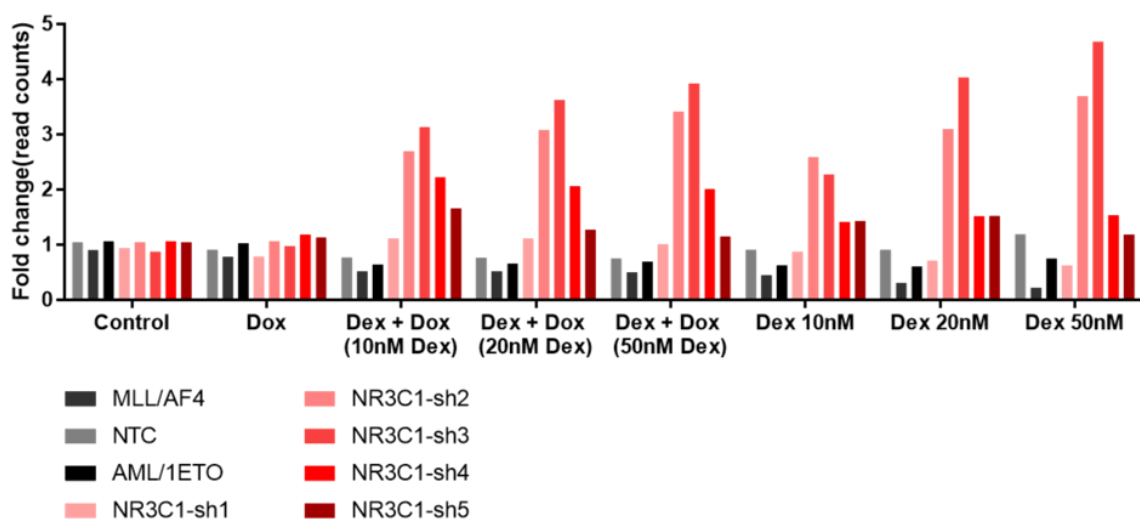


Figure 46: Fold change in the count number for the 5 separate NR3C1 targeting shRNA and the 3 control shRNA in 697 cells treated over a 13-day period with combinations of Dex and Dox for the second run of the experiment. Fold change was calculated using the normalised reads in the baseline compared to the normalised reads at the endpoint, n = 1.

5.2.2 *Survival of mice is not affected by induction of shRNA constructs*

The same experiment was done *in vivo* using 17 male NSG mice. Each mouse was intrafemorally injected with 10^4 transduced 697 cells and then split into 2 groups given either Dox containing food or normal food. These two groups of mice were then split further into control or Dex treatment groups, resulting in 4 different treatment groups. Dox food was given from 8 days after intrafemoral injection, and Dex (10 mg/kg) I.P. every weekday was started 2 days after that. Mice were monitored every day and were humanely killed when they reached license endpoints. As can be seen from Figure 47, Dex treated mice died slightly earlier than control mice, but not significantly earlier than any other treatment group. However, with such small group numbers the significance of this data is questionable. What was found with this experiment is that the 697 cells engraft and result in death very quickly, as 4 of the mice were found dead, which prompted the increase of checking to twice daily after 21 days.

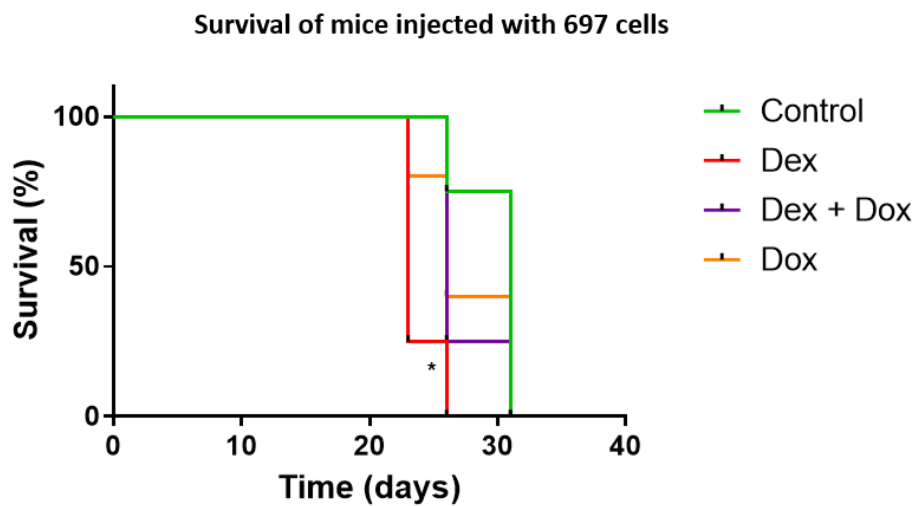


Figure 47: Survival of mice in the 4 different treatment groups. Mice were either fed with Dox containing food or normal food starting 8 days after intrafemoral injection. Mice were also treated with Dex (10 mg.kg) or saline I.P. every weekday started 10 days after intrafemoral injection. Dex treated mice die significantly earlier ($p<0.05$) than the other treatment groups when analysed using the Log-rank (Mantel-Cox) test. The other treatment groups are not significantly different from each other.

5.2.3 *The in vivo screen shows no correlation with treatment group and expression of NR3C1 expressing shRNA constructs*

When the data from the *in vivo* experiment were analysed it was found there was no consistent pattern between any of the groups (Figure 48-49). Some cells were tested for tRFP expression after collection from the mouse and this may provide a reason for why there was no increase in NR3C1 targeting shRNA in either the Dex + Dox treated mice or the Dex only mice. The tRFP expression was reduced from what would be expected in a spleen with high levels of engraftment (Figure 50), indicating that the tRFP and shRNA expression has been silenced. This is a problem that has been reported before with the use of the UBC promoter in our lab *in vivo* (unpublished data).

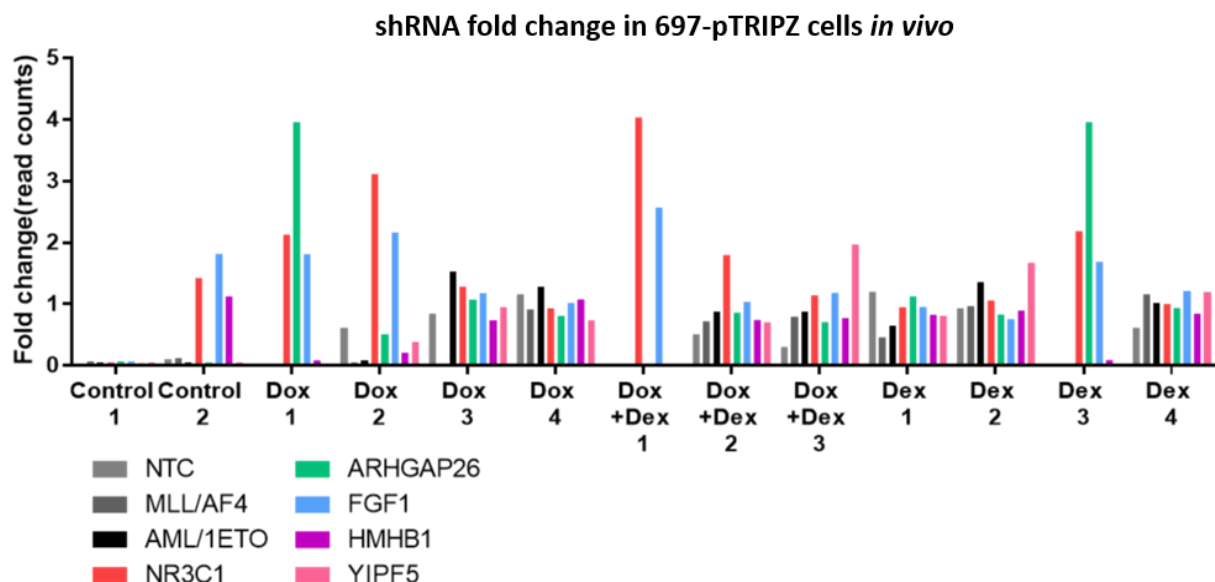


Figure 48: Fold change of shRNA counts from 697 cells engrafted into NSG mice. Control shRNA and the averages of targeting shRNA for each gene are shown. There is no correlation between any of the groups, as there is in vitro. This indicates that either the Dex or Dox is not reaching the cells or the cells are not reacting in the same way they do in vitro. Fold change was calculated using the normalised reads in the baseline compared to the normalised reads at the endpoint.

NR3C1 shRNA fold change in 697-pTRIPZ cells *in vivo*

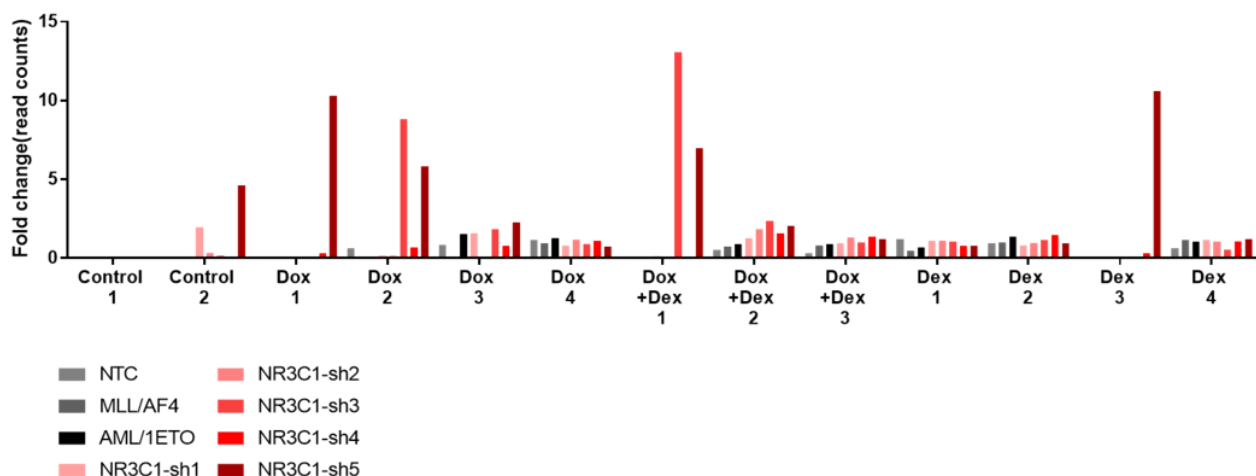


Figure 49: Fold change of shRNA counts from 697 cells engrafted into NSG mice. Control shRNA and the 5 NR3C1 targeting shRNA are shown. There is no correlation between any of the groups in NR3C1 targeting shRNA in the Dex + dox mice as there is in vitro. This indicates that either the Dex or Dox is not reaching the cells or the cells are not reacting in the same way they do in vitro. Fold change was calculated using the normalised reads in the baseline compared to the normalised reads at the endpoint.

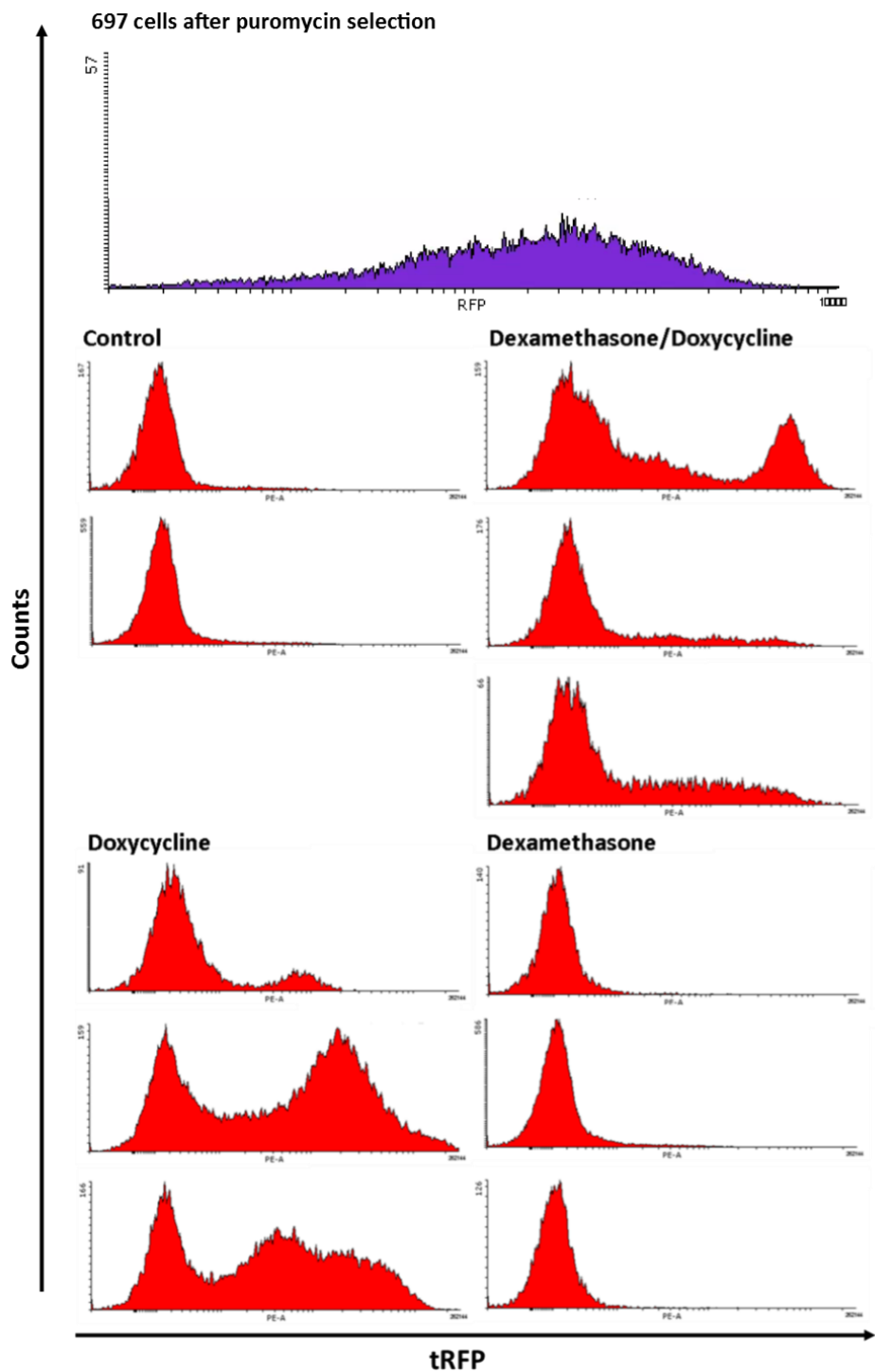


Figure 50: FACS analysis of 697 cells after puromycin selection before injection into mice, and spleen samples after collection from mice. Mouse spleens were very heavily engrafted upon collection, the amount of tRFP negative cells in samples treated with doxycycline is higher than expected indicating that the expression of tRFP and the shRNA under the same promoter is being silenced in these cases.

What can be taken from this experiment is that *in vitro*, the NR3C1 targeting shRNAs result in Dex resistance when induced by Dox treatment. These constructs are slightly leaky, and

there is an increase in NR3C1 targeting shRNA expression when cells are just treated with Dex. This does not appear to alter the Dex resistance of the sample, which has a similar cytotoxicity profile to the un-transduced 697 cells.

In vivo is a different story, and no useful data can be gleaned from this experiment other than the pTRIPZ plasmid is susceptible to silencing *in vivo* and should be avoided for future experiments. Despite a lack of data to support the original hypothesis, the use of the 697 cells for this experiment led to the incidental finding that the 697 cells appear to be Dex resistant *in vivo*. This led to further experiments to investigate this. It is also possible that the lack of changes in the enrichment of constructs may not just be a result of silencing but because the cells are not responding to Dex treatment in the murine microenvironment.

5.2.4 *Mifepristone acts as a partial agonist at NR3C1 in the 697 cells*

The next hypothesis was that if loss of NR3C1 is a disadvantage to cells, except in the presence of dexamethasone, then antagonism of the receptor may also be a disadvantage. To study this, mifepristone, a progesterone and glucocorticoid receptor antagonist with high binding affinity for NR3C1, was used (Bourgeois, Pfahl, and Baulieu 1984). Mifepristone treatment has been shown to be of use in spontaneous murine leukaemia, with treated mice having significantly better survival (Check et al. 2009).

Before the study was taken into mice, the effect of both Dex and mifepristone on the expression of several NR3C1 inducible genes was tested in the 697 cells to ensure they were having the desired effect. Treatment with 10nM or 100nM Dex increases the expression of GILZ (Glucocorticoid induced leucine zipper), NFKBIA (NFKB inhibitor alpha) and FKBP5 (FK506 binding protein 5), to different extents with GILZ being the most induced. This induction of expression is rapid and occurs within 2hr, whereas FKBP5 is slower to respond (Figure 51). As well as the induction of target genes there is also an auto induction of NR3C1 expression when cells are treated with Dex.

Mifepristone when tested had a somewhat surprising effect, Although NFKBIA expression in response to mifepristone reduced, as would be expected with an antagonist, with a steady decrease in both NFKBIA and NR3C1 mRNA over the time period. When GILZ was measured

it was found that within the first few hours after drug exposure there was an increase in GILZ mRNA. By 24hr this was reduced, as was NR3C1 expression, but there was an initial increase induced by mifepristone. FKBP5 expression had an initial decrease before recovering expression in response to mifepristone (Figure 52).

From this data it would appear that mifepristone is not a NR3C1 antagonist as there is little evidence for NR3C1 inhibition in cells treated with Mifepristone. Mifepristone does appear to be a partial antagonist with agonist activity at some concentrations and time points. The partial agonist activity of mifepristone has been reported in two kidney cell lines, and is reported to occur when there are high levels of NR3C1 present, which is sufficient to drive the formation of NR3C1 dimer DNA complexes, which can then become transcriptionally active (Zhang, Jonklaas, and Danielsen 2007).

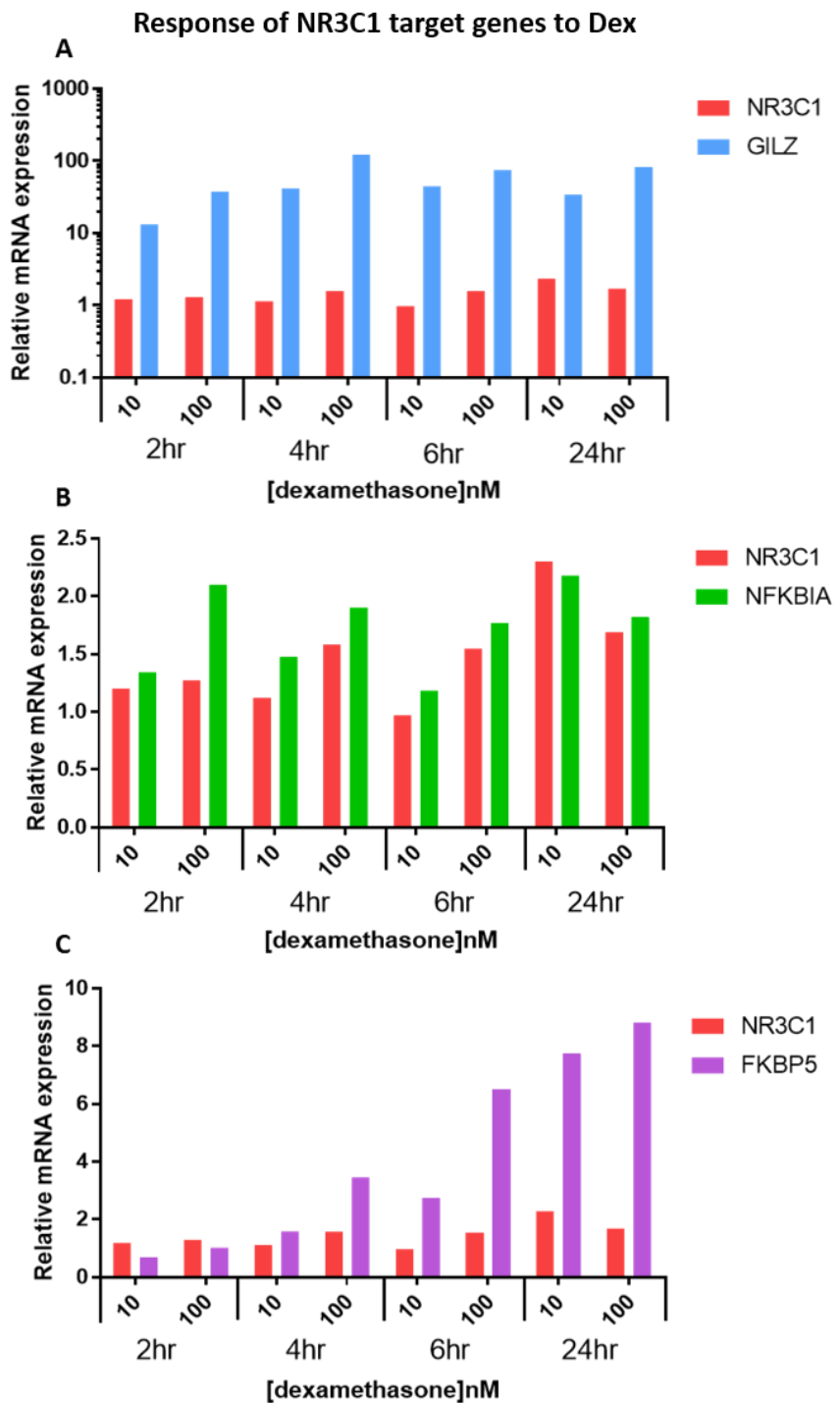


Figure 51: Response of NR3C1 target genes and NR3C1 to Dex treatment over a 24 hr period in the 697 cells, bars show mRNA level relative to GAPDH and control samples. A – The increase in GILZ mRNA is rapid and sustained over 24 hr. B- NFKBIA expression increases are much smaller than with GILZ, but there is an increase in expression correlated with increased dose, the auto induction of NR3C1 by Dex can also be seen. All data is relative to samples taken at 0 hr. n = 1.

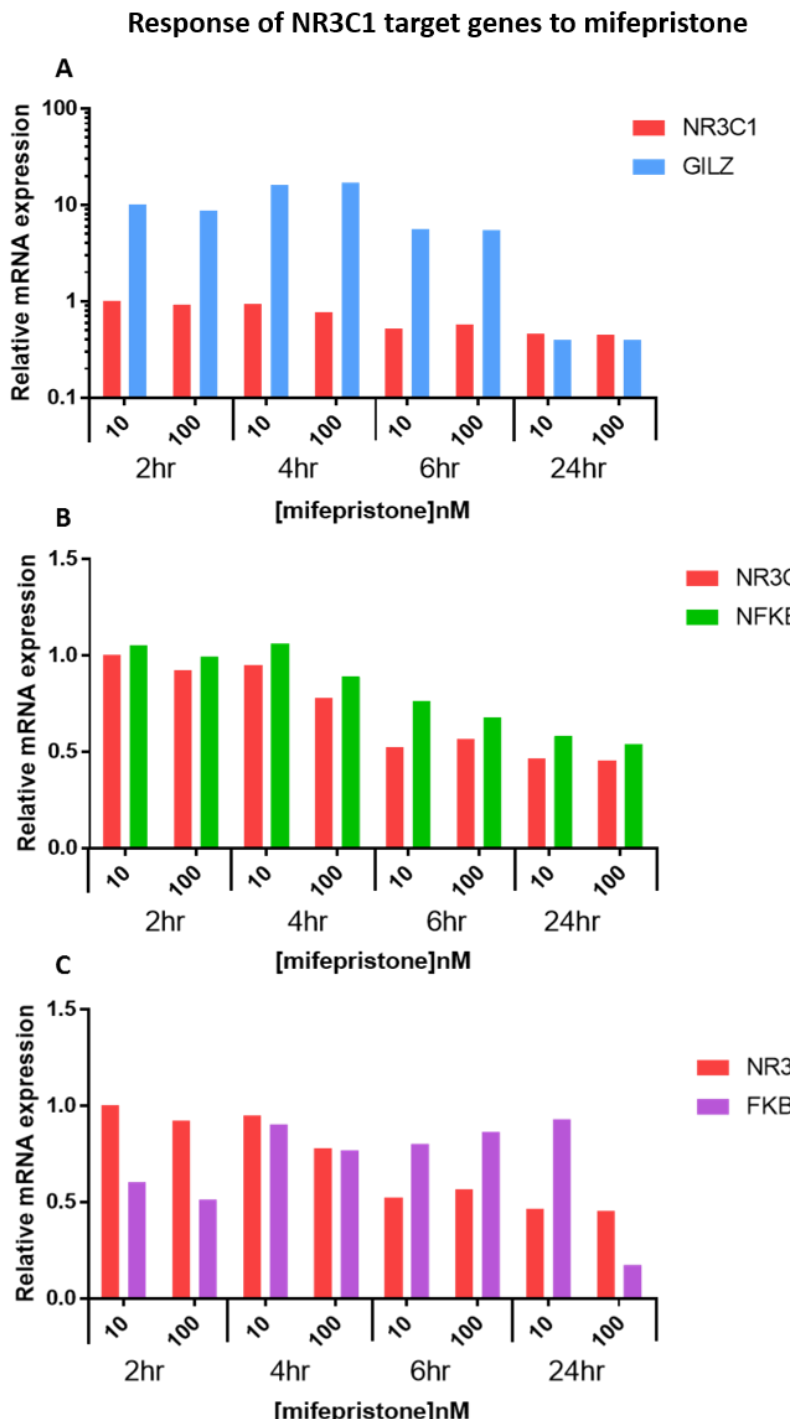


Figure 52: Response of NR3C1 target genes and NR3C1 to Mifepristone treatment over a 24 hr period in the 697 cells, bars show mRNA level relative to GAPDH and control samples.. A – There is an initial increase in GILZ mRNA before it is reduced by 24 hr. There is little increase in NR3C1 and this too is reduced by 24 hr. B – NFKBIA expression reduces over the time period but it is not a large difference. C – FKBP5 expression shows an initial decrease before recovering somewhat. All data is relative to samples taken at 0 hr. n =1.

5.2.4.1 Mifepristone is not toxic in mice up to doses of 100 mg/kg

Despite the apparent initial agonist activities of mifepristone, the reduction in GILZ mRNA by 24h was determined to be sufficient to warrant taking the hypothesis further and testing mifepristone *in vivo*.

As this drug is widely used for a number of medical conditions it has a well-known safety profile and so only a small toxicity study was needed to determine the concentrations that were tolerated in the NSG mice.

6 male NSG mice were intrafemorally injected with 1×10^5 L707 presentation cells, and 2 weeks later dosing with mifepristone was initiated for 3 mice. Three doses, 10, 30 and 100 mg/kg mifepristone were used. This was given in suspension in olive oil by oral gavage, with a dose escalation every 7 days to determine the highest tolerated dose. There was no effect of mifepristone dosing on the weight of treated mice compared to controls (Figure 53), and although mice tolerated the highest dose the suspension was very viscous and hard to administer, so to avoid possible injury from dosing with a thick liquid 30 mg/kg was chosen for further experiments.

Change in mouse weight over dosing period

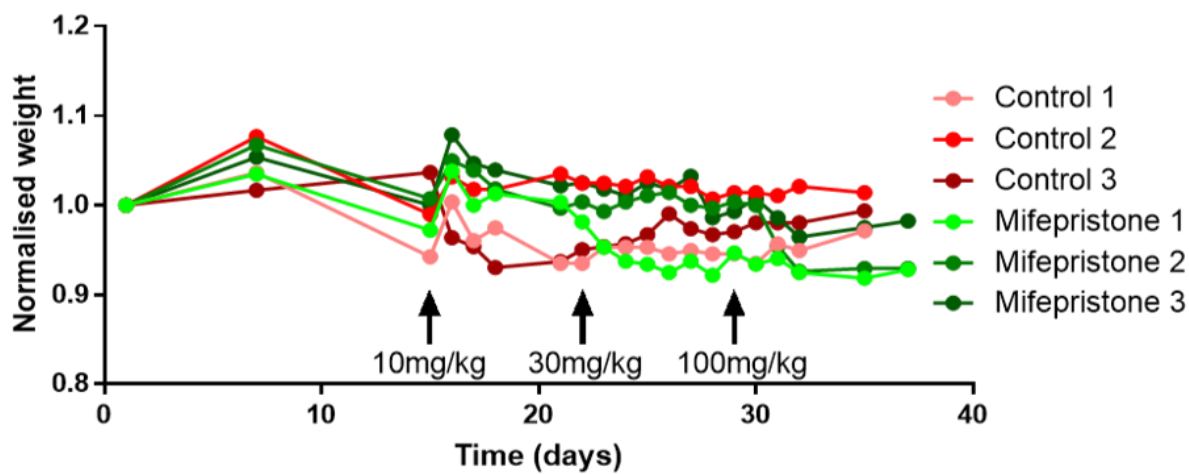


Figure 53: Weight of mice normalised to weight at the start of the experiment. Black arrows indicate start of dosing and the concentration of mifepristone given at these time points and for the next 7 days. The drop in weight seen in all but one mouse before the 10 mg/kg dosing was started was due to a blocked water bottle.

5.2.4.2 Mifepristone does not increase survival of mice engrafted with L707 presentation cells

Once the lack of toxicity of mifepristone in the NSG mice had been established, a larger study was run to determine mifepristone treatment had any effect on survival of mice engrafted with L707 presentation cells. The hypothesis was that treating the L707 presentation with mifepristone may result in a phenotype similar to the L707 relapse, with longer survival periods of mice.

11 male NSG mice were each injected with 5×10^5 L707 presentation cells transduced with the luciferase expressing lentiviral plasmid, pSLIEW. 13 days later, imaging was carried out using the *in vivo* imaging system (IVIS) to ensure mice were engrafted (Figure 54). Once engraftment was established dosing was started with either Dex (15 mg/kg), mifepristone (30 mg/kg) or control (olive oil). Dosing was done by oral gavage and was given every weekday. The different groups were separated by cage as mifepristone is excreted in the faeces and as mice are coprophagic, mixing mifepristone treated mice with other treatment groups might result in other mice also being dosed with mifepristone.

Survival of mice was increased significantly with Dex treatment as had been seen before, but mifepristone had no effect on survival (Figure 55).

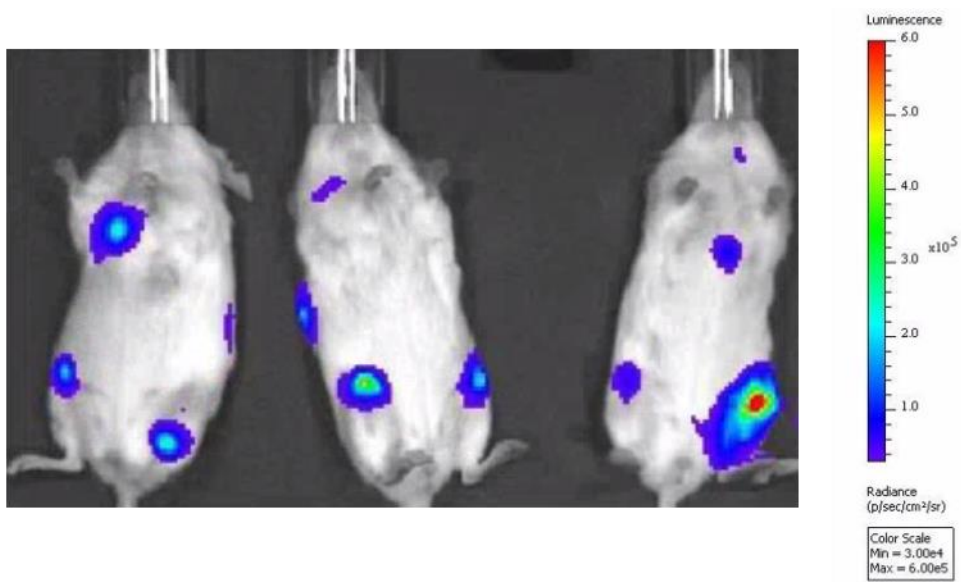


Figure 54: Representative IVIS image of 3 mice showing bioluminescence in the mouse 13 days after injection with L707 presentation pSLIEW cells. Bioluminescence is produced by the oxidation of uciferin to oxyluciferin, catalysed by luciferase, which is encoded in the pSLIEW plasmid which was used to transduce the L707 presentation cells before they were intra-femorally injected into the mice. Engraftment can be seen in the injected femur (right) and the contralateral femur as well as several other locations. This indicates that the leukaemia has spread beyond the site of injection.

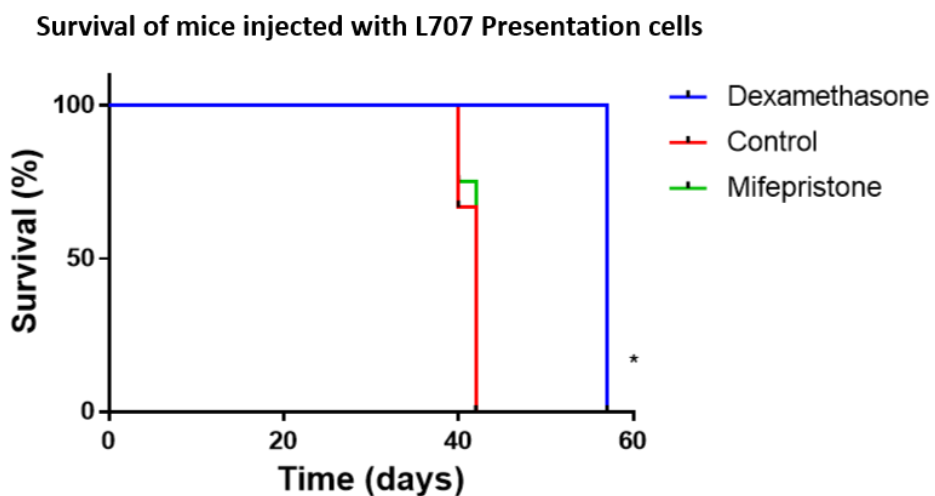


Figure 55: Survival of mice engrafted with L707 presentation pSLIEW cells. There is no effect of mifepristone (30 mg/kg) dosing on survival, Dex (15 mg/kg) treated mice survive significantly ($p<0.05$) longer than control and mifepristone treated mice. Dex and mifepristone groups n=4, control group n=3. Statistical analysis done using Log Rank (Mantel-Cox) test.

After mice were killed, FACS analysis was used to determine levels of CD19 positive human cells in the spleens as these were to be used for microarray analysis and needed to have low levels of murine cells that would contaminate the results. The percentage of L707 presentation cells was high in the spleens, with an average of 97% between all the spleens tested by FACS (Figure 56). The levels of GFP in the samples was very low, with an average of just 0.22% of cells expressing GFP, indicative of very low transduction levels with pSLIEW of these cells. This low amount is sufficient for mice engrafted with these cells to be analysed using IVIS imaging.

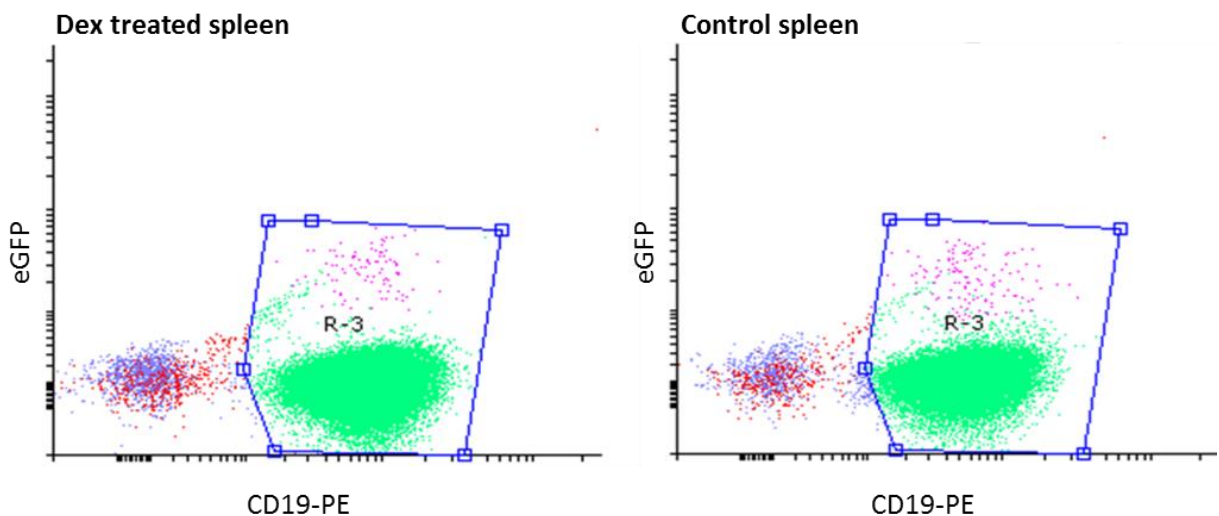


Figure 56: Two FACS plots showing the levels of CD19-PE and GFP positive cells. The majority of cells are CD19 positive, but only a small fraction is positive for GFP (average 0.22%). R3 shows CD19 positive cells, red cells within that show GFP positivity. There was no difference seen between the spleens of the Dex treated or Control spleens. Representative images, all plots showed a similar picture.

RNA was extracted from the spleen samples using the MirVana kit (Ambion). This RNA was then sent to Oxford Genomics for microarray analysis to determine the changes in the gene expression profile of the L707 presentation cells when treated with Dex, mifepristone or controls.

5.2.5 Microarray analysis

Data was returned from Oxford Genomics in the form of Illumina IDAT files. These were analysed in two ways, firstly using Genome studio for normalisation and then Excel to determine which genes have altered expression, and secondly in R using the microarray analysis programmes Lumi and Limma.

5.2.5.1 *Control vs Dex treatment shows reduction the anti-apoptotic gene BCL2 but no significant enrichment of pathways*

The genes that are differentially expressed between control and Dex treatment samples should give an indication of how Dex is resulting in apoptosis in the L707 presentation cells. Using the thresholds determined previously (>2 fold change in expression, p<0.01, binding >100 in either control or Dex treatment), 375 genes score as differentially up or down regulated; 144 are upregulated in Dex treatment compared to controls, and 231 are downregulated in response to Dex.

Two of the proteins upregulated in response to Dex are S100A8 and S100A9 (S100 Calcium binding proteins A8 and A9). These genes have been shown to result in glucocorticoid resistance when expression is increased in MLL rearranged ALL (Spijkers-Hagelstein et al. 2012). These proteins suppress the glucocorticoid induction of increased cytosolic calcium ions required to initiate apoptosis.

Gene ontology of the 144 genes upregulated with Dex treatment shows that positive regulation of biological processes (FDR=3.04e-5), cellular response to chemical stimuli (FDR=3.04e-5) and signal transduction (FDR=1.77e-4) pathways are enriched in the list.

The 231 genes that are downregulated more than 2 fold in response to Dex treatment have no pathways significantly enriched. Despite this, there are several genes which indicate the Dex treatment is having an effect, other than the increase in mouse survival. BCL2, an anti-apoptotic protein is reduced 2.2 fold in the Dex treatment samples. This gene has been reported to have a reduction in response to Dex in chondrocytes (Zaman et al. 2014). When

investigated in the gene expression data *BCL2* was found to be expressed at similar levels in the presentation and relapse.

5.2.5.2 *Control vs Mifepristone treatment shows little change in gene expression profile*

When looking at the cells which pass the thresholds in the mifepristone treatment group compared to control, only 6 genes have a p value of < 0.001 . If this is relaxed to 0.005 then the number of probes increases to 9, equating to 7 genes, this is still far less than was expected. This list of genes does not have any enriched pathways associated with it.

The reasons for this lack of differentially expressed genes in the cells treated with mifepristone were unclear at the time of initial microarray analysis and so the data was not used for any further experiments.

5.2.5.3 *Microarray analysis using R shows 2 samples do not cluster with the rest*

Analysis of the microarray data using the R programmes Lumi and Limma sheds a little more light on the apparent lack of data shown using Genome studio and Excel for analysis.

The data was imported into R and 3 probes were removed due to low numbers of beads in at least one sample. VST and RSN were used to transform and normalise the sample (Figure 57-58) before the clustering of samples was determined using PCA (Figure 59). It was found that the Mifepristone 1 and Dexamethasone 3 samples did not cluster with the other samples the way they were expected. This lack of clustering could possibly account for the lack of data found when all samples were analysed using Genome Studio and Excel. For further analysis these 2 samples were removed, which resulted in far closer clustering of treatment groups (Figure 60). The reason for these two samples not clustering together is not known.

When array quality control metrics were run on the arrays, only 35% of probes were left after filtering. This is lower than was expected and could indicate a poor array run but at the point of analysis it was too late to repeat the experiment.

As can be seen from the heat map (Figure 61), when the top differentially expressed genes in the Dex treatment group are used, the control and Dex samples have separate gene signatures. Mifepristone treated cells look more similar to the controls, indicating that the highly differential genes for Dex are not also differentially expressed in mifepristone treated cells.

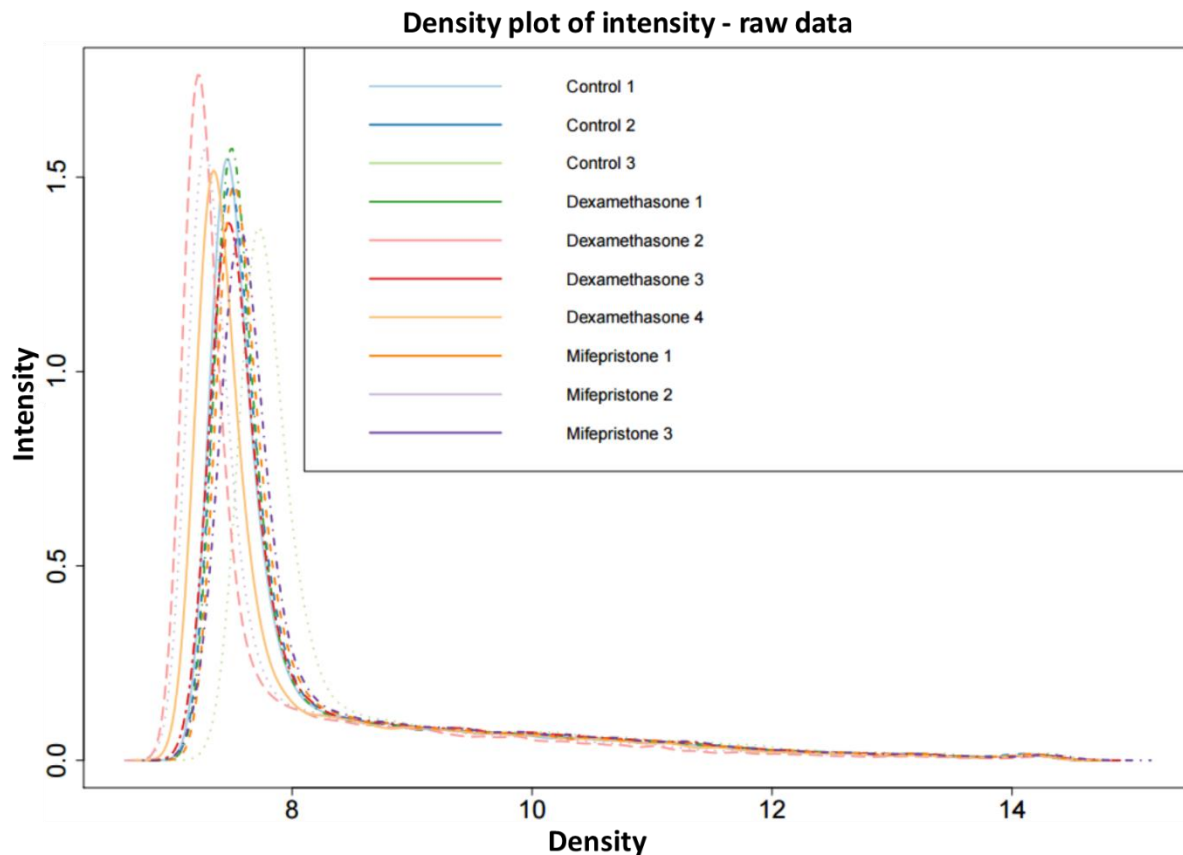


Figure 57: The Density plot of the raw microarray data for the L707 presentation cells treated with Dex, mifepristone or controls before normalisation. The plot gives an indication about the distribution of the intensity of probe binding (signal) across the chip. If chips have very different distribution patterns then they are normally removed from the data analysis. No chips were removed from the analysis at this point.

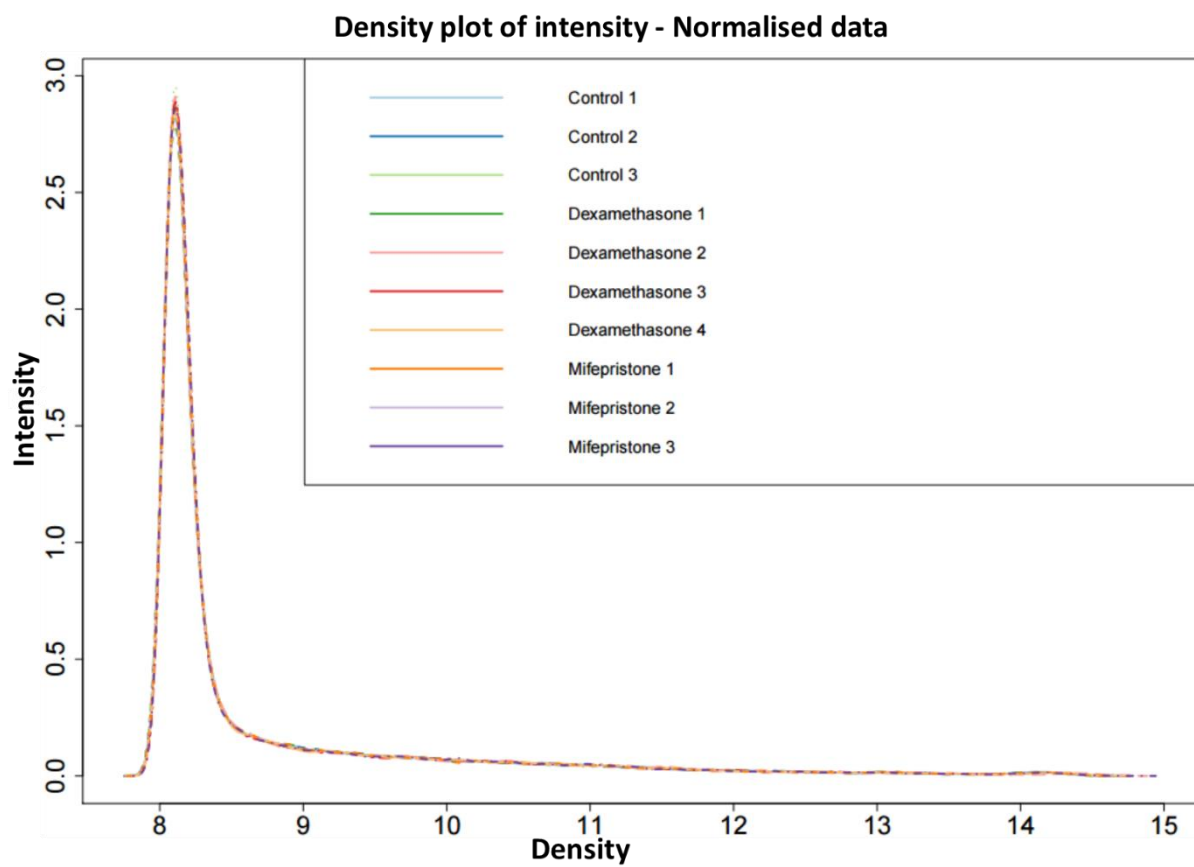


Figure 58: The Density plot of the microarray data for the L707 presentation cells treated with Dex, mifepristone or controls after robust spline normalisation (RSN) has been used. The plot shows that after normalisation the distribution of intensity, and thus probe binding across the chip is the same for all chips meaning they can be analysed together.

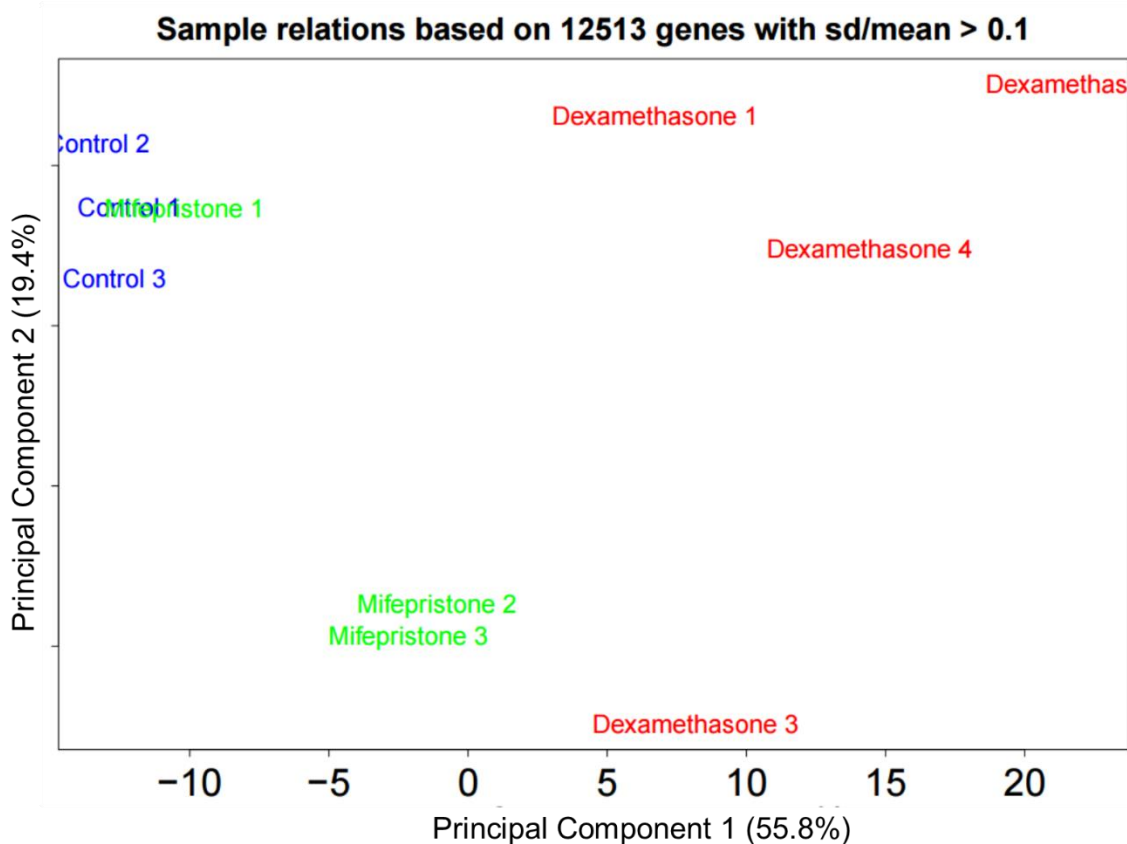


Figure 59: Principal component analysis showing all 10 samples run on the microarray for the L707 samples treated with either Dex, mifepristone or controls. The top 2 principle components are shown, including the percentage contribution of each to the distribution. Two samples, Dexamethasone 3 and Mifepristone 1, do not cluster closely with samples in the same group, the reason for this is not known.

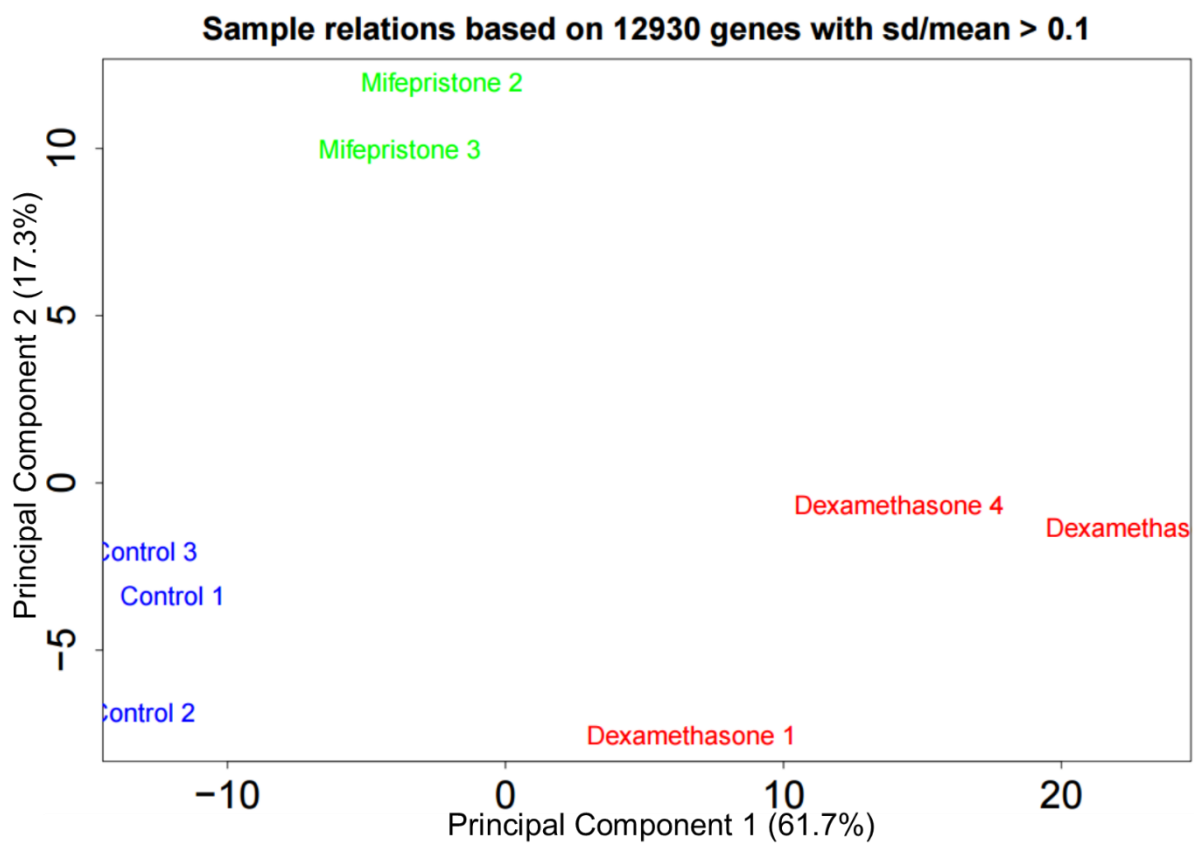


Figure 60: Principal component analysis of the microarray data for the L707 samples treated with either Dex, mifepristone or controls with the two outlying samples, dexamethasone 3 and mifepristone 1 removed. The top 2 principle components are shown, including the percentage contribution of each to the distribution. Samples cluster closer with samples of the same treatment.

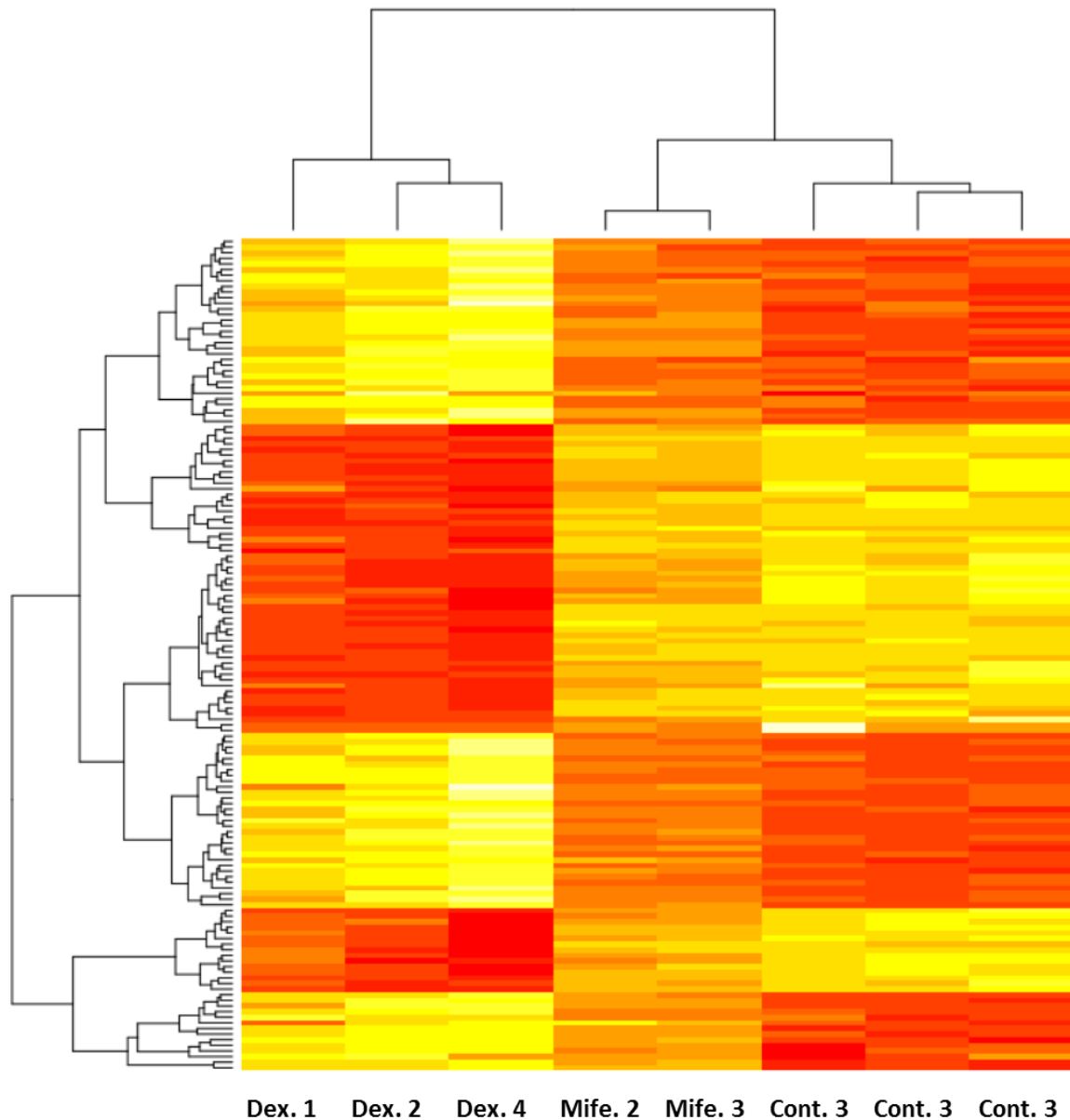


Figure 61: Heat map for the top 1000 differentially regulated genes in L707 presentation treated with Dex compared to L707 presentation cells treated as controls. Clustering shows that L707 cells with mifepristone treatment cluster with controls closer than dexamethasone treatment, this indicates that there may not be a lot of changes induced by mifepristone in the L707 presentation cells.

5.2.6 L707 Presentation; control vs Dex treatment

Once the two anomalous samples were removed from the data analysis was done to determine the differential gene expression in response to treatment with Dex and mifepristone. Analysis of the genes that are differentially regulated in response to Dex in the L707 presentation cells will give an indication of the pathways activated in these cells that result in apoptosis.

5.2.6.1 Up regulated genes in response to Dex

It is known from the survival data that treatment with Dex prolongs survival, so looking at genes which are upregulated should give an indication into how the cells are responding and what pathways are resulting in apoptosis.

1610 probes score as significant ($P<0.05$), which is 13% of all probes that passed through data filtering, but when applying fold change thresholds to this the number reduces dramatically. A p value of 0.05 was used rather than the 0.01 as with the other analyses as there were so few probes significant with the lower p value that no genes scored as significant. 14 genes are upregulated >2 fold in the L707 cells in response to Dex treatment, and these account for just 0.11% of the total probes that passed filtering. These 14 genes show an interconnected network of protein interactions (Figure 62).

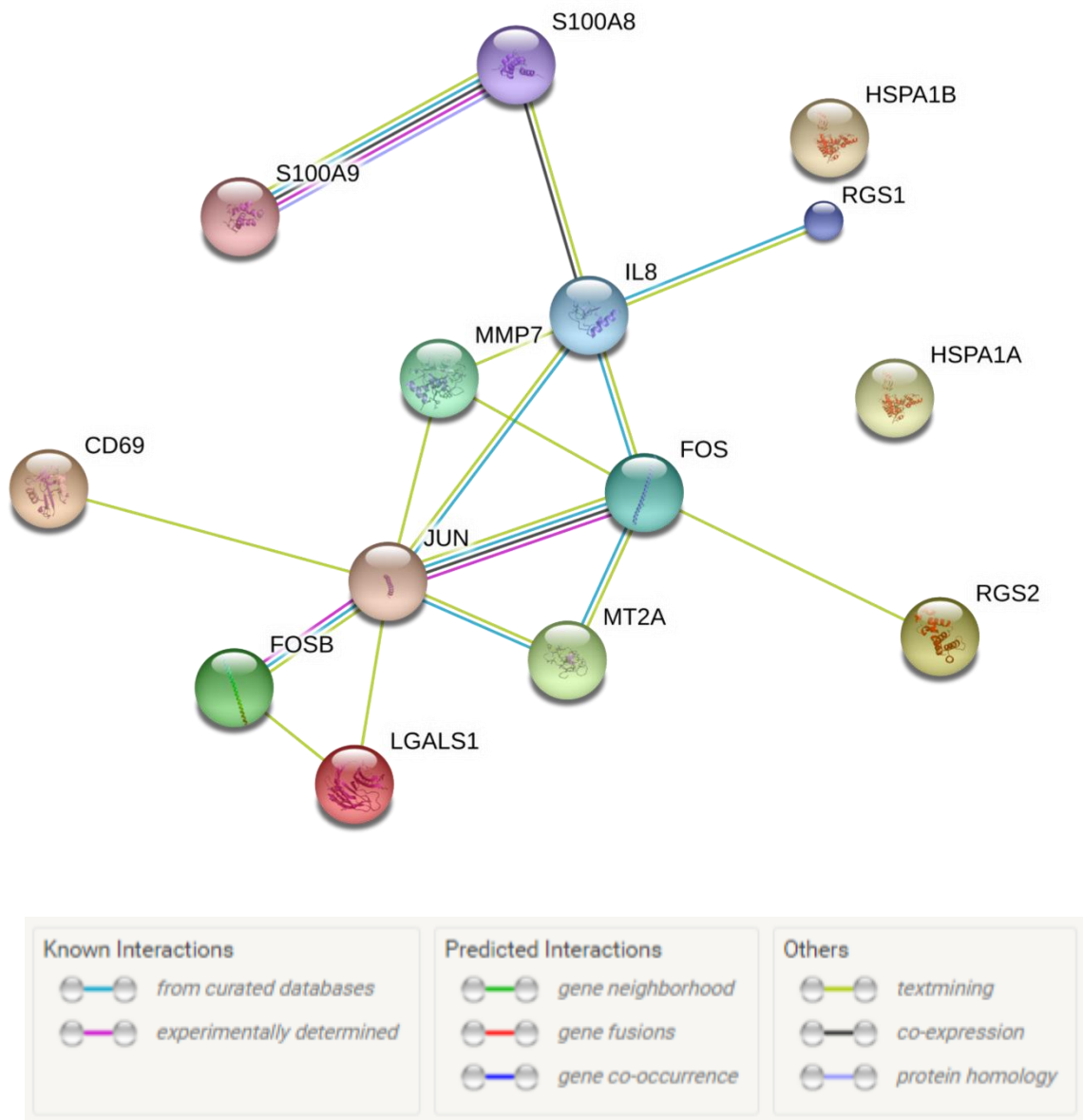


Figure 62: Protein interactions between the 14 genes with >2 fold increase in expression in response to Dex treatment in the L707 presentation cells. Interactions were determined using the online database Search Tool for the Retrieval of Interacting Genes/Proteins (STRING), version 10.0. The types of interactions are shown in the legend below the

Within these upregulated genes several pathways are significantly enriched including response to drugs ($FDR=4.07e-5$) and the immune response ($FDR=7.36e-5$). The upregulation of an immune response pathway could be linked to the presence of Activator protein (AP-1) subunit genes in this list, *Fos*, *Jun* and *FOSB*. AP-1 is involved in the immune response by way of induction of inflammatory mediators. If AP-1 is knocked down using RNAi then cells have been found to have reduced levels of IL6, IL8 and CD38, all inflammatory cytokines. In the

same study that showed this, it was also found that AP-1 protein subunits were regulated by the MAPK (Mitogen activated protein kinase) pathway member MAPK3K8 (Wang et al. 2013). Both MAPK pathway genes and AP-1 are some or the many factors that interact with NR3C1 to alter the activation and repression of target genes. In the case of AP-1 this occurs by AP-1 recruiting the glucocorticoid interacting protein (GRIP1) to initiate transrepression of target genes (Glass and Saijo 2010). Using ChIP seq it was been found that AP-1 was present in a high proportion of NR3C1 binding sites and that loss of AP-1 signalling resulted in a significant reduction in NR3C1 regulation of transcription indicating an interaction of the two transcription factors (John et al. 2011; Biddie, John, and Hager 2010).

As was seen with the analysis done using GenomeStudio and Excel, the calcium binding proteins S100A8 and S100A9 have increased expression in response to Dex in the L707 cells. These genes are 2 of the most differentially regulated genes with a fold change of 4.3 and 5 respectively. The Two other proteins in the list of upregulated genes are heat shock proteins, which form complexes with NR3C1 in the cytoplasm, HSPA1A and HSPA1B (Heat shock protein 1A and 1B). These proteins have been shown to be involved in the NR3C1 mediated regulation of genes (Prota et al. 2012).

5.2.6.2 *Downregulated genes in response to Dex*

The downregulation of genes in response to Dex is another indication of how the drug is affecting the cells. Just 8 probes have >2 fold decrease in expression in Dex treated samples, 0.06% of the total probes that passed filtering. These 8 genes include 5 protein coding genes, 2 SNORD RNA genes and one probe without a gene symbol. The 5 protein coding genes do not show enrichment of any pathways but includes 3 genes, PROM1 (promonin 1), SNORA79 (small nucleolar RNA, H/ACA Box 79) and LOC100132810 which are all significantly reduced in the L707 relapse, which might indicate a role for these genes in the L707 response to Dex in these cells.

If the thresholds are relaxed to include genes with >1.5 fold reduction, then the list of upregulated probes is increased to 19. These 19 probes include 10 protein coding genes, 5

RNA genes and 3 probes without gene symbols. There is still no enrichment of pathways in the gene list.

When the data is used for KEGG pathway analysis there are 17 significantly enriched KEGG pathways in the differentially expressed genes. These included TP53 signalling pathway, pathways in cancer and MAPK signalling pathway.

5.2.7 *Control vs Mifepristone treatment*

Although treatment with mifepristone did not result in a change in survival of mice, investigation of the differentially expressed genes may still prove interesting.

782 probes are significantly ($p<0.05$) differentially expressed between control and mifepristone treated mice. Of these, only 6 probes have >2 fold increase in expression, and none have >2 fold decrease. If the parameters are relaxed to include probes with >1.5 fold change then the number of upregulated probes increases to 14 probes, but still no probes that are downregulated.

The probes that are upregulated >1.5 fold with mifepristone treatment have several interconnecting protein associations (Figure 63). This list also includes 5 genes that are also upregulated in response to Dex, indicating similar pathways may be modulated in the L707 cells in response to these 2 drugs, possibly as a result of the partial agonist activity of mifepristone.

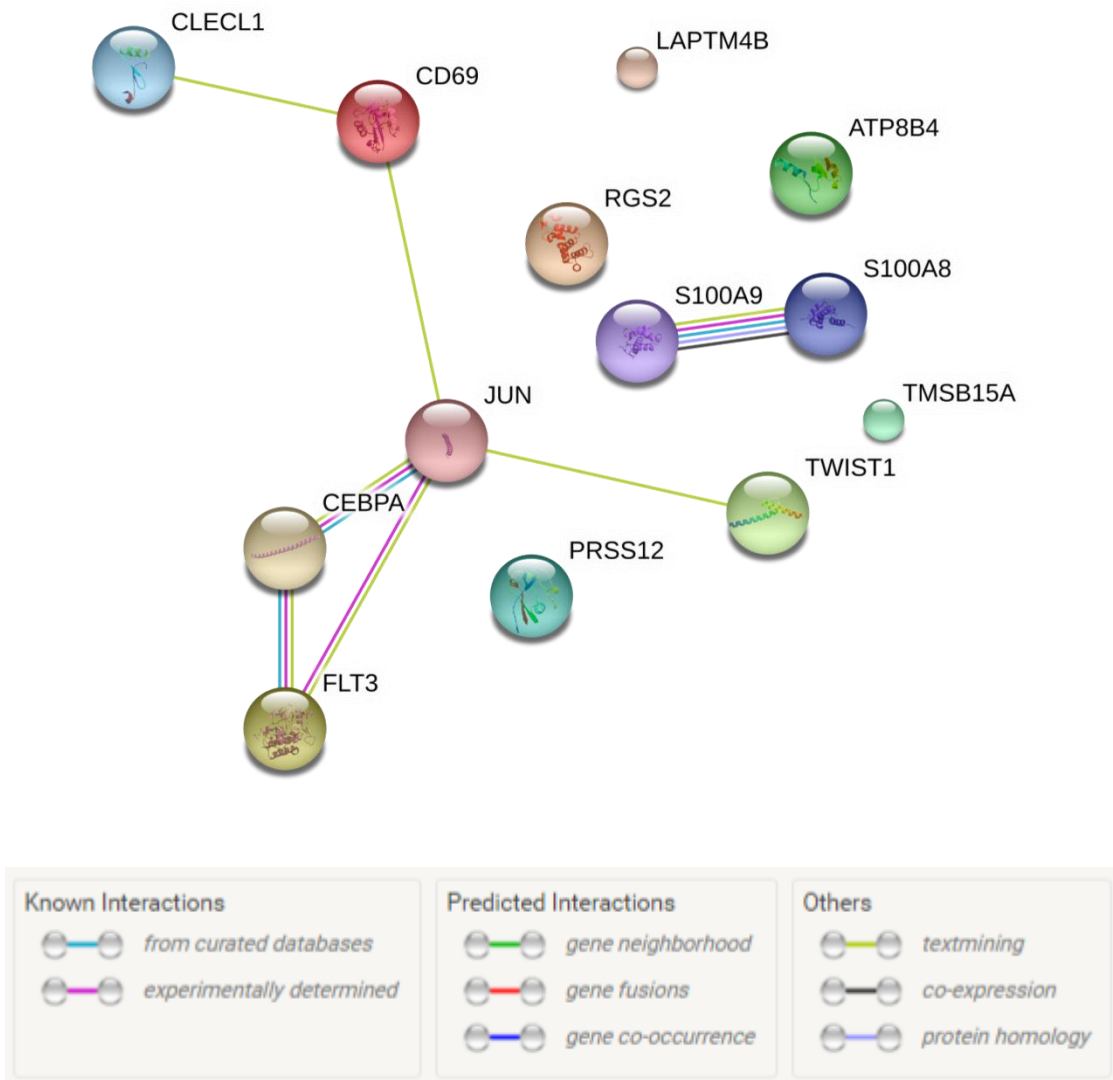


Figure 63: Protein association of the genes upregulated >1.5 fold in response to mifepristone treatment in the L707 presentation cells. Interactions were determined using the online protein interaction database, STRING (version 10.0), and the types of interaction are shown in the legend below.

From this data it would appear that treatment with mifepristone has little effect on the L707 presentation cells. Although pharmacokinetic studies have not been done to ensure that the drug has high bioavailability *in vivo*, the use of this drug orally in patients implies that it has a good oral bioavailability profile and the lack of differentially expressed genes stem from the L707 cells not having a large response. Possibly due to the dual action of the drug as an agonist and antagonist.

5.3 Summary

From the data obtained during these experiments it would appear that although NR3C1 knockdown results in Dex resistance *in vitro*, when cells are tested *in vivo* there is no enrichment of NR3C1 targeting constructs as is seen *in vitro*. This is highly suggestive of a loss of shRNA expression *in vivo*, which is supported by the finding that cells collected from the spleens of mice treated with doxycycline do not show high levels of tRFP expression. Another possible cause for this lack of library enrichment could be because there is a lack of Dex sensitivity of the 697 cells *in vivo* (Chapter 7). The cause for this silencing is not known, but it has been reported before in the lab (unpublished data). Furthermore, the use of the pTRIPZ plasmid with Dex may not be advised, as Dex activates the UBC promoter (Marinovic et al. 2002a). This could account for why in Dex treated *in vitro* samples there is an increase in NR3C1 targeting shRNAs. The hypothesis as to how this results in increased leakiness of shRNA expression is that over activation of the UBC promoter may be enough to drive rtTA3 expression, so that in the absence of Dox the TRE is activated, and transcription initiated (Figure 64).

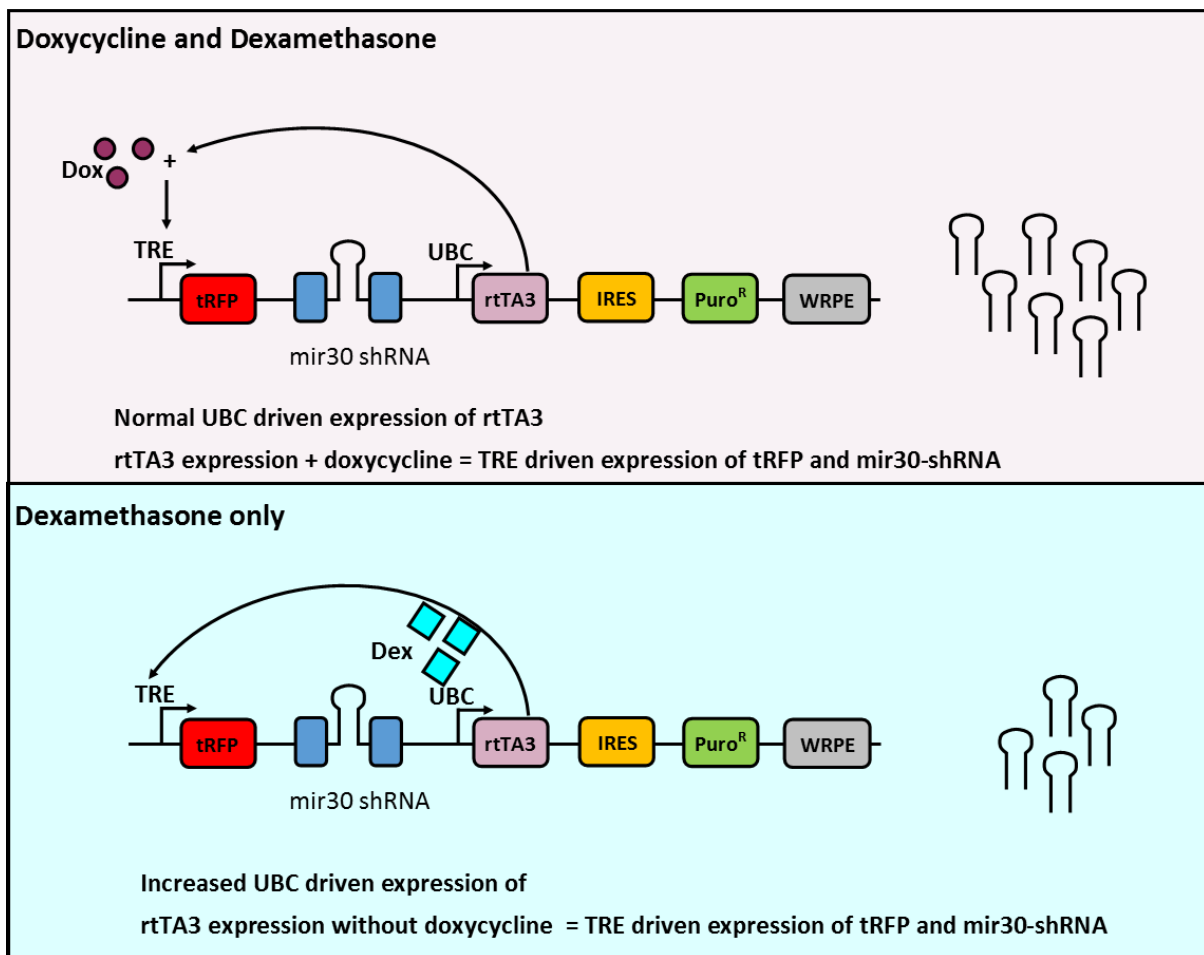


Figure 64: The hypothesised reaction of the UBC promoter in response to Dex treatment in ALL cells transduced with the pTIPZ plasmid. This shows how induction of shRNA expression can be brought about in the absence of Dox (Marinovic et al. 2002).

The response of the 697 cells to Dexamethasone was as expected according to the literature, with an auto induction of NR3C1 (Van Galen et al. 2010), and an upregulation in GILZ, FKBP5 and NFKBIA (Rainer et al. 2012). GILZ appears to be the most responsive of these genes, with more than 10-fold increase in mRNA expression even with just 10nM at 2h. Despite this increase, GILZ was not one of the significantly increased genes in the microarray analysis of Dex treated mice vs controls. One possible reason for this could be that increases in GILZ expression is transient, and by the time mouse samples are collected the effect has returned to normal levels. Another possibility is that GILZ is only upregulated in response to Dex at these levels *in vitro* and the response *in vivo* is different.

Another interesting finding from these experiments is that mifepristone acts as a partial agonist of NR3C1 within the first few hours of treatment. There is a basis for this in the literature; in an early paper on mifepristone the drug was found to have weak glucocorticoid

agonist activity but this was put down to the presence of an agonist impurity in the preparation or a non-specific effect (Bourgeois, Pfahl, and Baulieu 1984). Since then it has been found that increased NR3C1 levels are sufficient to cause the formation of transcriptionally active NR3C1 complexes in the presence of mifepristone, driving expression of NR3C1 target genes (S. Zhang, Jonklaas, and Danielsen 2007). Despite this finding, mifepristone was still tested *in vivo* because it was thought the antagonist activity at 24h could be sufficient for any effect on survival to manifest. The toxicity study with mifepristone confirmed that it was non-toxic in NSG mice but no differences in survival were found for mifepristone treated vs control mice, it was only when mice are treated with Dex that there was any increase in survival.

Despite no change in survival, mifepristone treated samples were still sent for microarray analysis along with the Dex treated and control samples. From this it can be seen that mifepristone does not result in many genes being significantly differentially regulated, but of those that are, several are also genes that are differentially regulated in Dex treated samples such as S100A8, S100A9, which have both been implicated in Dex resistance in ALL (Spijkers-Hagelstein et al. 2012) and JUN (Jun proto-oncogene). This indicates some cross over of pathways involved in the cellular response to these two drugs. The differential expression of these in both mifepristone and Dex treated samples gives further credence to the hypothesis that mifepristone is acting as a partial agonist at NR3C1.

The genes differentially regulated in mifepristone treated cells does not have complete crossover with Dex treated samples however. In Dex treated L707 presentation cells there is upregulation of JUN and FOS (Fos proto-oncogene). These genes are part of the AP-1 (Activator protein 1) transcription factor which has roles in cell cycle, the glucocorticoid response and oncogenesis (Helmburg et al. 1995; Bakiri et al. 2000; Yang-Yen et al. 1990; Kappelmann, Bosserhoff, and Kuphal 2014). These roles are initiated by the interaction between AP-1 and NR3C via intermediary proteins GIP1 and NTRIP6, which are required for NR3C1/ AP-1 driven transrepression of AP-1 target genes (Glass and Saijo 2010). The ability of NR3C1 to repress other transcription factors is not limited to AP-1, it is also known to modulate the expression of NF- κ B target genes. This was in part discovered by the inability of NR3C1 to bind to NF- κ B and induce repression of target genes when there was a loss of acetylation either through targeted mutagenesis or siRNA knockdown (Ito et al. 2006). Acetylation of NR3C1 was required for the two transcription factors to form a complex which

in turn represses NF- κ B activity. Interestingly, the differentially expressed genes S100A8 and S100A9 are both NF- κ B target genes (Nemeth et al. 2009)

The microarray analysis of Dex and mifepristone treated L707 presentation cells as well as controls did not yield as many results as was expected. The removal of the 2 anomalous samples will have reduced the power of the comparison, but not so much that there should be so few differentially expressed genes between the treatment groups. The lack of genes significantly down regulated by mifepristone is further support for the lack of effect of this drug in ALL cells, but the lack of other known NR3C1 target genes in the Dex treated samples implies that perhaps the microarray data quality was not high enough, which is supported by the fact only 35% of probes passed filtering.

The original hypothesis that NR3C1 is infrequently deleted because it results in reduced fitness has not been proven or disproven by this set of experiments. The loss of NR3C1 mRNA does result in Dex resistance but no alteration in proliferation. Loss of NR3C1 signalling pharmacologically through use of mifepristone has no effect on survival. This indicates that further work would be needed to prove this hypothesis.

Chapter 6: *In vivo* lentiCRISPR whole genome screen to determine genes implicated in dexamethasone treatment and the emergence of relapse

6.1 Introduction

Genome editing using CRISPR Cas9 is a relatively new technique that has really taken off in the past few years with several high profile papers being published (Sanjana, Shalem, and Zhang 2014; Shalem et al. 2014; Chen et al. 2015). The system utilizes the Cas9 endonuclease from *Streptococcus pyogenes* (*S. pyogenes*) to induce double strand breaks (DSB) in DNA; these are then repaired by homologous recombination or non-homologous end joining. The result of these repairs are either the repair of the target sequence or the creation of an indel, which may lead to disruption of gene function. The Cas9 enzyme is directed to the DNA using specific short guide RNA (sgRNA) sequences that can be targeted anywhere in the genome with a protospacer adjacent motif (PAM) sequence. The Cas9 endonuclease from *S. pyogenes* is specific to the PAM sequence NGG, and by taking the frequency of GG dinucleotides as around 5.2% in the 3 billion base pairs that make up the human genome, the number of possible PAM sites recognisable by *S. pyogenes* is over 161 million (Scherer 2008; Integrated DNA Technologies 2016). This number of possible sites means that virtually any gene in the genome will be targetable using the CRISPR Cas9 system.

The CRISPR Cas9 system was chosen over other whole-genome screening methods for several reasons. With RNAi-mediated screens, especially *in vivo* we have found silencing of the construct to be a problem (unpublished observations). This was demonstrated by the data in chapter 5, which found that when 697 cells that were transduced with the inducible lentiviral plasmid pTRIPZ and grown *in vivo*, there was a loss of tRFP expression *in vivo* despite mice being treated with Dox to induce expression. This was not seen when the same cells were grown *in vitro* suggesting a role for the murine microenvironment in facilitating silencing of the construct. Using CRISPR negates the risk of silencing as once Cas9 has caused a DSB and the gene is knocked out, it is a stable effect that is passed on to all daughter cells. This could result in problems such as off target effects, but as we felt siRNA and methods using transient Cas9 expression were not a viable option in primary derived cells, due to

both the high levels of cell death with electroporation of primary cells seen in our lab (unpublished results) and the transient effects, the lentiCRISPRv2 GeCKO plasmid library was chosen as the best choice.

The lentiCRISPRv2 GeCKO library is a commercially available CRISPR sgRNA library (Chen et al. 2015; Shalem et al. 2014). The library contains over 122000 sgRNA, with 6 sgRNA per gene, 4 for miRNA and 1000 non targeting controls. The lentiCRISPRv2 is a single plasmid system with both the sgRNA and Cas9 enzyme encoded by the same plasmid, this means that only one type of antibiotic selection, and one round of transduction is needed, both of which are preferable for use in primary ALL cells.

Although cell lines are often the model of choice for research due to their availability and relative ease of culturing *in vitro*, these may not be the best models to investigate the acquisition of Dex resistance. Several studies found that cell lines have increased sensitivity to cytotoxic agents compared to matched primary material (Stein et al. 2004; Wang et al. 2002), and that in cell lines there is no correlation between target expression and drug sensitivity (Jaeger, Duran-Frigola, and Aloy 2015) There is also evidence that following prolonged Dex exposure, cell lines have an increase in the acquisition of deletions or mutations in NR3C1 (Hala et al. 1996). Considering that deletions or mutations in NR3C1 are relatively rare in ALL, even at relapse when resistance to glucocorticoids is increased(Irving et al. 2005), this further supports the theory that cell lines may not be the best model for these investigations. As a result, it was decided that to investigate acquisition of drug resistance in ALL, drug naïve primary cells were the best model. It was hypothesised that if it was possible to transduce primary derived cells with the lentiCRISPRv2 plasmid (Sanjana, Shalem, and Zhang 2014; Shalem et al. 2014), with a high enough viral titre, it would represent a robust model in which to carry out a genome wide CRISPR screen. The use of primary cells may be a better model but there are technical issues with using them, most notably the amount of cells needed for a screen. For this reason, primary derived cells that have been grown *in vitro* after injection into NSG mice were used. Although primary derived cells are not directly primary cells, they still retain the characteristics of the primary sample. The cells chosen for this screen, the L707 presentation cells, do not proliferate *in vitro* without the support of a feeder layer and have a phenotype more similar to primary cells than a cell line. The L707 presentation xenograft cells have maintenance of genomic deletions from the patient sample and the phenotype of the cells once engrafted remains

stable over several engraftment passages (Latif 2012). This suggests that the primary derived L707 presentation cells are an accurate representation of the primary material.

The aims of this screen were

- to prove the feasibility of a genome-wide lentiCRISPR screen in primograft ALL cells *in vivo*, and
- to investigate mechanisms of Dex resistance in matched presentation and relapse ALL cells.

6.2 Transduction pilot

An initial transduction pilot was done before the screen was undertaken to determine the feasibility of the whole-genome approach in primary derived cells. L707 Presentation cells were transduced with lentiCRISPRv2 empty vector lentivirus and samples were taken at 3 and 5 days post transduction. As the plasmid does not contain a fluorescent marker for quantification of transduction, qPCR was used. Levels of cas9 DNA in the genomic DNA of samples were determined as a measure of transduction. Compared with the un-transduced L707 Presentation and SEM cells the transduced cells had significantly increased Cas9 DNA levels, over 1000 fold more than in the controls (Figure 65). This PCR represents the proof of concept that a sufficient viral titre could be achieved to go ahead with a full genome screen.

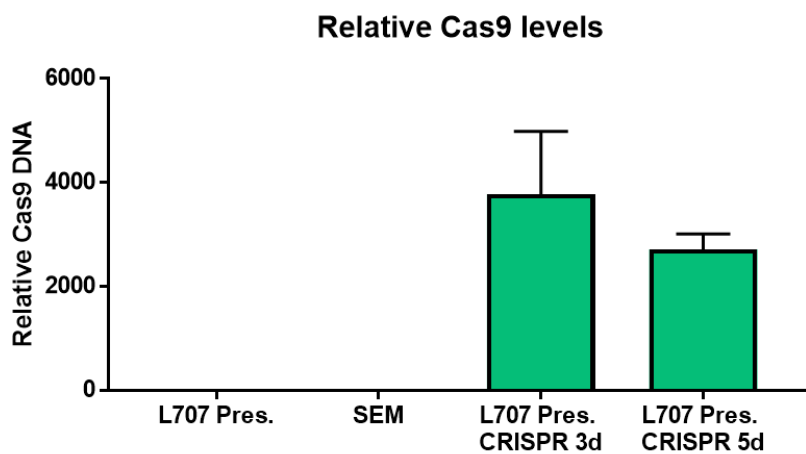


Figure 65: Relative Cas9 DNA levels in samples transduced with the lentiCRISPRv2 plasmid at 3 and 5 days post transduction. Negative controls of L707 Presentation and SEM cells without virus were also tested. L707 Presentation without virus was used as the control for $\Delta\Delta Ct$ calculations along with GAPDH levels. Data shows technical repeats of a single transduction, not biological repeats and error bars show SEM.

6.3 *in vivo* screen

Approximately 4.7×10^7 freshly thawed L707 Presentation cells were transduced with concentrated lentivirus before being grown *in vitro* and puromycin selected ($0.25\text{--}5 \mu\text{g/ml}$). The cells were then intra-femorally injected into 15 NSG mice and dosing with Dex started the next day (every weekday, 15 mg/kg for 5 weeks, 10 mg/kg thereafter). This was continued until the mice reached endpoints as defined on the license and were killed by cervical dislocation. Samples were extracted from several organs and DNA extracted before PCR was used to prepare amplicon libraries for next generation sequencing using an Illumina HiSeq2500.

Treatment with Dex is known to significantly prolong the survival of mice engrafted with the L707 presentation cells (Latif 2012). The treatment of mice engrafted with L707 CRISPR cells significantly increases survival compared to these mice, but as treatment is started straight away this is not a true comparison (Figure 66). No other experiments with the L707 presentation used Dex treatment straight away after engraftment and so the L707

presentation + Dex after 2 weeks represents the best data to compare the survival of mice engrafted with the L707 Presentation CRISPR cells to. Three mice did die earlier than expected, and on examination this was due to suspected liver toxicity, and this prompted the decrease in Dex dose and these mice were excluded from survival analysis.

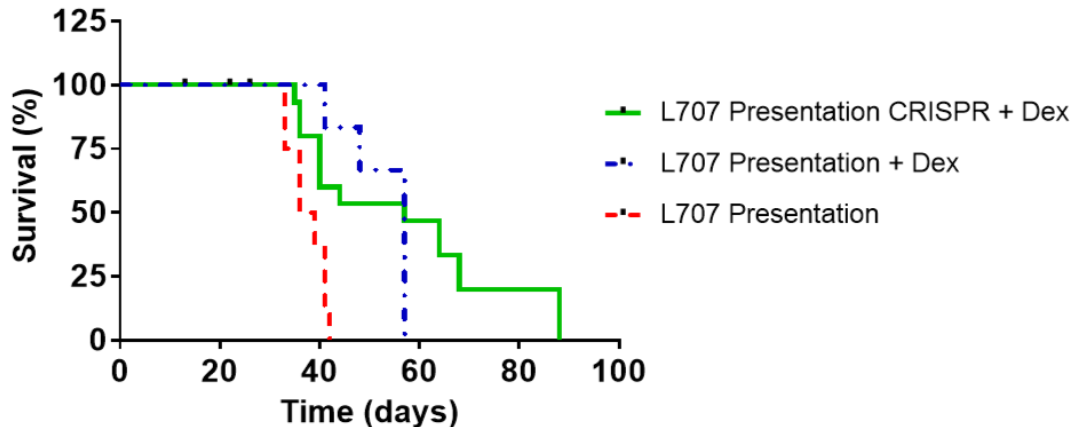


Figure 66: *Survival of mice engrafted with L707 Presentation cells; L707 Presentation (red), L707 Presentation + Dex (15 mg/kg) after 2 weeks engraftment (blue) and L707 Presentation CRISPR + Dex (15 mg/kg, then 10 mg/kg) (green). Censored mice are shown as black bars. Both L707 Presentation + Dex and L707 Presentation CRISPR + Dex have significantly longer survival than the untreated L707 Presentation ($p<0.005$). L707 Presentation + Dex and L707 Presentation CRISPR + Dex do not have significantly different survival. The L707 presentation + Dex engrafted mice were left for 2 weeks before dosing was started (I.P. every weekday) but the L707 Presentation CRISPR mice did not have a gap before treatment.*

Histology was done on the samples collected from the mice engrafted with L707 presentation CRISPR cells to determine if there were differences between the organs, or any abnormalities not normally seen in mice engrafted with L707 presentation cells. The spleens of NSG mice engrafted with L707 presentation CRISPR cells show the highest level of engraftment of human cells, which considering the splenomegaly seen in these mice is unsurprising (Figure 67). The BM in the vertebra (Figure 68) and tibia (not shown) were also highly engrafted with L707 presentation cells. The infiltration of human cells into the liver is more variable, with large areas not showing expression of CD19, indicating no human cells (Figure 69). This pattern of engraftment in the mouse implies that the BM is colonised first,

closely followed by the spleen and then later on the liver, but before the liver can reach significant levels of engraftment the mice succumb to the disease. In mice engrafted with L707 presentation CRISPR cells, several mice were killed due to loss of hind limb mobility, likely as a consequence of vertebral collapse resulting from high levels of engraftment in the vertebral BM. This was the same as for previous mice engrafted with L707 presentation without transduction, which suggests that the engraftment phenotype of these cells was not altered by the transduction with the CRISPR library.

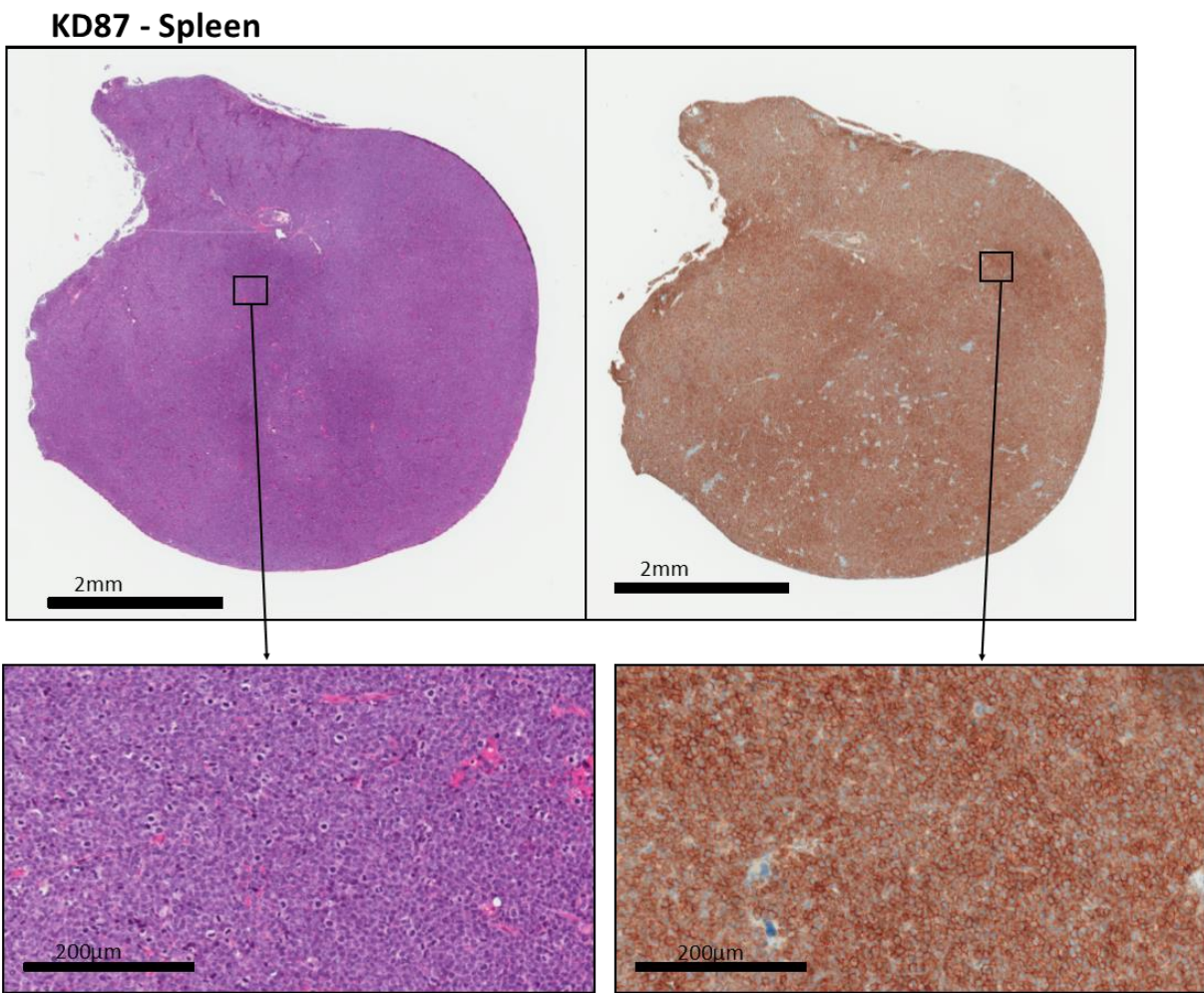


Figure 67: Histology of a section of spleen from an NSG mouse engrafted with L707 presentation CRISPR cells treated with Dex, left – H&E staining shows gross morphology is very homogenous in the spleen, Right – CD19 staining shows the entire spleen is heavily engrafted with human cells. Sectioning and staining was carried out by the histopathology department at the RVI hospital.

KD88 - Spine

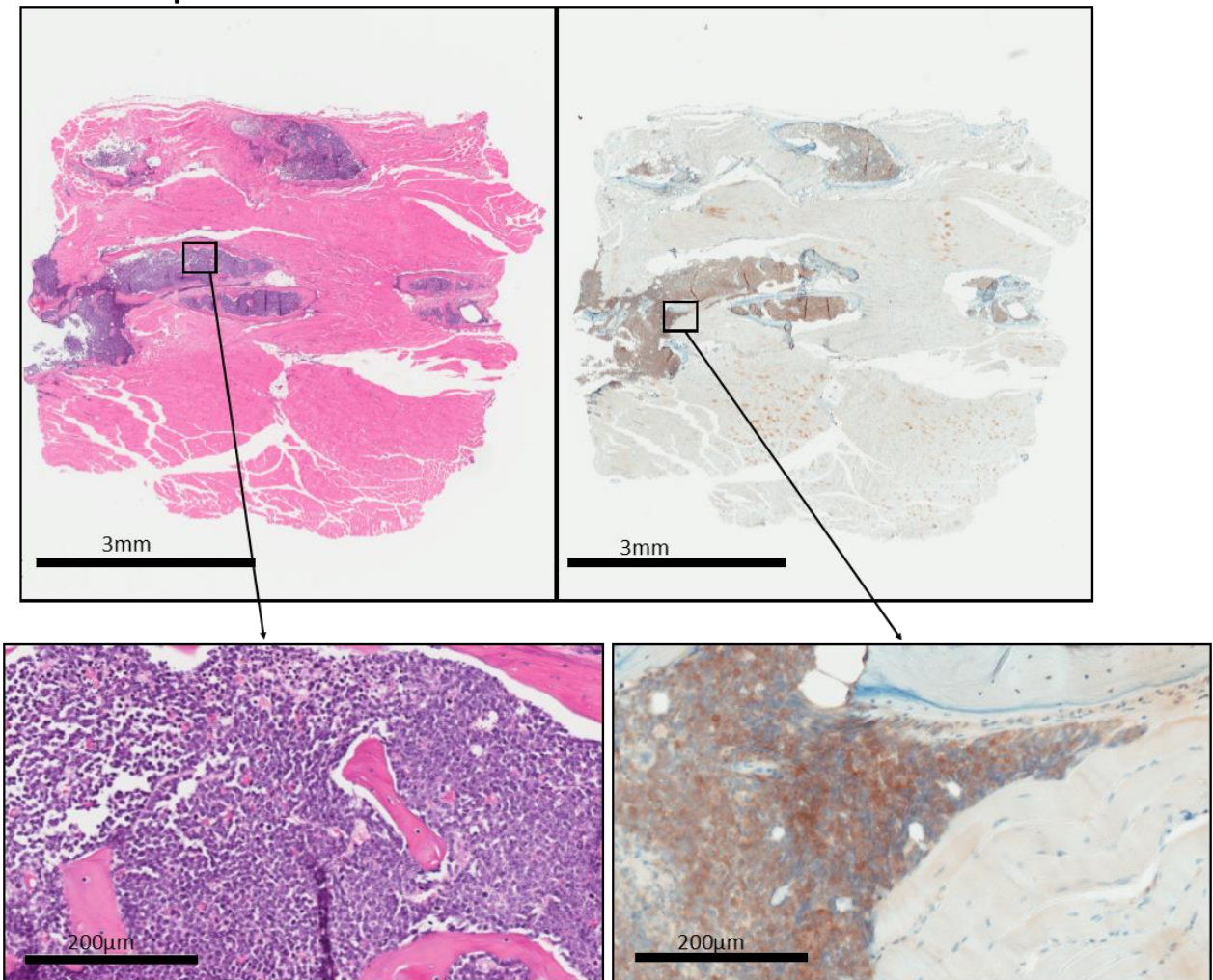


Figure 68: Histology from the spine of a mouse engrafted L707 presentation CRISPR cells treated with Dex. The muscle around the spine as well as the BM of the vertebra can be seen. Left – H&E staining shows muscles are not engrafted but the BM is homogenous with small lymphocyte like cells, Right – CD19 staining shows that the BM of the vertebra are engrafted with CD19 positive human cells. Sectioning and staining was carried out by the histopathology department at the RVI hospital. Sectioning and staining was carried out by the histopathology department at the RVI hospital

KD87 - Liver

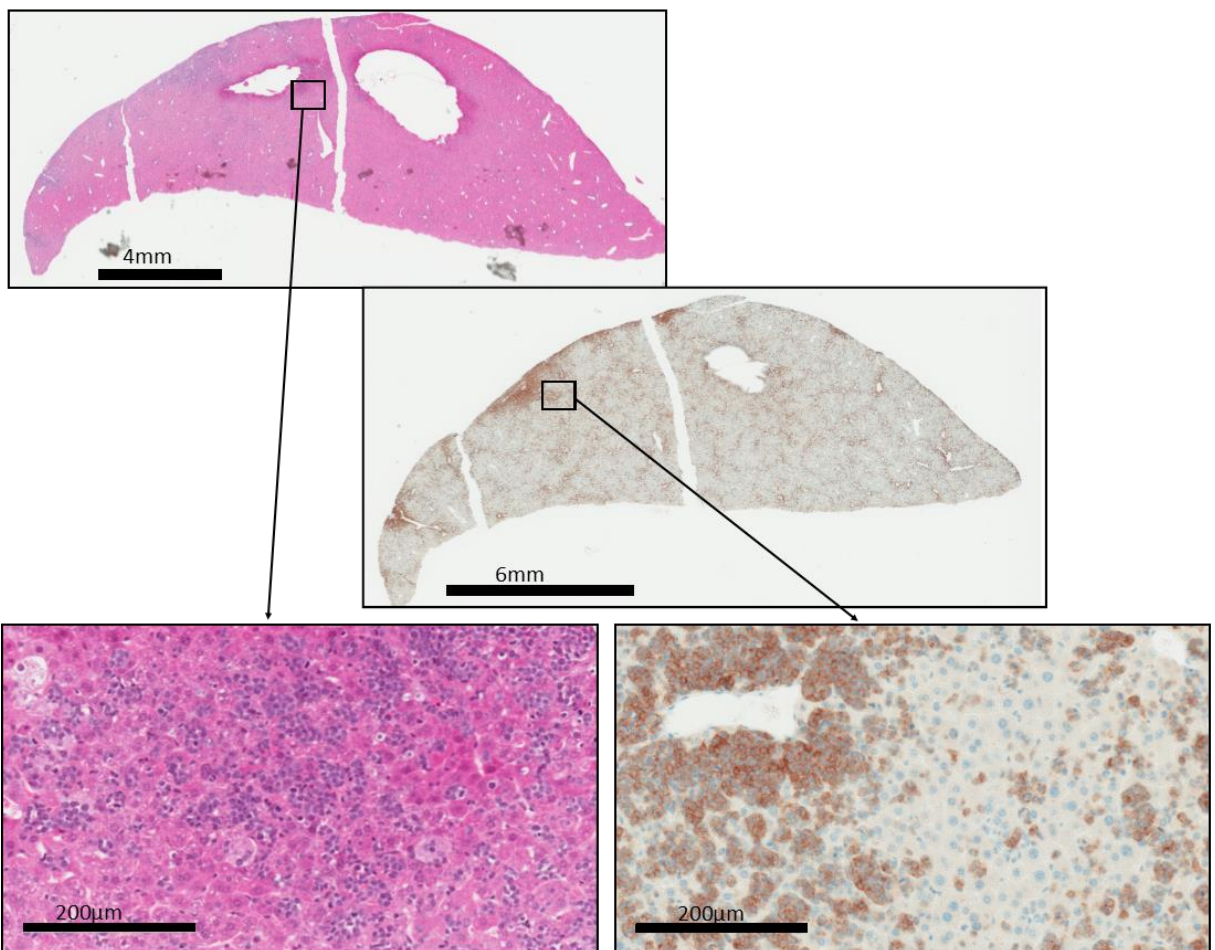


Figure 69: Histology from the liver of a mouse engrafted with L707 presentation CRISPR cells treated with Dex. Left – H&E staining shows engraftment of cells is not homogenous in the liver with areas of different cellular composition. Right –CD19 staining shows that only some areas of the liver are engrafted with human CD19 positive cells. The majority of the liver is not-engrafted. Sectioning and staining was carried out by the histopathology department at the RVI hospital.

6.3.1 Sample preparation

The sequencing run and data described in this chapter are from a second sequencing run as the initial one failed to produce usable data. This is thought to be a result of using a custom primer and the Fluidigm adaptors rather than the standard Illumina primer and adaptors. The custom primer likely did not have the right thermodynamic properties and as such there

was no hybridisation and the chemistry used with the HiSeq2500 did not work. As a result, not all samples sent for sequencing were amplified from genomic DNA, some were from pre-amplified DNA from the first run.

6.3.2 Analysis

When data were returned originally analysis was carried out but it was found that levels of NR3C1 and some non-targeting control (NTC) sgRNAs were unusually high (Figure 70). Plasmids containing these NR3C1 and control sgRNAs had been cloned in the lab for use in experiments knocking down NR3C1 individually before the library preparation. Given that the NTC were high in the list of hits along with NR3C1, this implied that there was a PCR contamination and the results for these constructs could not be trusted. High sensitivity of PCR to contamination by other sgRNA plasmids used in the same lab space has also been reported by other groups using the GeCKO library in the institute (unpublished results). As a result, the analysis was re-run without the 6 NR3C1 targeting sgRNA and the 20 NTC that were used. All data reported has had these 26 sgRNA removed.

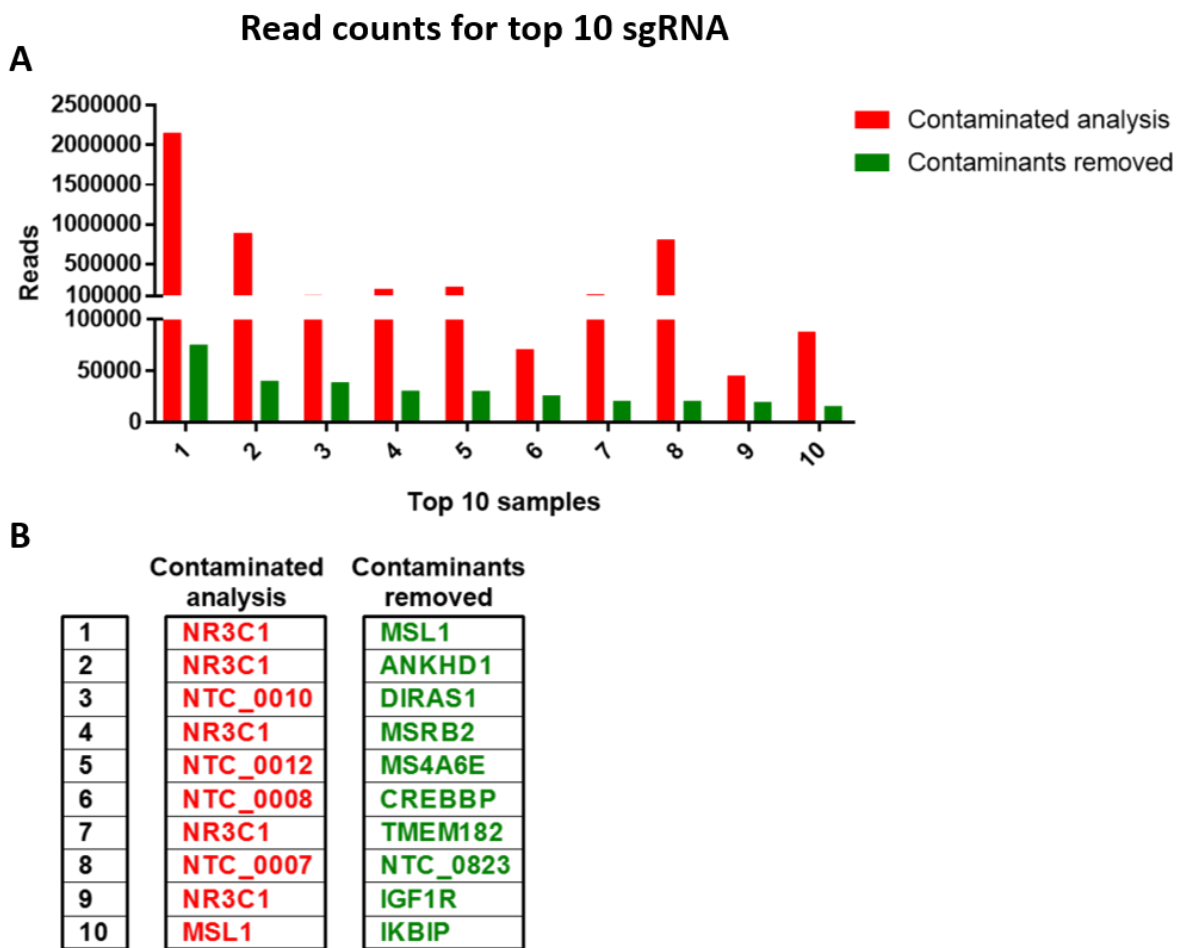


Figure 70: A - The number of reads for the top 10 highest reads for KD93 spleen in the contaminated analysis before removal of NR3C1 and NTC reads (red) and after these reads were removed (green). B – the names of these 10 genes for the contaminated reads (red) and reads after the contaminants were removed (green).

6.3.2.1 Data Analysis: Reads and coverage

Two types of analysis were used with this data. Firstly analysis of the normalised reads in excel which gives an overall view of the level of sgRNA lost and the coverage in different mice and organs, and secondly, analysis using the CRISPR specific statistical programme MAGeCK (Li et al. 2014), which allows for significance to be calculated for enriched and depleted sgRNA, genes to be ranked and enrichment of pathways to be determined.

AROS returned the data in the form of de-multiplexed FASTQ files, and analysis of the raw reads showed that all samples except one had >1 million reads, and only 3 were < 5 million reads (Figure 71). The high levels of reads for most samples means that even with reads removed there are enough left for statistical analysis. The differences in the number of reads between samples is not an issue due to the median normalisation that is used.

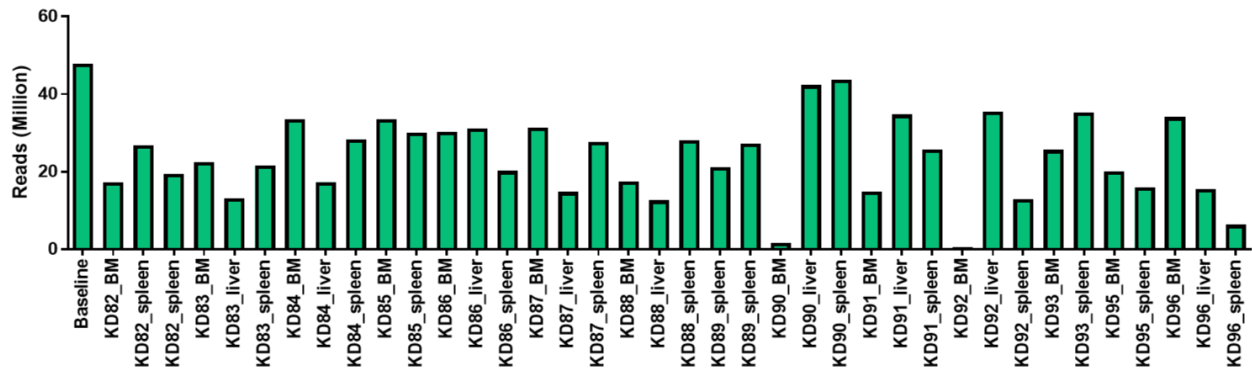


Figure 71: The reads per sample in the raw sequencing data returned from the HiSeq2500 sequencing run from AROS. The sequencing depth was varied between the samples but only 3 samples had <5 million reads and these were still analysed with the rest.

Coverage is an important issue in whole genome screens, and especially so with negative screens which look at drop out of sgRNA. This is due to the requirement of a high number of each sgRNA in the baseline in order to determine which drop-outs are significant and often 1000-fold coverage is the requirement. However, 1000-fold coverage in this screen would have required 1220 mice and assuming 30% transduction, the transduction of $>4 \times 10^8$ cells, which was not achievable with the number of cells, mice and time available. Instead, a positive screen was used to look for which sgRNA constructs were enriched in samples after treatment. 15 mice were injected with 10^5 L707 presentation CRISPR cells each, and the original pool had a complexity of ~122000 constructs. This results in 0.8-fold coverage per mouse, and when all mice are pooled a total coverage of 12.3-fold. With low coverage this screen was designed not to be negative, but a positive screen, identifying constructs that are enriched in samples compared to baseline.

Count data was used to investigate the coverage and loss of sgRNA in the mouse organs and a 10 read cut off was applied to the data to eliminate sequencing artefacts. Using this cut-off, the baseline maintains 94% coverage of the original GeCKO plasmid library (Figure 72).

This reduction in library complexity was to be expected, as with genome wide screens some constructs will be lost, partly due to actual drop out of constructs that negatively affect the cell and partly due to low read counts as a result of not having high coverage. The reduction in sgRNA from the baseline sample to the mouse organs ranges from 11% to 88% of the baseline sample (Figure 73). This variation is seen both between different mice, and within the organs from one mouse. As might be expected, those samples with more reads also had a higher percentage coverage (Figure 74). There does not appear to be any patterns in the coverage when looking at different organs.

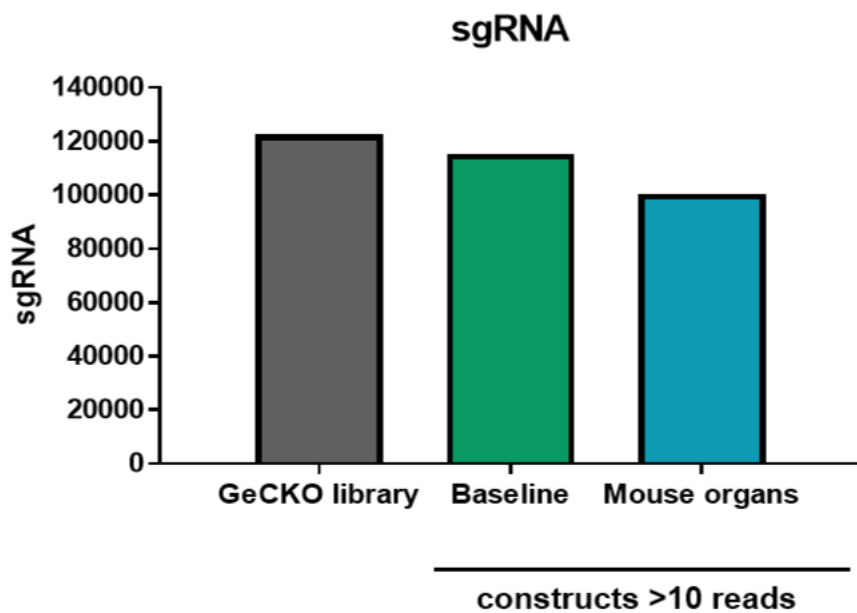


Figure 72: The reduction in the number of sgRNA found in the original GeCKO library (grey), number of sgRNA with >10 reads in the baseline sample (Green) and the combined mouse samples(blue). The reduction between the library and the two samples indicates a loss of complexity, which was expected. The loss is not too severe meaning there was engraftment of almost all sgRNA in the mice.

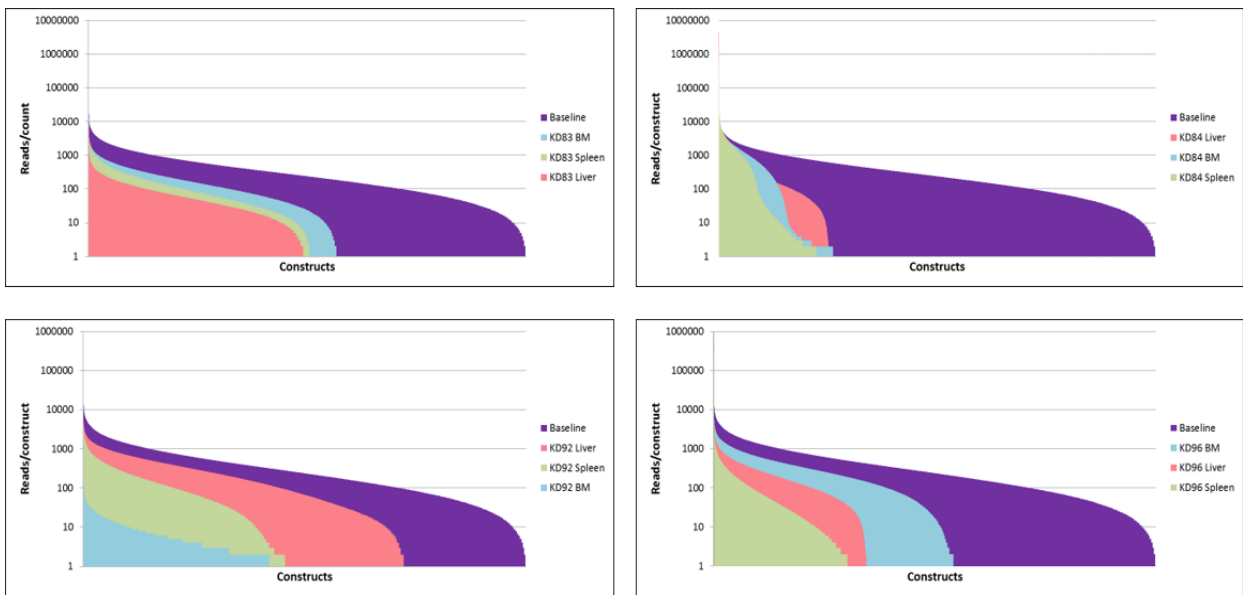


Figure 73: The reduction in sgRNA coverage in the organs of 4 representative mice compared to baseline. All sgRNA reads are included in charts, and loss in complexity between baseline and samples is shown by a reduction in the area of the plots. This shows the difference in the sgRNA distribution in the separate organs of the mice compared to the baseline sample.

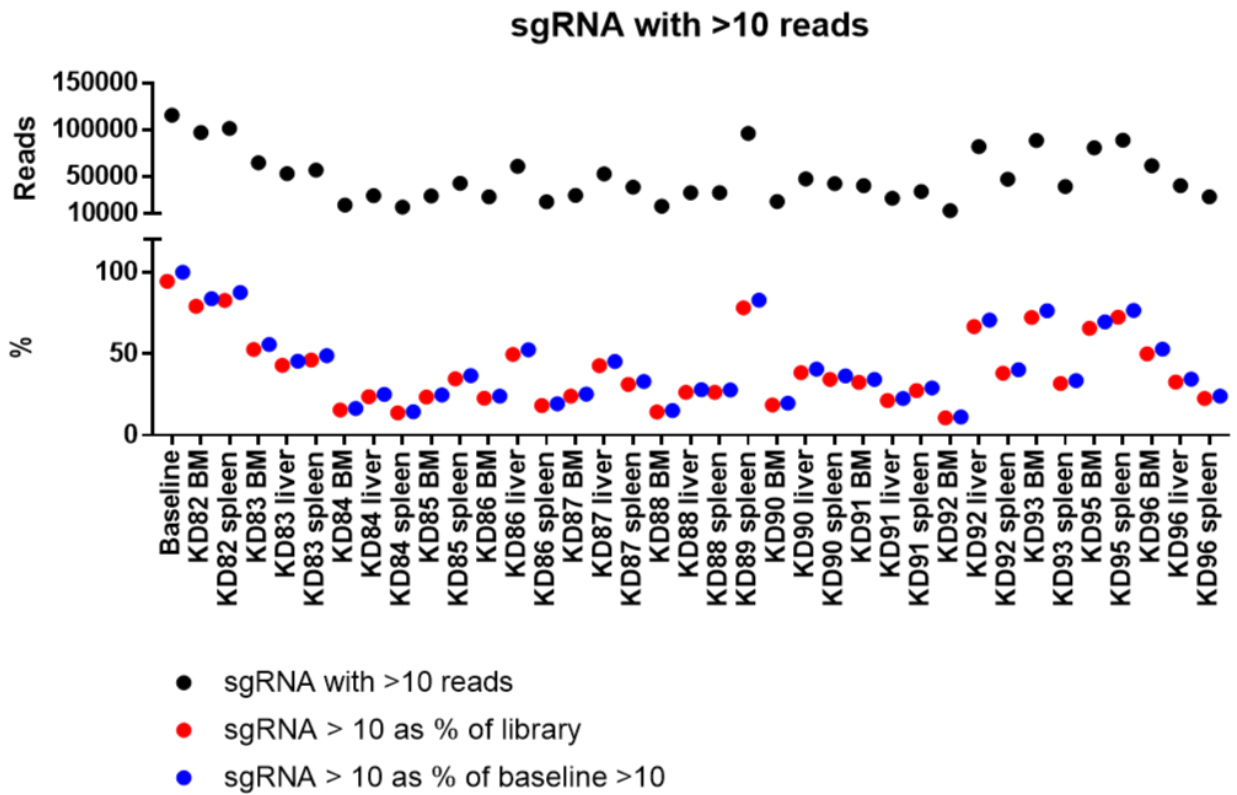


Figure 74: A comparison of sgRNA in separate organs. sgRNA with > 10 reads as percentages of the original GeCKO library are shown in red, and as a percentage of the baseline are shown in blue. The total reads for each sample is shown above those samples in black.

Principal component analysis (PCA) of the samples shows there is no clustering pattern, some samples show close association between different organs, but others do not (Figure 75). This would imply that despite the pool being spread across several mice, the inter mouse effect is not as significant as it could have been.

PCA plot — Mouse samples

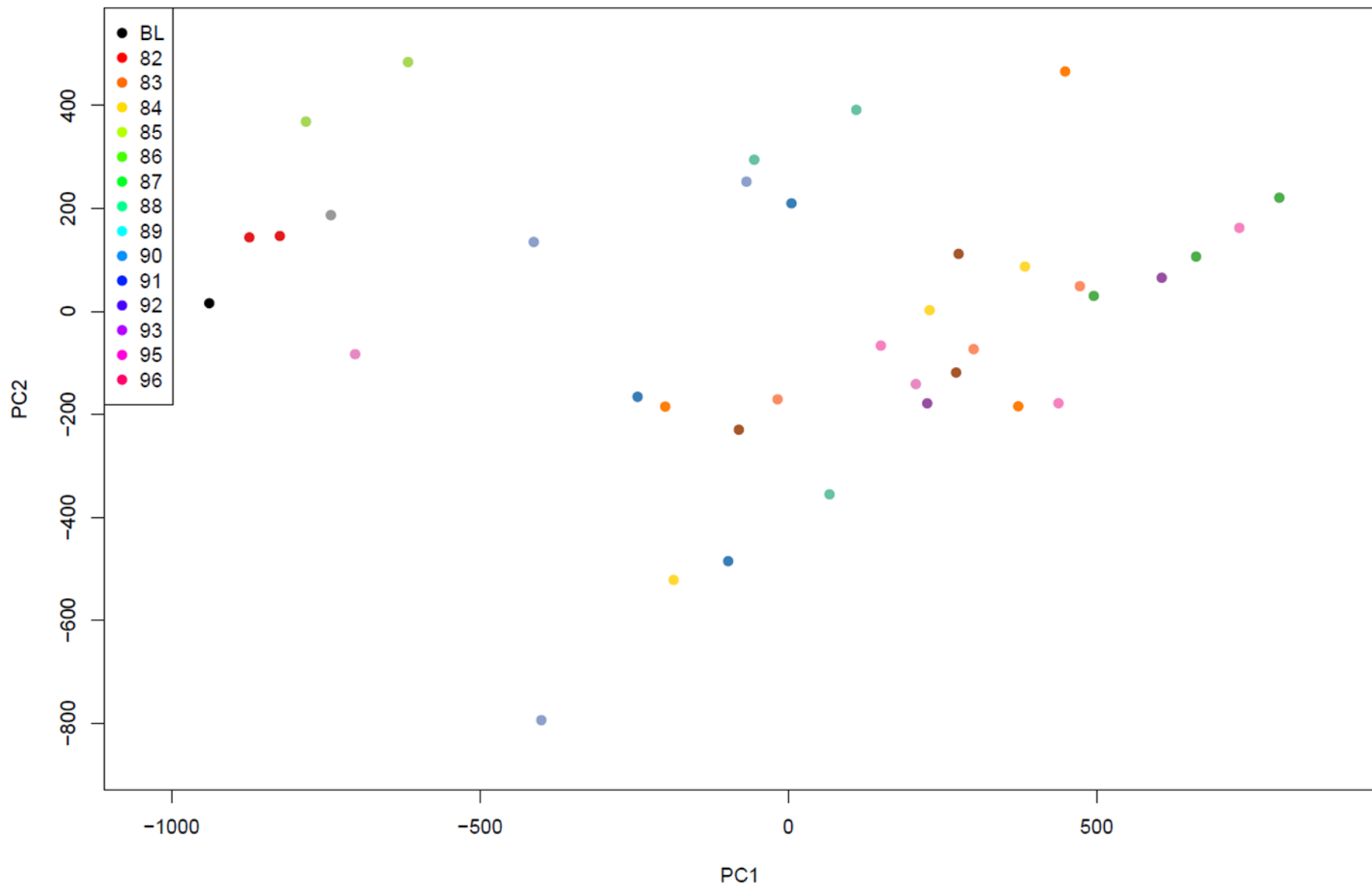


Figure 75: Principal component analysis plot for samples in the screen using the two principal components that contribute most to sample variance. Baseline sample is shown in black and each mouse a different colour, separate organs for each mouse are not differentiated by colour. Plot was produced by Dr. Matt Bashton.

6.3.2.2 Enriched sgRNA

sgRNA that are enriched in the mouse samples indicate genes with knockout by CRISPR induced indels, that has led to reduced sensitivity to Dex or enhanced growth *in vivo*. This list of genes can be used to determine which are important for engraftment and Dex response *in vivo* in the L707 presentation.

Of the top ten significantly enriched sgRNA (Figure 76) there are two non-targeting controls. This could be because they have off-target effects on cell function not calculated for when the sgRNA were designed using an algorithm. When the sequences are searched for using the online BLAST (Basic Local Alignment Search Tool) web interface (Madden 2002), NonTargetingControlForHuman_0823 (NTC_0823) has 95% sequence homology with PTPRN2 (Protein tyrosine phosphatase, receptor type N2), a protein with a similar sequence to known receptor protein tyrosine phosphatases. The other highly scoring NTC, NTC_0737 has 80% sequence homology to CNTN5 (Contactin 5) (Figure 77). Alternatively, because the NTC are a single sgRNA rather than a pool of 6 like protein coding genes, less of an increase is needed for them to score as highly significant. The top hit for a protein coding gene is MSRB2 (Methionine Sulfoxide Reductase B2). This gene is the catalyst in the reduction of methionine sulphoxide to methionine, and is thought to be protective against oxidative stress induced damage in cells (Sreekumar et al. 2005).

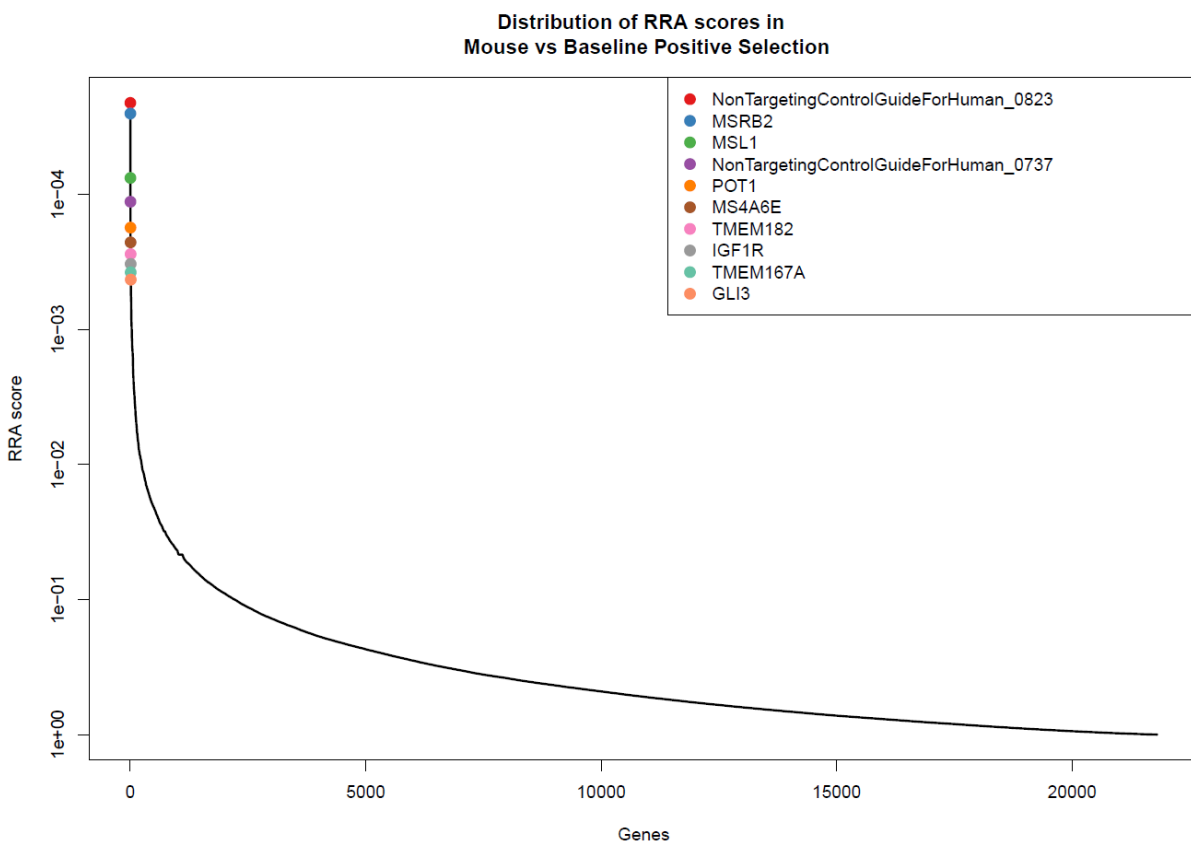


Figure 76: RRA (Robust rank aggregation) scores for positive selection of sgRNA in mouse samples vs baseline. Only the top 10 enriched sgRNA are shown as data points on the trend-line. A higher RRA score is associated with a reduced number of genes, with the vast majority of genes having a very low score. Data was produced using the in built functions of MAGeCK by Dr. Matt Bashton.

NTC_0823

sgRNA	1	TGAGTCTTACTAGGTCTTG	19
Sequence	152751	TGAGTCTTACTGGGTCTTG	152733
	PTPRN2		

NTC_0737

sgRNA	1	ATTTAGTAATGCACAC	16
Sequence	1007813	ATTTAGTAATGCACAC	1007828
	CNTN5		

Figure 77: Sequence homology, as determined using the NCBI blast online database. The top sequence shows the homology between 19 bp of NTC_0823 and PTPRN2, which is 95% and

the lower sequence shows the homology between 16bp of NTC_0737 and CNTN5, which is 80%. The homology between the NTC and known genes indicates that these may not be non targeting.

Analysis of all the genes with significantly enriched sgRNA with an FDR <0.05 after corrections for multiple testing (Figure 78) does not show any enrichment of gene ontology terms, or protein interactions between the genes, and when all the enriched sgRNA are analysed for pathway analysis, those that are significant include genes downregulated by NR2E1 (Nuclear receptor subfamily 2, group E member 1) and Multiple myeloma pathways. After corrections for multiple testing none of these pathways have an FDR <0.05.

The protein coding genes with significantly enriched sgRNA in the mouse samples compared to baseline, as determined by robust rank aggregation were investigated further. This was done using publically available ENCODE Chro-matin immunoprecipitation (ChIP) data obtained by treating the A549 human alveolar adenocarcinoma cell line with 100nM Dex and then testing for the presence of NR3C1 bound to the DNA (ENCODE project Consortium 2013) (GEO:GSM803371). Six of the genes investigated have NR3C1 binding at the start sites of the genes in the presence of Dex; MSRB2, MSL1 (Male specific lethal 1) and RRB1 (Ribosome binding protein 1), IKBIP (I Kappa B kinase interacting protein), POT1 (protection of telomeres 1) and MAPKBP1 (Mitogen activated protein kinase binding protein1) (Figure 79). This data combined with the fact that these genes have enriched sgRNA, and so decreased expression, indicates that these genes are likely to play a role in the response of Dex that is disadvantageous to the cells. However, it is important to note that the ChIP-seq data was obtained using an alvelolar adenocarcinoma cell line, and it is known that smooth muscle cells have a differential response to Dex compared to lymphocytes.

Some of the genes identified as significant using the MAGeCK analysis did not have any NR3C1 binding in the presence of Dex (Figure 80) which could indicate that these are not direct targets of NR3C1 but downstream targets, or that they are not affected by Dex treatment but are important for leukaemic growth.

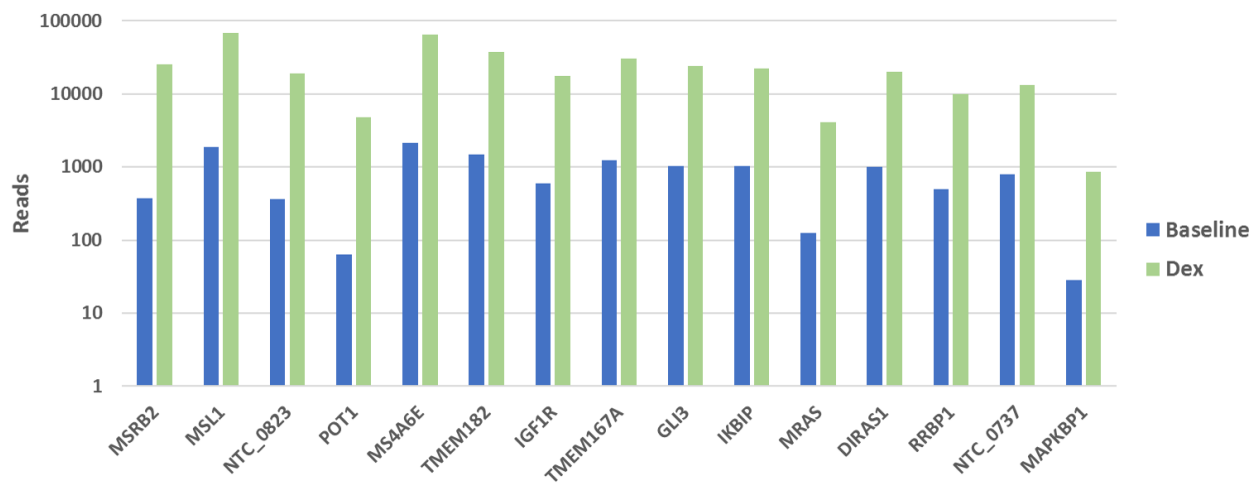


Figure 78: Plot showing the increase in sgRNA reads between the baseline to the endpoint samples (Dex) for all of the genes with significantly ($p < 0.05$) upregulated sgRNA calculated using the robust rank aggregation (RRA) score in the MAGECK analysis pipeline. Only genes with an FDR < 0.05 after correcting for multiple testing are shown.

MSRB2



MSL1



RRBP1



IKBIP



POT1



MAPKBP1



Figure 79: Genes with enriched sgRNA and NR31 binding at the transcription start site as determined by ChIP-seq. Traces produced using publicly available ENCODE ChIP-seq data for A549 cells, a human alveolar adenocarcinoma cell line, treated with 100nM Dex. The top part of each trace shows the gene and direction of transcription. The traces below that show two repeats of the ChIP seq with peaks for NR3C1 antibody binding. The blue peaks at the gene transcription sites, marked by the red boxes indicate locations of NR3C1 binding to the DNA. (ENCODE project Consortium 2013)



Figure 80: Genes with enriched sgRNA but no NR3C1 binding as determined by ChIP-seq data. Traces produced using publically available ENCODE ChIP-seq data for A549 cells, a human alveolar adenocarcinoma cell line, treated with 100nM Dex. The top part of each trace shows the gene and direction of transcription. The traces below that show two repeats of the ChIP seq with peaks for NR3C1 antibody binding. These traces show two genes, DDIRAS1 and MS4A6E that do not have NR3C1 binding sites at the transcriptional start site or anywhere within the gene. (ENCODE project Consortium 2013).

Of the genes with significantly enriched sgRNA, 9 are expressed in the L707 presentation and relapse as determined by the microarray data. Interestingly, MSRB2, the top protein coding gene hit for the CRISPR screen has a reduction in the relapse compared to the presentation. This reduction, is 0.45 fold but may indicate that the enrichment of this sgRNA is mirroring the phenotype in the relapse. Several of the top hit genes are not expressed, which indicates that these sgRNA may be high ranking because they have little effect in the cell. MS4A6E (Membrane spanning 4-domains A6E), TMEM182 (Transmembrane protein 182), IGF1R (Insulin like growth factor) and MRAS (Muscle Ras oncogene homolog) are not expressed in either the L707 presentation or relapse. All of the other genes have no difference in expression between the presentation and relapse.

6.3.2.3 *Depleted sgRNAs*

Depletion of an sgRNA indicates that the cell cannot function without the gene targeted by that sgRNA. Although there is not as high coverage in the screen as would usually be required to determine dropout with significance, looking at those genes for which sgRNA are lost can still reveal some targets of interest.

The top hit for depletion of sgRNA is PLXND1 (Plexin D1) (Figure 81). In several cancers PLXND1 and its ligand, SEMA3E (semaphorin 3E) expression are associated with increased invasiveness and malignancy (Casazza et al. 2010). Indeed PLXND1 has been postulated as a dependence receptor which when activated by ligand binding increases invasiveness, but without ligand binding can induce apoptosis by its interaction with NR4A1 (Nuclear receptor subfamily 4, group A member 1), and orphan receptor (Luchino et al. 2013). PLXND1 as well as 3 other of the top genes with depleted sgRNA have NR3C1 binding sites in the region near the transcriptional start site of the gene (Figure 82).

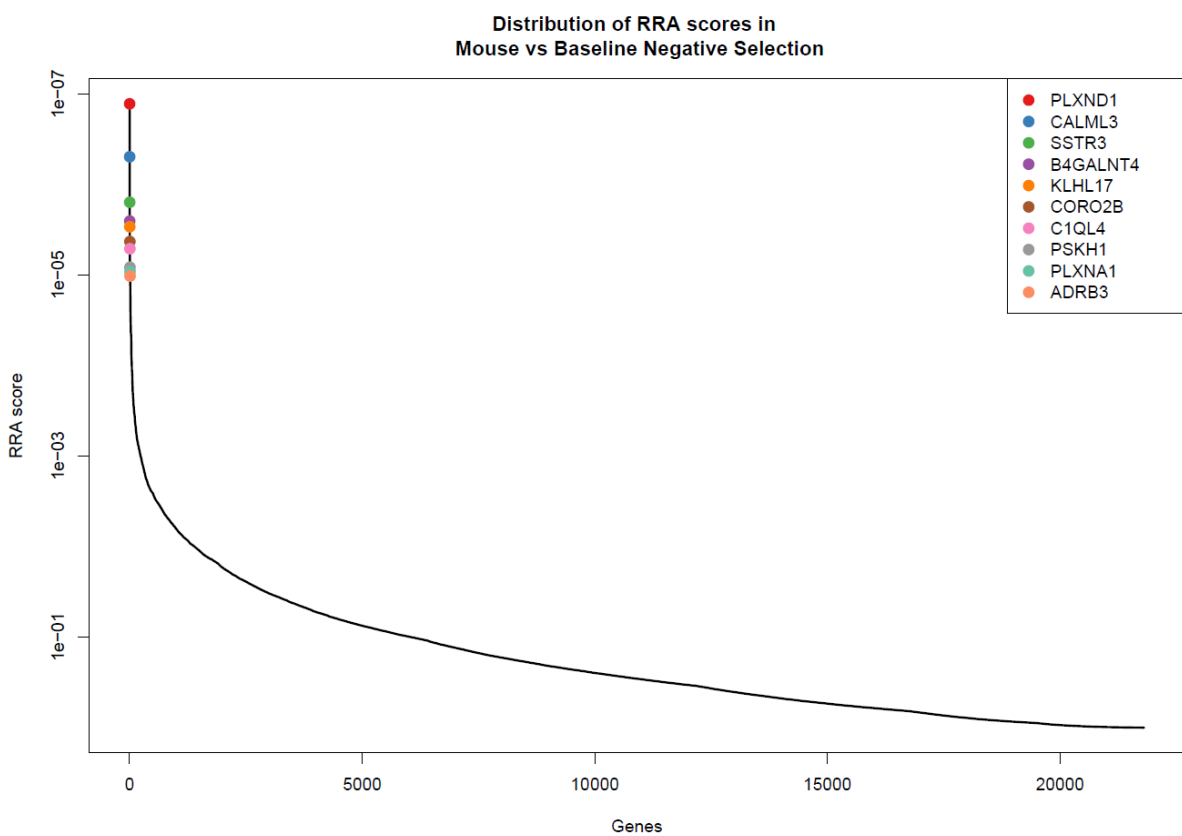


Figure 81: RRA scores for depletion of sgRNA in mouse samples vs baseline. Only the top ten depleted sgRNA are shown as data points on the trend-line. A higher RRA score is associated with fewer genes, the majority of shRNA in the screen will have a lower score which is why there is a correlation between the number of genes and a low RRA score. Data was produced using the in built functions of MAGeCK by Dr. Matt Bashton.



Figure 82: Traces for the genes with depleted sgRNA that have ChIP-seq peaks at the transcription start site. Produced using publically available ENCODE ChIP-seq data for A549 cells, a human alveolar adenocarcinoma cell line, treated with 100nM Dex. The top part of each trace shows the gene and direction of transcription. The traces below that show two repeats of the ChIP seq with peaks for NR3C1 antibody binding. The blue peaks at the gene transcription sites, marked by the red boxes indicate locations of NR3C1 binding to the DNA.

Unlike the enriched sgRNA analysis, when using the pathway analysis function of MAGeCK, several pathways had an FDR < 0.05. It should be noted that the pathway analysis takes into account the entire data set and so the top genes may not correlate as strongly as expected to the list of pathways. TP53 targets is one of these pathways. TP53 is well established as a tumour suppressor, and loss of genes associated with this pathway indicates a loss of tumour suppressive control in the L707 cells (Baker et al. 1989; Zilfou and Lowe 2009). Another significantly enriched pathway was EED (embryonic ectoderm development) targets. EED is a polycomb protein that forms part of the cellular machinery that represses transcription, it is also implicated in the proliferation of haematopoietic cells and loss of expression results in increased myeloid and lymphoid proliferation (Lessard et al. 1999). This pathway and the associated gene signature is correlated with an immature stem cell like phenotype (Ben-Porath et al. 2008), which implies that these sgRNA are not compatible with proliferation and engraftment *in vivo* due to their role in the L707 presentation cells as promoting the leukaemic phenotype. It should be noted that none of the genes in the top 10 depleted constructs appear to be associated with this pathway, so any investigations arising from the gene ontology output from MAGeCK, gene expression may have to be checked separately using alternative methods first.

PLXND1 mRNA is expressed in both the L707 presentation and relapse, but there is little difference between the expression, with just a 0.2-fold reduction in expression in the relapse. PLXNA1 is expressed at very low levels (average probe binding in presentation 31) in the presentation but is completely lost in the relapse. Considering the low expression in the presentation is, this might be an artefact of the microarray. The other genes with depleted sgRNA also show very low or no expression and only PLXND1 shows probe binding >100.

Although the low coverage means that loss of sgRNA data is not as robust as it could be, the results warrant further investigation, especially the loss of sgRNA targeting PLXND1 as this is expressed in both the L707 presentation and relapse.

6.3.3 Functional validation of targets

6.3.3.1 NR3C1

The results from the screen were further investigated to determine which genes may have an effect on dexamethasone resistance. Several genes were chosen for this from the ranked MAGeCK gene lists. Lentivirus was made from pools of sgRNA ordered based on sequences in the GeCKO library and transduced into the L707 Presentation cells, which were then puromycin selected whilst on MSC feeder cells. The cloning of these single sgRNA was the source of the PCR contamination in the screen, as the NR3C1 targeting sgRNA were used in the lab before the samples from the screen were sent away for sequencing.

As detailed previously, the L707 Presentation cells are Dex sensitive. They have an IC₅₀ of approximately 28 nM when treated with Dex *in vitro* whilst growing on an MSC feeder layer (Figure 83). After 96 hrs treatment of the L707 presentation with 25 nM Dex, 58% of cells are still viable, which is significantly less than the L707 relapse (87% survival). This resistance in the relapse is likely to be a direct result of the 5q deletion in the L707 relapse cells, which includes NR3C1. L707 Presentation CRISPR-NR3C1 cells showed Dex resistance at similar levels to the L707 Relapse cells (80% survival) at 25 nM, but were less resistant than the relapse at higher concentrations (Figure 84). This could possibly indicate a heterozygous mutation of NR3C1 rather than a homozygous loss. To determine any off target effects of Cas9 or transduction in general, cells were transduced with a pool of 6 non-targeting control CRISPR plasmids and tested in the same way. The Dex response of the L707 presentation control CRISPR-NTC (Non targeting control) cells was not significantly different from the L707 Presentation indicating no effect of Cas9 or transduction (Figure 84). Despite a significant gain of resistance in the L707 presentation CRISPR-NR3C1 cells there was no significant decrease in mRNA, although there was a trend for reduced mRNA in transduced cells (Figure 85). There was also no decrease seen in protein levels. A possible cause for this is that the sgRNA target the DNA binding and ligand binding domain, and instead of causing knockout of the gene entirely are just causing mutations in these critical regions for Dex response. This would explain the Dex resistance as well as lack of reduction in protein and also account for the modest loss of mRNA as the primers used span exons 2 and 3, separate from the sgRNA binding locations.

This data supports the idea that the NR3C1 deletions are the major causes of Dex resistance in the L707 relapse cells.

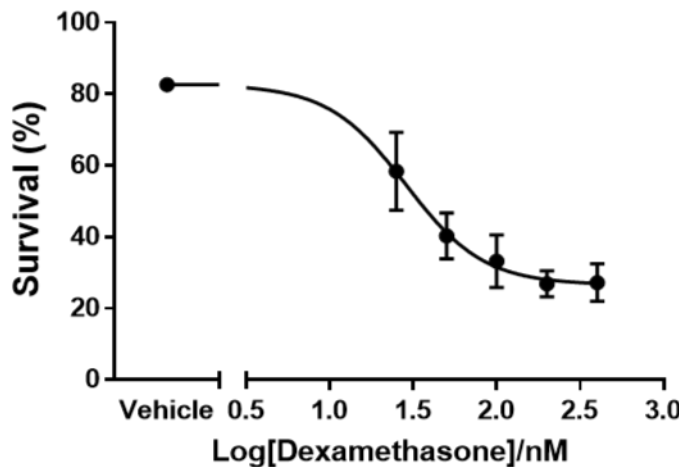


Figure 83: Survival of L707 presentation cells grown on an MSC feeder layer when treated with Dex over a 96 hr time period. L707 presentation cells were grown on MSC for 24hrs before addition of Dex, vehicle was 0.01% ethanol. Viability was assessed using the trypan blue exclusion method after 96h of Dex treatment and data was analysed using a 4 parameter dose response curve and the error bars show standard deviation.

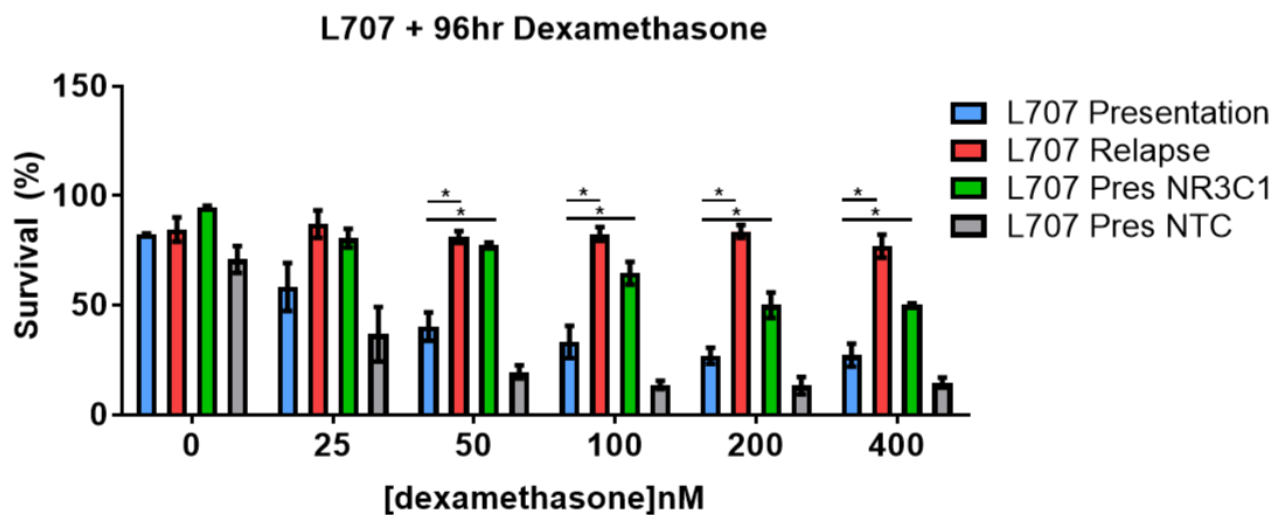


Figure 84: The percentage cell survival, assessed by the trypan blue exclusion method in L707 Presentation, L707 Relapse and L707 presentation CRISPR-NR3C1 and L707 presentation CRISPR-NTC (non targeting control) cells. Cells were grown on MSC for 24hrs before addition of Dex, vehicle was 0.01% ethanol. Viability was assessed after 96h of Dex treatment and Significance was tested using one-way ANOVA and Holm Sidak's multiple comparison test.

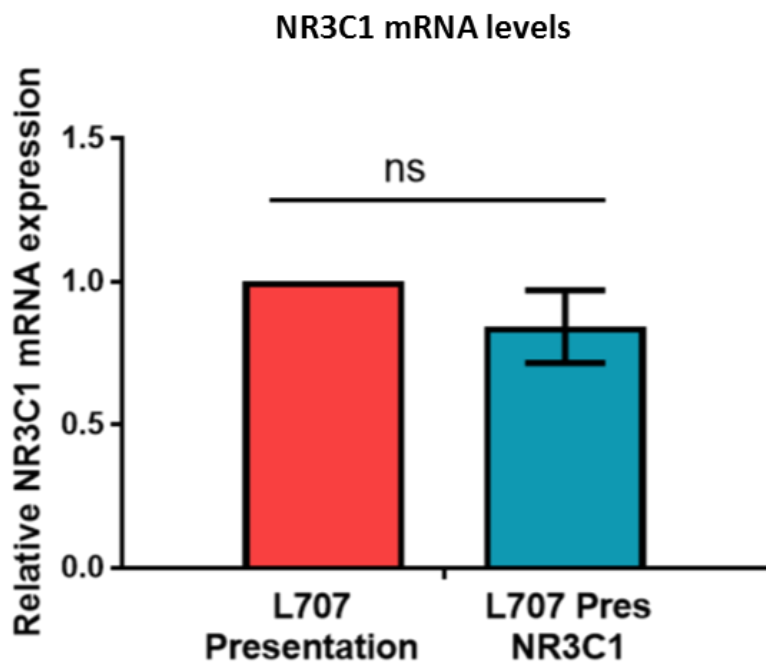


Figure 85: NR3C1 mRNA levels in the L707 presentation and L707 presentation cells transduced with a lentiCRISPR pool targeting NR3C1 cells (L707 Pres NR3C1), the two samples are not significantly different, as measured using the Wilcoxon signed rank test, p=0.125. Analysis was done using the ΔΔCt method and GAPDH as the housekeeping gene.

6.3.3.2 *PLXND1* and other genes

As well as NR3C1, several other genes were also selected from the screen for validation. These choices were based off the data from the ranked gene analysis done in MAGECK. As well as the genes from list of top enriched and depleted genes, SEMA3E was chosen as it is the ligand for PLXND1, which was initially thought to be of importance.

No sgRNA tested, other than NR3C1 showed any effect on dexamethasone resistance (Figure 86) or cell proliferation (Figure 87). Interestingly, despite no significant decrease in NR3C1 mRNA in cells transduced with NR3C1 targeting sgRNA, there was a significant reduction in PLXND1 mRNA (Figure 88). The reasons for this are unknown, but it does implicate NR3C1 in the control of PLXND1, and indeed when looking at the transcriptional start site of PLXND1 there are two consensus GRE (Glucocorticoid response element) upstream of the transcriptional start site. Indeed, when looking further into this using publically available ChIP-seq data (ENCODE project Consortium 2013) (GEO:GSM803371), there are 2 peaks around the start site of PLXND1 that have NR3C1 binding peaks in the same position as the consensus GRE (peaks 7082 and 7083). This gives further proof that NR3C1 is involved in the control of PLXND1 expression, and considering loss of NR3C1 signalling results in loss of PLXND1 mRNA this would indicate a positive relationship between the two genes.

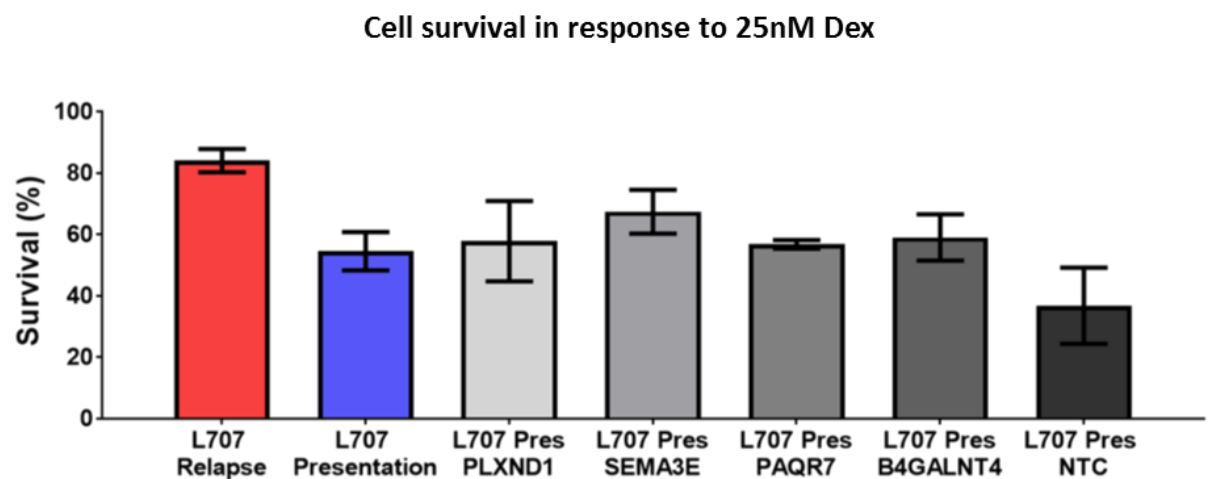


Figure 86: Percentage cell survival of L707 presentation cells with gRNA targeting PLXND1, SEMA3E, PAQR7 B4GALNT4 and NTC with 25nM Dex treatment. Only the survival of the L707 Relapse is significantly different to L707 Presentation ($p<0.05$). None of the transduced cells show a significantly different percentage of surviving cells compared to L707 Presentation cells, and all of the transduced cells were significantly different to L707 Relapse cells ($p<0.05$), apart from L707 Pres-SEMA3E. Significance was tested using one-way ANOVA and Holm Sidak's multiple comparison test. Analysis was done using the $\Delta\Delta Ct$ method and GAPDH as the housekeeping gene.

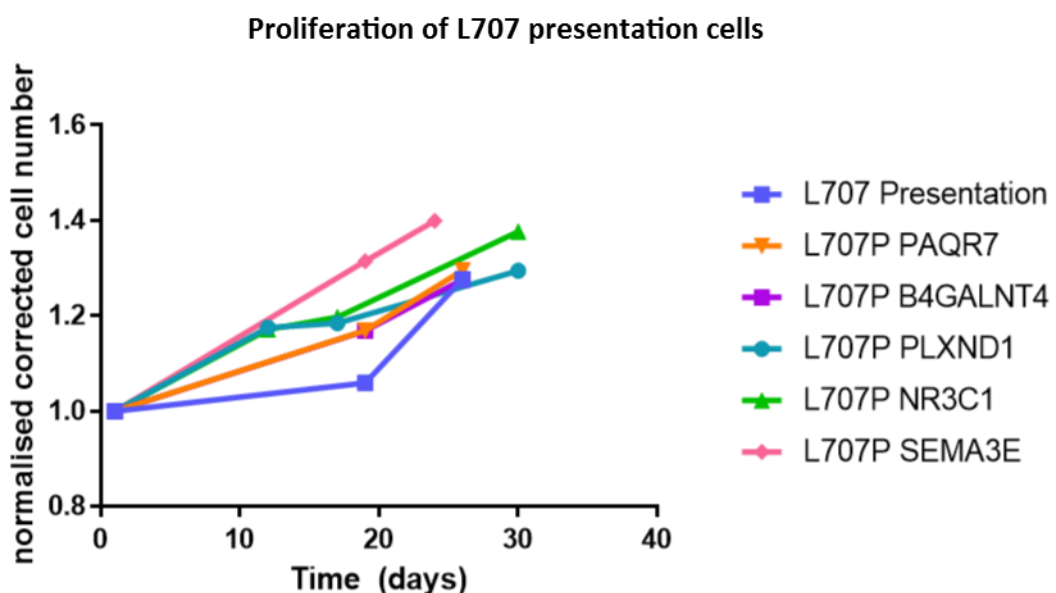


Figure 87: Proliferation of L707 Presentation cells and L707 Presentation cells transduced with several different pools of sgRNA over a 25-30 day period in SFEM-II media with an hMSC feeder layer for support. Cells were split when deemed necessary from the apparent confluence and seeded at $1 \times 10^6/\text{cm}^2$. No significant change in proliferation is seen with any of the constructs when analysed using ANOVA.

NR3C1 and PLXND1 mRNA expression in transduced cells

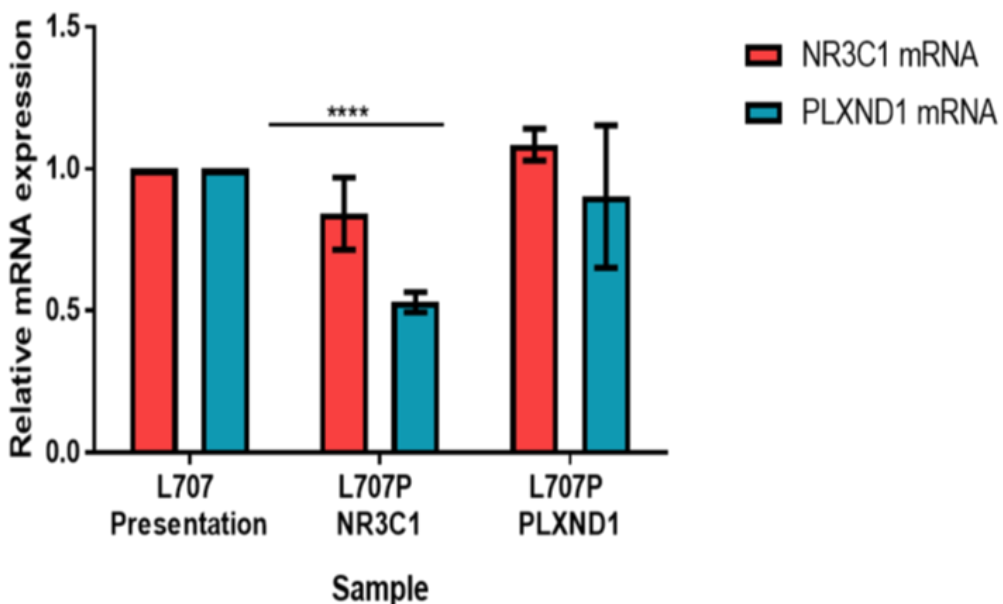


Figure 88: The decrease in NR3C1 mRNA in cells transduced with NR3C1 sgRNA is not significant. There is a significant reduction in PLXND1 mRNA in L707 Presentation cells transduced with sgRNA targeting NR3C1 but not in cells transduced with PLXND1, significance was determined using 2-way ANOVA with multiple testing, $p < 0.05$.

6.4 Summary

Despite the PCR contamination and the subsequent removal of NR3C1 targeting sgRNA from the pool, the CRISPR screen has still been successful. Firstly, a high transduction of the L707 presentation cells was achieved, and enough cells survived the puromycin selection to be injected into NSG mice. This shows that *in vivo* CRISPR screens are feasible which was not known when the screen was first proposed.

The validation of target genes has shown that loss of NR3C1 results in Dex resistance, and considering the deletion of this gene in the L707 relapse confirms NR3C1 deletion as likely the major driver for relapse in this case. Loss of the other genes did not have an effect on growth or Dex response *in vitro*. This implies that these genes are not involved in Dex response, and this combined with the lack of changes in proliferation rate could suggest that

loss of these genes only has impact *in vivo*. As growth *in vivo* and *in vitro* can result in different phenotypes of ALL cells, the loss of these genes *in vitro* may not result in a noticeable phenotypic change.

The top protein coding gene with significantly enriched sgRNA, MSRB2, is an interesting screen hit. With a GRE approximately 10,000 bp upstream of the transcription start site this gene may be modulated by Dex treatment. The probable mechanistic cause for loss of expression of this gene is through its actions protecting the cell against oxidative stress. Oxidative stress has been postulated to play a role in oncogenesis as well as leukaemic progression, as increased mutagenesis resulting from oxidative stress would result in increased clonal diversity (Udensi and Tchounwou 2014); and in ALL patients the expression of antioxidant genes has been found to be reduced (Battisti et al. 2008). This information potentially connects the loss of MSRB2 in this screen to leukaemia and gives a possible mechanistic reason why sgRNA targeting this gene are enriched.

The genes for which the sgRNA are depleted represent another potentially important list of genes, although the data is not as robust and would need further validation. The loss of sgRNA targeting PLXND1 could play a role in leukaemic growth and possibly response to Dex as PLXND1 signalling is implicated in metastatic growth and invasiveness in several types of cancer (Luchino et al. 2013; Casazza et al. 2010; Biankin et al. 2012). The expression of the PLXND1 ligand SEMA3E is correlated with metastatic disease in several solid tumours, and associated with reductions in patient survival. Loss of SEMA3E/PLXND1 signalling has been shown to reduce tumour cell growth and increase apoptosis. This loss is thought to be through ligand independent signalling of PLXND1, which can induce apoptosis through its interaction with NR4A1, an orphan receptor with both pro survival and pro apoptotic functions (Lee et al. 2011; Mohan et al. 2012). Another of the top hits for depleted sgRNA is PLXNA1 and although there is less of a role for this protein in cancers, the presence of 2 Plexins in the top ten hits is indicative of a role for Plexin signalling in engraftment of ALL *in vivo* or Dex response. Indeed, it is known that the Plexins have a role in the development of the immune system (Kumanogoh and Kikutani 2013). PLXNB1 (Plexin B1) is expressed by stromal cells in the BM and this interaction between B cells expressing SEMA4D, the ligand for PLXNB1, increases proliferation and life span of these cells. Chronic lymphocytic leukaemia cells have also been found to express this ligand, indicating that PLXNB1 may have a role in increasing the survival of malignant cells (Granziero et al. 2003). There is a lack of

data available for the role of PLXND1 and PLXNA1 in leukaemia and Dex response. How the roles of PLXND1 in apoptosis and PLXNA1 are linked to the loss of the sgRNA targeting these genes is not known, but it would appear that loss of expression is not tolerated in the L707 presentation cells.

This screen is currently being re done by Alex Elder, with both a Dex and Control arm. The DNA extraction and PCR steps will be done in a clean area where sgRNA have not been opened before, and so will not have the same issues with PCR contamination as this screen had. It should hopefully show the same genes with enriched or depleted sgRNA. Further work would then be needed to validate these genes and determine their role in leukaemia, Dex response and growth of cell *in vivo*.

Chapter 7: Dexamethasone resistance in Acute Lymphoblastic Leukaemia

cell lines

7.1 Introduction

Cell lines have been used to study cancer for over 60 years, the first being the HeLa cells in 1951. These cells were used widely for all types of research and were considered a good model for many studies. The first evidence that cell lines may not be a good model for the disease of origin came from a cell line that had been in culture for an extended period of time, and as a result had both morphological and karyotypic changes compared to the original cells (Nelson-Rees et al. 1976). Investigation of the differences between primary samples and cell lines has been greatly improved since this first report, with the advent of next generation sequencing hugely expanding the field. A large study that used microarray analysis of over 5000 cell lines, primary cancer samples and normal samples found that each group clustered together, not with samples from the same tissue of origin. Analysis of the genetic signature in cell lines compared to primary cancer samples found that genes involved in cell cycle, mitosis and metabolism were upregulated in cell lines (Gillet, Varma, and Gottesman 2013; Lukk et al. 2010). Despite this evidence the picture is muddied by studies that suggest cell lines are an accurate representation of the disease state they are modelling. For example 51 breast cancer cell lines were found to mirror the genomic and transcriptional signatures of primary samples with only a few significant differences (Neve et al. 2006). These differences have been suggested as artefacts of growing in a different microenvironment *in vitro* and the different signature could simply be subtracted to get useful information (Gillet, Varma, and Gottesman 2013).

Despite misgivings about the faithful representation of disease states, cell lines are still incredibly useful. Cell lines often grow well in culture and have shorter doubling times than primary cells (Czekanska et al. 2014). This makes them a very attractive option for drug screening, which may require very large numbers of cells. The investigation of drug resistance in cell lines may be problematic, due to the altered expression of cell cycle and apoptosis genes as a result of growing cells *in vitro*, as these genes may also have an effect on drug resistance. Cell lines have been shown to have different expression profiles of multi

drug resistance related genes which would undoubtedly alter the drug response profile of cells (Gillet et al. 2011; Gillet, Varma, and Gottesman 2013).

As already described, resistance to dexamethasone is a problem in ALL, and especially in relapsed ALL. For these reasons having the right model to study the emergence of drug resistance is important. Cells need to be sensitive to Dex, which considering the relapse origin of many cell lines is not often the case.

The 697 cells are a cell line derived from the BM of a 12 year old male at relapse, and were one of the first ALL cell lines to be derived from a paediatric patient (Findley et al. 1982). The patient had null cell ALL (non B, non T) ALL at presentation but cells cultured at relapse were found to have a pre-B phenotype. The 697 cells contain the translocation t(1;19) which generates the leukaemic fusion gene E2A/PBX1. Importantly the 697 cells are sensitive to Dex, with a reported IC₅₀ of 23.3±5.7nM (Inoue et al. 2002).

7.2 The 697 cells show dexamethasone resistance *in vivo*: An incidental finding

The 697 cells were initially chosen as a Dex sensitive cell line in which to carry out a small screen of pTRIPZ plasmids, containing shRNA thought to be important in the emergence of Dex resistance at relapse in pre B ALL. A pilot study was carried out with 7 NSG mice, engrafted with 10⁴ 697 cells each in order to determine the rate of engraftment in NSG mice and the concentration of Dex that could be well tolerated. Mice were either given saline control, 5 mg/kg or 10 mg/kg Dex I.P on weekdays starting 14 days after intrafemoral injection and continued until mice reached license endpoints. The 697 cells engrafted very quickly, and both Dex doses were well tolerated by the mice. Survival was not further investigated at the time, although analysis later on reveals that none of the groups had a significant difference in survival (Figure 89). The main pTRIPZ plasmid pool study was carried out in a larger group of 17 mice, split into 4 groups with combinations of Dex and doxycycline treatment, but essentially 8 control mice and 9 Dex (10 mg/kg) treated mice. Dex treatment was started 2 weeks after intra-femoral injection of 697 cells transduced with the luciferase expressing plasmid pSLIEW , 697pSLIEW cells. The mice in this study also had no significant differences in survival between the control and treated group (Figure 90). It

was at this point that the survival from the pilot study was investigated further and the differences in survival, or lack thereof were questioned.

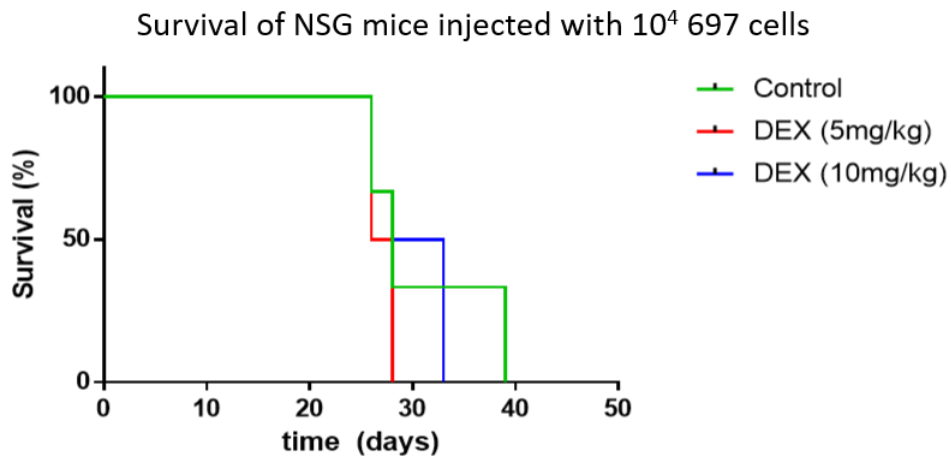


Figure 89: Survival of mice from first test of 697 engraftment in NSG mice. Dex treatment was started 14 days from intrafemoral injection and continued every weekday until mice were killed due to license defined endpoints. Survival is not significantly different between the 3 groups as determined using Log Rank (Mantel Cox) testing.

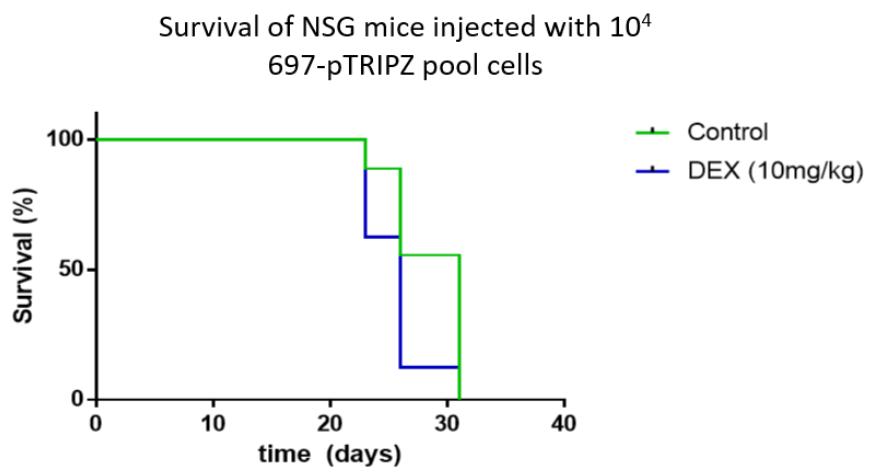


Figure 90: Survival of mice engrafted with 697 transduced with pTRIPZ shRNA pool treated with either saline or Dex (10 mg/kg). Treatment was started 2 weeks after intra-femoral injection of 697 cells and was give on weekdays after that until mice were killed as per license endpoints. Survival is not significantly different between the groups as determined using Log Rank (Mantel Cox) testing.

From this initial study it was determined that Dex treatment did not have any effect on the survival of mice engrafted with the 697 cells. This was surprising considering the IC₅₀ of the 697 cells *in vitro* was found to be around 25 nM in both the literature (Inoue et al. 2002) and with cytotoxicity experiments carried out over a 96hr time course *in vitro* (Figure 91). We therefore decided to further investigate the reasons for this *in vivo* resistance.

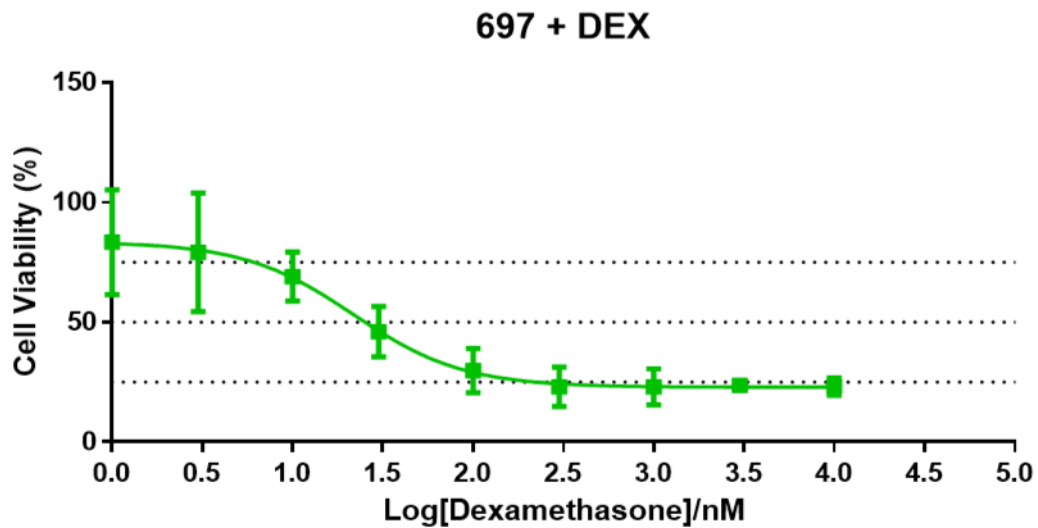


Figure 91: In vitro Dex sensitivity of the 697 cells. Determined using the WST-1 assay. Cells were seeded at 0.5×10^6 cells/ml and treated with Dex for 96 hours before readings were taken. The plotting method used was a 4 parameter dose response curve, error bars show standard deviation. n=3.

7.2.1 697 cell dexamethasone resistance is not mediated by adhesion *in vitro*

The initial hypothesis for this acquired resistance *in vivo* is that it was due to adhesion-mediated drug resistance. Increased resistance to chemotherapeutic agents caused by cell adhesion has been demonstrated in both multiple myeloma and chronic myelogenous leukaemia (Damiano, Hazlehurst, and Dalton 2001; Landowski et al. 2003). It is mediated through the cell surface integrins and NF-kappa β signalling.

In order to test this hypothesis, several lines of feeder cells were used to support 697 cells to mimic the *in vivo* niche, with adherence of the leukaemic cells to the stromal cells. These were the murine BM lines M210B5 and MS5 and primary human MSC. To increase the

likelihood of feeder dependency in these cells 2% FBS was used as well as 10%. The rationale behind this is that without high levels of FBS as is usual with culture of the 697 cell line, the cells would become dependent on the factors produced by the feeder cell layers. Before use, 697 cells previously transduced with the pSLIEW plasmid were sorted to enrich for GFP positivity (Figure 92). The pSLIEW plasmid contains GFP and luciferase so that cells can be quantified either using FACS or a luciferase assay, whereby the luciferase in the cells converts the substrate luciferin to oxyluciferin and light. Although for *in vivo* studies transduction efficiency does not need to be high to determine engraftment, when investigating the cells *in vitro* the entire population needs to have luciferase activity in order to get accurate readings.

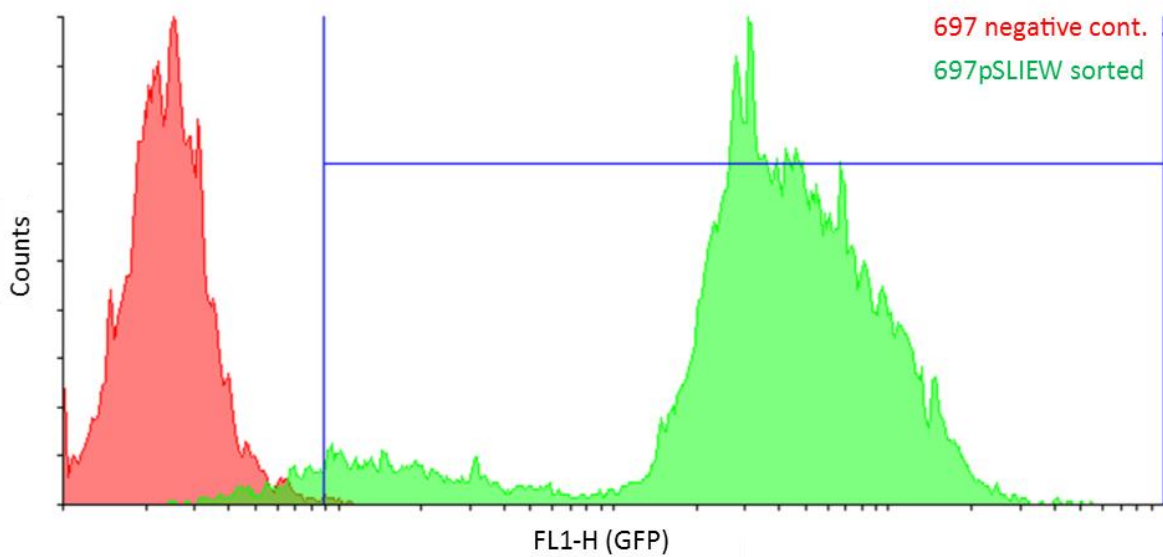


Figure 92: GFP expression in 697 pSLIEW cells after sorting (green) compared to 697 control cells without transduction (red). As can be seen from the plot there is GFP expression in approximately 98%.

Three types of supporting cells were used, 2 murine BM stromal cell lines, MS5 and M210B4 as well as human MSC. In order to test all possibilities in regards to feeder dependence, as this might alter the phenotype of the leukaemic cells, the 697pSLIEW cells were tested with 4 different conditions (Table 32). Feeder cells were seeded 24 hrs before addition of 697pSLIEW cells and dex at a range of 1-5,000nM. Co-cultures of cells were incubated with dex for 96hrs before cytotoxicity readings were taken. This was done using the luciferase assay as cytotoxicity assay that used metabolism as a readout for cell numbers such as the WST-1 assay would have been contaminated by contributing readings from the feeder cells.

Briefly, 10 µl of 7.5% luciferin was added to each well and bioluminescence readings taken at 3 minutes. Readings were used to calculate the number of cells in each well compared to the vehicle (0.05% ethanol). The luciferase assay is a measure of the level of luciferase enzyme activity in the sample, to determine the number of cells.

Cell concentration/ml	FBS concentration (%)
0.5x10 ⁶	10
0.5x10 ⁶	2
0.5x10 ⁴	10
0.5x10 ⁴	2

Table 32: The cell and FBS concentrations used for the four different conditions for testing 697pSLIEW cells on different supporting stromal cells.

None of the conditions used resulted in a significant increase in dex resistance when grown on any of the feeder cells (Figure 93-95). In fact, the opposite was seen all conditions for the M210B4 and MSC feeder cells, and one condition with the MS5 cells. The reasons for this are not known, but it would appear that growth on a BM stromal feeder layer does not induce dex resistance in the 697pSLIEW cells and is likely not the cause of the resistance seen *in vivo*.

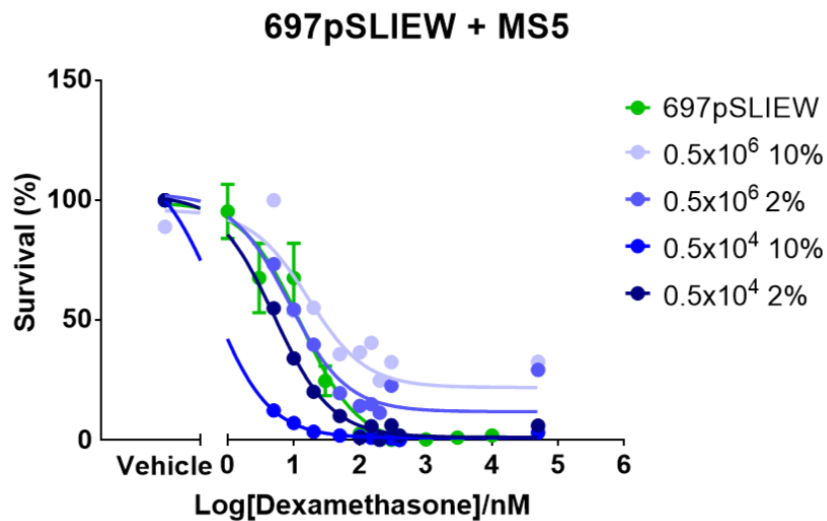


Figure 93: Dex cytotoxicity of 697 pSLIEW cells on a feeder layer of MS5 cells. 697 cells tested at 4 different conditions, (Table 32), error bars show standard deviation, n=1. No conditions other than 0.5x10⁴ cells/ml & 10% FBS show any significant difference ($p<0.05$) to 697pSLIEW cells, this difference is an increase in Dex sensitivity. Data shown is log2 transformed and normalised. The plotting and statistics used were a 4 parameter dose response curve and two way ANOVA. Error bars show standard deviation.

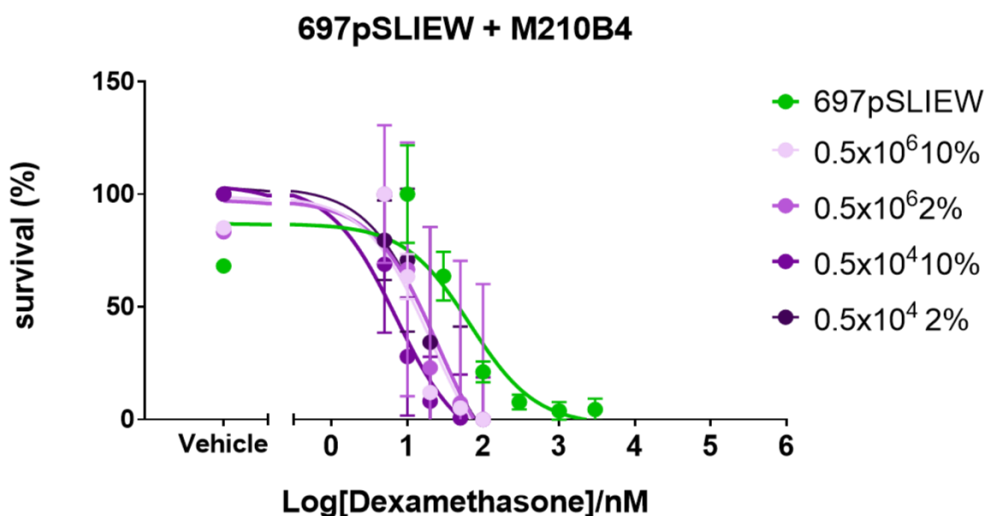


Figure 94: Dex cytotoxicity of 697 pSLIEW cells on a feeder layer of M210B4 cells. 697 cells tested at 4 different conditions, (Table 32), error bars show standard deviation, n=3. All samples on M210B4 cells are significantly less Dex resistant than the 697pSLIEW cells in normal culture conditions ($p<0.05$). Data shown is log2 transformed and normalised. The plotting and statistics used were a 4 parameter dose response curve and two way ANOVA. Error bars show standard deviation.

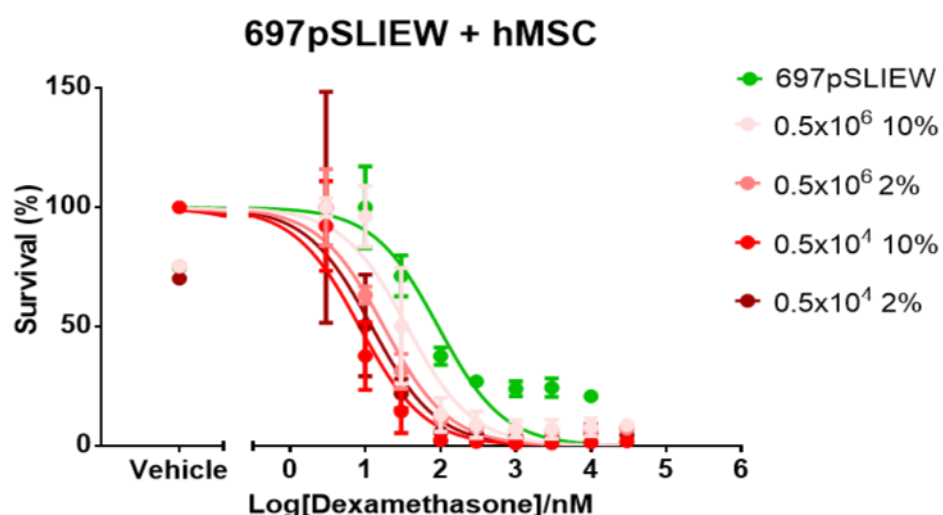


Figure 95: Dex cytotoxicity of 697 pSLIEW cells on a feeder layer of MSC cells. 697 cells were tested at 4 different conditions (Table 32), error bars show standard deviation, n=4. All conditions show significantly increased Dex sensitivity compared to the 697pSLIEW cells under normal culture conditions. (p<0.05). Data shown is log2 transformed and normalised. The plotting and statistics used were a 4 parameter dose response curve and two way ANOVA. Error bars show standard deviation.

7.2.2 Growth of 697 in vivo does not result in resistance when cells are tested in vitro

The finding that the Dex resistance in the 697 pSLIEW cells did not appear to be mediated by cell adhesion to stromal cells, at least not in an *in vitro* setting, resulted in another study *in vivo* to determine the mechanisms of this resistance. The hypothesis was that 697 cells that had been injected into mice, and then collected once mice were killed may retain Dex resistance when tested *in vitro*. Mice were injected with 10⁴ sorted 697pSLIEW cells and split into 3 treatment groups: control (saline), Dex the day after intrafemoral (7.5 mg/kg), and Dex after engraftment (7.5 mg/kg). A lower concentration of Dex was used for this study than the initial one because of concerns over potential toxicity and issues with weight loss seen in other studies using Dex with other ALL cells.

Engraftment was monitored using the IVIS to determine levels of bioluminescence produced by the luciferase in the 697pSLIEW cells engrafted in the mouse when the animal is dosed with luciferin, at day 14. Engraftment was determined sufficiently high and treatment was started for the later Dex treatment group. At this time point there was no difference in the

total bioluminescent flux (p/s^2) of the control mice compared to those that had already been treated with Dex for 2 weeks (Figure 96).

Overall survival was not affected by which group mice were in, and Dex treatment did not prolong survival (Figure 97), unlike the Dex sensitive L707 presentation ALL cells also used in this thesis. Mice were killed when they reached endpoints as defined on the license and samples collected from the BM of the femurs, the spleen and the liver. Spleen and liver samples were purified by ficoll separation before use *in vitro*.

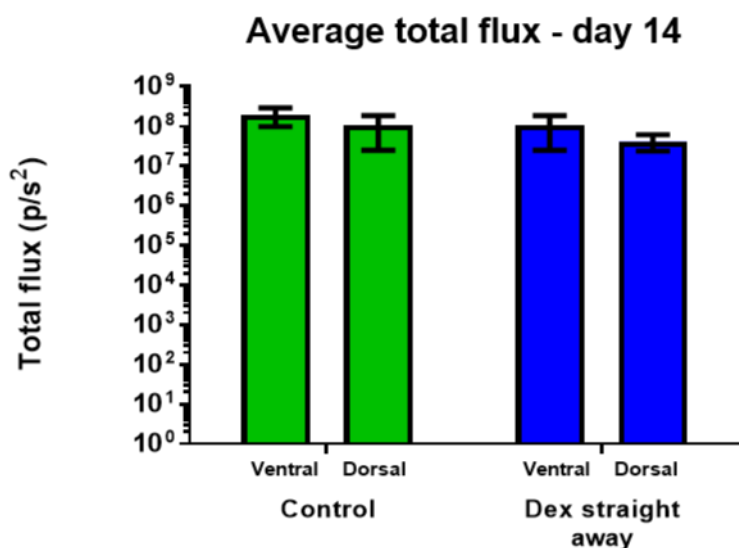


Figure 96: Total flux (photons/s^2) emitted from the mice in the two of the treatment groups after dosing with luciferin and imaging using the IVIS. No significant difference is seen after 13 days of treatment in the Dex treated group compared to the controls using multiple t tests.

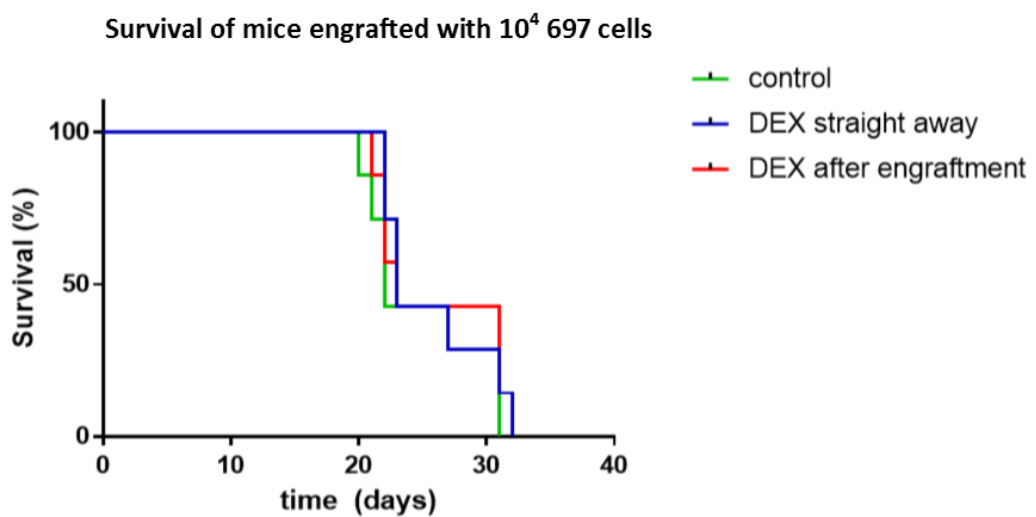


Figure 97: The survival of mice engrafted with 10^4 697 pSLIEW cells, dosed with Dex (10 mg/kg), every weekday; starting after intrafemoral injection, 2 weeks later, or controls. None of the groups are significantly different from each other using a Log Rank (Mantel ox) test.

To determine if the Dex resistance was retained after cells were grown *in vivo*, the 697pSLIEW cells from mouse organs were tested for Dex sensitivity *in vitro* after collection. Cells were seeded the day of collection in 96 well plates and Dex added, cytotoxicity was measured 96hrs later by luciferase assay.

Samples collected from the mice that were tested *in vitro* did not show any differences in Dex sensitivity between the three treatment groups (Figure 98-100). There was a significant increase in Dex sensitivity in the BM and spleen samples, similar to what was seen with the 697 pSLIEW cells with feeder support. The cause for this is not known, but it could possibly be a result of reduced viability in these samples. If there was an alteration to the phenotype of the cells induced by *in vivo* growth, it would be expected to be present in the cells collected from the liver as well. It would also, considering the Dex resistance of these cells in the mouse be expected to be shift towards resistance not away from it.

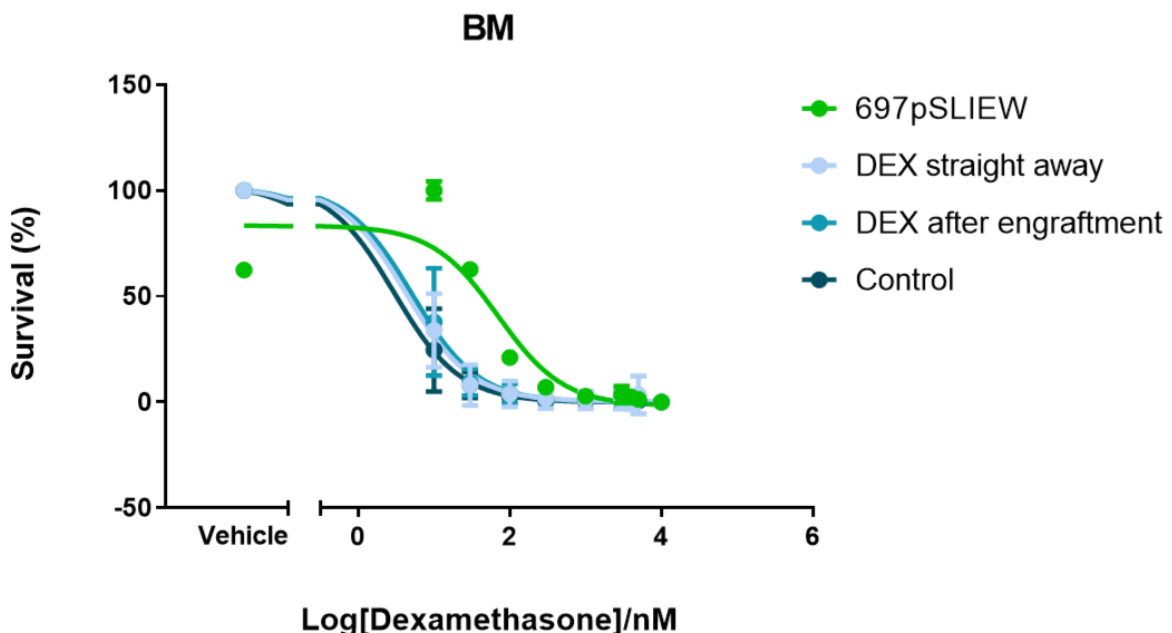


Figure 98: Dex sensitivity of 697pSLIEW cells collected from the BM of engrafted mice compared to 697pSLIEW that were not grown in vivo. BM 697pSLIEW cells are significantly more sensitive to Dex compared to 697pSLIEW in vitro samples ($p<0.001$) but are not significantly different to each other. Reduced viability of cells from BM samples could account for the increased sensitivity of BM 697pSLIEW cells compared to 697pSLIEW in vitro samples. Measured by luciferase assay after 96hrs incubation with Dex. The plotting and statistics used were a 4 parameter dose response curve and two way ANOVA. Error bars show standard deviation, 5 or 6 mice per group.

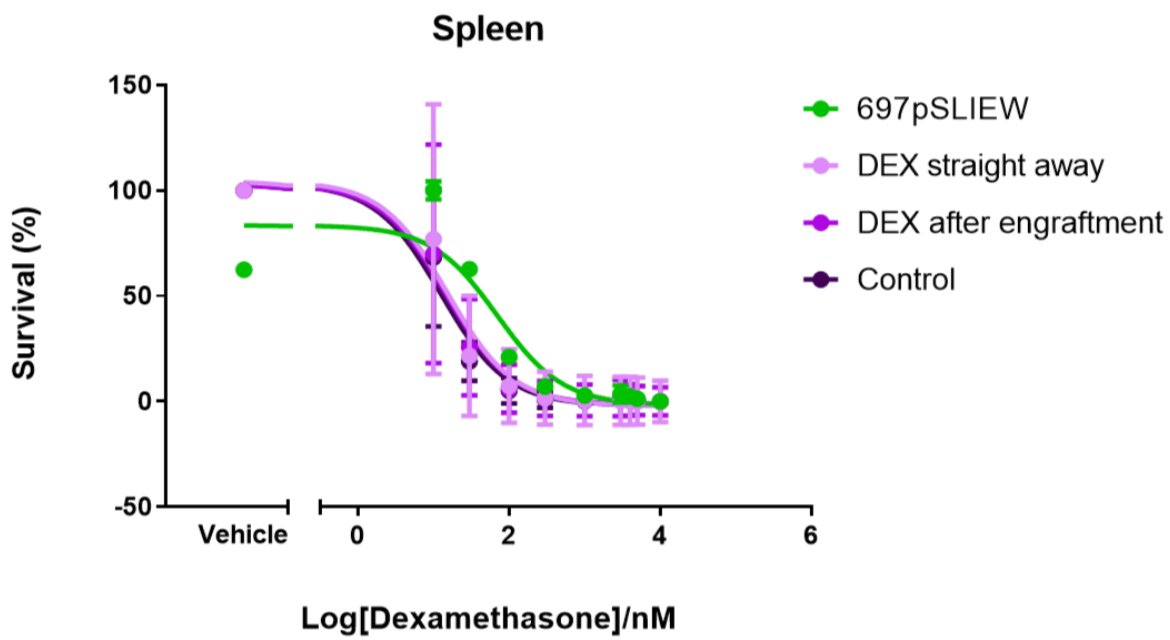


Figure 99: Dex sensitivity of 697pSLIEW cells collected from the spleens of engrafted mice compared to 697pSLIEW cells that were not grown in vivo. Spleen 697pSLIEW samples are significantly more sensitive to Dex compared to 697pSLIEW cells grown in vitro ($p<0.05$) but not significantly different to each other. Measured by luciferase assay after 96hrs incubation with Dex. The plotting and statistics used were a 4 parameter dose response curve and two way ANOVA. Error bars show standard deviation, 5 or 6 mice per group.

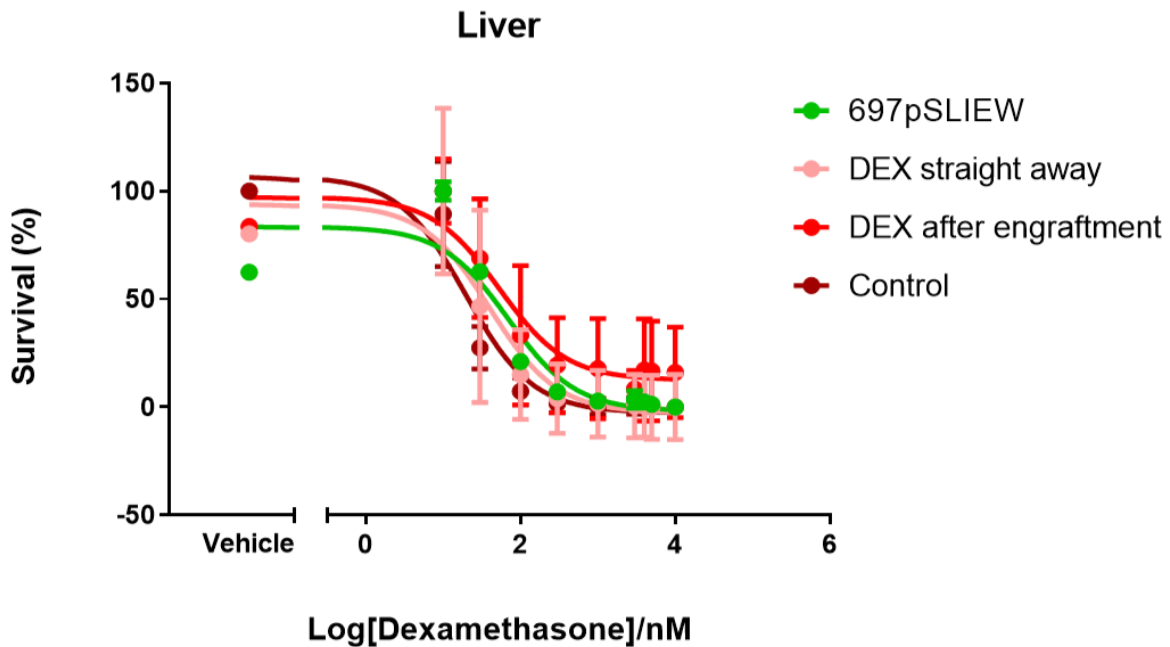


Figure 100: Dex sensitivity of the 697pSLIEW cells collected from the livers of engrafted mice compared to 697pSLIEW cells not grown in vivo. Liver 697pSLIEW cells are not significantly different from each other or the 697pSLIEW cells not grown in vivo. Measured by luciferase assay after 96hrs incubation with Dex. The plotting and statistics used were a 4 parameter dose response curve and two way ANOVA. Error bars show standard deviation, 5 or 6 mice per group.

7.2.3 No changes in histology are seen in mice from different treatment groups

Samples from the mice engrafted with 697 pSLIEW cells were sent for histology to discern if there were any differences in engraftment between the three groups. H/E staining was used to determine the tissue structure and CD45 and CD19 were used to mark human 697 cells. However, the CD45 staining was not very strong and so CD19 was used for all further investigations (Figure 101).

The engraftment in all three groups was similar, with the same picture in the organs of mice from all groups. The spleen has a relatively uniform engraftment with CD19⁺ 697 pSLIEW cells whereas the liver has more focal growth, indicating clonal growth may have more of a role in the liver (Figure 102-101). The 697 cells engraft very quickly in NSG mice. They also

have a slightly different phenotype to the other ALL cells used in this PhD, the L707, in as much that they engraft the liver heavily, not just the spleen. Analysis of peripheral blood of mice engrafted with 697 pSLIEW cells did not show engraftment, implying that the cells do not appear to circulate in the peripheral blood in any significant number.

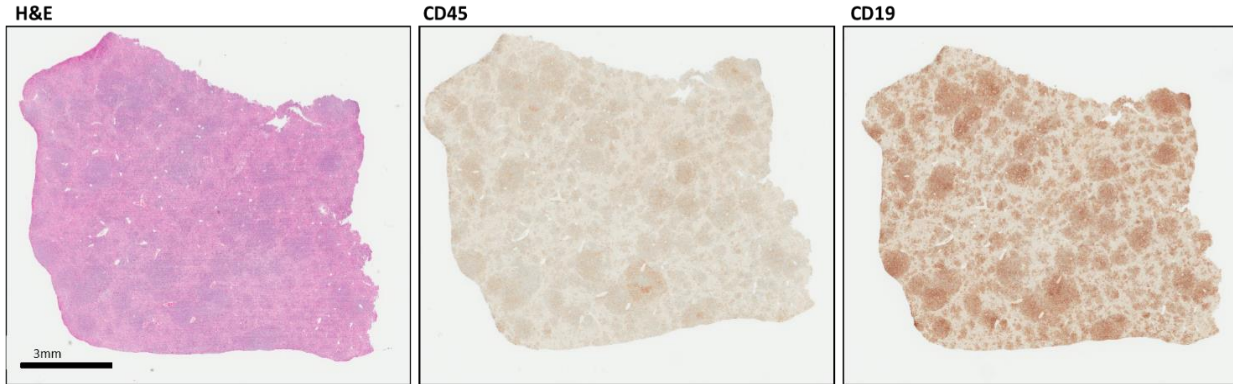


Figure 101: H&E, CD45 and CD19 staining of liver from an NSG mouse injected intra-femorally with 10^4 697 pSLIEW cells. 697pSLIEW cells are strongly positive for CD19, but CD45 staining is weak and so for further experiments only H&E and CD19 were used. Sectioning and staining was carried out by the histopathology department at the RVI hospital.

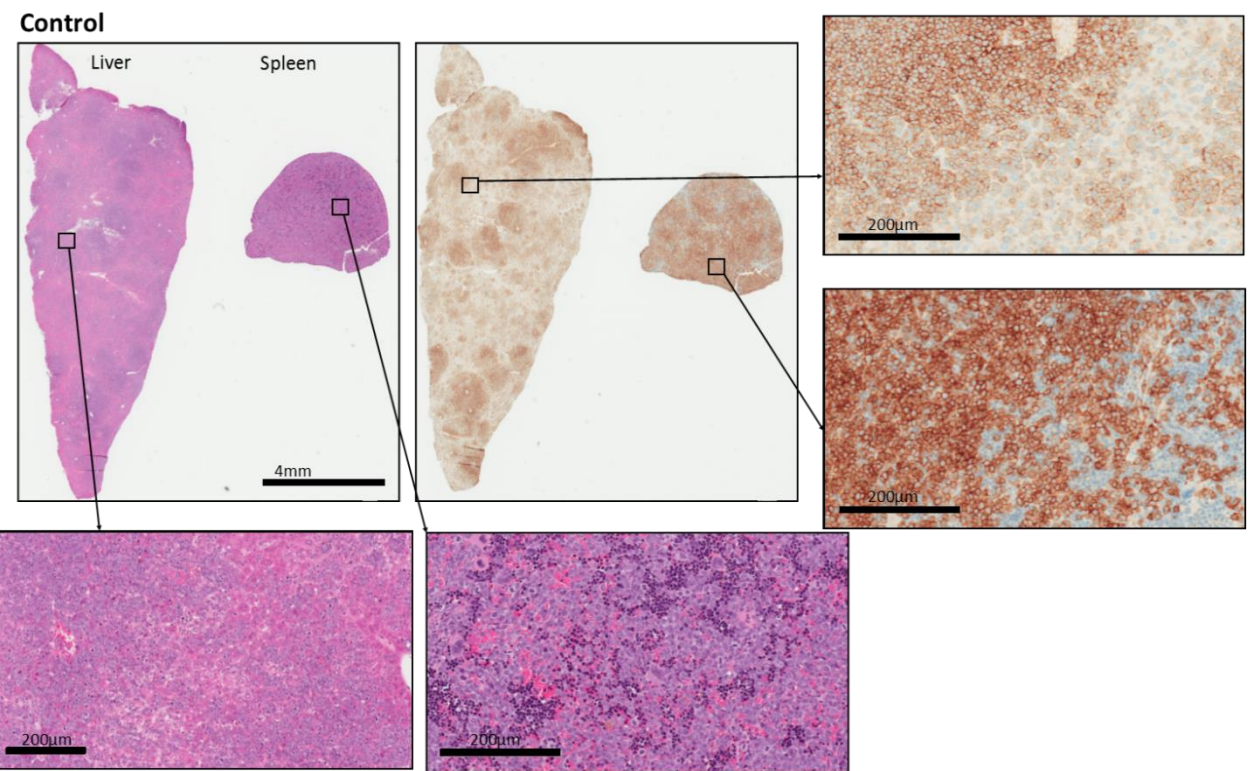


Figure 102: Liver (top) and spleen (bottom) samples from a control mouse that received saline injections after injection with 10^4 697 pSLIEW cells intra-femorally. H&E (pink and purple) and CD19 (brown and blue) staining are both shown. The liver shows less engraftment than the spleen, and the engraftment is also less uniform. Sectioning and staining was carried out by the histopathology department at the RVI hospital.

Dex straight after intra-femoral injection

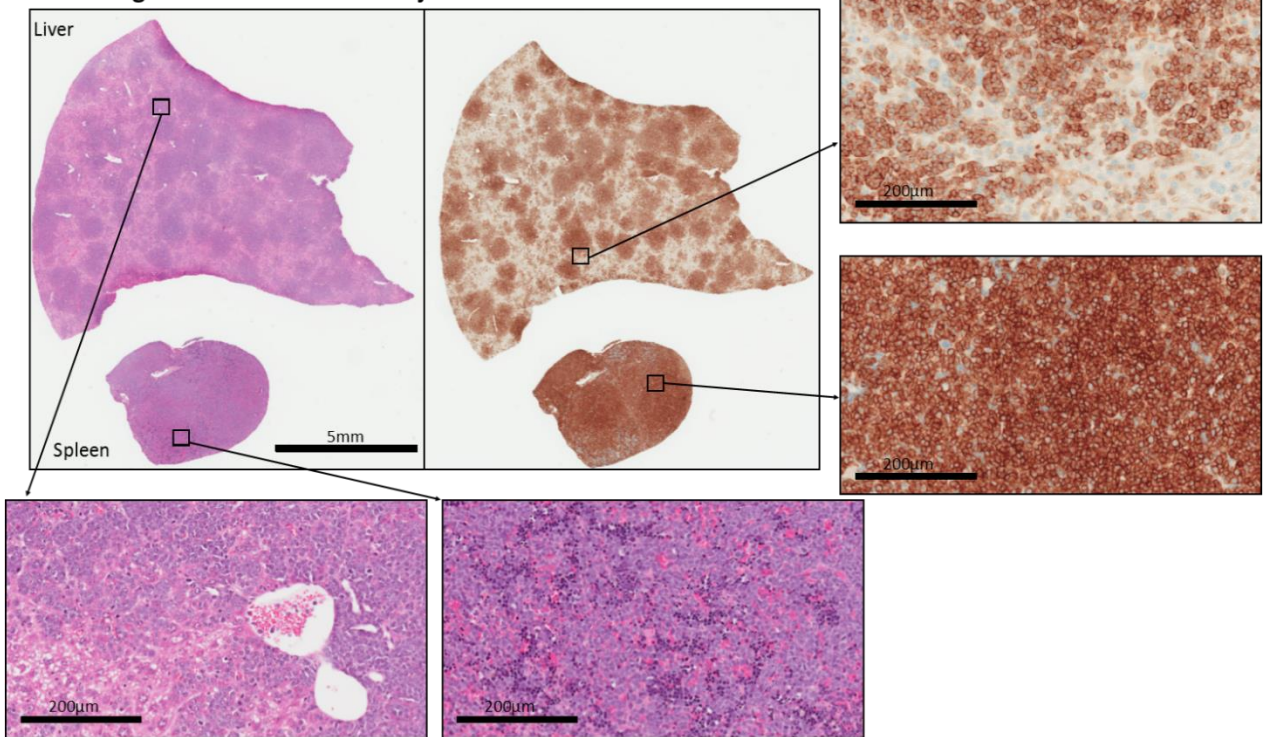


Figure 103: Liver (top) and spleen (bottom) samples from a mouse that received Dex straight after injection with 10^4 697 pSLIEW cells intra-femorally. H&E (pink and purple) and CD19 (brown and blue) staining are both shown. As can be seen from the images the liver shows a less uniform engraftment than the spleen, similar to the images for the control mice and the mice treated with Dex starting later. Sectioning and staining was carried out by the histopathology department at the RVI hospital.

Dex 14 days after intra-femoral injection

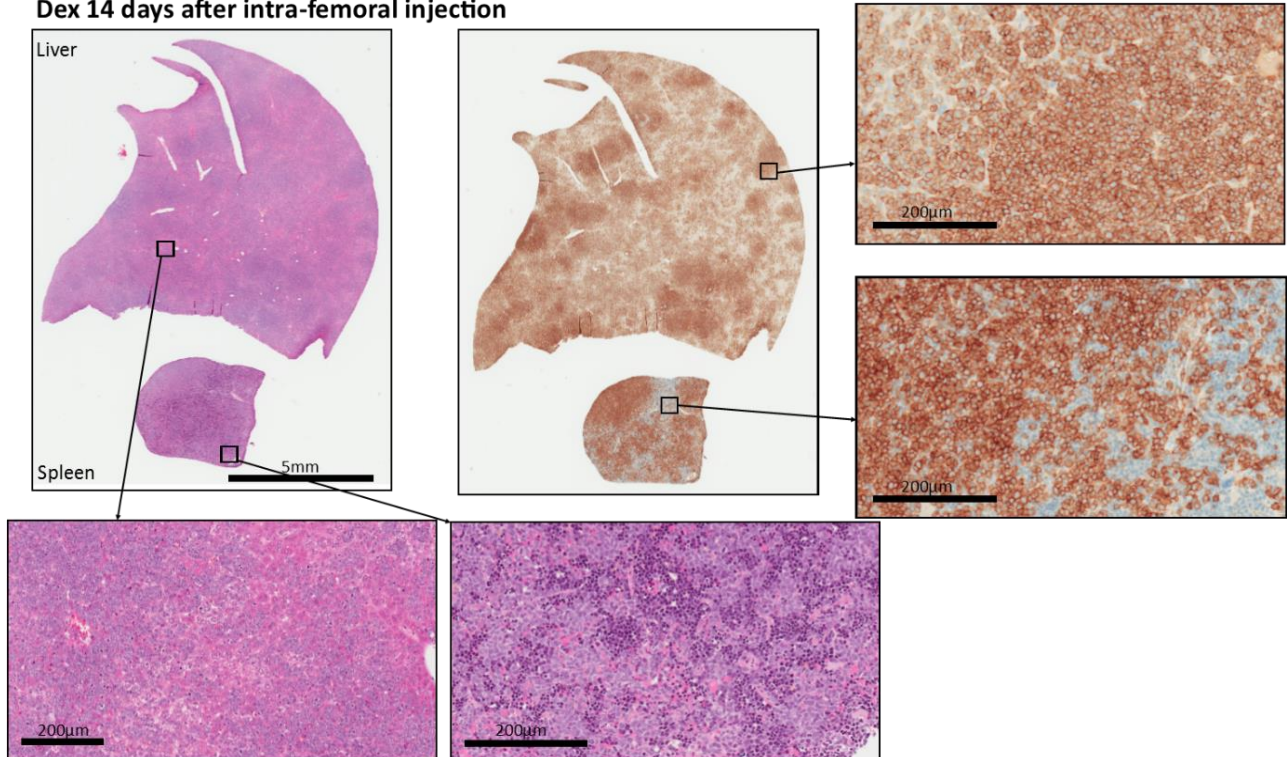


Figure 104: Liver (top) and spleen (bottom) samples from a mouse that received Dex 14 days after injection with 10^4 697 pSLIEW cells intra-femorally. H&E (pink and purple) and CD19 (brown and blue) staining are both shown. As can be seen from the images the liver shows a less uniform engraftment than the spleen. The reasons for this are not fully understood but it is seen with the majority of ALL engraftment in NSG mice where there is liver involvement. Sectioning and staining was carried out by the histopathology department at the RVI hospital.

7.3 Dexamethasone pharmacokinetics

To determine the levels of Dex *in vivo*, pharmacokinetic (PK) studies were carried out to check that the lack of Dex response *in vivo* was not due to insufficient concentrations reaching the cells.

Two PK studies were carried out; dosing by oral gavage, or dosing by I.P. injection, both with 7.5 mg/kg. Both routes of administration were tested as both methods were used throughout the PhD for Dex dosing.

For the oral gavage study 12 male CD1 mice were used and 6 time points were taken. For the I.P. PK study 9 male RAG2 mice were used and the last time point, at 72hrs, was removed as levels of Dex in the blood were reduced to zero by 48hr after dosing so it was considered unnecessary. Peripheral blood was collected by tail vein venepuncture or cardiac puncture, samples were centrifuged to separate the red cells and the serum collected and stored at -20°C. Dex concentrations in the peripheral blood were determined by mass spectroscopy by Rosie Jackson. Although there was a trend for higher concentrations with oral dosing this was not found to be significant (Figure 105). By 24hrs after dosing by either route Dex was cleared from the peripheral blood. Despite the fast clearance, for all time points taken before 24hrs the concentration of Dex in the peripheral blood was well above the IC₅₀ for 697 cells *in vitro* (~25nM). Although there is no significant difference between the two routes as determined using a one tailed T test ($p=0.68$), there is a slight trend that would imply oral dosing has a slower clearance. As most of the Dex is cleared relatively quickly this would have been a better experiment if more time points had been taken, especially between 6 and 24 hrs. However, due to limitations in the number of mice available this was not possible.

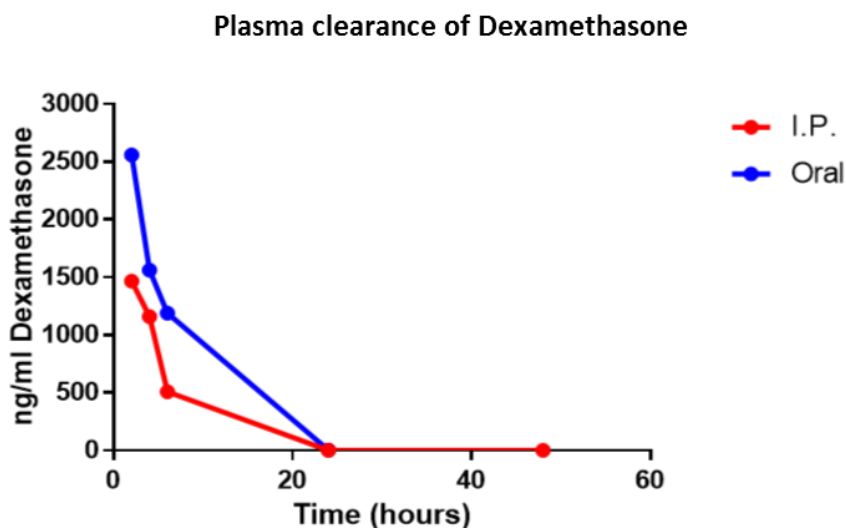


Figure 105: Concentration of Dex (ng/ml) in the peripheral blood of mice (oral – CD1 mice, I.P. – RAG2 mice) as measured by mass spectroscopy (done by Rosie Jackson). Blood was collected via tail venepuncture for the 2,4 and 6hr measurements and by cardiac puncture under terminal anaesthesia for the later time points. Both I.P. and Oral dosing of 7.5 mg/kg Dex are shown. Dosing routes are not significantly different to each other, determined by a T test, $p=0.68$.

The high levels of Dex in the peripheral blood imply that the cells are receiving a sufficient dose to induce apoptosis if they showed the same sensitivity as cells *in vitro*. This leads to the theory that although the cells are receiving the drug, they are not having the same reaction that would normally result in apoptosis. The fast clearance from the blood indicates that mice only have therapeutic levels of Dex for somewhere after 6 but before 24 hrs after dosing, which considering mice were not dosed over the weekend would leave long treatment free periods. Mice were only treated at the weekends due to the effect of Dex dosing on weight loss, it was found that if mice were given a break then the weight increased again. This was important due to restrictions on the license around the amount of weight mice are permitted to lose before they have to be killed. A slow release pump for Dex might be a good option to consider in future experiments.

7.4 RNA sequencing

With the failure to determine a mechanism for 697 cell *in vivo* Dex resistance using *in vitro* testing, another strategy had to be used. Without knowing how to test for this change in the cells, RNA sequencing was chosen as the best possible way to investigate the cells, as the expression profiles of the cells and the differences between *in vitro* and *in vivo* should provide evidence for the changes occurring that could account for the Dex resistance.

Mice were injected intrafemorally with 10^4 697 pSLIEW cells (98% GFP+). Mice were monitored for engraftment using IVIS and once they were engrafted, 5 days of Dex (7.5 mg/kg, I.P.) treatment was given, controls were dosed with saline. Six hours after dosing mice were humanely killed and the organs collected. Liver samples were purified using ficoll separation and RNA extracted using the RNeasy kit (Qiagen). RNA quality was determined using a Bioanalyser (Figure 106) and samples were sent for sequencing to AROS (Table 33). *In vitro* samples were grown at 0.5×10^6 cells/ml and treated with 20 nM Dex for 96hrs before samples were taken, washed with PBS and RNA extracted in the same way. Large numbers of cells were treated with Dex *in vitro* in order to have enough viable cells to use for RNA sequencing. A lower centrifugation speed (300g) was used when washing to increase removal of dead cells.

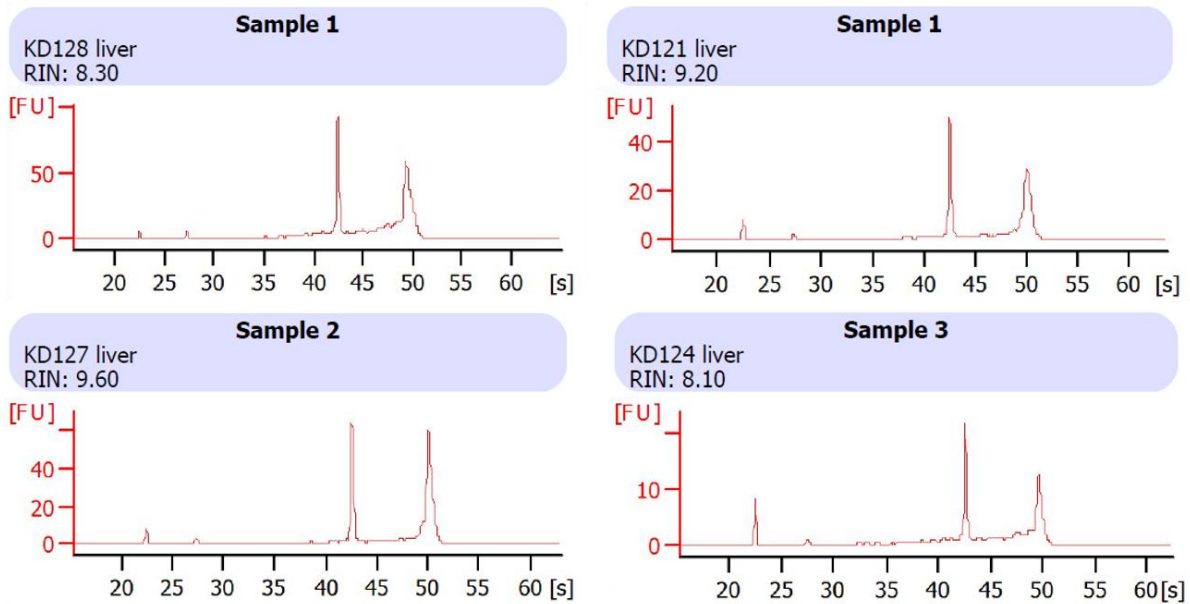


Figure 106: Bioanalyser traces for 4 of the representative mouse samples sent for RNA sequencing. The RNA Integrity Number (RIN) is determined by electrophoresis of the RNA sample, showing fluorescence (FU) over time. All of the samples show high RIN values indicating that the RNA was not degraded.

Sample	Group
697pSLIEW control (1)	<i>in vitro</i> control
697pSLIEW control (2)	<i>in vitro</i> control
697pSLIEW Dex 20 nM – 96 hrs (1)	<i>in vitro</i> DEX
697pSLIEW Dex 20 nM – 96 hrs (2)	<i>in vitro</i> DEX
KD111	Control Male
KD119	Control Male
KD121	DEX Male
KD124	DEX Male
KD127	DEX female
KD128	DEX female

Table 33: Samples used for the 697 Dex resistance RNA sequencing. Both male and female mice were used to eliminate sex specific differences. However, the sequencing for KD124 failed to produce reads and so is not included in any of the analysis. Male mice were originally used for the entire experiment but not enough samples were collected due to two mice dying early. As a result more mice were injected and treated with Dex, the only mice available at the time were female mice.

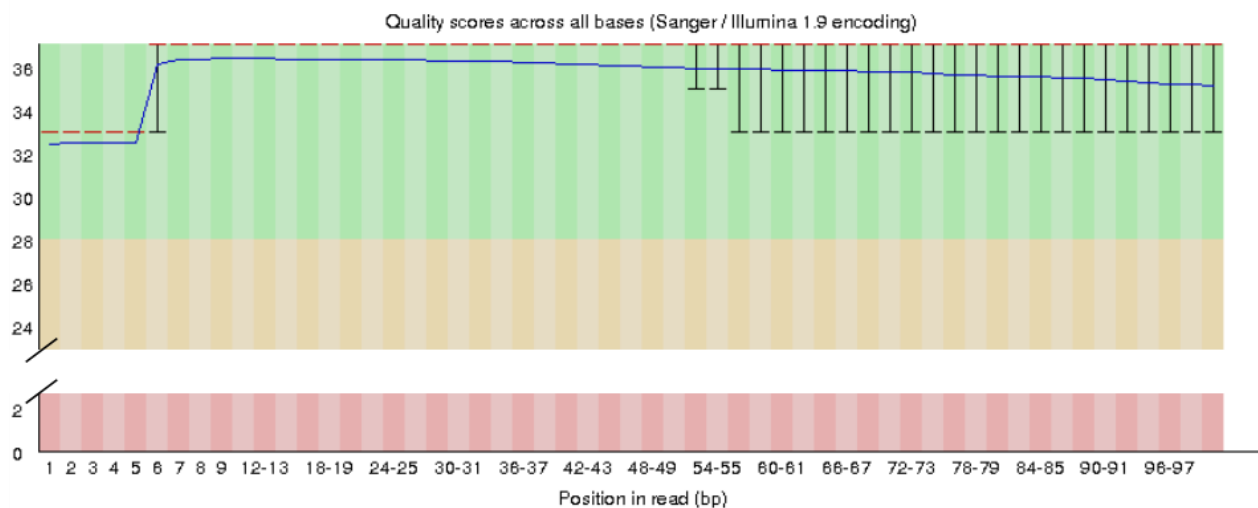
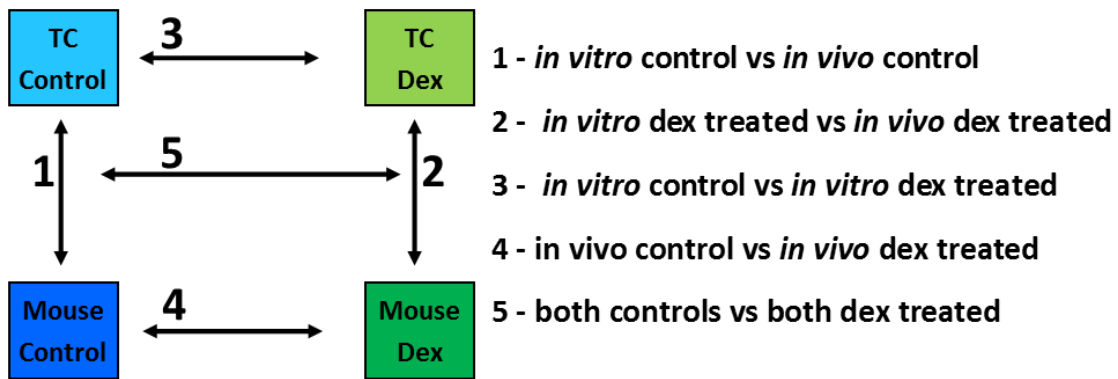


Figure 107: Quality score across the bases in the RNA sequencing reads for a representative FASTQ file. All bases are in the highest quality range (the green area). The plot was generated using the programme FASTQC which is used to run quality control on FASTQ files before they are used for downstream applications. The type of sequencing used was 100bp, paired end RNA sequencing.

Raw RNA sequencing data, from a 100bp paired end sequencing run was returned from AROS in the form of FASTQ files and quality control showed that the sequencing quality was very high (Figure 107). The Cufflinks suite was used to analyse data and produce plots.

In order to determine the differences between *in vitro* and *in vivo* samples as well as treatment vs control, several permutations of analysis were run (Figure 108). It should be noted that cuffdiff has a minimum p value of 5.00E-05, so if genes scored as significant they were then ranked by the log₂(fold change) FPKM. In RNA sequencing analysis expression is referred to in units of FPKM which is the fragments per kb of transcript per million mapped reads. As well as changes in FPKM and the subsequent fold change differences, with Cuffdiff the other possible option to use is the test statistic value which is used to determine significance of the change in FPKM between samples and thus relates to the effect size. However, it is more complicated to comprehend than the log₂ fold change and so is not often used, but may still be useful.



*Figure 108: The 5 comparisons that were run using the 697 RNA sequencing data in order to determine which genes might be important for the differences between *in vitro* and *in vivo* Dex response. Blue boxes indicate control samples and green boxes indicate Dex treated samples, the darker of the two for each represents the *in vivo* sample.*

Initial evaluation showed that the dispersion, and the squared coefficient of variation (CV_2) which are both measures of the biological variation between the samples is very similar for all of the samples tested. If these plots show the same pattern it means the data is not substantially different between groups, indicating lower variance and so a higher likelihood that genes with differential expression will be significant. The comparisons for all of the permutations of comparison are very similar (Figure 109-110).

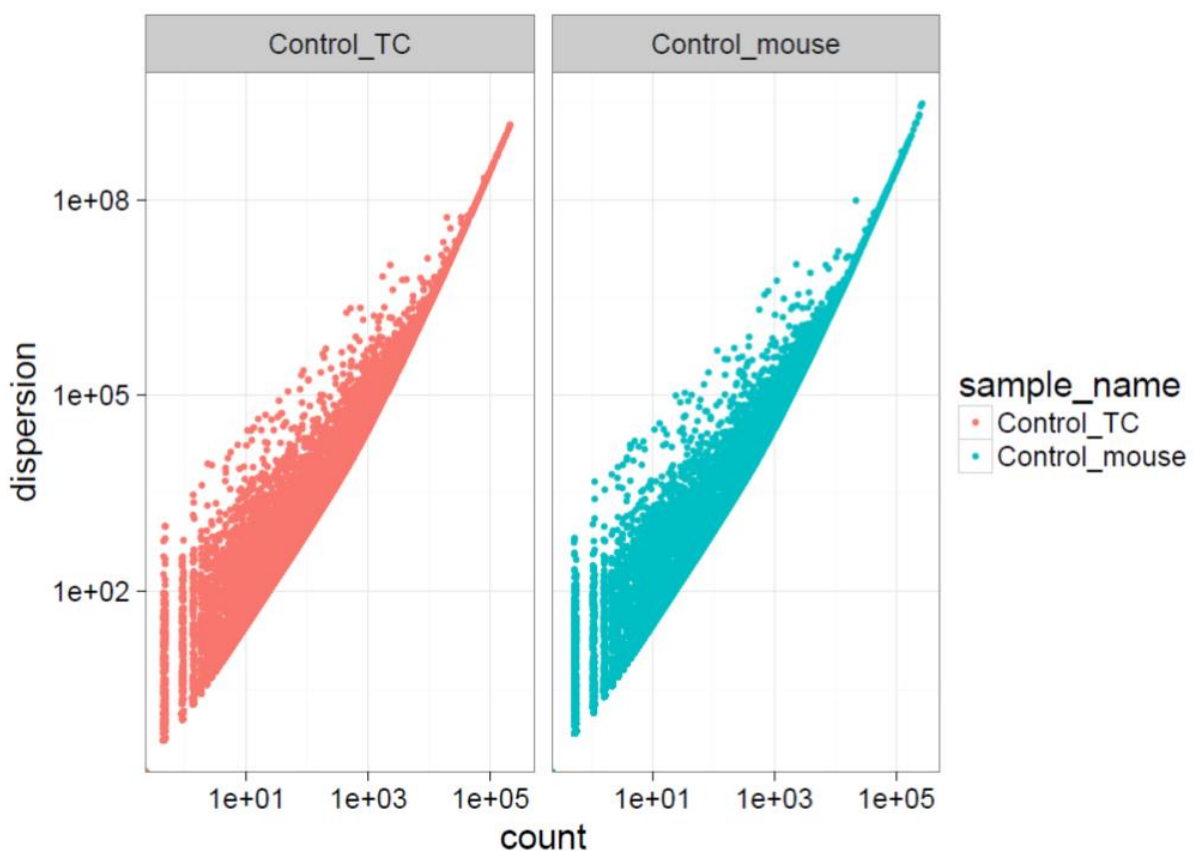


Figure 109: Dispersion plot for the RNA sequencing data of the 697 control TC samples and Control mouse samples. The dispersion is very similar between the two indicating low variance between samples. This indicates the raw data is high quality so can be used to generate robust results. Plots produced in CummRBund with CuffDiff analysed data.

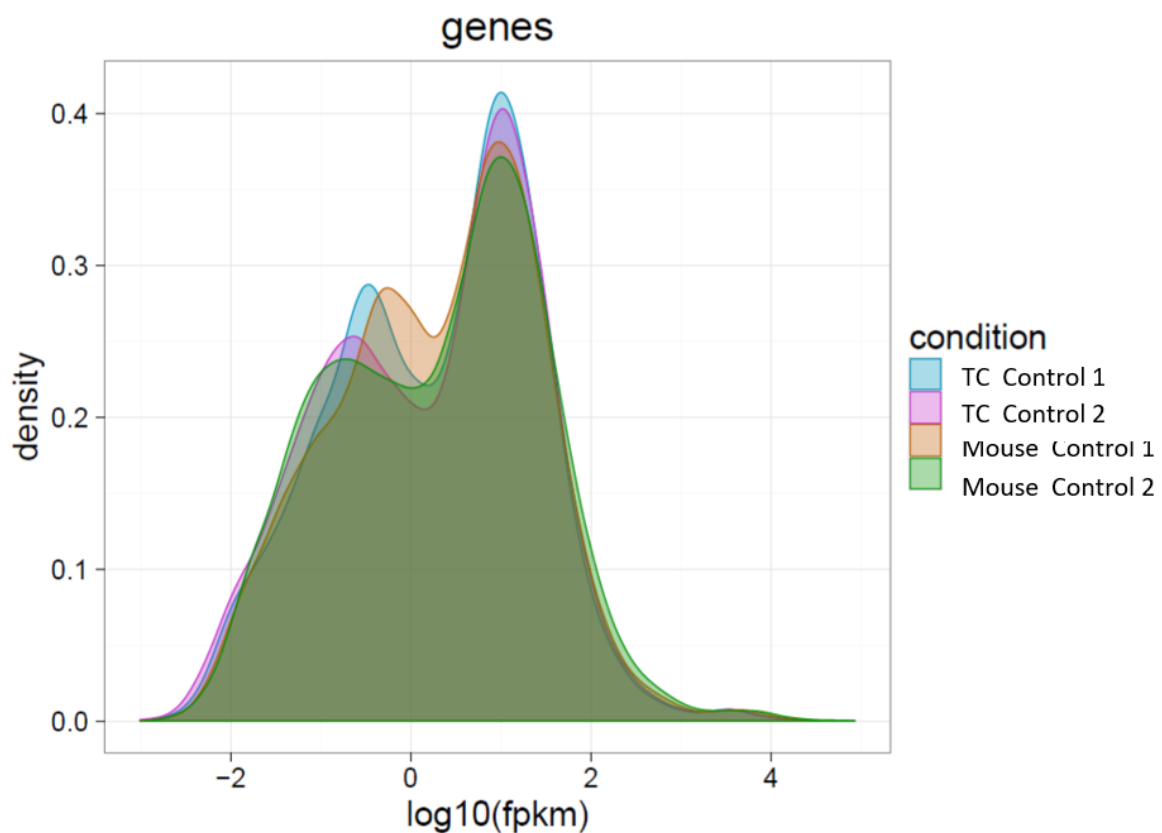


Figure 110: Density of the log₁₀ (FPKM) values for the 697 cell TC and mouse control sample data from the RNA sequencing analysis. Each replicate is shown separately but there is not a lot of variance between them. Plots produced in CummRBund with CuffDiff analysed data.

7.4.1 *in vitro control vs in vivo control*

Comparison of the *in vivo* and *in vitro* samples should allow for the elucidation of which genes are important for engraftment *in vivo*, and may provide insight for how the cell phenotype changes in response to the murine microenvironment.

TC samples cluster separately from the mouse samples (Figure 111), and 3225 genes were significantly ($P<0.05$) up or down regulated in the control TC vs control mouse samples (Figure 112). To narrow down this list, we only looked at genes which had a log₂ fold change of greater than two. This resulted in 139 genes with decreased *in vivo* expression and 253 genes with increased expression.

All Genes(Control samples)

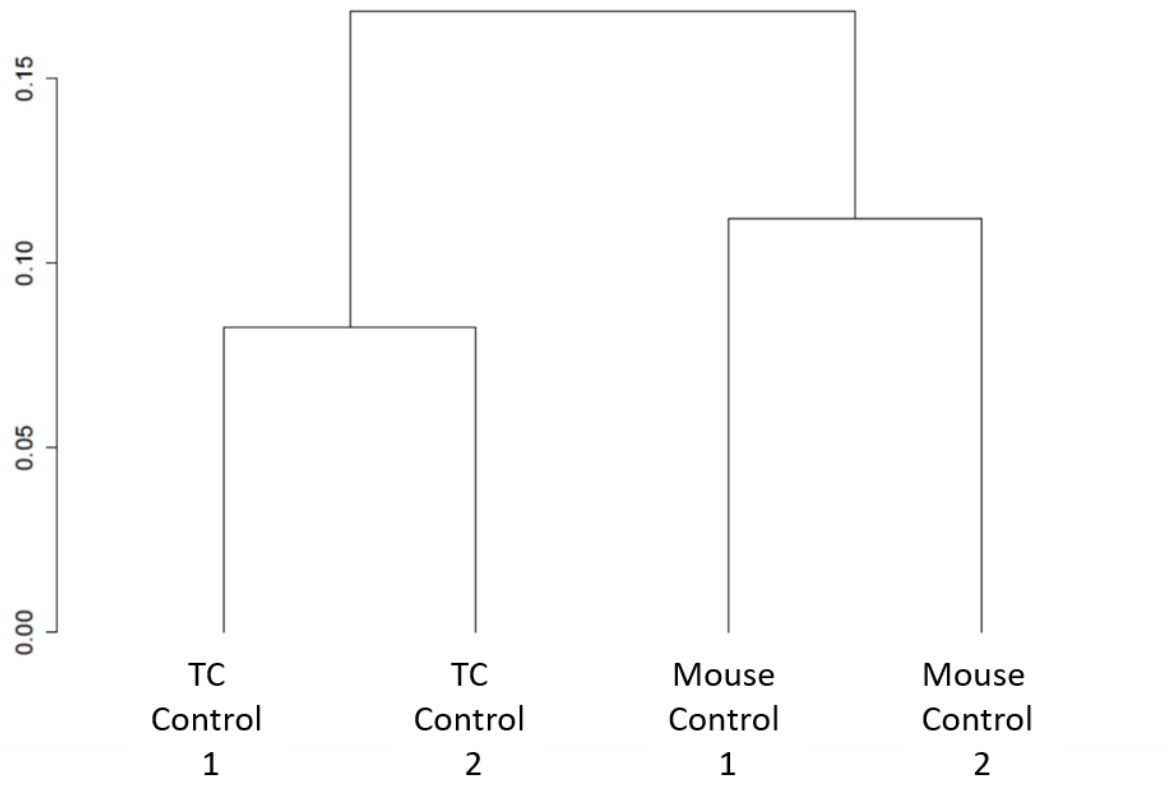


Figure 111: Dendrogram showing the 2 697 cell TC and 2 697 cell mouse control samples cluster separately from each other, but together with the treatment replicates indicating that even for control samples there is a lot of variance between mouse and TC samples. Ideally there would have been more biological repeats to make this data more robust.

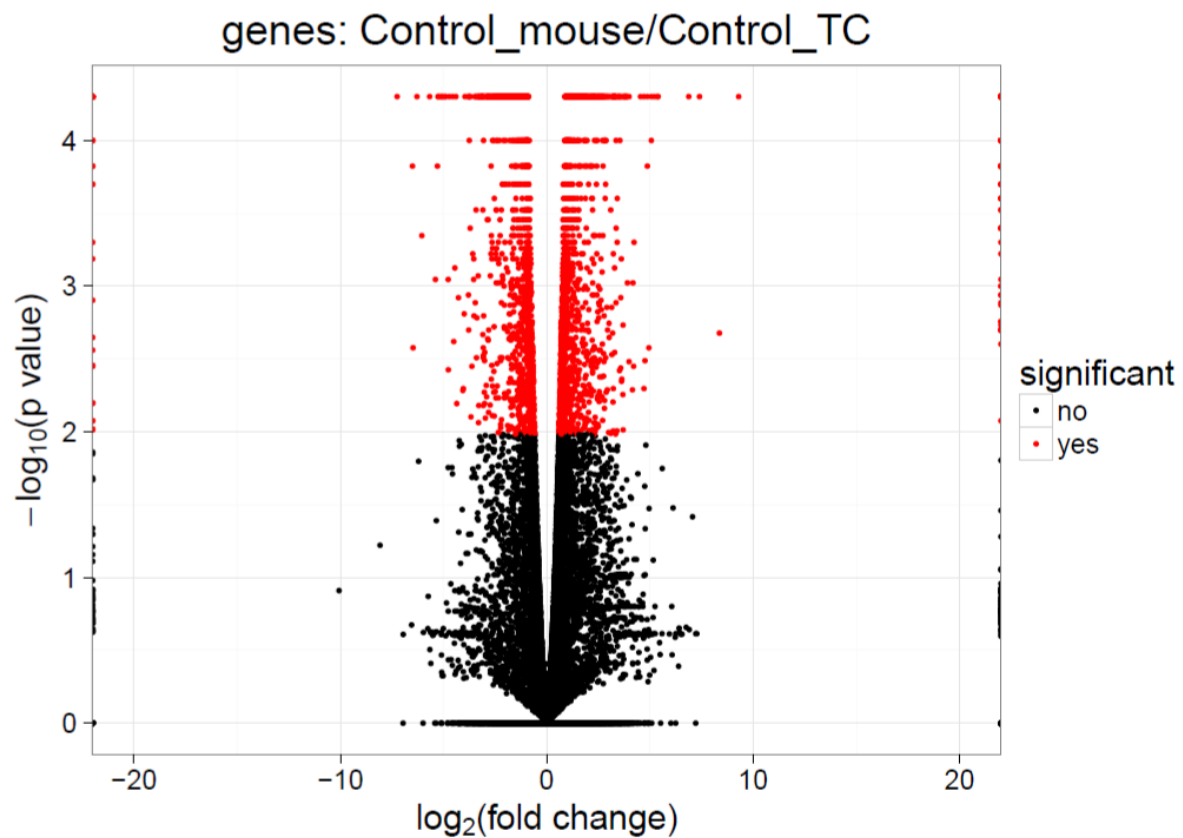


Figure 112: Volcano plot showing the spread of $\log_2(\text{fold change})$ of FPKM values for genes between control mouse samples compared to control TC samples. Data points in red indicate which genes are significant ($p < 0.01$). Points to the left of centre are down regulated and points to the right of centre are upregulated. Points at the edge of plot are those for which the fold change is inferred due to one of the conditions having an FPKM value of 0. Significance was calculated and the plot generated using the R package CummRBund, which is designed for the analysis and visualisation of CuffDiff RNA sequencing data.

7.4.1.1 Up regulated genes

FOS, FOSB (FosB proto oncogene) and JUN, were all highly upregulated in the mouse compared to TC. These genes are all components of the transcription factor AP-1, which is associated with proliferation. These genes have been demonstrated as oncogenes due to their ability to cause oncogenic transformation when overexpressed (Kappelmann, Bosserhoff, and Kuphal 2014; Castellazzi et al. 1993; Miller, Curran, and Verma 1984), which makes the upregulation in mice an interesting finding. These are not the only interconnected

genes in the upregulated gene list, as 7/10 of the top 10 hits are connected using the online functional protein association network, STRING (Figure 113). Gene ontology indicates an upregulation in the response to cAMP and Ca²⁺ as significantly enriched in the gene set (FDR<0.005), and the upregulation of the three most differentially regulated genes was seen in both replicates (Figure 114).

Despite the gene ontology for these upregulated genes indicating cAMP and Ca2 response, both FOS and JUN are both part of the AP-1 transcription factor and are associated with MAPK signalling which was not indicated in the gene ontology (Kappelmann, Bosserhoff, and Kuphal 2014; Jones et al. 2015; Bakiri et al. 2000).

Analysis of separate isoforms rather than genes shows that there is a mixed picture, with only some isoforms being upregulated (Figure 115). It is important to look at RNA sequencing both on a gene level and at isoforms due to different isoforms of a gene often having alternate functions and effects within different cells. The difference in isoform expression may represent isoforms with different functions, or isoforms that are not expressed at high levels in lymphocytes.

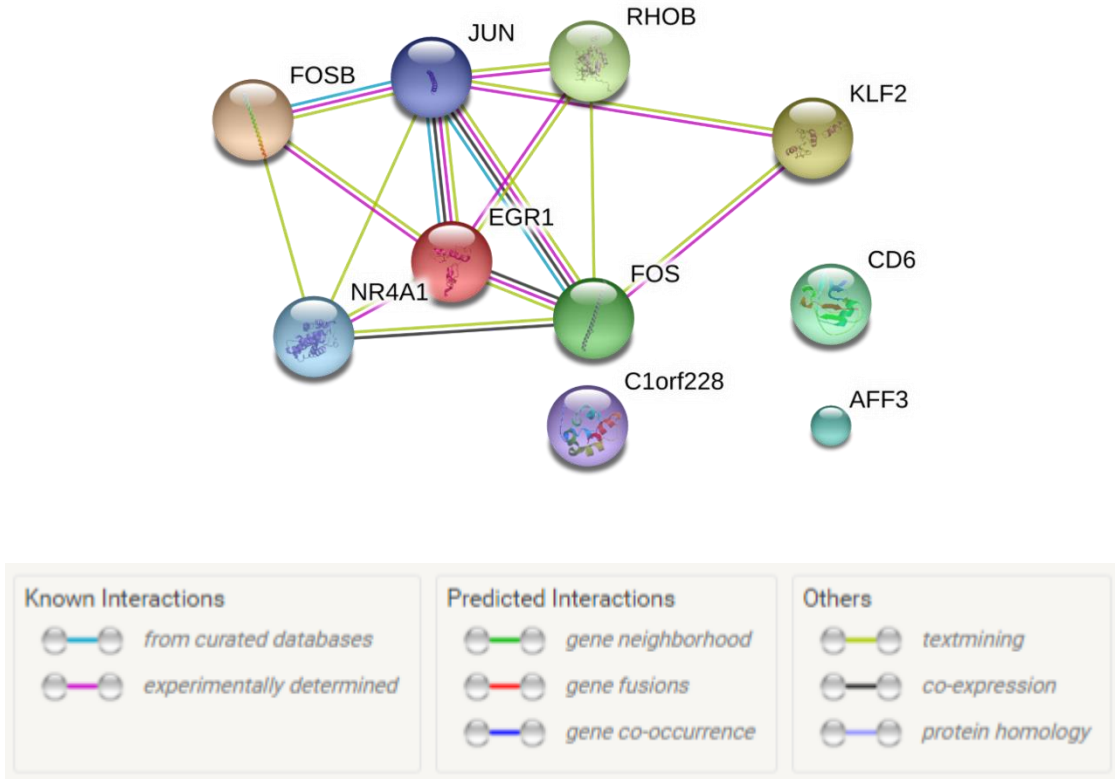


Figure 113: Interactions between the top 10 protein coding genes upregulated in mouse control samples compared to TC control samples. Interactions were determined using the online protein interaction database, STRING (version 10.0), and the types of interaction are shown in the legend below.

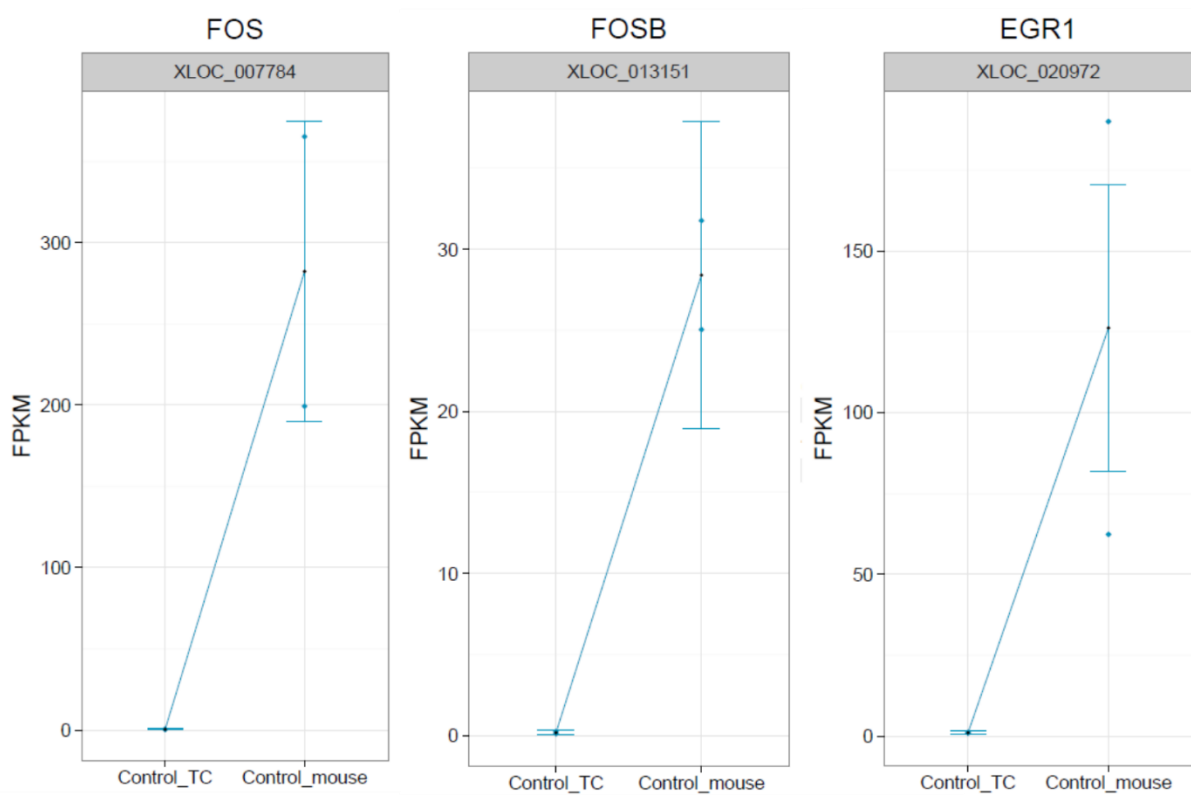


Figure 114: Differences in FPKM between control TC samples and control mouse samples for the 3 most differentially regulated genes in the control mouse samples. The 3 most differentially regulated genes, measured by fold change ($p<0.01$), FOS, FOSB and EGR1. Both replicates are shown in plots.

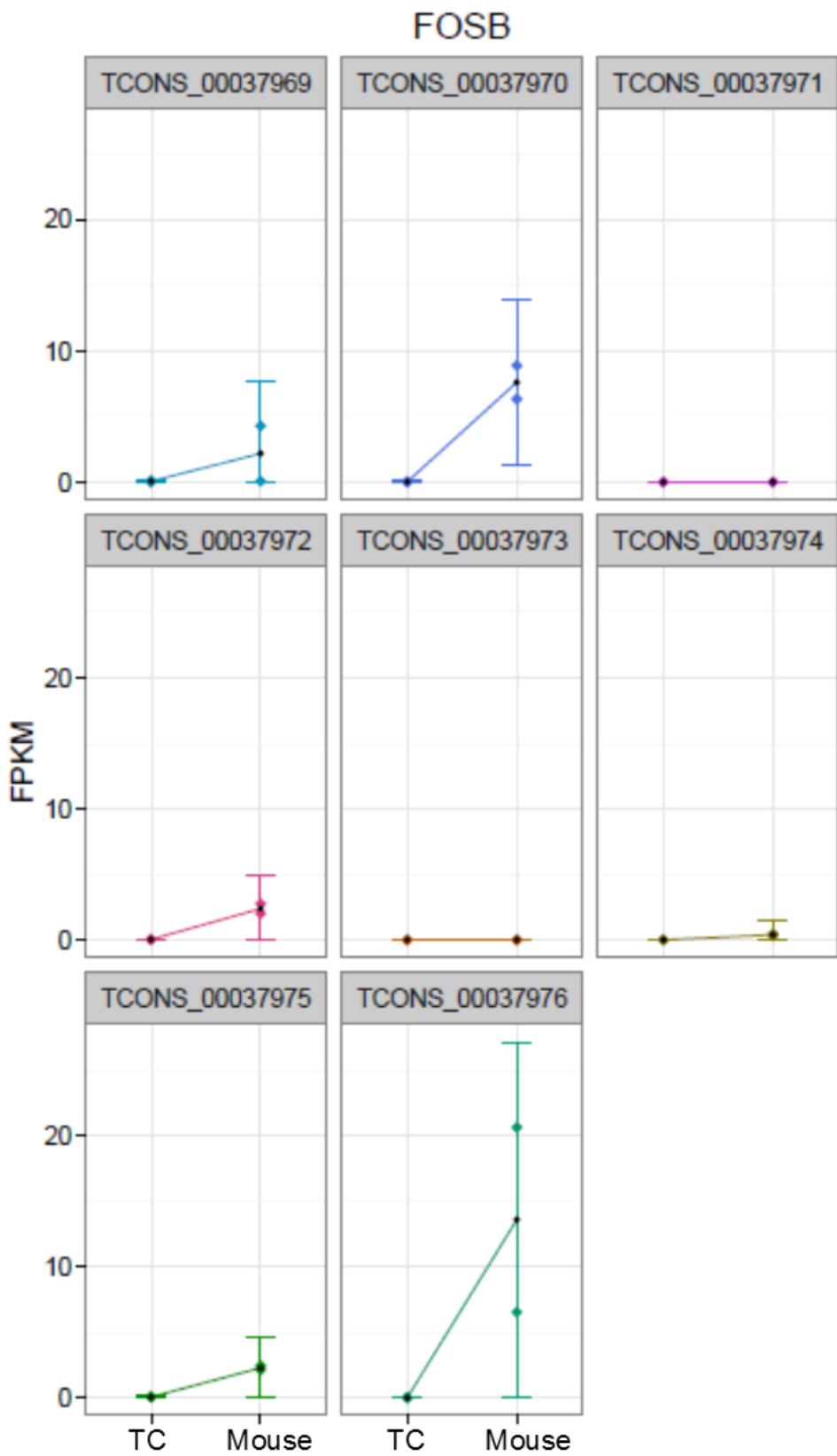


Figure 115: Differences in FPKM in the 697 cells between TC control samples and Mouse control samples for FOSB in the RNA sequencing data, both replicates are shown in plots. Changes for 8 isoforms are shown.

7.4.1.2 Downregulated genes

Amongst the genes downregulated in mice are several interesting candidates. ASS1 (Argininosuccinate synthase 1) and ASNS (Asparagine Synthetase (Glutamine-Hydrolyzing)) have both been identified in drug resistance to L-Asparaginase in T cell ALL (Estes et al. 2007) and have a log₂ fold decrease in mouse compared to TC of -4.5 and -2.9 respectively. Although the reduction in expression is the opposite to the literature, the differential expression of these genes may suggest a change in the drug sensitivity profile of the cells overall. Several other highly reduced genes are implicated in metabolism, such as SCD (Stearoyl-CoA Desaturase(Delta-9-Desaturase)) (log₂ fold(-7.2)) and LDLR (Low density lipoprotein receptor) (log₂ fold(-5)), which might indicate that there is an altered metabolic profile of the cells in the mouse compared to in tissue culture, which considering the different microenvironment and proliferation conditions is highly feasible. Protein association reveals a highly complex picture with many of the down-regulated genes interconnected. Ontology analysis of the genes with decreased expression in mice reveals down regulation of small molecules biosynthesis (Figure 116) (FDR=1.84e-11) and amino acid biosynthesis (FDR=1.31e-6), which support the theory of an altered metabolic processes.

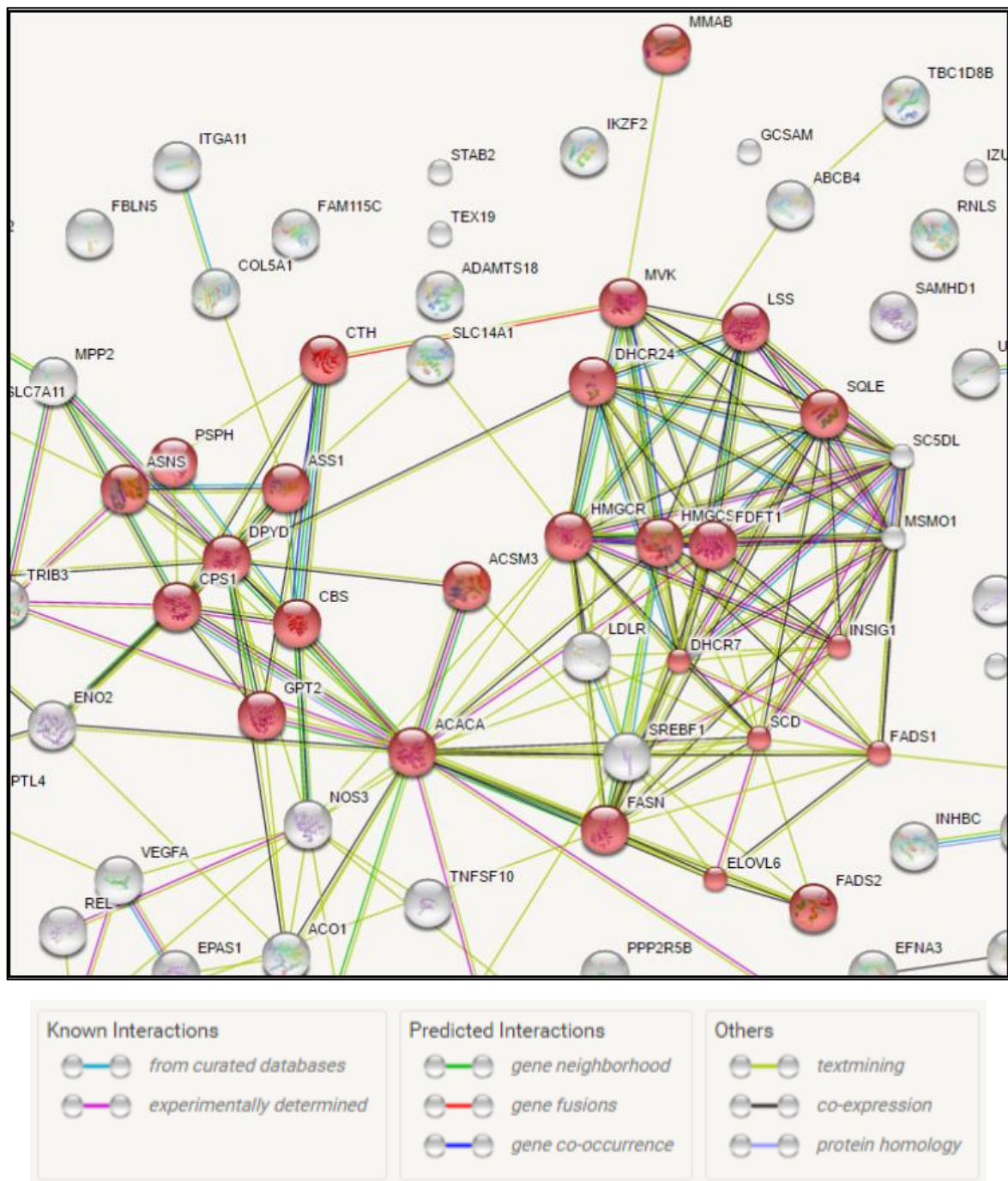


Figure 116: Snapshot from genes down regulated $>2 \log_2(\text{fold change})$ in control mouse vs control TC, genes in red are those involved in the biosynthesis of small molecules. Interactions were determined using the online protein interaction database, STRING (version 10.0), and the types of interaction are shown in the legend below.

7.4.2 Dexamethasone *in vitro* vs dexamethasone *in vivo*

The comparison of Dex TC and Dex mouse should allow for the identification of genes that are differentially expressed in response to Dex between the two. Any genes found in this set of comparisons could be effectors of resistance *in vivo*. Dispersion and CV_2 was the same as for the control vs control permutation, indicative of good quality data. Mouse and TC samples cluster separately (Figure 117) and 2035 genes were scored as significantly differently expressed between mouse and tissue culture .

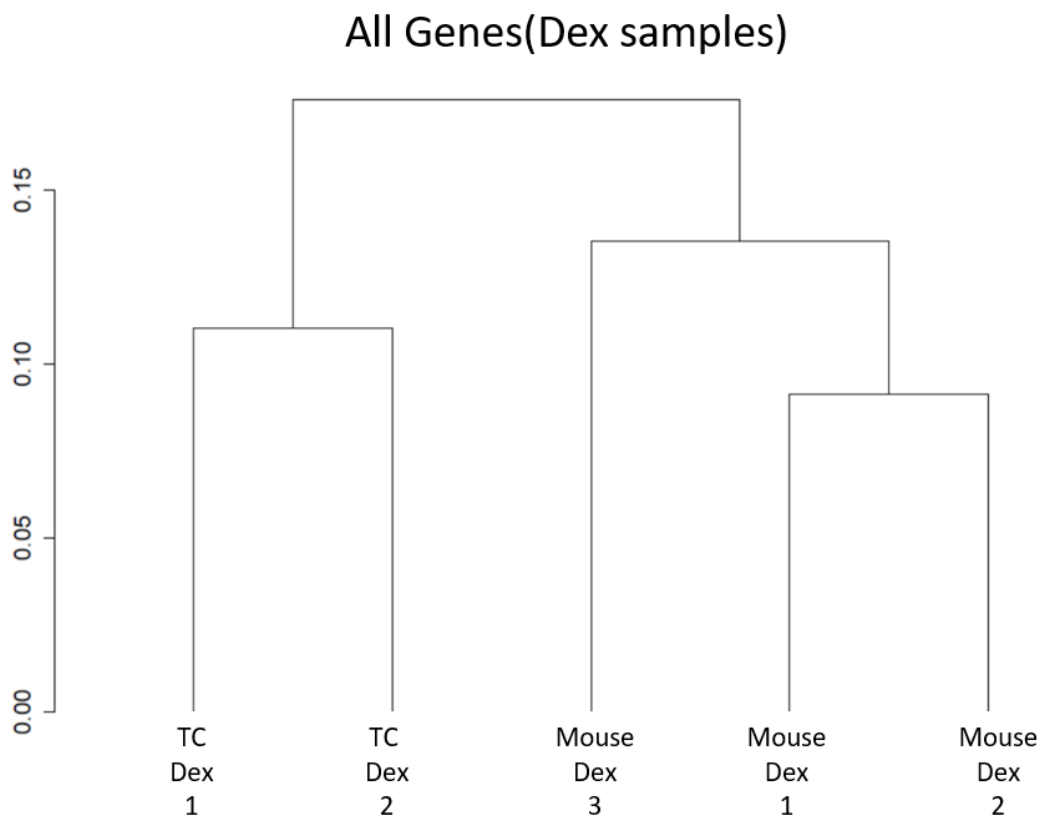


Figure 117: Dendrogram showing clustering of 697 cell TC and mouse samples with Dex treatment. TC samples cluster separately from mouse indicating a different expression profile in response to Dex between the two conditions.

7.4.2.1 Upregulated genes

The genes that are upregulated in the Dex mouse samples compared to Dex TC represent the genes required for engraftment in the mouse that are unaffected by Dex treatment, as well as genes responsible for the different actions of Dex *in vivo*, and possibly the resistance to Dex. Of the 2035 genes that were significantly different between Dex treated cells in TC and mouse, 74 have a greater than 2(log2) fold increase in FPKM in the mouse. The highest ranked of the upregulated genes in the mouse Dex group is the same as for the mouse control group, FOS (Figure 118). Four of the top eight upregulated genes for both control and Dex TC vs mouse are shared between both groups indicating a role for these genes in growth of ALL cells in the murine environment. Many of the genes are also interconnected when looking at protein interactions, including FOS, FOSB and JUN, further highlighting the likelihood that these genes are important in the growth of the 697pSLIEW cells *in vivo* (Figure 119).

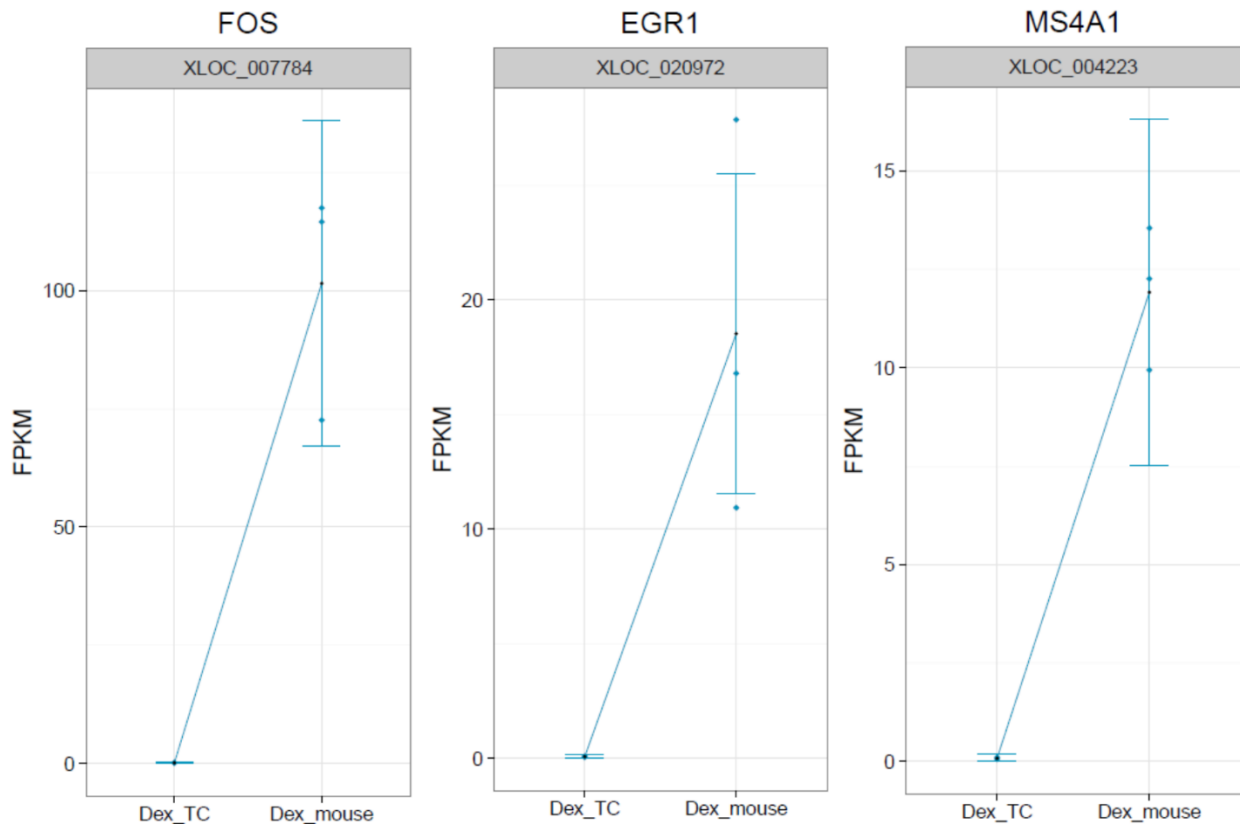


Figure 118: The top 3 upregulated genes in the 697 cells for TC Dex vs mouse Dex samples; FOS, EGR1 and MS4A1. Genes are ranked by log fold change and all replicates are shown on plots as separate data points. As can be seen the increase in FOS expression is around 10 fold higher than that of either EG1 or MS4A1.

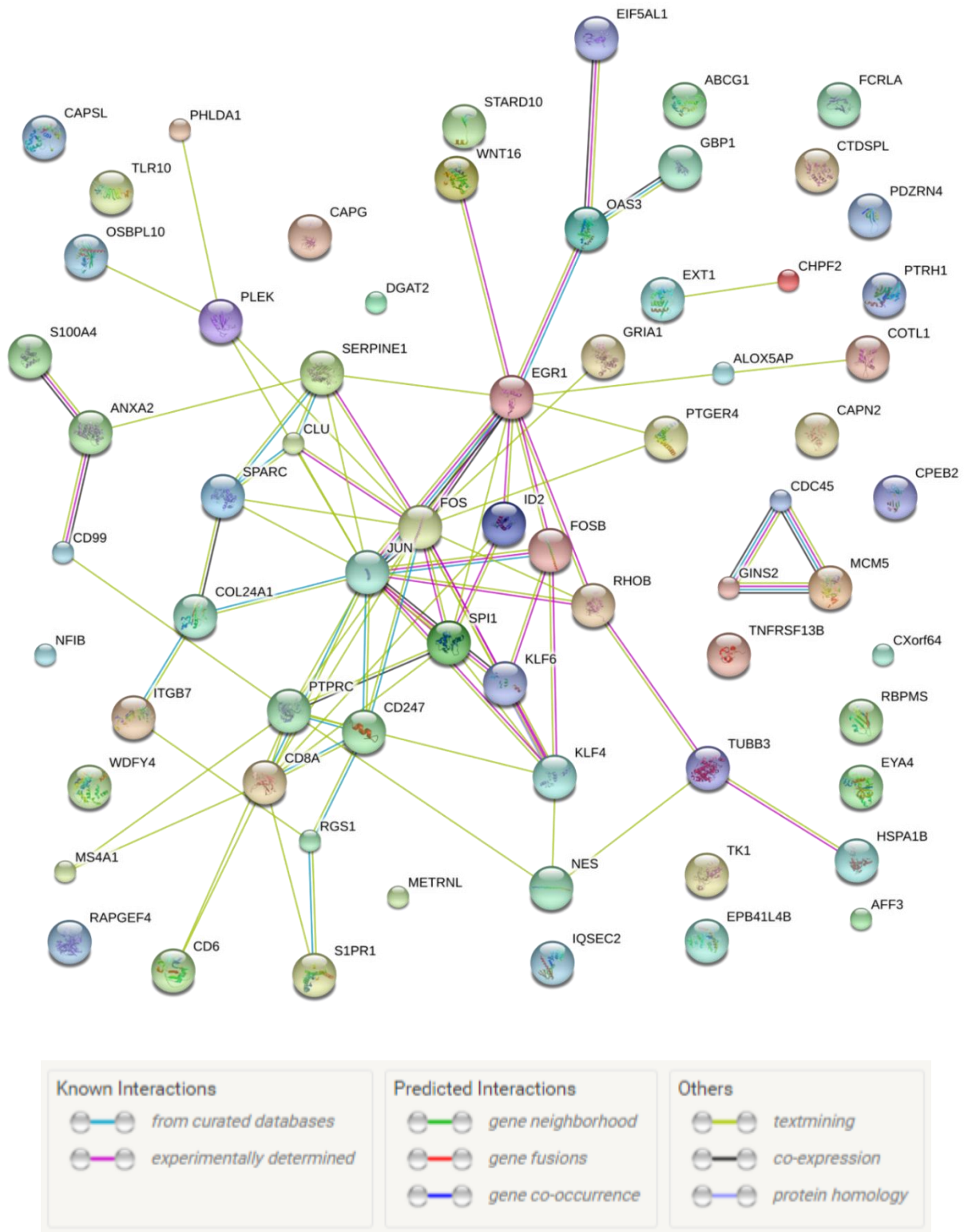


Figure 119: The protein interactions of all 74 genes with more than 2 log₂ (fold upregulation) in the 697 cells in the mouse vs tissue culture for Dex treated samples. Interactions were determined using the online protein interaction database, STRING (version 10.0), and the types of interaction are shown in the legend below.

7.4.2.2 Down regulated genes

Genes that show reduced expression in the Dex mouse samples compared to the Dex TC samples represent genes that are not induced in response to Dex in the mouse, thus any genes that are not induced by Dex in the mouse but are in TC may be Dex inducible genes important for the induction of apoptosis. There are 39 genes that have reduced expression in both control mouse and Dex mouse, and within this list of genes biosynthesis of amino acids and steroids is enriched in the list ($FDR < 0.05$). This would imply that the metabolism of the 697 cells is altered *in vivo*.

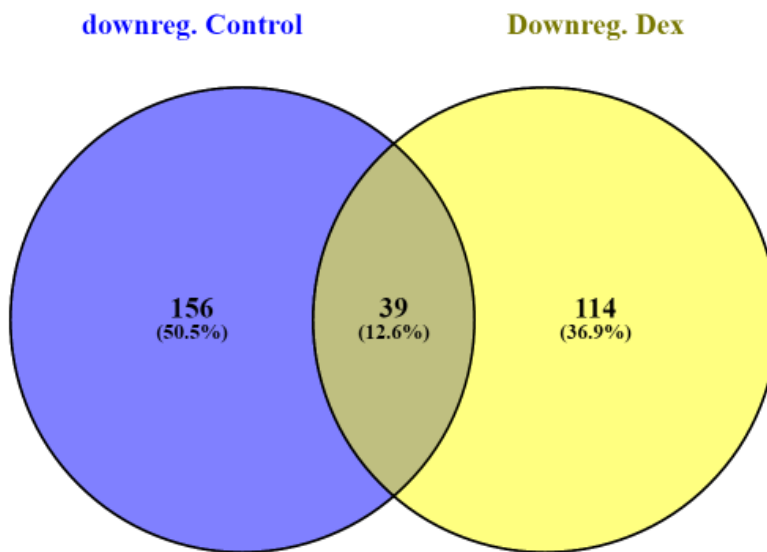


Figure 120: The overlap between the downregulated genes (with gene IDs only) in the 697 cells when control samples were compared to Dex treated samples for both the *in vitro* and *in vivo* conditions.

Perhaps the more interesting genes to investigate are those that have differential expression only in TC or mouse samples, as these might indicate a differential Dex response in the mouse compared TC. There are 114 genes downregulated in Dex TC vs Dex mouse treatment groups that are not downregulated in the control TC vs control mouse (Figure 120). Included in this list is RASD1 (Ras related Dex induced 1), a member of the RAS family of genes that is Dex induced. Further investigation shows this gene, which is downregulated in Dex TC vs Dex mouse, is actually upregulated in TC samples when Dex treatment is given. The mouse samples do have a higher basal level of expression than the TC samples, but this is less than

the levels seen with Dex induction of expression (Figure 121). This lack of RASD1 upregulation in response to Dex could be the cause for Dex resistance in the mouse.

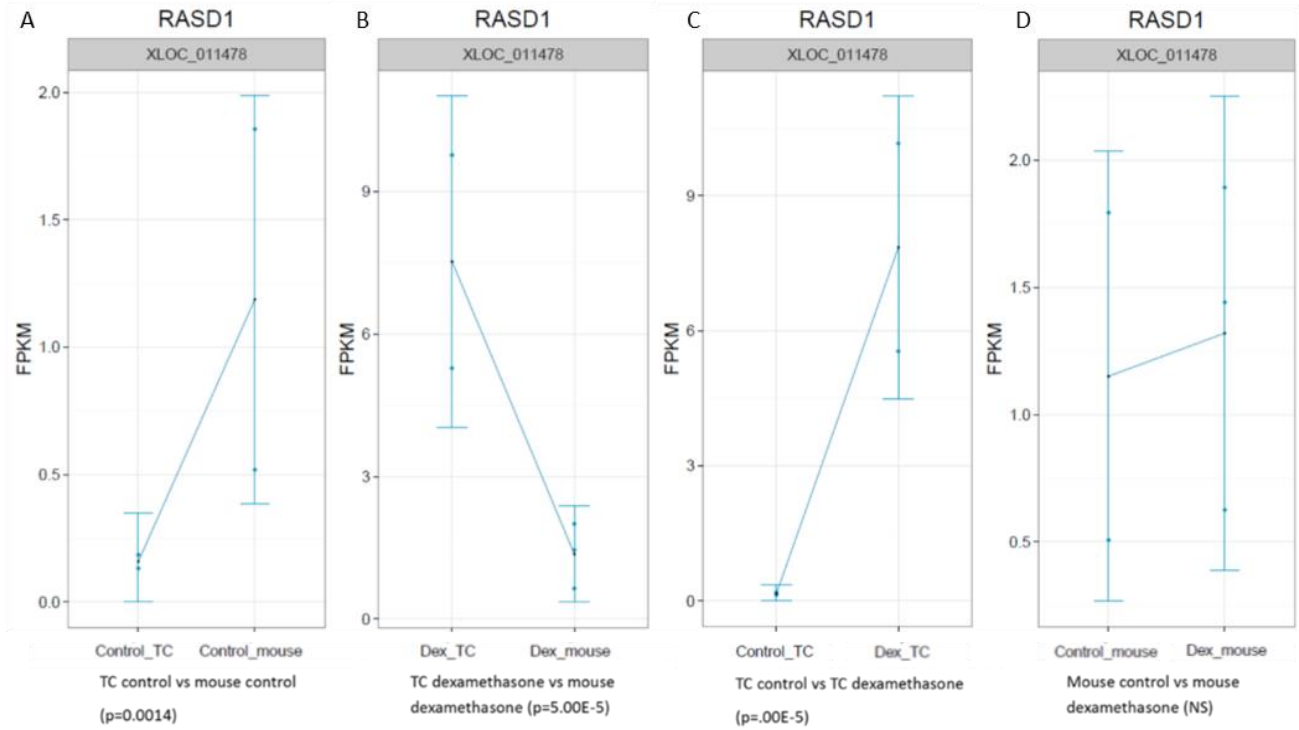


Figure 121: Changes in RASD1 FPKM in four of the analyses. Increased expression in response to Dex treatment is seen in the control samples (A), as well as an increased basal level in mouse control samples compared to TC control samples (C). There is no significant increase in RASD1 expression in mouse samples when they are treated with Dex (D) and the levels of RASD1 expression are much higher in the TC Dex treated samples (B)

7.4.3 Control vs Dexamethasone

7.4.3.1 Control vs dexamethasone *in vitro*

The comparison of the gene expression differences between the control TC samples and the Dex TC samples will show the expression changes that occur normally in Dex sensitive cells *in vitro* in response to Dex treatment. Analysis of control TC samples vs Dex TC samples shows the two treatment groups cluster separately (Figure 122). 1407 genes are significantly ($p<0.05$) up or down regulated between the two groups (Figure 123).

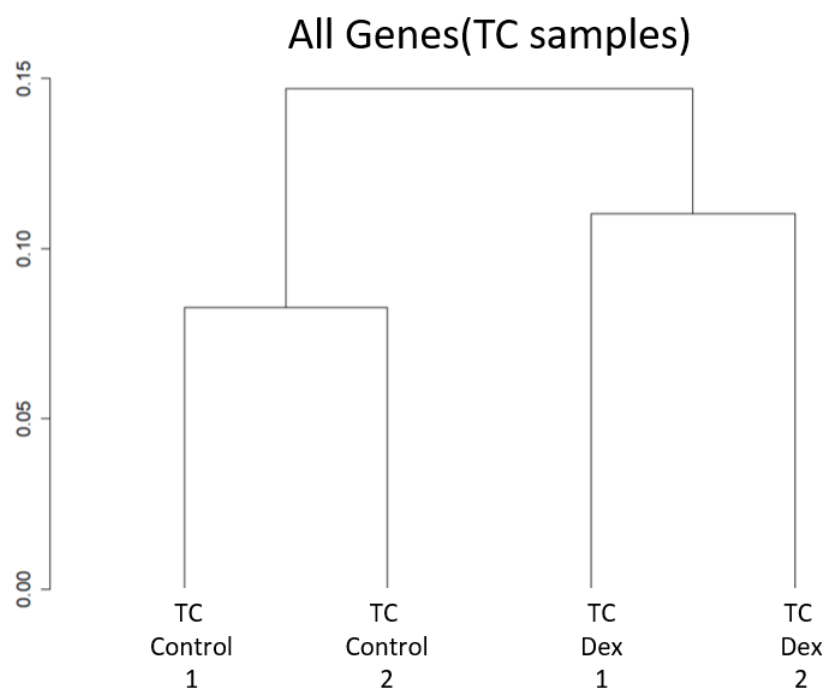


Figure 122: Dendrogram produced using the normalised read counts from the 697 RNA sequencing data with the CummeRbund programme in R. The dendrogram shows the treatment groups cluster separately from each other when the 697 TC samples are analysed.

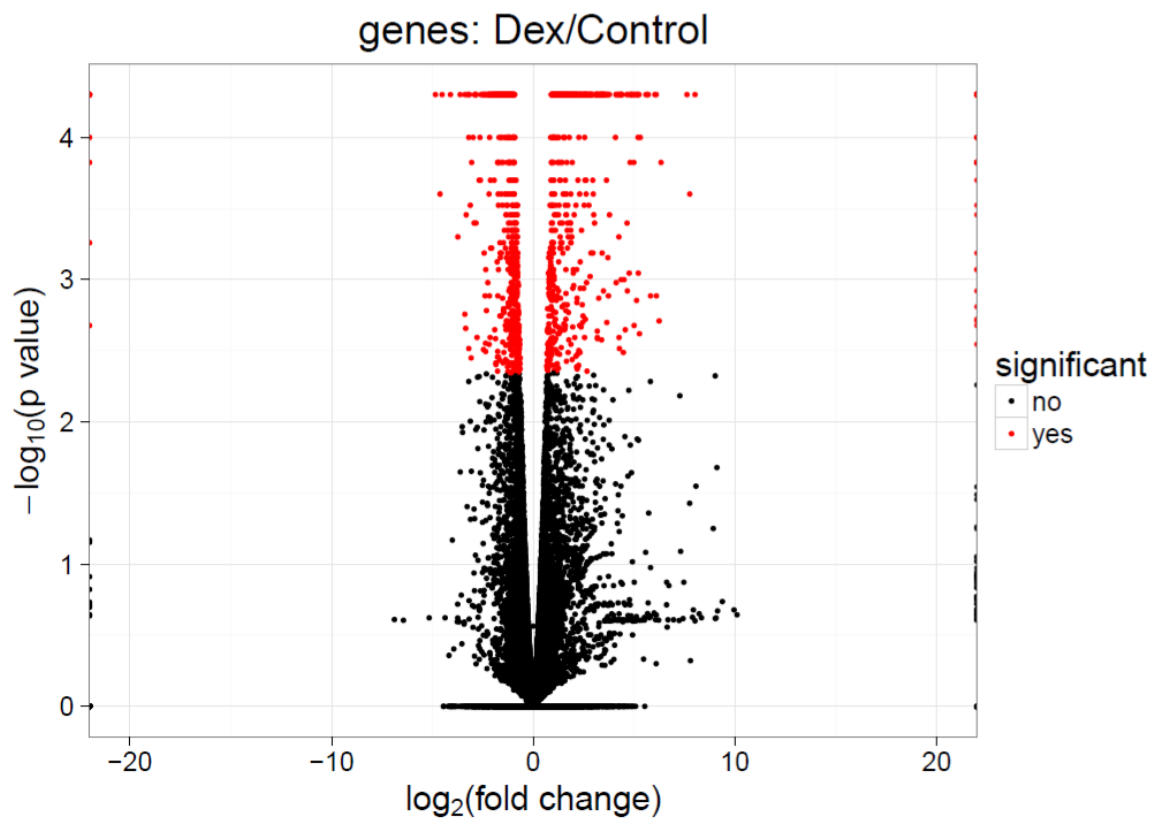


Figure 123: Log2 fold change in FPKM in the 697 cells between control and Dex treated samples in vitro. Red points indicate significant genes ($p<0.01$), data points to the left of centre indicate down regulated genes and points to the right indicate upregulated genes. Data points on the edge of the plot are those for which the $\log_2(\text{fold change})$ is inferred due to one of the conditions having an FPKM value of 0. Significance was calculated and the plot generated using the R package CummRBund, which is designed for the analysis and visualisation of CuffDiff RNA sequencing data.

7.4.3.2 Up regulated genes

The genes that show upregulation of expression in Dex TC compared to control TC will include the genes which are induced by Dex under normal conditions in the 697 cells. These genes will show the picture of which genes should be differentially expressed between control and Dex treatment. Of the 1407 genes significantly up or down regulated, 36 have more than 2 fold decrease in expression and 197 have more than 2 fold increased expression with Dex treatment. Of the genes upregulated in the Dex treated group there are several genes that are direct targets of NR3C1, such as UBA7 (Ubiquitin Like Modifier Activating

Enzyme 7) and FKBP5, which have several GRE within the area of the genes (Figure 124). Another gene, PLS3 (Plastin 3) (Figure 125) has a log₂ fold increase in FPKM of 3.3 in the Dex treatment group compared to control, this gene has been implicated in osteoporosis (van Dijk et al. 2013; Fahiminiya et al. 2014) and binds calcium. Given that osteonecrosis is a known side effect of treatment with synthetic glucocorticoids, upregulation of this gene is potentially interesting.

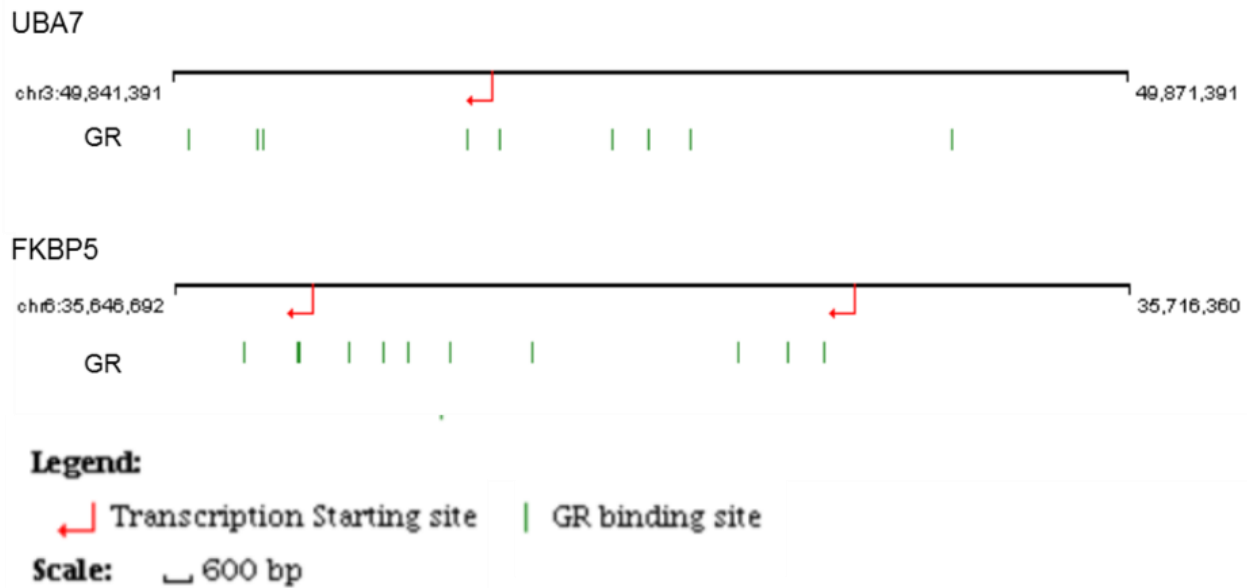


Figure 124: GRE consensus sequences indicated by the green lines in the genomic sequence of UBA7 (top) and FKBP5 (bottom). Data was obtained from the Qiagen website online function to search for Transcription factor binding sites.

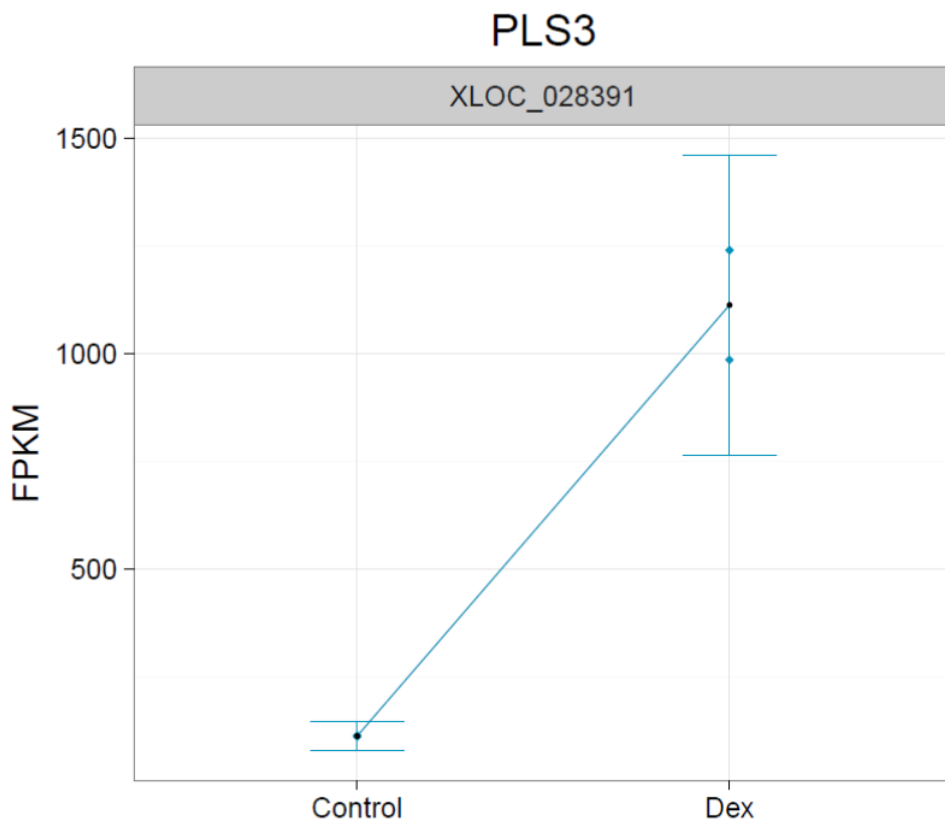


Figure 125: Increase in the FPKM of PLS3 seen in the 697 Dex TC samples compared to control TC samples. All replicates are shown in the plot.

7.4.3.3 Downregulated genes

The genes down regulated in the Dex TC samples will again represent the normal transcriptional changes occurring in the 697 cells upon Dex treatment. The most downregulated gene in Dex treatment compared to control in the tissue culture samples is INHBE (Inhibin Beta E), an activin, some of which have been shown to have reduced expression upon Dex treatment in adipose cells (Sethi 2010). Only one of the INHBE isoforms has a large reduction, but this is significant enough to make the gene the top hit. The third most down regulated gene, ITGB7 (Integrin subunit Beta 7), an integrin, which are proteins involved in extracellular signalling, has a reduction in more isoforms (3/5) than seen with INHBE (Figure 126), but still not all of the isoforms.

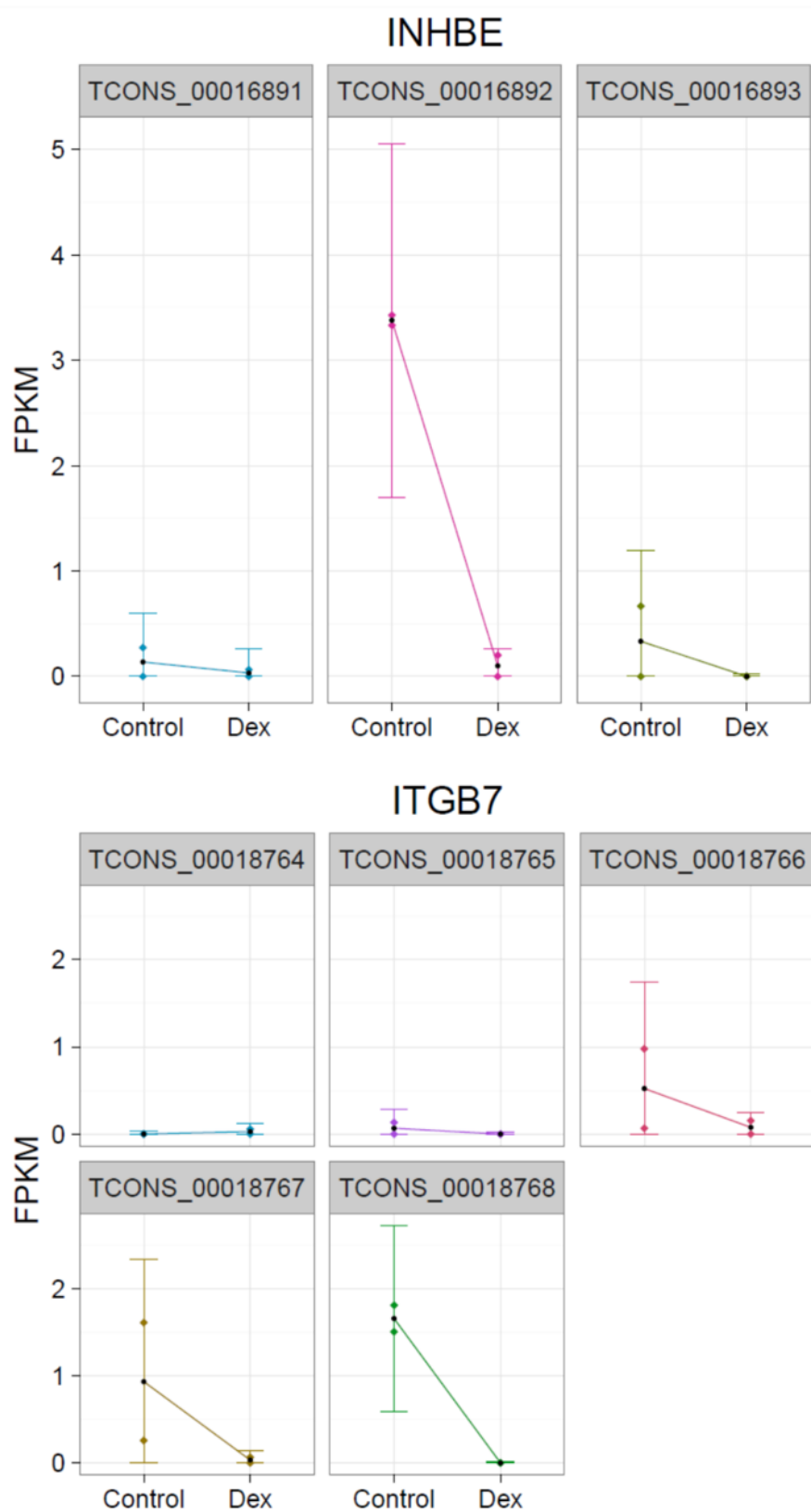


Figure 126: Plots showing the reduction in FPKM for 2 of the most significant genes down regulated in the 697 Dex TC samples compared to the 697 control TC samples. Plots show separate repeats to indicate the range seen between samples in the same condition.

The treatment of 697 cells *in vitro* with Dex results in the upregulation of several Dex inducible genes, such as FKBP5. This shows that there is not an issue with substrate binding to the receptor, or the subsequent homodimerisation, nuclear translocation and transcriptional regulation by NR3C1. Although not directly linked to Dex, INHBE is related to genes that are, and could well be another gene inhibited by Dex treatment.

7.4.4 Control vs dexamethasone *in vivo*

The comparison of control mouse samples and Dex treated mouse samples will allow for the changes induced by Dex treatment in an *in vivo* setting to be determined. Any overlapping genes with the *in vitro* expression changes would allow for the determination of whether the cells are still being affected by Dex *in vivo*. The differentially expressed genes would give clues to why this resistance is occurring and possible mechanisms.

As with all the other data, the dispersion and grouping of the control samples vs the Dex samples shows the same picture. The samples cluster dependent on treatment (Figure 127-129), and there are 2881 genes significantly ($p<0.05$) up or down regulated in the Dex treatment group (Figure 129).

All Genes(Mouse samples)

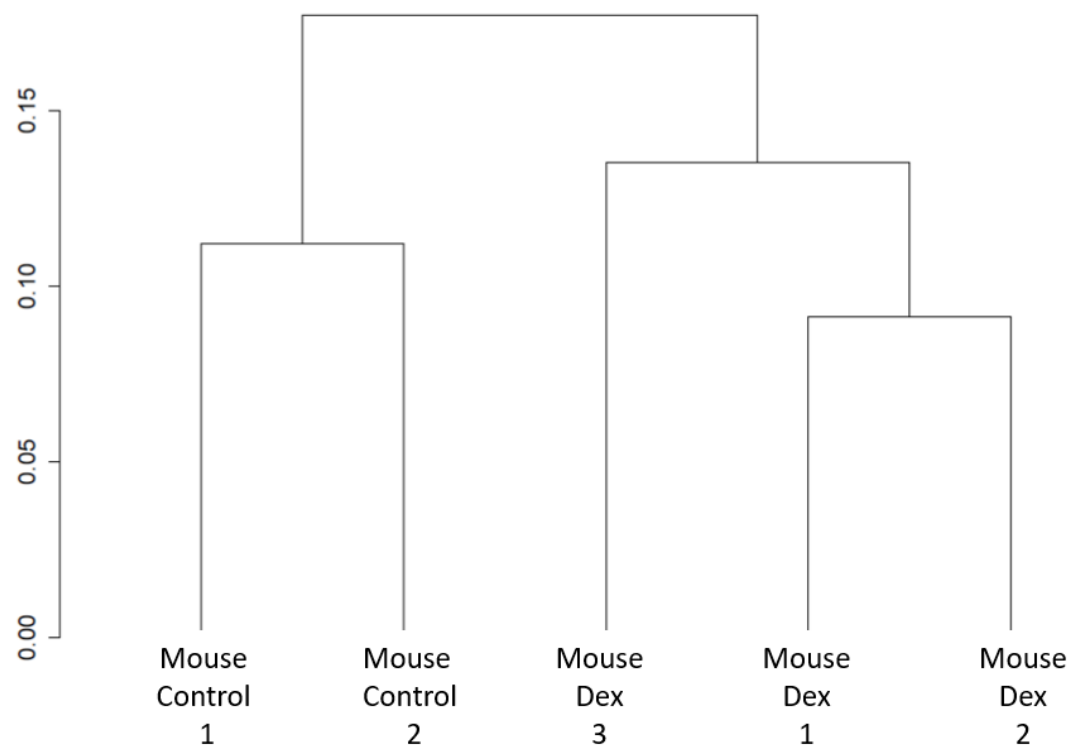


Figure 127: Dendrogram showing the clustering of mouse control and mouse Dex treated 697 samples. Dex treated 697 samples cluster together whilst the control treated 697 samples cluster separately.

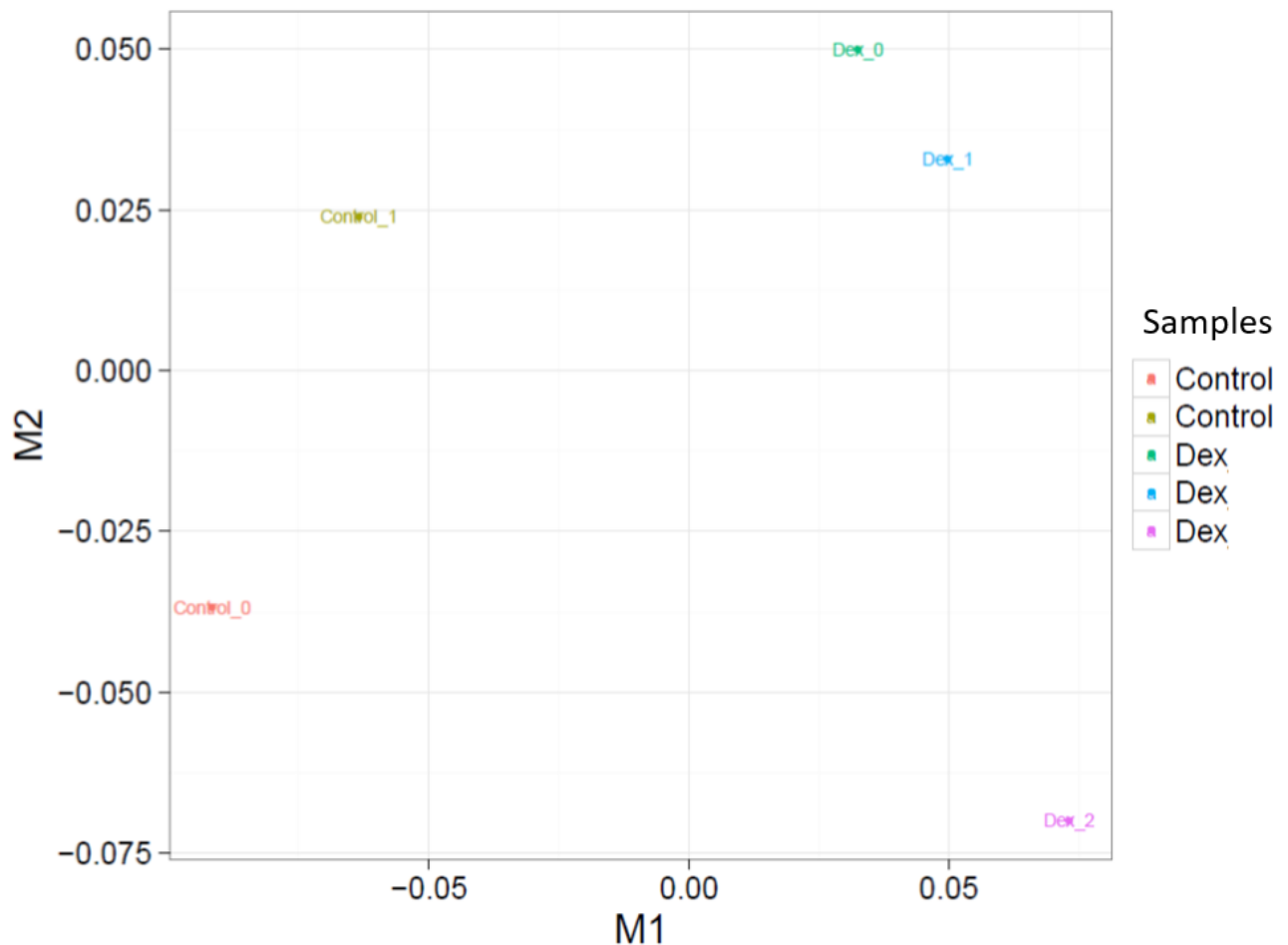


Figure 128: PCA plot for the in vivo samples, the control samples are separated from the Dex samples based on principle component M1, and from each other on M2. Two of the Dex samples cluster tightly whilst the other has more differences based on component M2. The Dex treated outlier is one of the female Dex treated mice, indicating the difference in expression was not due to sex differences.

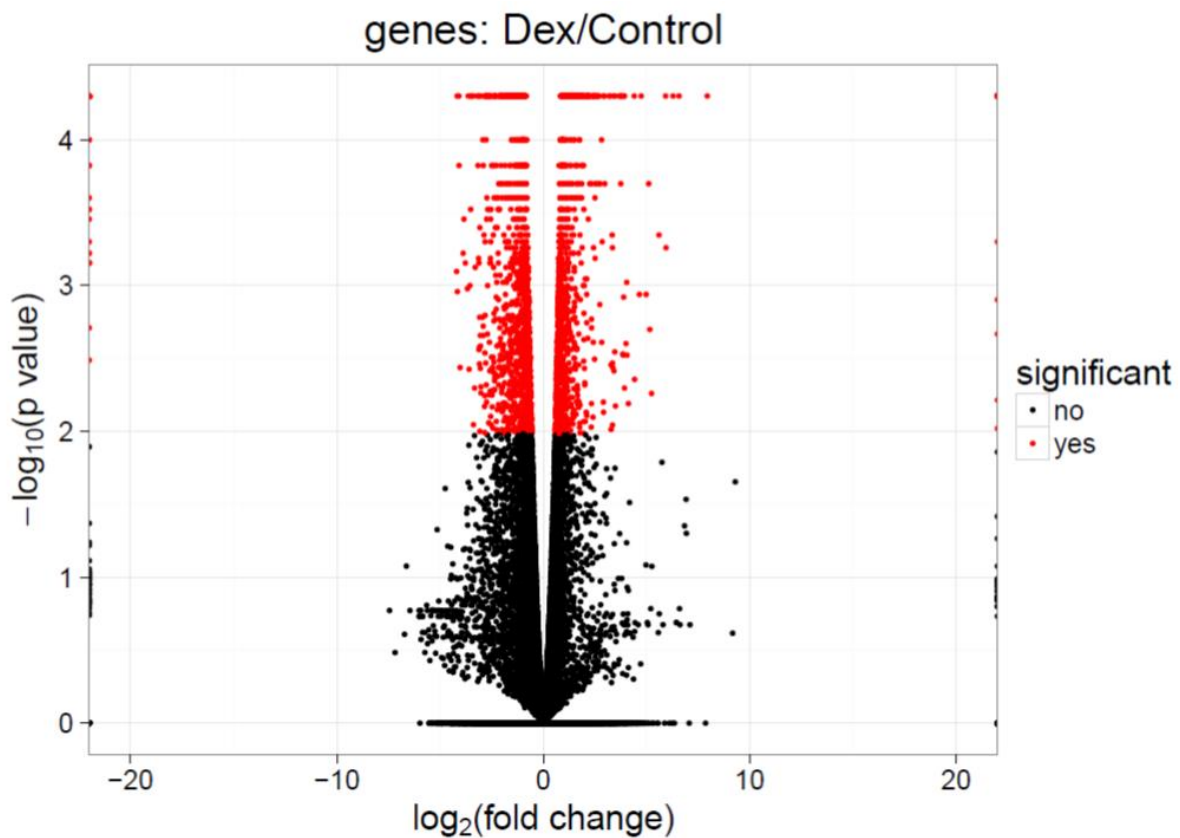


Figure 129: Log2 fold change in FPKM in the 697 cells between control and Dex treated samples in vivo. Red points indicate significant genes ($p<0.01$), data points to the left of centre indicate down regulated genes and points to the right indicate upregulated genes. Data points on the edge of the plot are those for which the $\log_2(\text{fold change})$ is inferred due to one of the conditions having an FPKM value of 0. Significance was calculated and the plot generated using the R package CummRBund, which is designed for the analysis and visualisation of CuffDiff RNA sequencing data.

7.4.4.1 Upregulated genes

The upregulation of genes in the Dex mouse group compared to control mouse give an idea of how Dex is affecting the cells. Of the significantly altered genes in the control mouse vs Dex mouse, 108 are more than 2 log₂ fold increased following Dex treatment. 22 of the genes with > 2 log₂ fold increase with Dex treatment are common between the two analyses

(Figure 130). These genes include the known NR3C1 targets FKBP5 and IL6ST (Interleukin 6 signal transducer).

The induction of these genes indicates that despite the Dex being cleared from the peripheral blood completely within 24hrs *in vivo* the downstream effects of NR3C1 induced transcriptional modulation is still present. This indicates that NR3C1 does indeed bind to Dex before homodimerizing and translocating to the nucleus where it interacts with GRE to induce gene modulation. The exact timescale of this is unknown in the 697 cells but NR3C1 is known to bind to GRE only transiently, this interaction is known as the ‘hit and run’ hypothesis. First described in 2000 by McNally et al the mechanism was based on the finding that the receptor moves from the chromatin to the nucleoplasm very rapidly (McNally et al. 2000). This finding that there was a dynamic exchange of transcription factors at chromatin binding sites changed the way that receptor binding was viewed. This mechanism was further supplemented by the finding that this rapid interaction the response element results in the ability of many transcription factors being able to bind in quick succession to induce transcriptional alteration, which results in a lack of competition between transcription factors binding to response elements in promoter regions (McNally et al. 2000; Ratman et al. 2013). The PK data shows that Dex is cleared from the peripheral blood completely by 24hrs of dosing, this combined with the induction of NR3C1 transcriptional modulation supports the hit and run hypothesis in this instance.

The mechanism of resistance therefore must be downstream of this process. Genes that are specific only to control mouse vs Dex mouse represent the genes that are affecting the differential response to Dex in the mouse compared to TC. Included in these genes is SCD, this gene is downregulated by Dex treatment (Daniel et al. 2004), and although this evidence is from adipose tissue rather than B cells, the reversal of this relationship, with an increase in SCD shows that the cells are not responding to Dex as expected *in vivo*.

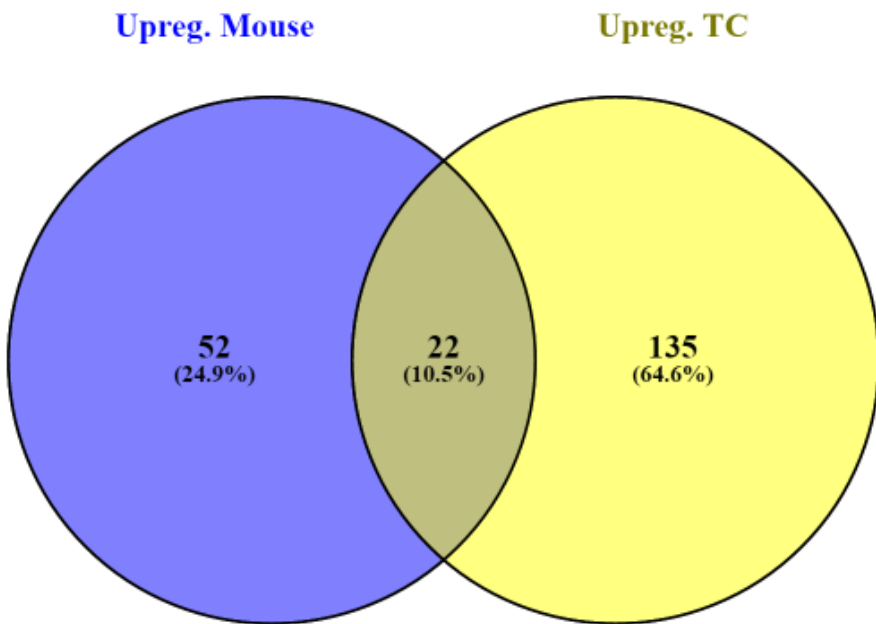


*Figure 130: Venn diagram showing the crossover between genes upregulated in the 697 cells control vs Dex for both the *in vivo* and *in vitro* conditions. There is only 10.5% of overlap between the two treatment conditions.*

7.4.4.2 Downregulated genes

The downregulation of genes in Dex mouse compared to Dex TC can be used to elucidate the difference in transcriptional regulation *in vivo* compared to *in vitro*. Between control and Dex treatment *in vivo*, 182 genes were reduced more than 2 log₂ fold. The top three of these are shown in Figure 131. In this list of down regulated genes are several JUN-EGR pathway genes such as JUNB (JunB proto-oncogene), and JUND (JunD proto-oncogene) as well as EGR1,2 and 3 (Early growth response 1-3). This indicates suppression of AP-1 driven transcription in response to Dex, and this same pathway was also found upregulated in the mouse in control samples, and mouse Dex samples. This pathway appears to be important for both engraftment and Dex response *in vivo*.

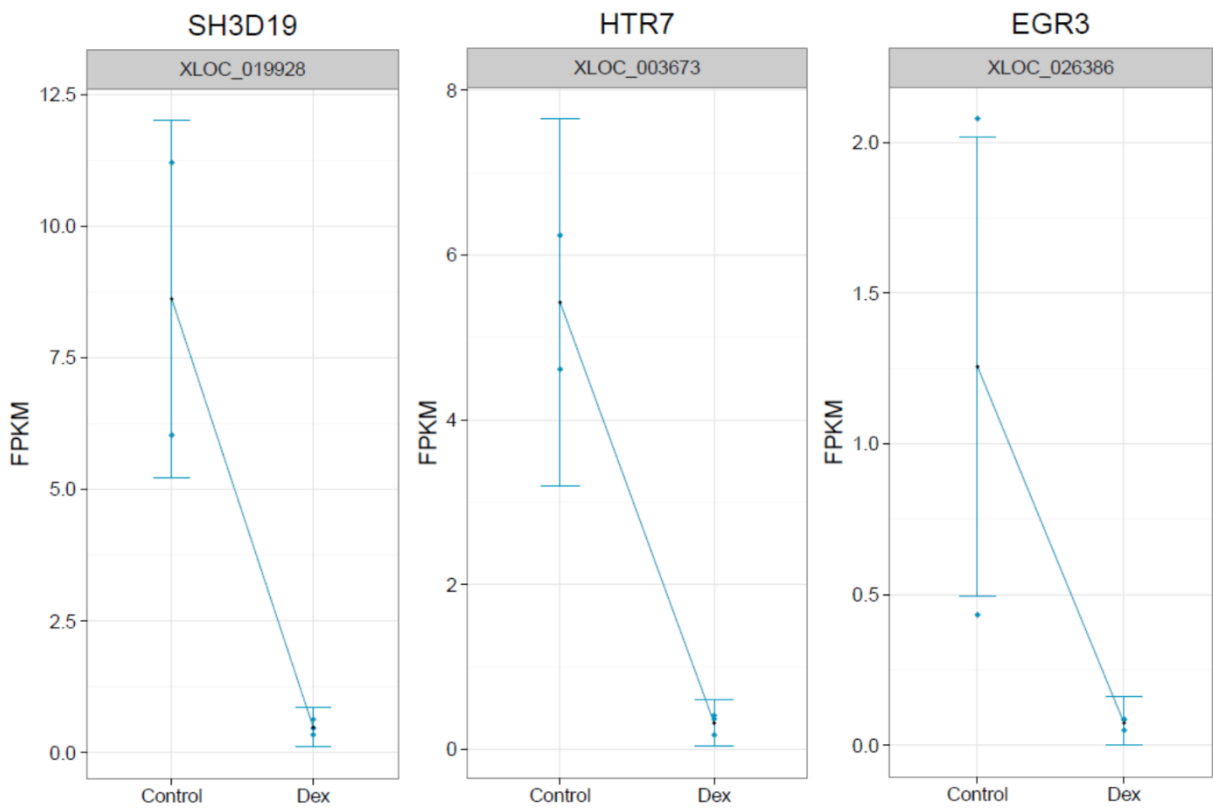


*Figure 131: Plots showing the reduction in FPKM for the top three down regulated genes in the 697 cells when the control samples are compared to the Dex treated samples *in vivo*. SH3D19 is the most down regulated, followed by HTR7 and EGR3. For each plot both of the data points representing each mouse is shown.*

The genes that might be most significant for the Dex response will be those that are down regulated in the Dex treated mouse samples but not the Dex treated TC samples. One of these such genes is SLAMF6 (Slam family member 6). This gene is reduced in the Dex treated mouse samples, but actually has increased expression in the Dex treated TC samples indicating opposing control between *in vivo* and *in vitro*. Although little evidence links this gene and Dex, it is involved in regulation of the immune system, in particular natural killer cells (N. Wu et al. 2016).

7.4.4.3 *Control vs dexamethasone, combined samples*

The combination of all control samples and all Dex samples will show which genes are important in the Dex response that is still shared between *in vitro* and *in vivo*, this could be important to determine how far downstream the loss of Dex responsiveness occurs *in vivo*.

When the samples are grouped into control vs Dex for TC and mouse samples combined, the data has the same dispersion and CV_2 profile as the other data sets. Despite this there are no significantly up or downregulated genes. Looking at the clustering of the samples shows why this might be the case, as the TC samples cluster separately from the mouse (Figure 132).

However, looking on an isoform level there are some isoforms that are significantly altered. Thirty-five of these isoforms have greater than 2 fold increase in expression. Within these 35 genes is FKBP5, a known NR3C1 target gene that is upregulated in both the TC and mouse Dex treatment samples compared to control. One isoform of FKBP5 is highly upregulated in all Dex samples compared to controls but the others have little or no change (Figure 133). Another high ranking isoform is TP53INP1 (Tumour protein P53 inducible nuclear protein 1), a pro-apoptotic gene that is involved in the stress response of the cell (Figure 134). TP53INP1 is also upregulated in Dex vs control for TC and mouse alone.

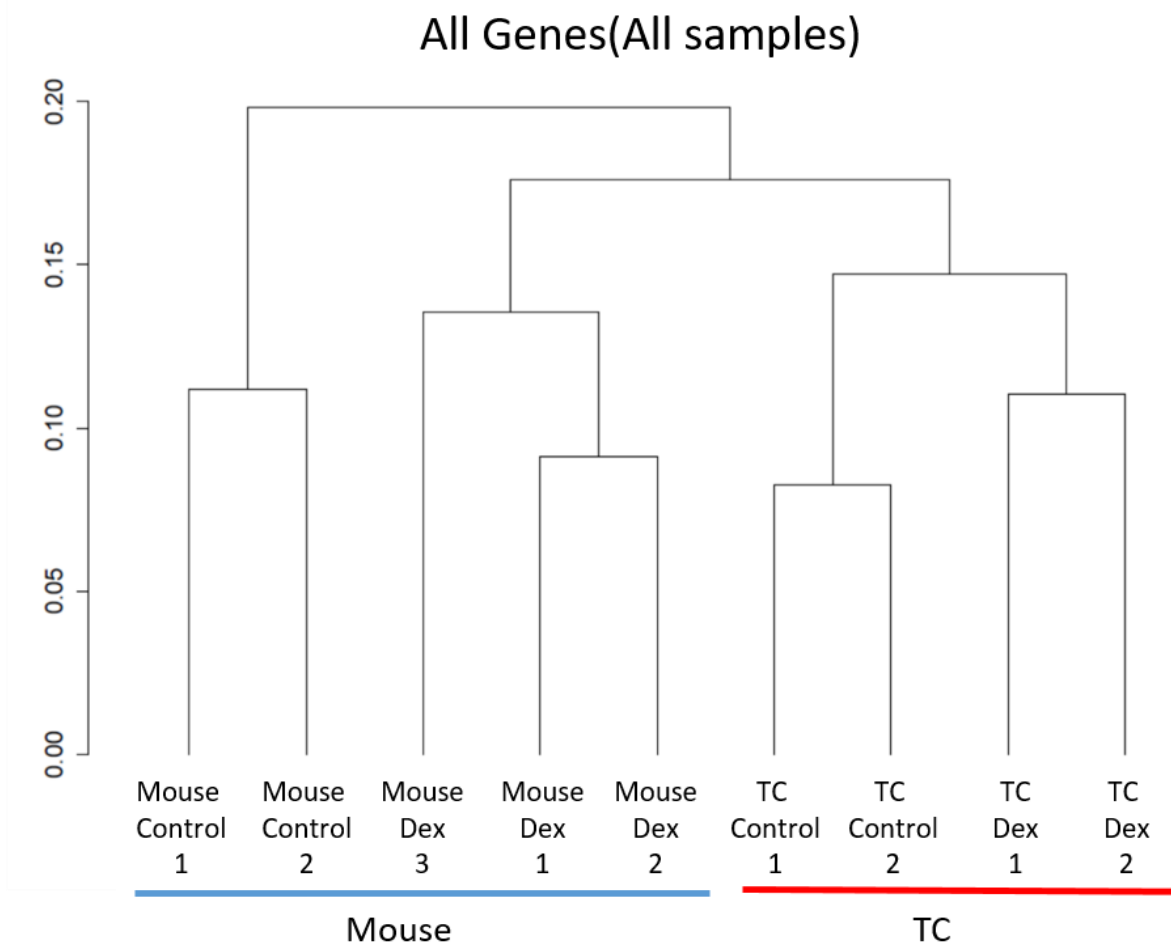


Figure 132: Dendrogram showing clustering of all 697 samples. They do not cluster into control and Dex but rather the samples from tissue culture (red line) cluster together, separate from the samples taken from the mice (blue line).

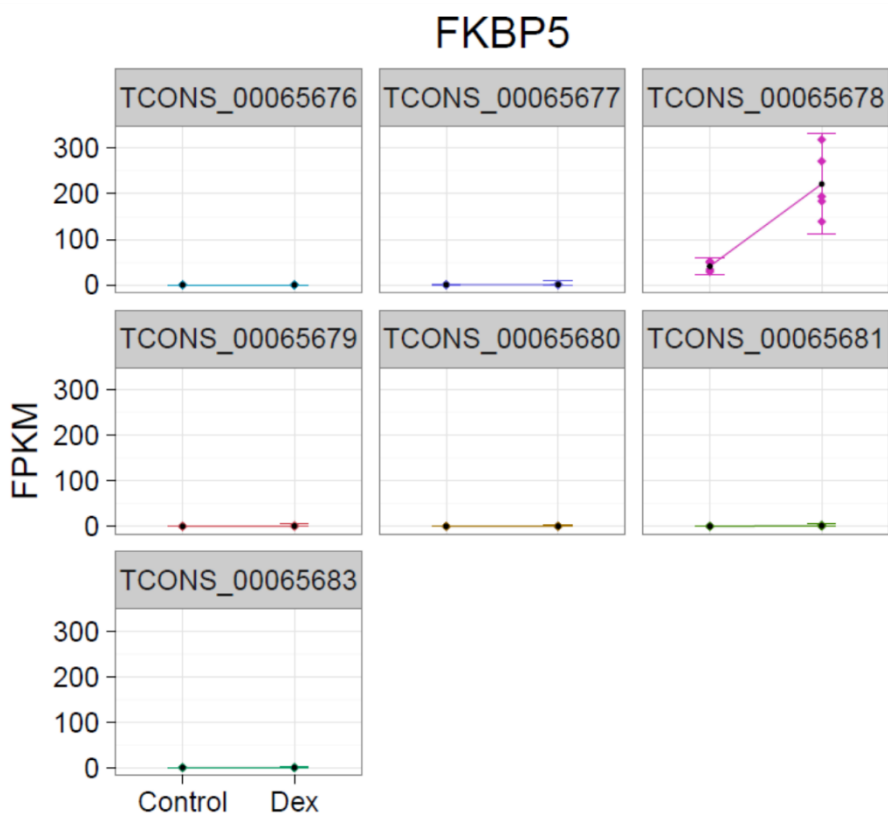


Figure 133: The change in expression of the isoforms of FKBP5 in the 697 cells control vs Dex treatment. All samples are included in the analysis. Just one isoform is significantly ($p<0.05$) upregulated in Dex treated samples as determined by CuffDiff and CummRBund, the RNA sequencing analysis software programmes.

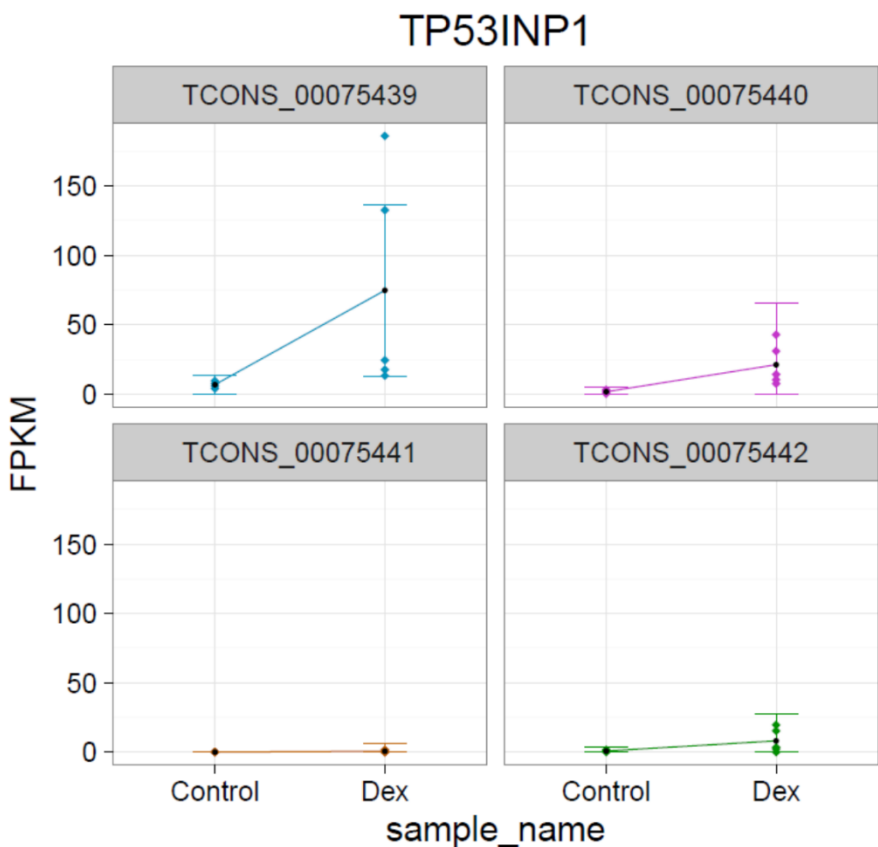


Figure 134: Transcripts of TP53INP1, a gene with one significantly upregulated isoform in Dex vs control in the 697 cells when both in vitro and in vivo samples are analysed together. 4 different isoforms are shown, and all repeats are shown as data point.

7.5 Summary

Despite several approaches being used to determine the cause for the apparent Dex resistance of the 697 cells to Dex *in vivo*, no definite mechanism has been found, although there are several possibilities.

All of the work on Dex treatment of the 697 cells *in vitro*, including treatment of cells collected from mice, did not show any increase in Dex resistance of the 697pSLIEW cells as was seen *in vivo*.

The lack of increased Dex resistance in the 697 cells when grown on the BM stromal feeder cells would indicate that these are not sufficient to provide the *in vivo* microenvironment that is required for the alteration in cell phenotype. The increase in Dex sensitivity seen in some of the conditions cannot be explained other than when the 697 cells are grown at low

density they do not have high viability, suggesting cell-cell interactions are important for this cell line.

The increase in Dex sensitivity observed in the 697pSLIEW cells collected from the spleen and BM of the mice is likely to be a result of reduced cell viability and it was most pronounced in the BM samples followed by spleen and not present in the liver. The number of leukaemic cells collected from the BM was the lowest, followed by the spleen whereas there was an abundance of cells collected from the liver, so this might have an effect. One reason why no resistance was seen in the samples collected from the mouse could be that testing was done 96 h after extraction from the mouse. This could be too long and any change in Dex sensitivity could already be lost. It could also have been a microenvironment-mediated effect that is lost once cells are cultured *in vitro*. One experiment that would have been useful would have been testing cells from the mouse with the support of a feeder layer such as the MSC or MS5. By supporting the cells with a feeder layer as soon as they are collected from the mouse the phenotype of the cells from growing *in vivo* might be retained.

The RNA sequencing of the cells that were collected from the mice compared to cells grown *in vitro* is the only experiment that has revealed anything that could account for the resistance. However, this data is convoluted with differences between each permutation of analysis. Further validation of the genes would be needed before a definite answer could be stated.

The upregulation of JUN and FOS mRNA in the mouse samples compared to tissue culture in both control and Dex treated samples is interesting. Similar genes are also downregulated in both the mouse and TC Dex samples compared to control, indicating a role in both engraftment in the mouse and Dex response. JUN and FOS are subunits of the AP-1 transcription factor, which is involved in proliferation, survival, oncogenic transformation and cell migration (Kappelmann, Bosserhoff, and Kuphal 2014). Furthermore, AP-1 has several possible subunits, and the dimer composition of the transcription factor affects transcription and which genes are targeted. The composition of subunits affects whether the transcription factor has oncogenic properties, whereby c-Jun homodimers have been shown to result in oncogenic transformation when artificially stabilised (Castellazzi et al. 1993). Over expression of c-FOS is also sufficient for oncogenic transformation (Miller, Curran, and Verma 1984). Upregulation of the specific subunits JUN and FOS may result in more dimers

with oncogenic potential, altering the phenotype of the cell. It is unlikely that the increases in FOS and JUN mRNA are directly responsible for the apparent Dex resistance in the 697 cells. A previous study of patient samples found no correlation between levels of AP-1 binding or expression of FOS and JUN with prednisolone response *in vitro* (Bailey et al. 1999).

Another group of genes that are upregulated in the same pattern as *FOS* and *JUN* are the *EGR* genes *EGR1*, 2 and 3 (Figure 135). *EGR1* is upregulated in both mouse control and Dex, and down regulated Dex treatment (Mouse and control). These genes encode zinc finger proteins, and *EGR1* is known to be down regulated by Dex treatment (Kharbanda et al. 1991) This has even been found in the 697 cells after 24hrs treatment with 100nM Dex (Yamada et al. 2003). The *EGR* genes are highly interconnected with the *FOS* and *JUN* related genes (Figure 136), and this network of genes is associated with response to cAMP (FDR=2.8e⁻¹⁵) and transcriptional activation (FDR=1.59e⁻⁷). The upregulation of these genes in mouse samples compared to TC would imply a role in engraftment and proliferation *in vivo*.

Combined with the negative effect of Dex on *EGR* transcription, this indicates that the cells in the mouse are getting sufficient Dex, but components downstream may induce resistance to Dex induced apoptosis. One gene that is downstream of NR3C1 that could be a cause for loss of apoptosis is *RCAN1* (regulator of calcineurin 1), which is upregulated upon Dex treatment in TC samples but not in the mouse. This gene is upregulated in response to Dex in ALL cells, and in the CEM cell line has been correlated with apoptosis. In Dex resistant CEM cells *RCAN1* is not upregulated as it is in the Dex sensitive cells which indicates a role in Dex resistance (Hirakawa, Nary, and Medh 2009; Bindreither et al. 2014) .

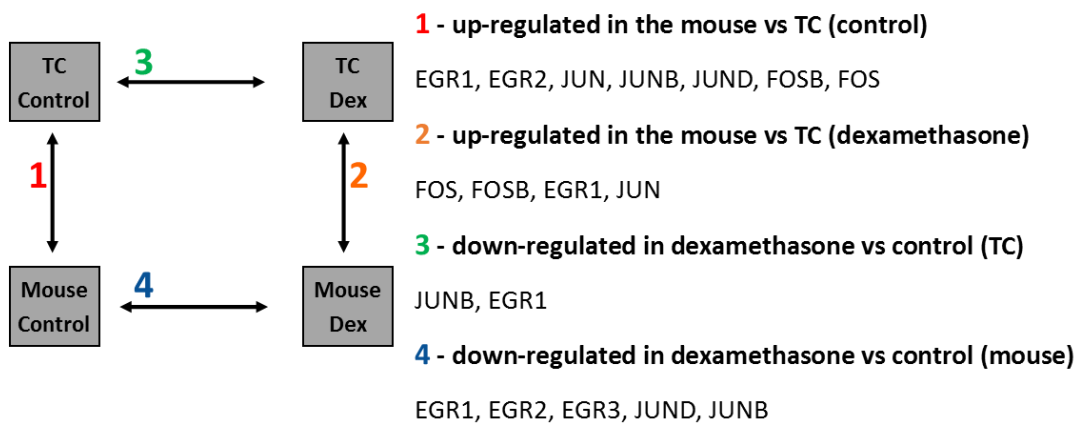


Figure 135: Schematic detailing the deregulation of *FOS*, *JUN* and *EGR* genes in the 697 cells *in vitro* and *in vivo*. The four different permutations of comparison are shown, and the differentially regulated genes including the direction of change for each. Although the picture is complicated, the same genes are repeatedly differentially expressed in the different conditions indicating a major role for these genes in why the 697 cells are not responsive to Dex *in vivo*,

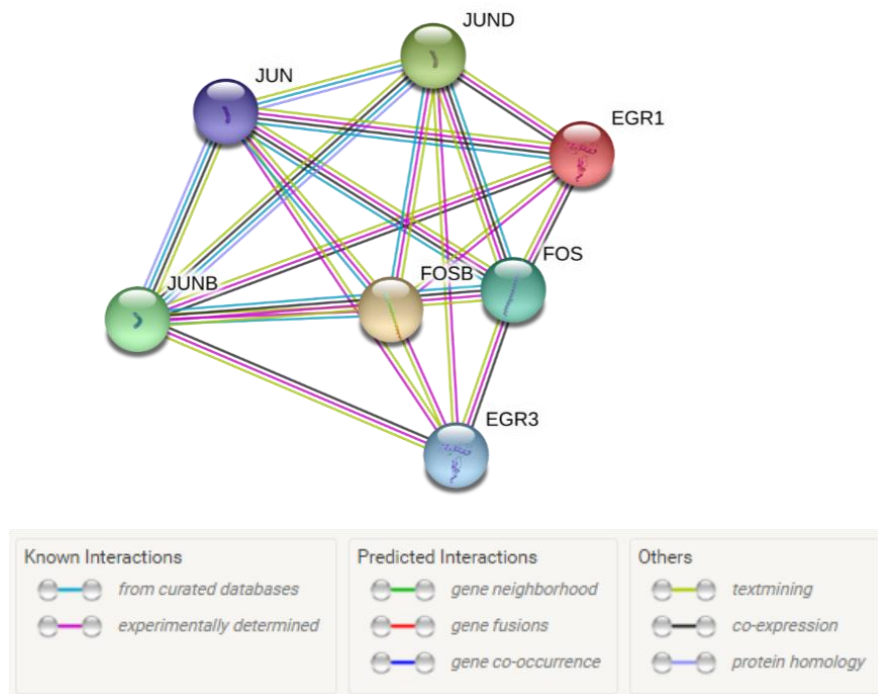


Figure 136: The known protein interactions between the *JUN*, *FOS* and *EGR* genes found differentially expressed in the analysis of Dex and control 697 samples both *in vivo* and *in vitro*. Interactions were determined using the online protein interaction database, STRING (version 10.0), and the types of interaction are shown in the legend below.

The differences between primary cells and cell lines include alterations in cell cycle and metabolism (Carette et al. 2010; Gillet et al. 2011). As well as the already outlined roles of AP-1, c-Jun has also been shown to increase transcription of Cyclin D, an important cell cycle regulator (Bakiri et al. 2000). Several metabolic genes were also differentially regulated in mouse samples compared to tissue culture. It could be that growth *in vivo* promotes a more primary cell like phenotype in the 697 cells, and this altered transcription is enough to render the cells resistant to Dex. The mechanisms of this are unknown.

Both mouse and tissue culture cells had a similar response to Dex with the induction of some NR3C1 target genes, including *FKBP5*, supporting the PK data that the bioavailability of Dex is sufficient. Only around 30% of genes with >2 log₂ fold change in mouse or tissue culture were shared between the two conditions indicating a different response in tissue culture compared to the mouse.

One gene that is differentially regulated in response to Dex in TC and the mouse is *RASD1*, a Dex inducible gene that is associated with control of aberrant growth, and control of proliferation of B cells (Vaidyanathan et al. 2004; Lindsey 2007).

Expression of *RASD1* is increased in response to Dex treatment in TC samples, but in mouse samples there is no increase, demonstrating a lack of Dex induced transcriptional activation of the gene. However, there is already higher basal expression of *RASD1* in mouse samples compared to TC. *RASD1* is found at low levels in freshly collected B cells from lymph nodes, but as cells are cultured *in vitro* the expression increases rapidly (Lindsey 2007). Although this is the opposite to what is seen in the samples run, this differential expression dependent on culture could account for why the mouse and tissue culture control samples have significantly different *RASD1* levels.

A role for *RASD1* in Dex resistance in the mouse could result from the lack of induction of *RASD1* expression in the mouse. *RASD1* has been proposed as an effector of apoptosis in response to chemotherapeutic agents in breast cancer (Tian et al. 2013), and expression of *RASD1* results in an inhibition of growth and increased apoptosis (Vaidyanathan et al. 2004). The lack of increase in response to Dex in the mouse samples could be the mechanism by

which these cells are resistant. However, what that does not explain is how the loss of RASD1 induction by Dex is mediated.

RASD1 signalling, or lack thereof provides a probable cause for the Dex resistance of the 697pSLIEW cells *in vivo*. The lack of effect once cells are removed from the mouse implies that there is signalling within the murine microenvironment that is needed to support this change in transcription, and when the microenvironment is lost, so too are the transcriptional changes and the cells revert to a sensitive phenotype. The changes in the 697pSLIEW cell line between *in vitro* and *in vivo* culture also appears to involve AP-1 transcription factor mediated changes. This change in transcription could be the cause for de-regulation of RASD1 signalling. RASD1 has been shown to be increased in EGR1 over expressing non-small cell lung carcinoma cell lines (Zhang et al. 2014) but there is little other data to support this hypothesis.

The 697 cells, although Dex sensitive *in vitro* should not be used as a model for Dex sensitivity due to the change in sensitivity that is seen when cells are grown *in vivo*. This altered drug sensitivity profile may not just be for Dex, as genes implicated in asparaginase resistance were also found differentially regulated in mouse samples compared to tissue culture samples (Estes et al. 2007). Although these genes are downregulated, which is counterintuitive to their role in resistance it might indicate an underlying alteration in drug sensitivity when these cells are cultured *in vivo* compared to *in vitro*. Unfortunately, asparaginase was not tested in the 697pSLIEW cells during these experiments, as this would be an interesting experiment to do in the future.

The differences between engraftment and drug sensitivity to chemotherapeutic agents of ALL cell lines *in vitro* and *in vivo* culture are part of the larger issue of finding the right model to examine drug resistance in ALL. An interesting experiment, if it could ever be done would be the culture of a cell line and the parental primary cell sample *in vitro* and *in vivo* to investigate the changes and the clustering of the samples, to determine if growth of a cell line *in vivo* results in a phenotype closer to the primary cell sample.

Other future experiments would be to validate some of the targets found through this RNA sequencing through knock out and pharmacological inhibition. Genes that would be interesting to investigate further include RCAN1, RASD1 and several of the AP-1 transcription

factor subunits. How the loss of these genes affect engraftment of the 697 cells *in vivo* as well as response to Dex could prove important for the study of Dex resistance in ALL.

Chapter 8: Discussion

The issue of Dex resistance in ALL has important prognostic implications, as patients that do not respond well to Dex at presentation, or become resistant, have a significantly worse outcome (Moricke et al. 2008; Bachmann et al. 2005). The high frequency of Dex resistance in relapsed ALL is not normally mirrored by mutations or deletions in *NR3C1*, the target for Dex (Klumper et al. 1995; Mullighan et al. 2007). This discrepancy and the resulting hypothesis that *NR3C1* is important for the fitness of ALL resulted in the investigations into the role of *NR3C1* in the evolution of Dex resistance that was carried out as part of this PhD.

8.1 Paired primary presentation and relapse cells

Comparison of the L707 presentation and relapse using gene expression microarrays confirmed what was known about the 5q deletion from work previously done by Dr. Elda Latif. The loss of *NR3C1* and *HMHB1* expression in the relapse pointed to one of these two genes as drivers for relapse, and the other 4 genes as passengers due to lack of expression in the presentation determined by the microarray analysis. The enrichment of pathways involved in chromatin silencing in the relapse is perhaps more interesting and might indicate a role for altered epigenetic and transcriptional programmes in the L707 cells. More work would need to be done to determine exactly what this is, and comparison to online data sets for presentation and relapse cases may have proven useful.

Without a germline sample, the WGS data for the L707 presentation and relapse could not identify cancer specific mutations in these samples. Despite this, several interesting SNPs and indels were found in the relapse specific variants. These SNPs and indels could be involved in the genesis of relapse and several of these warrant further investigation, especially those that are already associated with cancers such as the variants in *CLEC1A*, *TTRAP* and *NDUFB11*. Despite the lack of a germline sample, the SNPs and Indels that are shared between the L707 presentation and relapse provide perhaps the most interest. The presence of variants in known tumour suppressors (*BRCA2*), cell cycle proteins (*ATR*, *CHEK1*) and *TP53* associated genes (*TP53BP1*, *TP53RK*, *MDM2*) all point to possible oncogenic

mechanisms. However, to determine whether these variants are significant, a large pool of reference genomes would be needed in place of a germline sample. This data is available through the 1000 genomes project but the analysis was determined to not be feasible after talking with Dr Matt Bashton due to the time constraints of this PhD and my own limited bioinformatics experience.

The possibility of a cell with a pre-existing heterozygous deletion in the L707 presentation, which then emerges when treated with Dex has not been robustly proven with this work, as all but one sample were below the cut-off for positivity. Despite there being no robust proof of this clone being present, with more rounds of engraftment and treatment it is likely to be identified.

8.2 Role of NR3C1 in ALL

The original hypothesis for this work was that loss of NR3C1 would result in reduced fitness of the ALL cells. This was tested in several ways using the 697 cell line and the L707 presentation cells. In the 697 cells this was tested using a pool of pTRIPZ shRNA constructs targeting the genes in the L707 relapse 5q deletion. This showed that NR3C1 knockdown results in Dex resistance, and further supported the idea that the other genes are likely passenger deletions as they appear to have no effect on proliferation or Dex sensitivity. There is no evidence that there is a deleterious effect of loss of NR3C1 as it would be expected that if loss of signalling through RNAi was harmful to the cells then these constructs would be lost when cells are induced by Dox but without Dex treatment.

The same screen when the cells were engrafted *in vivo* did not produce the expected results, and there are several possible reasons why. Firstly, the silencing of constructs *in vivo*, which has been seen in these samples and in other work in our groups (unpublished data) could be responsible, as if shRNA is not expressed then the construct will have no effect on the expression of genes. It does highlight the need to use plasmids with promoters that are less susceptible to silencing when the cells will be used *in vivo*. The second possibility is that, as well as the silencing, the lack of Dex sensitivity of the 697 cells *in vivo* could be a reason that

there is no correlation in construct enrichment or depletion. If the cells are not responding to Dex, then the NR3C1 targeting constructs will have little effect.

In order to test if the loss of NR3C1 signalling had an effect on the L707 cells, which could not be transduced with pTRIPZ, pharmacological inhibition was used. Mifepristone was chosen for this as the only commercially available NR3C1 antagonist. There has also been evidence for the use of mifepristone in murine models of leukaemia (Check et al. 2009). However, the treatment of the L707 presentation cells with mifepristone had no effect on survival and very little effect on the expression profile of the L707 cells when tested by gene expression microarray. This could be because mifepristone was found to work as a partial agonist in the 697 cells *in vitro*.

Lastly, the treatment of the L707 presentation with Dex did result in prolonged survival of mice, as had been seen previously. When the gene expression changes were analysed by microarray there was a change in the expression profile consistent with Dex treatment. This included the upregulation heat shock proteins, which are known to mediate the action of NR3C1 (Prota et al. 2012) and the upregulation of S1100A8 and S100A9, which have been implicated in Dex resistance (Spijkers-Hagelstein et al. 2012).

8.3 lentiCRISPR screen

The aims of the lentiCRISPR screen was to prove the feasibility of a genome-wide lentiCRISPR screen in primograft ALL cells using the *in vivo* NSG mouse model and to use this screen to investigate the mechanisms of Dex resistance in matched presentation and relapse ALL cells. This is the first time to our knowledge that a genome wide lentiCRISPR screen has been carried out in primary derived material *in vivo* and despite encountering many issues with the sequencing and PCR contamination, this work represents a major technical advance.

Both of the aims were completed, with the successful transduction of the L707 presentation cells with the lentiCRISPR GeCKO library, puromycin selection and injection of cells into mice. The investigation of genes responsible for Dex resistance was partly hampered by the finding that the library was contaminated with NR3C1 targeting sgRNA during the production of the amplicon library by PCR and the subsequent removal of these sequences from the analysis.

Several genes that could have implications in Dex resistance were highlighted and when the expression of the L707 presentation is taken into account with the enrichment and depletion of sgRNA, several genes warrant further investigation.

Amongst the genes identified by the CRISPR screen was MSRB2 which is expressed in both the L707 presentation and relapse, with a modest reduction at relapse (0.45 fold). This gene also has GRE binding sites upstream of the transcriptional start site, and there is binding of NR3C1 to these in A549 cells when treated with 100nM Dex (ENCODE project Consortium 2013). This combination of evidence presents this gene as an interesting possible driver gene in leukaemia. Its roles in oxidative stress, and the finding that oxidative stress genes are reduced in leukaemia (Battisti et al. 2008), points to a probable mechanistic reason for the loss of expression of this gene. Other sgRNA that are enriched in the L707 presentation cells when treated with Dex, MSL1 and RRB1P also have NR3C1 binding peaks when ChIP-seq data from A549 cells treated with Dex is analysed (ENCODE project Consortium 2013). These genes have an enrichment of sgRNA targeting them when the L707 cells are treated with Dex but in the microarray data there is no difference in expression between the presentation and relapse and neither of the genes are expressed at very high levels, they might still represent interesting genes to investigate further.

Although no effect was seen when L707 presentation cells were transduced with PLXND1 targeting sgRNA, this gene warrants further investigation due to the significant reduction in PLXND1 mRNA when NR3C1 signalling is disrupted by sgRNA in the L707 cells. As well as this, there are consensus GRE sites upstream of the transcriptional start site, and when ChIP-seq data is analysed, there are binding peaks from NR3C1 binding to this region in the presence of 100nM Dex (ENCODE project Consortium 2013).

8.4 Dex resistance in an ALL cell line

The last, and in my opinion most fascinating part of this PhD was the incidental finding that the 697 cells were Dex sensitive *in vitro* with an IC₅₀ of just 20 nM but appear completely Dex resistant *in vivo*. This Dex resistance is not a result of the cellular interactions with murine BM stromal cells, or if they do play a role which is likely, this is not evident *in vitro*.

The effect also appears to be transient, as once cells are removed from the mice they are no longer Dex resistant. The RNA sequencing data for these cells revealed the most about possible mechanisms for this Dex resistance.

There are two areas that could provide the mechanistic cause for this resistance. Firstly, the upregulation of *FOS*, *FOSB* and *JUN* in the mouse samples compared to TC indicate a role for these genes in the engraftment of cells *in vivo* and growth in the murine microenvironment. These genes have been found to be oncogenic, and overexpression results in oncogenic transformation (Kappelmann, Bosserhoff, and Kuphal 2014; Castellazzi et al. 1993; A. D. Miller, Curran, and Verma 1984). Not only are the individual proteins oncogenic but they are all components of the AP-1 transcription factor. Signalling through AP-1 has been found to be involved in several cellular processes that could be important in leukaemia cells including, proliferation, survival and cell migration (Kappelmann, Bosserhoff, and Kuphal 2014). No correlation between AP-1 expression and Dex resistance in ALL cells has been found (Bailey et al. 1999). *c-JUN* also increases transcription of Cyclin D (Bakiri et al. 2000) indicating a role for altered cell cycle in the possible mechanisms.

Another possible cause for the *in vivo* Dex resistance is the de-regulation of *RASD1* (Ras related Dex induced 1). *RASD1* is a Dex induced gene that is upregulated in response to Dex *in vitro* but not *in vivo*. Lack of RASD1 induction *in vivo* indicates that although the leukaemic cells are receiving adequate Dex treatment, as shown by PK studies, the response to the Dex *in vivo*.

To fully understand how this is occurring the genes which appear to have an effect would have to be investigated separately through other methods. The best option for this would be to use lentiCRISPR, as this should not be affected by the *in vivo* silencing of RNAi transcripts that was seen in the 697 cells in the pTRIPZ plasmid transduction experiments.

To summarise, loss of NR3C1 in ALL cells results in Dex resistance, but does not appear to affect fitness of these cells. There is another mechanism that is the cause of this in the L707 relapse, and although several possible genes have been highlighted through microarray analyses and WGS this is still unknown.

Despite this, the L707 cells are a good model to use for whole genome lentiCRISPR screening. We were able to retain 12X screen coverage but with changed parameters higher

yield and coverage would be attainable. The issue with PCR contamination in the screen carried out for this PhD did not render the data useless but does highlight the need for care when carrying out such sensitive PCR reactions. PCR contamination is a known problem but it was not considered in this screen which was a mistake. In future to avoid this issue, separate areas should be used for PCR set up and use of products. Single constructs should also not be taken from the library sequences, so that if contamination does occur it can easily be removed from analysis.

Lastly, the emergence of Dex resistance in cell lines is unpredictable, and the 697 cells are testament to this as they are sensitive to Dex *in vitro* but resistant *in vivo*. The causes for this were explored but no firm mechanism was found, although several possibilities were found. This data is both interesting and highlights the need for careful consideration of models when investigating drug resistance.

The work carried out in this PhD has both given insight into the genesis of relapse and Dex resistance in ALL and provided excellent training in research science.

- Abrams, Marc T., Noreen M. Robertson, Kyonggeun Yoon, and Eric Wickstrom. 2004. "Inhibition of Glucocorticoid-Induced Apoptosis by Targeting the Major Splice Variants of BIM mRNA with Small Interfering RNA and Short Hairpin RNA." *Journal of Biological Chemistry* 279 (53): 55809–17. doi:10.1074/jbc.M411767200.
- Abu-Shakra, M, D D Gladman, and M B Urowitz. 1996. "Malignancy in Systemic Lupus Erythematosus." *Arthritis Rheum* 39 (6): 1050–54.
- Adolfsson, Jörgen, Robert Måansson, Natalija Buza-Vidas, Anne Hultquist, Karina Liuba, Christina T Jensen, David Bryder, et al. 2005. "Identification of Flt3 + Lympho-Myeloid Stem Cells Lacking Erythro-Megakaryocytic Potential: A Revised Road Map for Adult Blood Lineage Commitment." *Cell* 121 (2): 295–306. doi:10.1016/j.cell.2005.02.013.
- Akasaka, Takashi, Theodore Balasas, Lisa J Russell, Kei-ji Sugimoto, Aneela Majid, Renata Walewska, E Loraine Karran, et al. 2007. "Five Members of the CEBP Transcription Factor Family Are Targeted by Recurrent IGH Translocations in B-Cell Precursor Acute Lymphoblastic Leukemia (BCP-ALL)." *Blood* 109 (8). American Society of Hematology: 3451–61. doi:10.1182/blood-2006-08-041012.
- Aken, Bronwen L, Sarah Ayling, Daniel Barrell, Laura Clarke, Valery Curwen, Susan Fairley, Julio Fernandez Banet, et al. 2016. "The Ensembl Gene Annotation System." *Database* 2016 (January): baw093-baw093. <http://dx.doi.org/10.1093/database/baw093>.
- Alcalay, Myriam, Natalia Meani, Vania Gelmetti, Anna Fantozzi, Marta Fagioli, Annette Orleth, Daniela Riganelli, et al. 2003. "Acute Myeloid Leukemia Fusion Proteins Deregulate Genes Involved in Stem Cell Maintenance and DNA Repair." *The Journal of Clinical Investigation* 112 (11): 1751–61. doi:10.1172/JCI17595.
- Anderer, G, M Schrappe, a M Brechlin, M Lauten, P Muti, K Welte, and M Stanulla. 2000. "Polymorphisms within Glutathione S-Transferase Genes and Initial Response to Glucocorticoids in Childhood Acute Lymphoblastic Leukaemia." *Pharmacogenetics* 10 (8): 715–26. doi:10.1097/00008571-200011000-00006.
- Anderson, Kristina, Christoph Lutz, Frederik W. van Delft, Caroline M. Bateman, Yanping Guo, Susan M. Colman, Helena Kempski, et al. 2011. "Genetic Variegation of Clonal Architecture and Propagating Cells in Leukaemia." *Nature* 469 (7330). Nature Publishing Group, a division of Macmillan Publishers Limited. All Rights Reserved.: 356–61.

doi:10.1038/nature09650.

Babovic, Sonja, and Connie J. Eaves. 2014. "Hierarchical Organization of Fetal and Adult Hematopoietic Stem Cells." *Experimental Cell Research*. doi:10.1016/j.yexcr.2014.08.005.

Bachmann, Petra S., Rosemary Gorman, Karen L. MacKenzie, Louise Lutze-Mann, and Richard B. Lock. 2005. "Dexamethasone Resistance in B-Cell Precursor Childhood Acute Lymphoblastic Leukemia Occurs Downstream of Ligand-Induced Nuclear Translocation of the Glucocorticoid Receptor." *Blood* 105 (6): 2519–26. doi:10.1182/blood-2004-05-2023.

Bachmann, Petra S., Rosemary Gorman, Rachael A. Papa, Jane E. Bardell, Jette Ford, Ursula R. Kees, Glenn M. Marshall, and Richard B. Lock. 2007. "Divergent Mechanisms of Glucocorticoid Resistance in Experimental Models of Pediatric Acute Lymphoblastic Leukemia." *Cancer Research* 67 (9): 4482–90. doi:10.1158/0008-5472.CAN-06-4244.

Bachmann, Petra S., Rocco G. Piazza, Mary E. Janes, Nicholas C. Wong, Carwyn Davies, Angela Mogavero, Vivek A. Bhadri, et al. 2010. "Epigenetic Silencing of BIM in Glucocorticoid Poor-Responsive Pediatric Acute Lymphoblastic Leukemia, and Its Reversal by Histone Deacetylase Inhibition." *Blood* 116 (16): 3013–22. doi:10.1182/blood-2010-05-284968.

Bai, Ying, Guang Rong Qiu, Fan Zhou, Li Ying Gong, Feng Gao, and Kai Lai Sun. 2013. "Overexpression of DICER1 Induced by the Upregulation of GATA1 Contributes to the Proliferation and Apoptosis of Leukemia Cells." *International Journal of Oncology* 42 (4): 1317–24. doi:10.3892/ijo.2013.1831.

Bailey, S, A G Hall, A D Pearson, M M Reid, and C P Redfern. 1999. "Glucocorticoid Resistance and the AP-1 Transcription Factor in Leukaemia." *Adv Exp Med Biol* 457: 615–19. <http://www.ncbi.nlm.nih.gov/pubmed/10500841>.

Bain, G, E C Maandag, D J Izon, D Amsen, a M Kruisbeek, B C Weintraub, I Krop, M S Schlissel, a J Feeney, and M van Roon. 1994. "E2A Proteins Are Required for Proper B Cell Development and Initiation of Immunoglobulin Gene Rearrangements." *Cell* 79 (5): 885–92. doi:0092-8674(94)90077-9 [pii].

Baker, S J, E R Fearon, J M Nigro, S R Hamilton, A C Preisinger, J M Jessup, P van Tuinen, et al. 1989. "Chromosome 17 Deletions and p53 Gene Mutations in Colorectal Carcinomas." *Science* 244. doi:10.1126/science.2649981.

Bakiri, L, D Lallemand, E Bossy-Wetzel, and M Yaniv. 2000. "Cell Cycle-Dependent Variations in c-Jun and JunB Phosphorylation: A Role in the Control of Cyclin D1 Expression." *The EMBO Journal* 19 (9): 2056–68. doi:10.1093/emboj/19.9.2056.

Balmano, K, and S J Cook. 2009. "Tumour Cell Survival Signalling by the ERK1/2 Pathway." *Cell Death and Differentiation* 16 (3): 368–77. doi:10.1038/cdd.2008.148.

Baron, Margaret H., Joan Isern, and Stuart T. Fraser. 2012. "The Embryonic Origins of Erythropoiesis in Mammals." *Blood*. doi:10.1182/blood-2012-01-153486.

Barrangou, Rodolphe, Christophe Fremaux, Hélène Deveau, Melissa Richards, Patrick Boyaval, Sylvain Moineau, Dennis Romero, and Philippe Horvath. 2007. "CRISPR Provides Acquired Resistance Against Viruses in Prokaryotes." *Science* 315 (March): 1709–12. doi:10.1126/science.1138140.

Basak, Nandini Pal, and Subrata Banerjee. 2015. "Mitochondrial Dependency in Progression of Acute Myeloid Leukemia." *Mitochondrion*. doi:10.1016/j.mito.2015.01.006.

Battisti, Vanessa, Liési D K Maders, Margarete D. Bagatini, Karen F. Santos, Rosélia M. Spanevello, Paula A. Maldonado, Alice O. Brulé, Maria do Carmo Araújo, Maria R C Schetinger, and Vera M. Morsch. 2008. "Measurement of Oxidative Stress and Antioxidant Status in Acute Lymphoblastic Leukemia Patients." *Clinical Biochemistry* 41 (7–8): 511–18. doi:10.1016/j.clinbiochem.2008.01.027.

Beesley, Alex H., Aaron J. Cummings, Joseph R. Freitas, Katrin Hoffmann, Martin J. Firth, Jette Ford, Nicolas H. De Klerk, and Ursula R. Kees. 2005. "The Gene Expression Signature of Relapse in Paediatric Acute Lymphoblastic Leukaemia: Implications for Mechanisms of Therapy Failure." *British Journal of Haematology* 131 (4): 447–56. doi:10.1111/j.1365-2141.2005.05785.x.

Ben-Porath, Ittai, Matthew W Thomson, Vincent J Carey, Ruping Ge, George W Bell, Aviv Regev, and Robert A Weinberg. 2008. "An Embryonic Stem Cell-like Gene Expression Signature in Poorly Differentiated Aggressive Human Tumors." *Nature Genetics* 40 (5):

499–507. doi:10.1038/ng.127.An.

Benz, Claudia, Michael R. Copley, David G. Kent, Stefan Wohrer, Adrian Cortes, Nima Aghaeepour, Elaine Ma, et al. 2012. "Hematopoietic Stem Cell Subtypes Expand Differentially during Development and Display Distinct Lymphopoietic Programs." *Cell Stem Cell* 10 (3): 273–83. doi:10.1016/j.stem.2012.02.007.

Bertrand, Julien Y, Neil C Chi, Buyung Santoso, Shutian Teng, Didier Y R Stainier, and David Traver. 2010. "Haematopoietic Stem Cells Derive Directly from Aortic Endothelium during Development." *Nature* 464 (7285): 108–11. doi:10.1038/nature08738.

Bertrand, Julien Y, Guillaume E Desanti, Richard Lo-Man, Claude Leclerc, Ana Cumano, and Rachel Golub. 2006. "Fetal Spleen Stroma Drives Macrophage Commitment." *Development (Cambridge, England)* 133 (18): 3619–28. doi:10.1242/dev.02510.

Bhadri, Vivek A., Toby N. Trahair, and Richard B. Lock. 2012. "Glucocorticoid Resistance in Paediatric Acute Lymphoblastic Leukaemia." *Journal of Paediatrics and Child Health* 48 (8): 634–40. doi:10.1111/j.1440-1754.2011.02212.x.

Bhatla, Teena, Courtney L Jones, Julia A Meyer, Nicholas A Vitanza, Elizabeth A Raetz, and William L Carroll. 2014. "The Biology of Relapsed Acute Lymphoblastic Leukemia: Opportunities for Therapeutic Interventions." *Journal of Pediatric Hematology/oncology* 36 (6): 413–18. doi:10.1097/MPH.0000000000000179.

Bhatla, Teena, Jinhua Wang, Debra J. Morrison, Elizabeth A. Raetz, Michael J. Burke, Patrick Brown, and William L. Carroll. 2012. "Epigenetic Reprogramming Reverses the Relapse-Specific Gene Expression Signature and Restores Chemosensitivity in Childhood B-Lymphoblastic Leukemia." *Blood* 119 (22): 5201–10. doi:10.1182/blood-2012-01-401687.

Bhojwani, Deepa, Huining Kang, Naomi P. Moskowitz, Dong Joon Min, Hokyung Lee, Jeffrey W. Potter, George Davidson, et al. 2006. "Biologic Pathways Associated with Relapse in Childhood Acute Lymphoblastic Leukemia: A Children's Oncology Group Study." *Blood* 108 (2): 711–17. doi:10.1182/blood-2006-02-002824.

Bhojwani, Deepa, and Ching-Hon Pui. 2013. "Relapsed Childhood Acute Lymphoblastic Leukaemia." *The Lancet Oncology* 14 (6): e205-17. doi:10.1016/S1470-2045(12)70580-

6.

Biankin, Andrew V, Nicola Waddell, Karin S Kassahn, Marie-Claude Gingras, Lakshmi B Muthuswamy, Amber L Johns, David K Miller, et al. 2012. "Pancreatic Cancer Genomes Reveal Aberrations in Axon Guidance Pathway Genes." *Nature* 491 (7424). Nature Publishing Group, a division of Macmillan Publishers Limited. All Rights Reserved.: 399–405. <http://dx.doi.org/10.1038/nature11547>.

Biddie, Simon C, Sam John, and Gordon L Hager. 2010. "Genome-Wide Mechanisms of Nuclear Receptor Action." *Trends in Endocrinology and Metabolism: TEM* 21 (1). United States: 3–9. doi:10.1016/j.tem.2009.08.006.

Bindreither, Daniel, Simone Ecker, Barbara Gschirr, Anita Kofler, Reinhard Kofler, and Johannes Rainer. 2014. "The Synthetic Glucocorticoids Prednisolone and Dexamethasone Regulate the Same Genes in Acute Lymphoblastic Leukemia Cells." *BMC Genomics* 15 (1): 1–8. doi:10.1186/1471-2164-15-662.

Blazsek, I, J Chagraoui, and B Péault. 2000. "Ontogenic Emergence of the Hematon, a Morphogenetic Stromal Unit That Supports Multipotential Hematopoietic Progenitors in Mouse Bone Marrow." *Blood* 96 (12): 3763–71.

Boden, Daniel, Oliver Pusch, Rebecca Silbermann, Fred Lee, Lynne Tucker, and Bharat Ramratnam. 2004. "Enhanced Gene Silencing of HIV-1 Specific siRNA Using microRNA Designed Hairpins." *Nucleic Acids Research* 32 (3). England: 1154–58. doi:10.1093/nar/gkh278.

Boettcher, Michael, and Michael T. McManus. 2015. "Choosing the Right Tool for the Job: RNAi, TALEN, or CRISPR." *Molecular Cell*. doi:10.1016/j.molcel.2015.04.028.

Boissel, Nicolas, Marie-Françoise Auclerc, Véronique Lhéritier, Yves Perel, Xavier Thomas, Thierry Leblanc, Philippe Rousselot, et al. 2003. "Should Adolescents With Acute Lymphoblastic Leukemia Be Treated as Old Children or Young Adults? Comparison of the French FRALLE-93 and LALA-94 Trials." *Journal of Clinical Oncology* 21 (5). American Society of Clinical Oncology: 774–80. doi:10.1200/JCO.2003.02.053.

Bolotin, Alexander, Benoit Quinquis, Alexei Sorokin, and S. Dusko Ehrlich. 2005. "Clustered Regularly Interspaced Short Palindrome Repeats (CRISPRs) Have Spacers of

Extrachromosomal Origin." *Microbiology* 151 (8): 2551–61. doi:10.1099/mic.0.28048-0.

Bomken, S, L Buechler, K Rehe, F Ponthan, A Elder, H Blair, C M Bacon, J Vormoor, and O Heidenreich. 2013. "Lentiviral Marking of Patient-Derived Acute Lymphoblastic Leukaemic Cells Allows in Vivo Tracking of Disease Progression." *Leukemia* 27 (3): 718–21. doi:10.1038/leu.2012.206.

Bondy-Denomy, Joseph, and Alan R. Davidson. 2014. "To Acquire or Resist: The Complex Biological Effects of CRISPR-Cas Systems." *Trends in Microbiology*. doi:10.1016/j.tim.2014.01.007.

Borowitz, Michael J., Brent L. Wood, Meenakshi Devidas, Mignon L. Loh, Elizabeth A. Raetz, Wanda L. Salzer, James B. Nachman, et al. 2015. "Prognostic Significance of Minimal Residual Disease in High Risk B-ALL: A Report from Children's Oncology Group Study AALL0232." *Blood* 126 (8): 964–71. doi:10.1182/blood-2015-03-633685.

Bourgeois, S, M Pfahl, and E E Baulieu. 1984. "DNA Binding Properties of Glucocorticosteroid Receptors Bound to the Steroid Antagonist RU-486." *The EMBO Journal* 3 (4): 751–55.

Breaks, D N a Double-strand, Margaret Nieborowska-skorska, Tomasz Stoklosa, Mandrita Datta, Agnieszka Czechowska, Lori Rink, Artur Slupianek, et al. 2006. "ATR-Chk1 Axis Protects BCR / ABL Leukemia Cells from the Lethal Effect Report ACKNOWLEDGEMENTS KEY WORDS RIB." *Cell Cycle*, no. May: 994–1000.

Buijs, Arjan, Marian J P L Stevens-Kroef, Edwin Sonneveld, and Lars T van der Veken. 2014. "Paired Analyses of Diagnostic and Relapse Samples of MLL Rearranged Infant Acute Lymphoblastic Leukemia Reveals Potential Therapy-Resistant Genomic Alterations." *Blood* 124 (21): 5345 LP-5345.
<http://www.bloodjournal.org/content/124/21/5345.abstract>.

Carette, Jan E, Carla P Guimaraes, Irene Wuethrich, Vincent A Blomen, Malini Varadarajan, Chong Sun, George Bell, et al. 2010. "A Global Map of Human Gene Expression." *Nat Biotechnol* 28 (4): 322–24. doi:10.1038/nbt0410-322.

Carroll, William L., Mignon L. Loh, Andrea Biondi, and Willman. 2009. *Childhood Leukemia*. Edited by Franklin O Smith Gregory H. Reaman. *Childhood Leukemia: A Practical Handbook*. Springer. doi:10.1007/BF02908298.7.

Casazza, Andrea, Veronica Finisguerra, Lorena Capparuccia, Andrea Camperi, Jakub M.

Swiercz, Sabrina Rizzolio, Charlotte Rolny, et al. 2010. "Sema3E-Plexin D1 Signaling Drives Human Cancer Cell Invasiveness and Metastatic Spreading in Mice." *Journal of Clinical Investigation* 120 (8): 2684–98. doi:10.1172/JCI42118.

Case, Marian, Elizabeth Matheson, Lynne Minto, Rosline Hassan, Christine J. Harrison, Nick

Bown, Simon Bailey, Josef Vormoor, Andrew G. Hall, and Julie A E Irving. 2008.

"Mutation of Genes Affecting the RAS Pathway Is Common in Childhood Acute Lymphoblastic Leukemia." *Cancer Research* 68 (16): 6803–9. doi:10.1158/0008-5472.CAN-08-0101.

Castellazzi, M, L Loiseau, F Piu, and A Sergeant. 1993. "Chimeric c-Jun Containing an

Heterologous Homodimerization Domain Transforms Primary Chick Embryo

Fibroblasts." *Oncogene* 8 (5). ENGLAND: 1149–60.

Catlin, Sandra N., Lambert Busque, Rosemary E. Gale, Peter Guttorp, and Janis L. Abkowitz.

2011. "The Replication Rate of Human Hematopoietic Stem Cells in Vivo." *Blood* 117 (17): 4460–66. doi:10.1182/blood-2010-08-303537.

Cella, Marina, Christian Döhring, Jacqueline Samardis, Mark Dessing, Manfred Brockhaus,

Antonio Lanzavecchia, and Marco Colonna. 1997. "A Novel Inhibitory Receptor (ILT3) Expressed on Monocytes, Macrophages, and Dendritic Cells Involved in Antigen

Processing." *Journal of Experimental Medicine* 185 (10): 1743–51.

doi:10.1084/jem.185.10.1743.

Chang, F., J. T. Lee, P. M. Navolanic, L. S. Steelman, J. G. Shelton, W. L. Blalock, R. A. Franklin,

and J. A. McCubrey. 2003. "Involvement of PI3K/Akt Pathway in Cell Cycle Progression,

Apoptosis, and Neoplastic Transformation: A Target for Cancer Chemotherapy."

Leukemia 17 (3): 590–603. doi:10.1038/sj.leu.2402824.

Check, Jerome H, Lynn Sansoucie, Joshua Chern, Nkechinyere Amadi, and Youval Katz. 2009.

"Mifepristone Treatment Improves Length and Quality of Survival of Mice with

Spontaneous Leukemia." *Anticancer Research* 29 (8). Greece: 2977–80.

Chen, Sidi, Neville E. Sanjana, Kaijie Zheng, Ophir Shalem, Kyungheon Lee, Xi Shi, David A.

Scott, et al. 2015. "Genome-Wide CRISPR Screen in a Mouse Model of Tumor Growth and Metastasis." *Cell* 160 (6): 1246–60. doi:10.1016/j.cell.2015.02.038.

Chiruvella, Kishore K., Zhuobin Liang, and Thomas E. Wilson. 2013. "Repair of Double-Strand Breaks by End Joining." *Cold Spring Harbor Perspectives in Biology* 5 (5): a012757. doi:10.1101/cshperspect.a012757.

Cho, Rebecca H., Hans B. Sieburg, and Christa E. Muller-Sieburg. 2008. "A New Mechanism for the Aging of Hematopoietic Stem Cells: Aging Changes the Clonal Composition of the Stem Cell Compartment but Not Individual Stem Cells." *Blood* 111 (12): 5553–61. doi:10.1182/blood-2007-11-123547.

Cifone, M G, G Migliorati, R Parroni, C Marchetti, D Millimaggi, a Santoni, and C Riccardi. 1999. "Dexamethasone-Induced Thymocyte Apoptosis: Apoptotic Signal Involves the Sequential Activation of Phosphoinositide-Specific Phospholipase C, Acidic Sphingomyelinase, and Caspases." *Blood* 93 (7): 2282–96.

Cobaleda, César, and Isidro Sánchez-García. 2009. "B-Cell Acute Lymphoblastic Leukaemia: Towards Understanding Its Cellular Origin." *BioEssays* 31 (6): 600–609. doi:10.1002/bies.200800234.

Cohen, J. 1988. "Statistical Power Analysis for the Behavioral Sciences." *Statistical Power Analysis for the Behavioral Sciences*. doi:10.1234/12345678.

Collonnier, Cécile, Aline Epert, Kostlend Mara, François Maclot, Anouchka Guyon-Debast, Florence Charlot, Charles White, Didier G. Schaefer, and Fabien Nogué. 2016. "CRISPR-Cas9 Mediated Efficient Directed Mutagenesis and RAD51-Dependent and -Independent Gene Targeting in the Moss *Physcomitrella Patens*." *Plant Biotechnology Journal*. doi:10.1111/pbi.12596.

Colucci, Francesco, Claire Soudais, Eleftheria Rosmaraki, Lesley Vanes, Victor LJ Tybulewicz, and James P Di Santo. 1999. "Dissecting NK Cell Development Using a Novel Alymphoid Mouse Model: Investigating the Role of the c-Abl Proto-Oncogene in Murine NK Cell Differentiation." *The Journal of Immunology* 162 (5): 2761–65. <http://www.jimmunol.org/cgi/content/abstract/162/5/2761>.

Cooper, Stacy L., and Patrick A. Brown. 2015. "Treatment of Pediatric Acute Lymphoblastic Leukemia." *Pediatric Clinics of North America*. doi:10.1016/j.pcl.2014.09.006.

Costa, Guilherme, Valerie Kouskoff, and Georges Lacaud. 2012. "Origin of Blood Cells and

HSC Production in the Embryo." *Trends in Immunology* 33 (5). Elsevier Ltd: 215–23.
doi:10.1016/j.it.2012.01.012.

Costas, M a, Müller Igaz L, F Holsboer, and E Arzt. 2000. "Transrepression of NF-kappaB Is Not Required for Glucocorticoid-Mediated Protection of TNF-Alpha-Induced Apoptosis on Fibroblasts." *Biochimica et Biophysica Acta* 1499 (1–2): 122–29.
doi:S0167488900001130 [pii].

Cox, Charlotte V., Roger S. Evely, Anthony Oakhill, Derwood H. Pamphilon, Nicholas J. Goulden, and Allison Blair. 2004. "Characterization of Acute Lymphoblastic Leukemia Progenitor Cells." *Blood* 104 (9): 2919–25. doi:10.1182/blood-2004-03-0901.

Cumano, Ana, and Isabelle Godin. 2007. "Ontogeny of the Hematopoietic System." *Annual Review of Immunology* 25. United States: 745–85.
doi:10.1146/annurev.immunol.25.022106.141538.

Czekanska, E. M., M. J. Stoddart, J. R. Ralphs, R. G. Richards, and J. S. Hayes. 2014. "A Phenotypic Comparison of Osteoblast Cell Lines versus Human Primary Osteoblasts for Biomaterials Testing." *Journal of Biomedical Materials Research - Part A* 102 (8): 2636–43. doi:10.1002/jbm.a.34937.

Damiano, J S, L a Hazlehurst, and W S Dalton. 2001. "Cell Adhesion-Mediated Drug Resistance (CAM-DR) Protects the K562 Chronic Myelogenous Leukemia Cell Line from Apoptosis Induced by BCR/ABL Inhibition, Cytotoxic Drugs, and Gamma-Irradiation." *Leukemia : Official Journal of the Leukemia Society of America, Leukemia Research Fund, U.K* 15 (8): 1232–39. doi:10.1038/sj.leu.2402179.

Dang, J, T Inukai, H Kurosawa, K Goi, T Inaba, N T Lenny, J R Downing, S Stifani, and A T Look. 2001. "The E2A-HLF Oncoprotein Activates Groucho-Related Genes and Suppresses Runx1." *Mol Cell Biol* 21 (17): 5935–45. doi:10.1128/MCB.21.17.5935.

Daniel, Z. C T R, S. E. Richards, A. M. Salter, and P. J. Buttery. 2004. "Insulin and Dexamethasone Regulate Stearyl-CoA Desaturase mRNA Levels and Fatty Acid Synthesis in Ovine Adipose Tissue Explants." *Journal of Animal Science* 82 (1): 231–37.

Das, Atze T, Xue Zhou, Monique Vink, Bep Klaver, Koen Verhoef, Giuseppe Marzio, and Ben Berkhout. 2004. "Viral Evolution as a Tool to Improve the Tetracycline-Regulated Gene

Expression System." *The Journal of Biological Chemistry* 279 (18). United States: 18776–82. doi:10.1074/jbc.M313895200.

David Wyatt, Dale Ramsden. 2015. "CRISPR 101: Non-Homologous End Joining."
<http://blog.addgene.org/crispr-101-non-homologous-end-joining>.

De Braekeleer, Etienne, Audrey Basinko, Nathalie Douet-Guilbert, Frederic Morel, Marie Jose Le Bris, Christian Berthou, Patrick Morice, Claude Ferec, and Marc De Braekeleer. 2010. "Cytogenetics in Pre-B and B-Cell Acute Lymphoblastic Leukemia: A Study of 208 Patients Diagnosed between 1981 and 2008." *Cancer Genetics and Cytogenetics* 200 (1): 8–15. doi:10.1016/j.cancergenryo.2010.03.004.

Den Boer, Monique L., Marjon van Slegtenhorst, Rene X. De Menezes, Meyling H. Cheok, Jessica GCAM Buijs-Gladdines, Susan TCJM Peters, Laura JCM Van Zutven, et al. 2009. "A Subtype of Childhood Acute Lymphoblastic Leukaemia with Poor Treatment Outcome: A Genome-Wide Classification Study." *The Lancet Oncology* 10 (2): 125–34. doi:10.1016/S1470-2045(08)70339-5.

DePristo, Mark A, Eric Banks, Ryan Poplin, Kiran V Garimella, Jared R Maguire, Christopher Hartl, Anthony A Philippakis, et al. 2011. "A Framework for Variation Discovery and Genotyping Using next-Generation DNA Sequencing Data." *Nature Genetics* 43 (5): 491–98. doi:10.1038/ng.806.

Drickamer, Kurt. 1999. "C-Type Lectin-like Domains." *Current Opinion in Structural Biology*. doi:10.1016/S0959-440X(99)00009-3.

Du, Pan, Warren A Kibbe, and Simon Lin. 2016. "Using Lumi , a Package Processing Illumina Microarray Overview of Lumi."

Dzierzak, E, and N A Speck. 2008. "Of Lineage and Legacy: The Development of Mammalian Hematopoietic Stem Cells." *Nat Immunol* 9 (2): 129–36. doi:ni1560 [pii]\r10.1038/ni1560.

Eijssen, Lars M T, Varshna S Goelela, Thomas Kelder, Michiel E Adriaens, Chris T Evelo, and Marijana Radonjic. 2015. "A User-Friendly Workflow for Analysis of Illumina Gene Expression Bead Array Data Available at the Arrayanalysis.org Portal." *BMC Genomics* 16 (1): 1–5. doi:10.1186/s12864-015-1689-8.

Emadali, Anouk, Neda Hoghoughi, Samuel Duley, Azadeh Hajmirza, Els Verhoeven, Francois-Loic Cosset, Philippe Bertrand, et al. 2016. "Haploinsufficiency for NR3C1, the Gene Encoding the Glucocorticoid Receptor, in Blastic Plasmacytoid Dendritic Cell Neoplasms." *Blood* 127 (24). Washington, DC: American Society of Hematology: 3040–53. doi:10.1182/blood-2015-09-671040.

ENCODE project Consortium. 2013. "An Integrated Encyclopedia of DNA Elements in the Human Genome." *Nature* 489 (7414): 57–74. doi:10.1038/nature11247.An.

Ender, Christine, Azra Krek, Marc R Friedländer, Michaela Beitzinger, Lasse Weinmann, Wei Chen, Sébastien Pfeffer, Nikolaus Rajewsky, and Gunter Meister. 2008. "A Human snoRNA with MicroRNA-Like Functions." *Molecular Cell* 32 (4): 519–28. doi:<http://dx.doi.org/10.1016/j.molcel.2008.10.017>.

Estes, David A, Debbie M Lovato, Hadya M Khawaja, Stuart S Winter, and Richard S Larson. 2007. "Genetic Alterations Determine Chemotherapy Resistance in Childhood T-ALL: Modelling in Stage-Specific Cell Lines and Correlation with Diagnostic Patient Samples." *British Journal of Haematology* 139 (1). England: 20–30. doi:10.1111/j.1365-2141.2007.06763.x.

Evans-Storms, Rosemary B., and John A. Cidlowski. 2000. "Delineation of an Antiapoptotic Action of Glucocorticoids in Hepatoma Cells: The Role of Nuclear Factor-Kb." *Endocrinology* 141 (5): 1854–62. doi:10.1210/en.141.5.1854.

Eveillard, Marion, Richard Garand, Nelly Robillard, Soraya Wuilleme, Caroline Thomas, Marion Strullu, Fanny Rialland, et al. 2013. "Paired Immunophenotype Comparison Of Diagnosis and Relapse Samples In B-Lineage Acute Lymphoblastic Leukemia." Edited by Marie-Christine Bene. *Blood* 122 (21): 4954 LP-4954. <http://www.bloodjournal.org/content/122/21/4954.abstract>.

Fahiminiya, Somayyeh, Jacek Majewski, Hadil Al-Jallad, Pierre Moffatt, John Mort, Francis H. Glorieux, Paul Roschger, Klaus Klaushofer, and Frank Rauch. 2014. "Osteoporosis Caused by Mutations in PLS3: Clinical and Bone Tissue Characteristics." *Journal of Bone and Mineral Research* 29 (8): 1805–14. doi:10.1002/jbmr.2208.

Filipovich, Alexandra, Rajesh K Gandhirajan, Iris Gehrke, Simon J Poll-Wolbeck, and Karl-Anton Kreuzer. 2010. "Evidence for Non-Functional Dickkopf-1 (DKK-1) Signaling in

Chronic Lymphocytic Leukemia (CLL)." *European Journal of Haematology* 85 (4). England: 309–13. doi:10.1111/j.1600-0609.2010.01494.x.

Findley, H W, M D Cooper, T H Kim, C Alvarado, and A H Ragab. 1982. "Two New Acute Lymphoblastic Leukemia Cell Lines with Early B-Cell Phenotypes." *Blood* 60 (6): 1305–9. <http://www.bloodjournal.org/content/60/6/1305.abstract>.

Fischer, Ute, Michael Forster, Anna Rinaldi, Thomas Risch, Stéphanie Sungalee, Hans-Jörg Warnatz, Beat Bornhauser, et al. 2015. "Genomics and Drug Profiling of Fatal TCF3-HLF-Positive Acute Lymphoblastic Leukemia Identifies Recurrent Mutation Patterns and Therapeutic Options." *Nature Genetics* 47 (9): 1020–29. doi:10.1038/ng.3362.

Forster, V J, M H Nahari, N Martinez-Soria, a K Bradburn, a Ptasinska, S a Assi, S E Fordham, et al. 2015. "The Leukemia-Associated RUNX1/ETO Oncoprotein Confers a Mutator Phenotype." *Leukemia* 30 (June). Macmillan Publishers Limited: 1–4. doi:10.1038/leu.2015.133.

Freedman, D. M., P. Stewart, R. A. Kleinerman, S. Wacholder, E. E. Hatch, R. E. Tarone, L. L. Robison, and M. S. Linet. 2001. "Household Solvent Exposures and Childhood Acute Lymphoblastic Leukemia." *American Journal of Public Health* 91 (4): 564–67. <http://www.ncbi.nlm.nih.gov/pmc/articles/PMC1446651/>.

Freedman, L. P., and B. F. Luisi. 1993. "On the Mechanism of DNA Binding by Nuclear Hormone Receptors: A Structural and Functional Perspective." *Journal of Cellular Biochemistry* 51 (2): 140–50. doi:10.1002/jcb.240510205.

Freireich, EMIL J, EDMUND Gehan, EMIL Frei, LESLIE R Schroeder, IRVING J Wolman, RACHAD ANBARI, E OMAR BURGERT, et al. 1963. "The Effect of 6-Mercaptopurine on the Duration of Steroid-Induced Remissions in Acute Leukemia: A Model for Evaluation of Other Potentially Useful Therapy." *Blood* 21 (6): 699–716. <http://www.bloodjournal.org/content/21/6/699.abstract>.

Friedenson, Bernard. 2007. "The BRCA1/2 Pathway Prevents Hematologic Cancers in Addition to Breast and Ovarian Cancers." *BMC Cancer* 7 (1): 1–11. doi:10.1186/1471-2407-7-152.

Fu, Lin, Jinlong Shi, Kai Hu, Jijun Wang, Weidong Wang, and Xiaoyan Ke. 2015. "Mitogen-

Activated Protein Kinase Binding Protein 1 (MAPKBP1) Is an Unfavorable Prognostic Biomarker in Cytogenetically Normal Acute Myeloid Leukemia." *Oncotarget* 6 (10): 8144–54. doi:10.18632/oncotarget.3519.

Gaj, Thomas, Charles A. Gersbach, and Carlos F. Barbas. 2013. "ZFN, TALEN, and CRISPR/Cas-Based Methods for Genome Engineering." *Trends in Biotechnology* 31 (7): 397–405. doi:10.1016/j.tibtech.2013.04.004.

Gale, K B, a M Ford, R Repp, a Borkhardt, C Keller, O B Eden, and M F Greaves. 1997. "Backtracking Leukemia to Birth: Identification of Clonotypic Gene Fusion Sequences in Neonatal Blood Spots." *Proceedings of the National Academy of Sciences of the United States of America* 94 (25): 13950–54. doi:10.1073/pnas.94.25.13950.

Garrett, Roger A., Gisle Vestergaard, and Shiraz A. Shah. 2011. "Archaeal CRISPR-Based Immune Systems: Exchangeable Functional Modules." *Trends in Microbiology* 19 (11): 549–56. doi:10.1016/j.tim.2011.08.002.

Geng, Huimin, Christian Hurtz, Kyle B. Lenz, Zhengshan Chen, Dirk Baumjohann, Sarah Thompson, Natalya A. Goloviznina, et al. 2015. "Self-Enforcing Feedback Activation between BCL6 and Pre-B Cell Receptor Signaling Defines a Distinct Subtype of Acute Lymphoblastic Leukemia." *Cancer Cell* 27 (3): 409–25. doi:10.1016/j.ccr.2015.02.003.

Gillet, Jean-Pierre, Anna Maria Calcagno, Sudhir Varma, Miguel Marino, Lisa J Green, Meena I Vora, Chirayu Patel, et al. 2011. "Redefining the Relevance of Established Cancer Cell Lines to the Study of Mechanisms of Clinical Anti-Cancer Drug Resistance." *Proceedings of the National Academy of Sciences of the United States of America* 108 (46): 18708–13. doi:10.1073/pnas.1111840108.

Gillet, Jean-Pierre, Sudhir Varma, and Michael M Gottesman. 2013. "The Clinical Relevance of Cancer Cell Lines." *Journal of the National Cancer Institute* 105 (7): 452–58. doi:10.1093/jnci/djt007.

Glass, Christopher K, and Kaoru Saijo. 2010. "Nuclear Receptor Transrepression Pathways That Regulate Inflammation in Macrophages and T Cells." *Nat Rev Immunol* 10 (5). Nature Publishing Group: 365–76. <http://dx.doi.org/10.1038/nri2748>.

Gobeil, Stephane, Xiaochun Zhu, Charles J. Doillon, and Michael R. Green. 2008. "A Genome-

Wide shRNA Screen Identifies GAS1 as a Novel Melanoma Metastasis Suppressor Gene." *Genes and Development* 22 (21): 2932–40. doi:10.1101/gad.1714608.

Godin, Isabelle, and Ana Cumano. 2005. "Of Birds and Mice: Hematopoietic Stem Cell Development." *The International Journal of Developmental Biology* 49 (2–3): 251–57. doi:10.1387/ijdb.041945ig.

Godley, Lucy A., and Richard A. Larson. 2008. "Therapy-Related Myeloid Leukemia." *Seminars in Oncology* 35 (4): 418–29. doi:10.1053/j.seminoncol.2008.04.012.

González, D, A Balanzategui, R García-Sanz, N Gutiérrez, C Seabra, J J M van Dongen, M González, and J F San Miguel. 2003. "Incomplete DJH Rearrangements of the IgH Gene Are Frequent in Multiple Myeloma Patients: Immunobiological Characteristics and Clinical Implications." *Leukemia* 17 (7). Nature Publishing Group: 1398–1403. doi:10.1038/sj.leu.2402964.

Granziero, Luisa, Paola Circosta, Cristina Scielzo, Elisa Frisaldi, Stefania Stella, Massimo Geuna, Silvia Giordano, Paolo Ghia, and Federico Caligaris-Cappio. 2003. "CD100/plexin-B1 Interactions Sustain Proliferation and Survival of Normal and Leukemic CD5+ B Lymphocytes." *Blood* 101 (5): 1962–69. doi:10.1182/blood-2002-05-1339.

Greaves, M F. 1997. "Aetiology of Acute Leukaemia." *Lancet (London, England)* 349 (9048). England: 344–49.

Gruber, G, M Carlet, E Türtscher, B Meister, J a E Irving, C Ploner, and R Kofler. 2009. "Levels of Glucocorticoid Receptor and Its Ligand Determine Sensitivity and Kinetics of Glucocorticoid-Induced Leukemia Apoptosis." *Leukemia : Official Journal of the Leukemia Society of America, Leukemia Research Fund, U.K* 23 (4): 820–23. doi:10.1038/leu.2009.35.

Grzegorz, Ira, Achille Pellicioli, Alitukiriza Balija, Xuan Wang, Simona Fiorani, Walter Carotenuto, Giordano Liberi, et al. 2004. "DNA End Resection, Homologous Recombination and DNA Damage Checkpoint Activation Require CDK1." *Nature* 431 (October): 1011–17. doi:10.1038/nature02991.1.

Hala, Monika, Bernd L. Hartmann, Günther Bock, Stephan Geley, and Reinhard Kofler. 1996. "Glucocorticoid-Receptor-Gene Defects and Resistance to Glucocorticoid-Induced

Apoptosis in Human Leukemic Cell Lines." *International Journal of Cancer* 68 (5): 663–68. doi:10.1002/(SICI)1097-0215(19961127)68:5<663::AID-IJC17>3.0.CO;2-2.

Harrison, Christine J. 2009. "Cytogenetics of Paediatric and Adolescent Acute Lymphoblastic Leukaemia." *British Journal of Haematology* 144 (2): 147–56. doi:10.1111/j.1365-2141.2008.07417.x.

Helmborg, A, N Auphan, C Caelles, and M Karin. 1995. "Glucocorticoid-Induced Apoptosis of Human Leukemic Cells Is Caused by the Repressive Function of the Glucocorticoid Receptor." *The EMBO Journal* 14 (3): 452–60.

<http://www.ncbi.nlm.nih.gov/pmc/articles/PMC144333/>

Hirakawa, Yasuko, Laura J Nary, and Rheem D Medh. 2009. "Glucocorticoid Evoked Upregulation of RCAN1-1 in Human Leukemic CEM Cells Susceptible to Apoptosis." *Journal of Molecular Signaling* 4: 6. doi:10.1186/1750-2187-4-6.

Hogan, Laura E., Julia A. Meyer, Jun Yang, Jinhua Wang, Nicholas Wong, Wenjian Yang, Gregory Condos, et al. 2011. "Integrated Genomic Analysis of Relapsed Childhood Acute Lymphoblastic Leukemia Reveals Therapeutic Strategies." *Blood* 118 (19): 5218–26. doi:10.1182/blood-2011-04-345595.

Housden, Benjamin E, and Norbert Perrimon. 2016. "Comparing CRISPR and RNAi-Based Screening Technologies." *Nat Biotech* 34 (6). Nature Publishing Group, a division of Macmillan Publishers Limited. All Rights Reserved.: 621–23.

<http://dx.doi.org/10.1038/nbt.3599>.

Huguet, Françoise, Thibaut Leguay, Xavier Thomas, Nicolas Boissel, Martine Escoffre-Barbe, Patrice Chevallier, Mathilde Hunault, et al. 2016. "The Upper Age Limit for a Pediatric-Inspired Therapy in Younger Adults with Ph-Negative Acute Lymphoblastic Leukemia (ALL)? Analysis of the Graall-2005 Study." *Blood* 128 (22). American Society of Hematology: 762. <http://www.bloodjournal.org/content/128/22/762>.

Hunger, S P, P E Devaraj, L Foroni, L M Secker-Walker, and M L Cleary. 1994. "Two Types of Genomic Rearrangements Create Alternative E2A-HLF Fusion Proteins in t(17;19)-ALL." *Blood* 83 (10): 2970–77.

<http://www.ncbi.nlm.nih.gov/pmc/articles/PMC144333/>

brary.org/content/83/10/2970.full.pdf.

Hunger, S P, K Ohyashiki, K Toyama, and M L Cleary. 1992. "Hlf, a Novel Hepatic bZIP Protein, Shows Altered DNA-Binding Properties Following Fusion to E2A in t(17;19) Acute Lymphoblastic Leukemia." *Genes & Development* 6 (9). United States: 1608–20.

Huo, Yanwu, Ki Hyun Nam, Fang Ding, Heejin Lee, Lijie Wu, Yibei Xiao, M Daniel Farchione, et al. 2014. "Structures of CRISPR Cas3 Offer Mechanistic Insights into Cascade-Activated DNA Unwinding and Degradation." *Nature Structural & Molecular Biology* 21 (9): 771–77. doi:10.1038/nsmb.2875.

Inaba, Hiroto, and Ching-hon Pui. 2010. "Glucocorticoid Use in Acute Lymphoblastic Leukaemia." *The Lancet. Oncology* 11 (11): 1096–1106. doi:10.1016/S1470-2045(10)70114-5.

Infante-Rivard, C, I Fortier, and E Olson. 2000. "Markers of Infection, Breast-Feeding and Childhood Acute Lymphoblastic Leukaemia." *British Journal of Cancer* 83 (11). Nature Publishing Group: 1559–64. doi:10.1054/bjoc.2000.1495.

Inoue, H, H Takemura, Y Kawai, A Yoshida, T Ueda, and T Miyashita. 2002. "Dexamethasone-Resistant Human Pre-B Leukemia 697 Cell Line Evolving Elevation of Intracellular Glutathione Level: An Additional Resistance Mechanism." *Jpn J Cancer Res* 93 (5): 582–90.
http://www.ncbi.nlm.nih.gov/entrez/query.fcgi?cmd=Retrieve&db=PubMed&dopt=Citation&list_uids=12036455.

Integrated DNA Technologies. 2016. "CRISPR Frequently Asked Questions." *Integrated DNA Technologies*, 1–9. www.idtdna.com.

Inukai, T, T Inaba, S Ikushima, and A T Look. 1998. "The AD1 and AD2 Transactivation Domains of E2A Are Essential for the Antiapoptotic Activity of the Chimeric Oncoprotein E2A-HLF." *Mol Cell Biol* 18 (10): 6035–43.
[http://www.ncbi.nlm.nih.gov/pubmed/9742120%5Cnhttp://www.ncbi.nlm.nih.gov/pmc/articles/PMC109189/pdf/mb006035.pdf%5Cnhttp://mcb.asm.org/content/18/10/6035.full.pdf#page=1&view=FitH%5Cnhttp://www.ncbi.nlm.nih.gov/p](http://www.ncbi.nlm.nih.gov/pubmed/9742120%5Cnhttp://www.ncbi.nlm.nih.gov/pmc/articles/PMC109189/pdf/mb006035.pdf%5Cnhttp://mcb.asm.org/content/18/10/6035.full.pdf%5Cnhttp://mcb.asm.org/content/18/10/6035.full.pdf#page=1&view=FitH%5Cnhttp://www.ncbi.nlm.nih.gov/p).

Inukai, Takeshi, Akira Inoue, Hidemitsu Kurosawa, Kumiko Goi, Tetsuharu Shinjyo, Keiya Ozawa, Mao Mao, Toshiya Inaba, and A. Thomas Look. 1999. "SLUG, a Ces-1-Related Zinc Finger Transcription Factor Gene with Antiapoptotic Activity, Is a Downstream Target of the E2A-HLF Oncoprotein." *Molecular Cell* 4 (3): 343–52. doi:10.1016/S1097-2765(00)80336-6.

Irving, J., L. Minto, S. Bailey, and A. Hall. 2005. "Loss of Heterozygosity and Somatic Mutations of the Glucocorticoid Receptor Gene Are Rarely Found at Relapse in Pediatric Acute Lymphoblastic Leukemia but May Occur in a Subpopulation Early in the Disease Course." *Cancer Research* 65 (21): 9712–18. doi:10.1158/0008-5472.CAN-05-1227.

Irving, Julie, Elizabeth Matheson, Lynne Minto, Helen Blair, Marian Case, Christina Halsey, Isabella Swidenbank, et al. 2014. "Ras Pathway Mutations Are Prevalent in Relapsed Childhood Acute Lymphoblastic Leukemia and Confer Sensitivity to MEK Inhibition." *Blood* 124 (23): 3420–30. doi:10.1182/blood-2014-04-531871.

Ishino, Y, H Shinagawa, K Makino, M Amemura, and A Nakata. 1987. "Nucleotide Sequence of the lap Gene, Responsible for Alkaline Phosphatase Isozyme Conversion in Escherichia Coli, and Identification of the Gene Product." *Journal of Bacteriology* 169 (12): 5429–33.

<http://www.ncbi.nlm.nih.gov/pmc/articles/PMC213968/>&tool=pmcentrez&rendertype=abstract.

Ito, Kazuhiro, Satoshi Yamamura, Sarah Essilfie-Quaye, Borja Cosio, Misako Ito, Peter J Barnes, and Ian M Adcock. 2006. "Histone Deacetylase 2-Mediated Deacetylation of the Glucocorticoid Receptor Enables NF-kappaB Suppression." *The Journal of Experimental Medicine* 203 (1). United States: 7–13. doi:10.1084/jem.20050466.

Itoh, K, H Tezuka, H Sakoda, M Konno, K Nagata, T Uchiyama, H Uchino, and K J Mori. 1989. "Reproducible Establishment of Hemopoietic Supportive Stromal Cell Lines from Murine Bone Marrow." *Experimental Hematology* 17 (2). UNITED STATES: 145–53.

Ivanovs, Andrejs, Stanislav Rybtsov, Lindsey Welch, Richard A. Anderson, Marc L. Turner, and Alexander Medvinsky. 2011. "Highly Potent Human Hematopoietic Stem Cells First Emerge in the Intraembryonic Aorta-Gonad-Mesonephros Region." *The Journal of Experimental Medicine* 208 (12): 2417–27. doi:10.1084/jem.20111688.

Jaeger, Samira, Miquel Duran-Frigola, and Patrick Aloy. 2015. "Drug Sensitivity in Cancer Cell Lines Is Not Tissue-Specific." *Molecular Cancer* 14 (February). London: BioMed Central: 40. doi:10.1186/s12943-015-0312-6.

Jagannathan-Bogdan, M., and L. I. Zon. 2013. "Hematopoiesis." *Development* 140 (12): 2463–67. doi:10.1242/dev.083147.

Jasin, Maria, and Rodney Rothstein. 2013. "Repair of Strand Breaks by Homologous Recombination." *Cold Spring Harbor Perspectives in Biology* 5 (11). Cold Spring Harbor Laboratory Press: a012740. doi:10.1101/cshperspect.a012740.

Jinek, Martin, Krzysztof Chylinski, Ines Fonfara, Michael Hauer, Jennifer A Doudna, and Emmanuelle Charpentier. 2012. "A Programmable Dual-RNA – Guided DNA Endonuclease in Adaptive Bacterial Immunity." *Science (New York, N.Y.)* 337 (August): 816–22. doi:10.1126/science.1225829.

Jinek, Martin, Fuguo Jiang, David W Taylor, Samuel H Sternberg, Emine Kaya, Enbo Ma, Carolin Anders, et al. 2014. "Structures of Cas9 Endonucleases Reveal RNA-Mediated Conformational Activation." *Science (New York, N.Y.)* 343 (6176): 1247997. doi:10.1126/science.1247997.

Jing, Duohui, Vivek A. Bhadri, Dominik Beck, Julie A I Thoms, Nurul A. Yakob, Jason W H Wong, Kathy Knezevic, John E. Pimanda, and Richard B. Lock. 2015. "Opposing Regulation of BIM and BCL2 Controls Glucocorticoid-Induced Apoptosis of Pediatric Acute Lymphoblastic Leukemia Cells." *Blood* 125 (2): 273–83. doi:10.1182/blood-2014-05-576470.

Johanssen, Sarah, and Bruno Allolio. 2007. "Mifepristone (RU 486) in Cushing's Syndrome." *European Journal of Endocrinology*. doi:10.1530/EJE-07-0458.

John, Sam, Peter J Sabo, Robert E Thurman, Myong-Hee Sung, Simon C Biddie, Thomas A Johnson, Gordon L Hager, and John A Stamatoyannopoulos. 2011. "Chromatin Accessibility Pre-Determines Glucocorticoid Receptor Binding Patterns." *Nat Genet* 43 (3). Nature Publishing Group, a division of Macmillan Publishers Limited. All Rights Reserved.: 264–68. <http://dx.doi.org/10.1038/ng.759>.

Johnson, T.A., C. Elbi, B.S. Parekh, G.L. Hager, and S. John. 2008. "Chromatin Remodeling

Complexes Interact Dynamically with a Glucocorticoid Receptor–regulated Promoter.”
Molecular Biology of the Cell 82 (19): 3308–22. doi:10.1091/mbc.E08.

Jones, B, A I Freeman, J J Shuster, C Jacquillat, M Weil, C Pochedly, L Sinks, L Chevalier, H M Maurer, and K Koch. 1991. “Lower Incidence of Meningeal Leukemia When Prednisone Is Replaced by Dexamethasone in the Treatment of Acute Lymphocytic Leukemia.”
Medical and Pediatric Oncology 19 (4): 269–75. doi:10.1002/mpo.2950190411.

Jones, Courtney L., Christy M. Gearheart, Susan Fosmire, Cristina Delgado-Martin, Nikki A. Evensen, Karen Bride, Angela J. Waanders, et al. 2015. “MAPK Signaling Cascades Mediate Distinct Glucocorticoid Resistance Mechanisms in Pediatric Leukemia.” *Blood* 126 (19): 2202–12. doi:10.1182/blood-2015-04-639138.

Kanz, Dirk, Martina Konantz, Elisa Alghisi, Trista E. North, and Claudia Lengerke. 2016. “Endothelial-to-Hematopoietic Transition: Notch-Ing Vessels into Blood.” *Annals of the New York Academy of Sciences*. doi:10.1111/nyas.13030.

Kappelmann, Melanie, Anja Bosserhoff, and Silke Kuphal. 2014. “AP-1/c-Jun Transcription Factors: Regulation and Function in Malignant Melanoma.” *European Journal of Cell Biology* 93 (1–2). Germany: 76–81. doi:10.1016/j.ejcb.2013.10.003.

Kaspers, G J, R Pieters, E Klumper, F C De Waal, and A J Veerman. 1994. “Glucocorticoid Resistance in Childhood Leukemia.” *Leukemia & Lymphoma* 13 (3–4): 187–201. doi:10.3109/10428199409056282.

Kelly, Audrey, Holly Bowen, Young Koo Jee, Nabila Mahfiche, Cecilia Soh, Tak Lee, Catherine Hawrylowicz, and Paul Lavender. 2008. “The Glucocorticoid Receptor β Isoform Can Mediate Transcriptional Repression by Recruiting Histone Deacetylases.” *Journal of Allergy and Clinical Immunology* 121 (1): 203–208.e1. doi:10.1016/j.jaci.2007.09.010.

Kennedy, Marion, Sunita L. D’Souza, Macarena Lynch-Kattman, Staci Schwantz, and Gordon Keller. 2007. “Development of the Hemangioblast Defines the Onset of Hematopoiesis in Human ES Cell Differentiation Cultures.” In *Blood*, 109:2679–87. doi:10.1182/blood-2006-09-047704.

Kharbanda, S, T Nakamura, R Stone, R Hass, S Bernstein, R Datta, V P Sukhatme, and D Kufe. 1991. “Expression of the Early Growth Response 1 and 2 Zinc Finger Genes during

Induction of Monocytic Differentiation." *The Journal of Clinical Investigation* 88 (2): 571–77. doi:10.1172/JCI115341.

Kinyamu, H Karimi, Jennifer B Collins, Sherry F Grissom, Pratibha B Hebbar, and Trevor K Archer. 2008. "Genome Wide Transcriptional Profiling in Breast Cancer Cells Reveals Distinct Changes in Hormone Receptor Target Genes and Chromatin Modifying Enzymes after Proteasome Inhibition." *Molecular Carcinogenesis* 47 (11). United States: 845–85. doi:10.1002/mc.20440.

Klein, F, N Feldhahn, L Harder, H Wang, M Wartenberg, W K Hofmann, P Wernet, R Siebert, and M Muschen. 2004. "The BCR-ABL1 Kinase Bypasses Selection for the Expression of a Pre-B Cell Receptor in Pre-B Acute Lymphoblastic Leukemia Cells." *J Exp Med* 199 (5): 673–85. doi:10.1084/jem.20031637.

Klumper, E, R Pieters, a J Veerman, D R Huismans, a H Loonen, K Hählen, G J Kaspers, E R van Wering, R Hartmann, and G Henze. 1995. "In Vitro Cellular Drug Resistance in Children with Relapsed/refractory Acute Lymphoblastic Leukemia." *Blood* 86 (10): 3861–68. <http://www.ncbi.nlm.nih.gov/pubmed/7579354>.

Koper, J W, R P Stolk, P de Lange, N a Huizenga, G J Molijn, H a Pols, D E Grobbee, et al. 1997. "Lack of Association between Five Polymorphisms in the Human Glucocorticoid Receptor Gene and Glucocorticoid Resistance." *Human Genetics* 99 (5): 663–68. doi:10.1007/s004390050425.

Kumanogoh, Atsushi, and Hitoshi Kikutani. 2013. "Immunological Functions of the Neuropilins and Plexins as Receptors for Semaphorins." *Nature Reviews. Immunology* 13 (11): 802–14. doi:10.1038/nri3545.

Kuscu, C, S Arslan, R Singh, J Thorpe, and M Adli. 2014. "Genome-Wide Analysis Reveals Characteristics of off-Target Sites Bound by the Cas9 Endonuclease." *Nat Biotechnol* 32 (7): 677–83. doi:10.1038/nbt.2916.

Kuster, Lilian, Reinhard Grausenburger, Gerhard Fuka, Ulrike Kaindl, Gerd Krapf, Andrea Inthal, Georg Mann, et al. 2011. "ETV6/RUNX1-Positive Relapses Evolve from an Ancestral Clone and Frequently Acquire Deletions of Genes Implicated in Glucocorticoid Signaling." *Blood* 117 (9): 2658–67. doi:10.1182/blood-2010-03-275347.

Landau, D a, S L Carter, G Getz, and C J Wu. 2014. "Clonal Evolution in Hematological Malignancies and Therapeutic Implications." *Leukemia* 28 (1): 34–43. doi:10.1038/leu.2013.248.

Landowski, Terry H, Nancy E Olashaw, Deepak Agrawal, and William S Dalton. 2003. "Cell Adhesion-Mediated Drug Resistance (CAM-DR) Is Associated with Activation of NF-Kappa B (RelB/p50) in Myeloma Cells." *Oncogene* 22 (16): 2417–21. doi:10.1038/sj.onc.1206315.

Lapidot, T, C Sirard, J Vormoor, B Murdoch, T Hoang, J Caceres-Cortes, M Minden, B Paterson, M a Caligiuri, and J E Dick. 1994. "A Cell Initiating Human Acute Myeloid Leukaemia after Transplantation into SCID Mice." *Nature* 367 (6464): 645–48. doi:10.1038/367645a0.

Latchoumanin, Olivier, Vanessa Mynard, Jocelyne Devin-Leclerc, Marie-Annick Dugué, Xavier Bertagna, and Maria Grazia Catelli. 2007. "Reversal of Glucocorticoids-Dependent Proopiomelanocortin Gene Inhibition by Leukemia Inhibitory Factor." *Endocrinology* 148 (1): 422–32. <http://dx.doi.org/10.1210/en.2006-0460>.

Latif, Elda. 2012. "Understanding the Proliferative and Self Renewal Potential of Different Leukaemic Stem Cell Populations." Doctoral thesis, Retrieved from Newcastle University eThesis database. <http://hdl.handle.net/10443/1828>

le Viseur, Christoph, Marc Hotfilder, Simon Bomken, Kerrie Wilson, Silja Rottgers, Andre Schrauder, Annegret Rosemann, Julie Irving, Ronald W. Stam, Leonard D. Shultz, Jochen Harbott, Heribert Jurgens, et al. 2008. "In Childhood Acute Lymphoblastic Leukemia, Blasts at Different Stages of Immunophenotypic Maturation Have Stem Cell Properties." *Cancer Cell* 14 (1): 47–58. doi:10.1016/j.ccr.2008.05.015.

le Viseur, Christoph, Marc Hotfilder, Simon Bomken, Kerrie Wilson, Silja Rottgers, Andre Schrauder, Annegret Rosemann, Julie Irving, Ronald W. Stam, Leonard D. Shultz, Jochen Harbott, Heribert Jurgens, et al. 2008. "In Childhood Acute Lymphoblastic Leukemia, Blasts at Different Stages of Immunophenotypic Maturation Have Stem Cell Properties." *Cancer Cell* 14 (1). Elsevier: 47–58. doi:10.1016/j.ccr.2008.05.015.

LeBien, T W. 2000. "Fates of Human B-Cell Precursors." *Blood* 96 (1): 9–23. <http://www.ncbi.nlm.nih.gov/pubmed/10891425>.

Leclerc, Gilles M, Shuhua Zheng, Guy J Leclerc, Joanna DeSalvo, Ronan T Swords, and Julio C Barredo. 2016. "The NEDD8-Activating Enzyme Inhibitor Pevonedistat Activates the eIF2 α ; and mTOR Pathways Inducing UPR-Mediated Cell Death in Acute Lymphoblastic Leukemia." *Leukemia Research* 50 (September). Elsevier: 1–10. doi:10.1016/j.leukres.2016.09.007.

Lee, Syng-Ook, Xi Li, Shaheen Khan, and Stephen Safe. 2011. "Targeting NR4A1 (TR3) in Cancer Cells and Tumors." *Expert Opinion on Therapeutic Targets* 15 (2). Taylor & Francis: 195–206. doi:10.1517/14728222.2011.547481.

Lee, Yoontae, Chiyoung Ahn, Jinju Han, Hyounjeong Choi, Jaekwang Kim, Jeongbin Yim, Junho Lee, et al. 2003. "The Nuclear RNase III Drosha Initiates microRNA Processing." *Nature* 425 (6956): 415–19. <http://dx.doi.org/10.1038/nature01957>.

Lemoine, F M, R K Humphries, S D Abraham, G Krystal, and C J Eaves. 1988. "Partial Characterization of a Novel Stromal Cell-Derived Pre-B-Cell Growth Factor Active on Normal and Immortalized Pre-B Cells." *Experimental Hematology* 16 (8). UNITED STATES: 718–26.

Lessard, Julie, Armin Schumacher, Unnur Thorsteinsdottir, Maarten Van Lohuizen, Terry Magnuson, and Guy Sauvageau. 1999. "Functional Antagonism of the Polycomb-Group Genes Eed and Bmi1 in Hemopoietic Cell Proliferation." *Genes and Development* 13 (20): 2691–2703. doi:10.1101/gad.13.20.2691.

Lewis-Tuffin, Laura J, Christine M Jewell, Rachelle J Bienstock, Jennifer B Collins, and John A Cidlowski. 2007. "Human Glucocorticoid Receptor Beta Binds RU-486 and Is Transcriptionally Active." *Molecular and Cellular Biology* 27 (6): 2266–82. doi:10.1128/MCB.01439-06.

Li, Wei, Han Xu, Tengfei Xiao, Le Cong, Michael I Love, Feng Zhang, Rafael a Irizarry, Jun S Liu, Myles Brown, and X Shirley Liu. 2014. "MAGECK Enables Robust Identification of Essential Genes from Genome-Scale CRISPR/Cas9 Knockout Screens." *Genome Biology* 15 (12): 554. doi:10.1186/s13059-014-0554-4.

Liem, Natalia L M, Rachael A. Papa, Christopher G. Milross, Michael A. Schmid, Mayamin Tajbakhsh, Seoyeon Choi, Carole D. Ramirez, et al. 2004. "Characterization of Childhood Acute Lymphoblastic Leukemia Xenograft Models for the Preclinical Evaluation of New

- Therapies." *Blood* 103 (10): 3905–14. doi:10.1182/blood-2003-08-2911.
- Lim, Joshua Yew-Suang, Smita Bhatia, Leslie L Robison, and Jun J Yang. 2014. "Genomics of Racial and Ethnic Disparities in Childhood Acute Lymphoblastic Leukemia." *Cancer* 120 (7): 955–62. doi:10.1002/cncr.28531.
- Lin, Simon M, Pan Du, Wolfgang Huber, and Warren A Kibbe. 2008. "Model-Based Variance-Stabilizing Transformation for Illumina Microarray Data." *Nucleic Acids Research* 36 (2). England: e11. doi:10.1093/nar/gkm1075.
- Lindsey, J W. 2007. "Dexamethasone-Induced Ras-Related Protein 1 Is a Potential Regulatory Protein in B Lymphocytes." *International Immunology* 19 (5). England: 583–90. doi:10.1093/intimm/dxm023.
- Linet, M S, E E Hatch, R A Kleinerman, L L Robison, W T Kaune, D R Friedman, R K Severson, et al. 1997. "Residential Exposure to Magnetic Fields and Acute Lymphoblastic Leukemia in Children." *N Engl J Med* 337 (1): 1–7. doi:10.1056/NEJM199707033370101.
- Little, Marie-térèse, and Rainer Storb. 2002. "History of Haematopoietic Stem-Cell Transplantation." *Nature Reviews. Cancer* 2 (3): 231–38. doi:10.1038/nrc748.
- Liu, Grace J., Luisa Cimmino, Julian G. Jude, Yifang Hu, Matthew T. Witkowski, Mark D. McKenzie, Mutlu Kartal-Kaess, et al. 2014. "Pax5 Loss Imposes a Reversible Differentiation Block in B-Progenitor Acute Lymphoblastic Leukemia." *Genes and Development* 28 (12): 1337–50. doi:10.1101/gad.240416.114.
- Lock, Richard B, Natalia Liem, Monica L Farnsworth, Christopher G Milross, Chengyuan Xue, Mayamin Tajbakhsh, Michelle Haber, Murray D Norris, Glenn M Marshall, and Alison M Rice. 2002. "The Nonobese Diabetic/severe Combined Immunodeficient (NOD/SCID) Mouse Model of Childhood Acute Lymphoblastic Leukemia Reveals Intrinsic Differences in Biologic Characteristics at Diagnosis and Relapse." *Blood* 99 (11). United States: 4100–4108.
- Lu, Desheng, Yandong Zhao, Rommel Tawatao, Howard B Cottam, Malini Sen, Lorenzo M Leoni, Thomas J Kipps, Maripat Corr, and Dennis A Carson. 2004. "Activation of the Wnt Signaling Pathway in Chronic Lymphocytic Leukemia." *Proceedings of the National Academy of Sciences of the United States of America* 101 (9). United States: 3118–23.

doi:10.1073/pnas.0308648100.

- Lu, Nick Z., and John A. Cidlowski. 2005. "Translational Regulatory Mechanisms Generate N-Terminal Glucocorticoid Receptor Isoforms with Unique Transcriptional Target Genes." *Molecular Cell* 18 (3): 331–42. doi:10.1016/j.molcel.2005.03.025.
- Lu, Qing, David C Pallas, Howard K Surks, Wendy E Baur, Michael E Mendelsohn, and Richard H Karas. 2004. "Striatin Assembles a Membrane Signaling Complex Necessary for Rapid, Nongenomic Activation of Endothelial NO Synthase by Estrogen Receptor Alpha." *Proceedings of the National Academy of Sciences of the United States of America* 101 (49): 17126–31. doi:10.1073/pnas.0407492101.
- Luchino, Jonathan, Mélanie Hocine, Marie Claude Amoureaux, Benjamin Gibert, Agnès Bernet, Amélie Royet, Isabelle Treilleux, et al. 2013. "Semaphorin 3E Suppresses Tumor Cell Death Triggered by the Plexin D1 Dependence Receptor in Metastatic Breast Cancers." *Cancer Cell* 24 (5): 673–85. doi:10.1016/j.ccr.2013.09.010.
- Lukk, Margus, Misha Kapushesky, Janne Nikkilä, Helen Parkinson, Angela Goncalves, Wolfgang Huber, Esko Ukkonen, and Alvis Brazma. 2010. "A Global Map of Human Gene Expression." *Nature Biotechnology* 28 (4): 322–24. doi:10.1038/nbt0410-322.
- Ma, Xiaotu, Michael Edmonson, Donald Yergeau, Donna M Muzny, Oliver A Hampton, Michael Rusch, Guangchun Song, et al. 2015. "Rise and Fall of Subclones from Diagnosis to Relapse in Pediatric B-Acute Lymphoblastic Leukaemia." *Nature Communications* 6 (March). England: 6604. doi:10.1038/ncomms7604.
- MacArthur, Amy C, Mary L McBride, John J Spinelli, Sharon Tamaro, Richard P Gallagher, and Gilles P Theriault. 2008. "Risk of Childhood Leukemia Associated with Vaccination, Infection, and Medication Use in Childhood: The Cross-Canada Childhood Leukemia Study." *American Journal of Epidemiology* 167 (5). United States: 598–606. doi:10.1093/aje/kwm339.
- Madden, Tom. 2002. "The BLAST Sequence Analysis Tool." *The NCBI Handbook [Internet]*, 1–15. <http://www.ncbi.nlm.nih.gov/books/NBK21097/>.
- Maia, Raquel da Rocha Paiva, and Victor Wünsch. 2013. "Infection and Childhood Leukemia: Review of Evidence." *Revista de Saúde Pública* 47 (6). Faculdade de Saúde Pública da

Universidade de São Paulo: 1172–85. doi:10.1590/S0034-8910.2013047004753.

Makarova, Kira S, Daniel H Haft, Rodolphe Barrangou, Stan J J Brouns, Emmanuelle Charpentier, Philippe Horvath, Sylvain Moineau, et al. 2011. “Evolution and Classification of the CRISPR–Cas Systems.” *Nature Reviews Microbiology* 9 (6). Nature Publishing Group, a division of Macmillan Publishers Limited. All Rights Reserved.: 467–77. doi:10.1038/nrmicro2577.

Manwani, Neetu, Stephane Gagnon, Martin Post, Stephen Joza, Louis Muglia, Salomon Cornejo, Feige Kaplan, and Neil B Sweezey. 2010. “Reduced Viability of Mice with Lung Epithelial-Specific Knockout of Glucocorticoid Receptor.” *American Journal of Respiratory Cell and Molecular Biology* 43 (5). United States: 599–606. doi:10.1165/rcmb.2009-0263OC.

Marchetti, Maria Cristina, Barbara Di Marco, Grazia Cifone, Graziella Migliorati, and Carlo Riccardi. 2003. “Dexamethasone-Induced Apoptosis of Thymocytes: Role of Glucocorticoid Receptor-Associated Src Kinase and Caspase-8 Activation.” *Blood* 101 (2): 585–93. doi:10.1182/blood-2002-06-1779.

Marinovic, Anne C., Bin Zheng, William E. Mitch, and S. Russ Price. 2002a. “Ubiquitin (UbC) Expression in Muscle Cells Is Increased by Glucocorticoids through a Mechanism Involving Sp1 and MEK1.” *Journal of Biological Chemistry* 277 (19): 16673–81. doi:10.1074/jbc.M200501200.

Marinovic, Anne C, Bin Zheng, William E Mitch, and S Russ Price. 2002b. “Ubiquitin (UbC) Expression in Muscle Cells Is Increased by Glucocorticoids through a Mechanism Involving Sp1 and MEK1.” *The Journal of Biological Chemistry* 277 (19). United States: 16673–81. doi:10.1074/jbc.M200501200.

Marjon, K D, C M Termini, K L Karlen, C Saito-Reis, C E Soria, K A Lidke, and J M Gillette. 2015. “Tetraspanin CD82 Regulates Bone Marrow Homing of Acute Myeloid Leukemia by Modulating the Molecular Organization of N-Cadherin.” *Oncogene*, no. October: 1–9. doi:10.1038/onc.2015.449.

Marke, R, J Havinga, J Cloos, M Demkes, G Poelmans, L Yuniati, D van Ingen Schenau, et al. 2015. “Tumor Suppressor IKZF1 Mediates Glucocorticoid Resistance in B-Cell Precursor Acute Lymphoblastic Leukemia.” *Leukemia* 30 (7): 1599–1603.

doi:10.1038/leu.2015.359.

Maroney, Patricia A, Yang Yu, Jesse Fisher, and Timothy W Nilsen. 2006. "Evidence That microRNAs Are Associated with Translating Messenger RNAs in Human Cells." *Nat Struct Mol Biol* 13 (12): 1102–7. <http://dx.doi.org/10.1038/nsmb1174>.

Marwaha, Ram K, Ketan P Kulkarni, Deepak Bansal, and Amita Trehan. 2010. "Central Nervous System Involvement at Presentation in Childhood Acute Lymphoblastic Leukemia: Management Experience and Lessons." *Leukemia & Lymphoma* 51 (2): 261–68. doi:10.3109/10428190903470323.

Marzluff, William F, Preetam Gongidi, Keith R Woods, Jianping Jin, and Lois J Maltais. 2002. "The Human and Mouse Replication-Dependent Histone Genes." *Genomics* 80 (5). United States: 487–98.

McConkey, David J., Pierluigi Nicotera, Pia Hartzell, Giorgio Bellomo, Andrew H. Wyllie, and Sten Orrenius. 1989. "Glucocorticoids Activate a Suicide Process in Thymocytes through an Elevation of Cytosolic Ca²⁺ Concentration." *Archives of Biochemistry and Biophysics* 269 (1): 365–70. doi:10.1016/0003-9861(89)90119-7.

McKenna, Aaron, Matthew Hanna, Eric Banks, Andrey Sivachenko, Kristian Cibulskis, Andrew Kernytsky, Kiran Garimella, et al. 2010. "The Genome Analysis Toolkit: A MapReduce Framework for Analyzing next-Generation DNA Sequencing Data." *Genome Research* 20 (9): 1297–1303. doi:10.1101/gr.107524.110.

McKinney, P A, F E Alexander, R A Cartwright, and L Parker. 1991. "Parental Occupations of Children with Leukaemia in West Cumbria, North Humberside, and Gateshead." *BMJ (Clinical Research Ed.)* 302 (6778): 681–87.
<http://www.pubmedcentral.nih.gov/articlerender.fcgi?artid=1669138&tool=pmcentrez&rendertype=abstract>.

McLaren, William, Laurent Gil, Sarah E Hunt, Harpreet Singh Riat, Graham R. S. Ritchie, Anja Thormann, Paul Flicek, and Fiona Cunningham. 2016. "The Ensembl Variant Effect Predictor." *bioRxiv*. doi:10.1101/042374.

Medvinsky, A L, N L Samoylina, A M Müller, and E A Dzierzak. 1993. "An Early Pre-Liver Intraembryonic Source of CFU-S in the Developing Mouse." *Nature* 364: 64–67.

doi:10.1038/364064a0.

Mendoza, Michelle C., E. Emrah Er, and John Blenis. 2011. "The Ras-ERK and PI3K-mTOR Pathways: Cross-Talk and Compensation." *Trends in Biochemical Sciences* 36 (6): 320–28. doi:10.1016/j.tibs.2011.03.006.

Miller, A D, T Curran, and I M Verma. 1984. "C-Fos Protein Can Induce Cellular Transformation: A Novel Mechanism of Activation of a Cellular Oncogene." *Cell* 36 (1). UNITED STATES: 51–60.

Miller, Gregory E, Edith Chen, and Eric S Zhou. 2007. "If It Goes Up, Must It Come down? Chronic Stress and the Hypothalamic-Pituitary-Adrenocortical Axis in Humans." *Psychological Bulletin* 133 (1): 25–45. doi:10.1037/0033-2909.133.1.25.

Minegishi, N, J Ohta, H Yamagiwa, N Suzuki, S Kawauchi, Y Zhou, S Takahashi, N Hayashi, J D Engel, and M Yamamoto. 1999. "The Mouse GATA-2 Gene Is Expressed in the Para-Aortic Splanchnopleura and Aorta-Gonads and Mesonephros Region." *Blood* 93 (12): 4196–4207. <http://www.ncbi.nlm.nih.gov/pubmed/10361117>.

Mohan, Helen M., Carol M. Aherne, Ailin C. Rogers, Alan W. Baird, Des C. Winter, and Evelyn P. Murphy. 2012. "Molecular Pathways: The Role of NR4A Orphan Nuclear Receptors in Cancer." *Clinical Cancer Research* 18 (12): 3223–28. doi:10.1158/1078-0432.CCR-11-2953.

Mojica, F. J M, César Díez-Villaseñor, Jesús García-Martínez, and Elena Soria. 2005. "Intervening Sequences of Regularly Spaced Prokaryotic Repeats Derive from Foreign Genetic Elements." *Journal of Molecular Evolution* 60 (2): 174–82. doi:10.1007/s00239-004-0046-3.

Moore, Malcolm A S. 2009. "The Ontogeny of the Hematopoietic System." *Essentials of Stem Cell Biology*, 199–209. doi:10.1016/B978-0-12-374729-7.00023-8.

Moorman, Anthony V. 2012. "The Clinical Relevance of Chromosomal and Genomic Abnormalities in B-Cell Precursor Acute Lymphoblastic Leukaemia." *Blood Reviews* 26 (3): 123–35. doi:10.1016/j.blre.2012.01.001.

Moorman, Anthony V., Hannah M. Ensor, Sue M. Richards, Lucy Chilton, Claire Schwab, Sally E. Kinsey, Ajay Vora, Chris D. Mitchell, and Christine J. Harrison. 2010. "Prognostic Effect

of Chromosomal Abnormalities in Childhood B-Cell Precursor Acute Lymphoblastic Leukaemia: Results from the UK Medical Research Council ALL97/99 Randomised Trial." *The Lancet Oncology* 11 (5): 429–38. doi:10.1016/S1470-2045(10)70066-8.

Mori, Hiroshi, Susan M Colman, Zhijian Xiao, Anthony M Ford, Lyn E Healy, Craig Donaldson, Jill M Hows, Cristina Navarrete, and Mel Greaves. 2002. "Chromosome Translocations and Covert Leukemic Clones Are Generated during Normal Fetal Development." *Proceedings of the National Academy of Sciences of the United States of America* 99 (12): 8242–47. doi:10.1073/pnas.112218799.

Moricke, Anja, Alfred Reiter, Martin Zimmermann, Helmut Gadner, Martin Stanulla, Michael Dordelmann, Lutz Luning, et al. 2008. "Risk-Adjusted Therapy of Acute Lymphoblastic Leukemia Can Decrease Treatment Burden and Improve Survival: Treatment Results of 2169 Unselected Pediatric and Adolescent Patients Enrolled in the Trial ALL-BFM 95." *Blood* 111 (9): 4477–89. doi:10.1182/blood-2007-09-112920.

Morishima, Yoshihiro, Kimon C. Kanelakis, Patrick J M Murphy, Ezra R. Lowe, Gary J. Jenkins, Yoichi Osawa, Roger K. Sunahara, and William B. Pratt. 2003. "The Hsp90 Chaperone p23 Is the Limiting Component of the Multiprotein Hsp90/Hsp70-Based Chaperone System in Vivo Where It Acts to Stabilize the Client Protein-Hsp90 Complex." *Journal of Biological Chemistry* 278 (49): 48754–63. doi:10.1074/jbc.M309814200.

Morrison, Sean J., and Irving L. Weissman. 1994. "The Long-Term Repopulating Subset of Hematopoietic Stem Cells Is Deterministic and Isolatable by Phenotype." *Immunity* 1 (8): 661–73. doi:10.1016/1074-7613(94)90037-X.

Muench, David E, Chinavenmeni S Velu, Andre Olsson, Sara E Meyer, and H Leighton Grimes. 2015. "Transcriptional Control of HSC Fitness." *Blood* 126 (23): 1161. <http://www.bloodjournal.org/content/126/23/1161.abstract>.

Müller, Albrecht M, Alexander Medvinsky, John Strouboulis, Frank Grosveld, and Elanie Dzierzak. 1994. "Development of Hematopoietic Stem Cell Activity in the Mouse Embryo." *Immunity* 1 (4): 291–301. doi:1074-7613(94)90081-7 [pii].

Mullighan, Charles G. 2012. "The Molecular Genetic Makeup of Acute Lymphoblastic Leukemia." *Hematology / the Education Program of the American Society of Hematology. American Society of Hematology. Education Program* 2012: 389–96.

doi:10.1182/asheducation-2012.1.389.

Mullighan, Charles G., Letha A. Phillips, Xiaoping Su, Jing Ma, Christopher B. Miller, Sheila A. Shurtleff, and James R. Downing. 2008. "Genomic Analysis of the Clonal Origins of Relapsed Acute Lymphoblastic Leukemia." *Science (New York, N.Y.)* 322 (5906): 1377–80. doi:10.1126/science.1164266.

Mullighan, Charles G, Salil Goorha, Ina Radtke, Christopher B Miller, Elaine Coustan-Smith, James D Dalton, Kevin Girtman, et al. 2007. "Genome-Wide Analysis of Genetic Alterations in Acute Lymphoblastic Leukaemia." *Nature* 446 (7137): 758–64. doi:10.1038/nature05690.

Mullighan, Charles G, Jinghui Zhang, Richard C Harvey, J Racquel Collins-Underwood, Brenda a Schulman, Letha a Phillips, Sarah K Tasian, et al. 2009. "JAK Mutations in High-Risk Childhood Acute Lymphoblastic Leukemia." *Proceedings of the National Academy of Sciences of the United States of America* 106 (23): 9414–18. doi:10.1073/pnas.0811761106.

Murr, R., T. Vaissière, C. Sawan, V. Shukla, and Z. Herceg. 2007. "Orchestration of Chromatin-Based Processes: Mind the TRRAP." *Oncogene* 26 (37): 5358–72. doi:10.1038/sj.onc.1210605.

Nelson-Rees, W. A., R. B. Owens, P. Arnstein, and A. J. Kniazeff. 1976. "Source, Alterations, Characteristics and Use of a New Dog Cell Line (Cf2Th)." *In Vitro* 12 (10): 665–69. doi:10.1007/BF02797468.

Nemeth, Julia, Ilan Stein, Daniel Haag, Astrid Riehl, Thomas Longerich, Elad Horwitz, Kai Breuhahn, et al. 2009. "S100A8 and S100A9 Are Novel Nuclear Factor Kappa B Target Genes during Malignant Progression of Murine and Human Liver Carcinogenesis." *Hepatology (Baltimore, Md.)* 50 (4). United States: 1251–62. doi:10.1002/hep.23099.

Neve, Richard M., Koei Chin, Jane Fridlyand, Jennifer Yeh, Frederick L. Baehner, Tea Fevr, Laura Clark, et al. 2006. "A Collection of Breast Cancer Cell Lines for the Study of Functionally Distinct Cancer Subtypes." *Cancer Cell* 10 (6): 515–27. doi:10.1016/j.ccr.2006.10.008.

Nguyen, K, M Devidas, S-C Cheng, M La, E A Raetz, W L Carroll, N J Winick, S P Hunger, P S

- Gaynon, and M L Loh. 2008a. "Factors Influencing Survival after Relapse from Acute Lymphoblastic Leukemia: A Children's Oncology Group Study." *Leukemia* 22 (12): 2142–50. doi:10.1038/leu.2008.251.
- . 2008b. "Factors Influencing Survival after Relapse from Acute Lymphoblastic Leukemia: A Children's Oncology Group Study." *Leukemia* 22 (12): 2142–50. doi:10.1038/leu.2008.251.
- Niu, Tong-Hong, Man Jiang, Yong-Ning Xin, Xiang-Jun Jiang, Zhong-Hua Lin, and Shi-Ying Xuan. 2014. "Lack of Association between Apolipoprotein C3 Gene Polymorphisms and Risk of Nonalcoholic Fatty Liver Disease in a Chinese Han Population." *World Journal of Gastroenterology* 20 (13): 3655–62. doi:10.3748/wjg.v20.i13.3655.
- Notta, Faiyaz, Charles G Mullighan, Jean C Y Wang, Armando Poepll, Sergei Doulatov, Letha A Phillips, Jing Ma, Mark D Minden, James R Downing, and John E Dick. 2011. "Evolution of Human BCR-ABL1 Lymphoblastic Leukaemia-Initiating Cells." *Nature* 469 (7330). Nature Publishing Group, a division of Macmillan Publishers Limited. All Rights Reserved.: 362–67. doi:10.1038/nature09733.
- Nottrott, Stephanie, Martin J Simard, and Joel D Richter. 2006. "Human Let-7a miRNA Blocks Protein Production on Actively Translating Polyribosomes." *Nature Structural & Molecular Biology* 13 (12). United States: 1108–14. doi:10.1038/nsmb1173.
- Nuñez, James K, Philip J Kranzusch, Jonas Noeske, Addison V Wright, Christopher W Davies, and Jennifer A Doudna. 2014. "Cas1-Cas2 Complex Formation Mediates Spacer Acquisition during CRISPR-Cas Adaptive Immunity." *Nature Structural & Molecular Biology* 21 (6): 528–34. doi:10.1038/nsmb.2820.
- Nutt, Stephen L., Pavel Urbanek, Antonius Relink, and Meinrad Busslinger. 1997. "Essential Functions of Pax5 (BSAP) in pro-B Cell Development: Difference between Fetal and Adult B Lymphopoiesis and Reduced V-to-DJ Recombination at the IgH Locus." *Genes and Development* 11 (4): 476–91. doi:10.1101/gad.11.4.476.
- Nutt, Stephen L, Barry Heavey, Antonius G Rolink, and Meinrad Busslinger. 1999. "Commitment to the B-Lymphoid Lineage Depends on the Transcription Factor Pax5." *Nature* 401 (6753): 556–62. doi:10.1038/44076.

O'Riordan, Mary, and Rudolf Grosschedl. 1999. "Coordinate Regulation of B Cell Differentiation by the Transcription Factors EBF and E2A." *Immunity* 11 (1): 21–31. doi:10.1016/S1074-7613(00)80078-3.

Okuda, Tsukasa, Jan Van Deursen, Scott W. Hiebert, Gerard Grosveld, and James R. Downing. 1996. "AML1, the Target of Multiple Chromosomal Translocations in Human Leukemia, Is Essential for Normal Fetal Liver Hematopoiesis." *Cell* 84 (2): 321–30. doi:10.1016/S0092-8674(00)80986-1.

Osawa, Masatake, Ken-ichi Hanada, Hirofumi Hamada, and Hiromitsu Nakauchi. 1996. "Long-Term Lymphohematopoietic Reconstitution by a Single CD34-Low/Negative Hematopoietic Stem Cell." *Science* 273 (5272): 242–45. doi:10.1126/science.273.5272.242.

Pal, D, H J Blair, A Elder, K Dormon, K J Rennie, D J L Coleman, J Weiland, et al. 2016. "Long-Term in Vitro Maintenance of Clonal Abundance and Leukaemia-Initiating Potential in Acute Lymphoblastic Leukaemia." *Leukemia*, no. August 2015: 1–36. doi:10.1038/leu.2016.79.

Palis, J, S Robertson, M Kennedy, C Wall, and G Keller. 1999. "Development of Erythroid and Myeloid Progenitors in the Yolk Sac and Embryo Proper of the Mouse." *Development (Cambridge, England)* 126 (22): 5073–84.

Palmi, Chiara, Maria Grazia Valsecchi, Giulia Longinotti, Daniela Silvestri, Valentina Carrino, Valentino Conter, Giuseppe Basso, Andrea Biondi, Geertruy Te Kronnie, and Giovanni Cazzaniga. 2013. "What Is the Relevance of Ikaros Gene Deletions as a Prognostic Marker in Pediatric Philadelphia-Negative B-Cell Precursor Acute Lymphoblastic Leukemia?" *Haematologica* 98 (8): 1226–31. doi:10.3324/haematol.2012.075432.

Park, Kyung-Soon, Young Cha, Chun-Hyung Kim, Hee-Jin Ahn, Dohoон Kim, Sanghyeok Ko, Kyeoung-Hwa Kim, et al. 2013. "Transcription Elongation Factor Tceal3 Regulates the Pluripotent Differentiation Potential of Mouse Embryonic Stem Cells via the Lefty1-Nodal-Smad2 Pathway." *Stem Cells (Dayton, Ohio)* 31 (2). United States: 282–92. doi:10.1002/stem.1284.

Paulsson, Kajsa, Andrea Horvat, Bodil Strömbeck, Fredrik Nilsson, Jesper Heldrup, Mikael Behrendtz, Erik Forestier, Anna Andersson, Thoas Fioretos, and Bertil Johansson. 2008.

"Mutations of FLT3, NRAS, KRAS, and PTPN11 Are Frequent and Possibly Mutually Exclusive in High Hyperdiploid Childhood Acute Lymphoblastic Leukemia." *Genes Chromosomes and Cancer* 47 (1): 26–33. doi:10.1002/gcc.20502.

Payne, Kimberly J. and Sinisa Dovat. 2011. "Ikaros and Tumor Suppression in Acute Lymphoblastic Leukemia." *Crit Rev Oncog.* 16 (1–2): 3–12. doi:10.1016/j.beha.2011.02.009.Rituximab.

Pear, Warren S, Garry P Nolan, Martin L Scott, and David Baltimore. 1993. "Production of High-Titer Helper-Free Retroviruses by Transient Transfection (Retroviral Packaing Cells/gene Therapy)." *Cell Biology* 90 (September): 8392–96. doi:10.1073/pnas.90.18.8392.

Pearson, O H, and L P Eleil. 1950. "Use of Pituitary Adrenocorticotrophic Hormone (ACTH) and Cortisone in Lymphomas and Leukemias." *Journal of the American Medical Association* 144 (16): 1349–53. doi:10.1001/jama.1950.02910340025007.

Persing, D H. 1991. "Polymerase Chain Reaction: Trenches to Benches." *Journal of Clinical Microbiology* 29 (7): 1281–85. <http://www.ncbi.nlm.nih.gov/pmc/articles/PMC270100/>.

Pieters, Rob, Martin Schrappe, Paola De Lorenzo, Ian Hann, Giulio De Rossi, Maria Felice, Liisa Hovi, et al. 2007. "A Treatment Protocol for Infants Younger than 1 Year with Acute Lymphoblastic Leukaemia (Interfant-99): An Observational Study and a Multicentre Randomised Trial." *Lancet* 370 (9583). Elsevier: 240–50. doi:10.1016/S0140-6736(07)61126-X.

Pourcel, C., G. Salvignol, and Gilles Vergnaud. 2005. "CRISPR Elements in Yersinia Pestis Acquire New Repeats by Preferential Uptake of Bacteriophage DNA, and Provide Additional Tools for Evolutionary Studies." *Microbiology* 151 (3): 653–63. doi:10.1099/mic.0.27437-0.

Pratt, William B, and David O Toft. 1997. "Steroid Receptor Interactions with Heat Shock Protein and Immunophilin Chaperones 1." *Endocrine Reviews* 18 (3): 306–60. doi:10.1210/edrv.18.3.0303.

Prota, Luiz Felipe M, Liudmila Cebotaru, Jie Cheng, Jerry Wright, Neeraj Vij, Marcelo M Morales, and William B Guggino. 2012. "Dexamethasone Regulates CFTR Expression in

- Calu-3 Cells with the Involvement of Chaperones HSP70 and HSP90." *PLoS ONE* 7 (12). Public Library of Science: e47405.
- <http://dx.doi.org/10.1371%252Fjournal.pone.0047405>.
- Pui, C H, J M Boyett, M V Relling, P L Harrison, G K Rivera, F G Behm, J T Sandlund, et al. 1999. "Sex Differences in Prognosis for Children with Acute Lymphoblastic Leukemia." *Journal of Clinical Oncology : Official Journal of the American Society of Clinical Oncology* 17 (3): 818–24. <http://www.ncbi.nlm.nih.gov/pubmed/10071272>.
- Pui, C H, W L Carroll, S Meshinchi, and R J Arceci. 2011. "Biology, Risk Stratification, and Therapy of Pediatric Acute Leukemias: An Update." *J Clin Oncol* 29 (5): 551–65. doi:JCO.2010.30.7405 [pii]10.1200/JCO.2010.30.7405.
- Pui, Ching-hon, and William E Evans. 2006. "Treatment of Acute Lymphoblastic Leukemia." *Njm* 354 (2). Massachusetts Medical Society: 166–78. doi:10.1056/NEJMra052603.
- Pui, Ching-Hon, and Leslie Robison. 2008. "Acute Lymphoblastic Leukaemia." *Lancet* 371 (9617): 1030–43. doi:10.1016/S0140-6736(12)62187-4.
- Pui, Ching Hon, Charles G. Mullighan, William E. Evans, and Mary V. Relling. 2012. "Pediatric Acute Lymphoblastic Leukemia: Where Are We Going and How Do We Get There?" *Blood* 120 (6): 1165–74. doi:10.1182/blood-2012-05-378943.
- Put, Natalie, Katrien Van Roosbroeck, Isabelle Vande Broek, Lucienne Michaux, and Peter Vandenberghe. 2012. "PDS5A, a Novel Translocation Partner of MLL in Acute Myeloid Leukemia." *Leukemia Research* 36 (4): e87–89. doi:<http://dx.doi.org/10.1016/j.leukres.2011.12.006>.
- Raimondi, Susana C., Frederick G. Behm, Paula K. Roberson, Dorothy L. Williams, Ching Hon Pui, William M. Crist, A. Thomas Look, and Gaston K. Rivera. 1990. "Cytogenetics of Pre-B-Cell Acute Lymphoblastic Leukemia with Emphasis on Prognostic Implications of the t(1;19)." *Journal of Clinical Oncology* 8 (8): 1380–88.
- Rainer, J, J Lelong, D Bindreither, C Mantinger, C Ploner, S Geley, and R Kofler. 2012. "Research Resource: Transcriptional Response to Glucocorticoids in Childhood Acute Lymphoblastic Leukemia." *Mol Endocrinol* 26. doi:10.1210/me.2011-1213.
- Rath, Devashish, Lina Amlinger, Archana Rath, and Magnus Lundgren. 2015. "The CRISPR-Cas

Immune System: Biology, Mechanisms and Applications." *Biochimie* 117: 119–28.
doi:10.1016/j.biochi.2015.03.025.

Ratman, Dariusz, Wim Vanden Berghe, Lien Dejager, Claude Libert, Jan Tavernier, Ilse M Beck, and Karolien De Bosscher. 2013. "How Glucocorticoid Receptors Modulate the Activity of Other Transcription Factors: A Scope beyond Tethering." *Molecular and Cellular Endocrinology* 380 (1–2): 41–54.
doi:<http://dx.doi.org/10.1016/j.mce.2012.12.014>.

Rehe, Klaus, Kerrie Wilson, Simon Bomken, Daniel Williamson, Julie Irving, Monique L. den Boer, Martin Stanulla, et al. 2013. "Acute B Lymphoblastic Leukaemia-Propagating Cells Are Present at High Frequency in Diverse Lymphoblast Populations." *EMBO Molecular Medicine* 5 (1). WILEY-VCH Verlag: 38–51. doi:10.1002/emmm.201201703.

Reiter, A, M Schrappe, W D Ludwig, W Hiddemann, S Sauter, G Henze, M Zimmermann, F Lampert, W Havers, and D Niethammer. 1994. "Chemotherapy in 998 Unselected Childhood Acute Lymphoblastic Leukemia Patients. Results and Conclusions of the Multicenter Trial ALL-BFM 86." *Blood* 84 (9): 3122–33.
<http://www.ncbi.nlm.nih.gov/pubmed/7949185>.

Relaix, Frédéric, Xiao-jun Wei, Wei Li, Jianjing Pan, Yahong Lin, David D Bowtell, David A Sassoon, and Xiangwei Wu. 2000. "Pw1/Peg3 Is a Potential Cell Death Mediator and Cooperates with Siah1a in p53-Mediated Apoptosis." *Proceedings of the National Academy of Sciences of the United States of America* 97 (5). The National Academy of Sciences: 2105–10. <http://www.ncbi.nlm.nih.gov/pmc/articles/PMC15761/>.

Rieger, Michael A., and Timm Schroeder. 2012. "Hematopoiesis." *Cold Spring Harbor Perspectives in Biology* 4 (12). doi:10.1101/cshperspect.a008250.

Ringold, Gordon M, Keith R Yamamoto, J M Bishop, and H E Varmus. 1977. "Glucocorticoid-Stimulated Accumulation of Mouse Mammary Tumor Virus RNA: Increased Rate of Synthesis of Viral RNA." *Proceedings of the National Academy of Sciences of the United States of America* 74 (7): 2879–83.
<http://www.ncbi.nlm.nih.gov/pmc/articles/PMC15761/>
<http://www.ncbi.nlm.nih.gov/pmc/articles/PMC15761/>

Rivera, Gaston K., Yinmei Zhou, Michael L. Hancock, Amar Gajjar, Jeffrey Rubnitz, Raul G.

Ribeiro, John T. Sandlund, et al. 2005. "Bone Marrow Recurrence after Initial Intensive Treatment for Childhood Acute Lymphoblastic Leukemia." *Cancer* 103 (2): 368–76. doi:10.1002/cncr.20743.

Rossi, Derrick J, David Bryder, Jacob M Zahn, Henrik Ahlenius, Rebecca Sonu, Amy J Wagers, and Irving L Weissman. 2005. "Cell Intrinsic Alterations Underlie Hematopoietic Stem Cell Aging." *Source: Proceedings of the National Academy of Sciences of the United States of America* 102 (26): 9194–99. doi:10.1073/pnas.0503280102.

Rousseau, Guy G, John D Baxter, Stephen J Higgins, and Gordon M Tomkins. 1973. "Steroid-Induced Nuclear Binding of Glucocorticoid Receptors in Intact Hepatoma Cells." *Journal of Molecular Biology* 79 (3): 539–54. doi:[http://dx.doi.org/10.1016/0022-2836\(73\)90405-1](http://dx.doi.org/10.1016/0022-2836(73)90405-1).

Sakai, D. D., S. Helms, J. Carlstedt-Duke, J. A. Gustafsson, F. M. Rottman, and K. R. Yamamoto. 1988. "Hormone-Mediated Repression: A Negative Glucocorticoid Response Element from the Bovine Prolactin Gene." *Genes & Development* 2 (9): 1144–54. doi:10.1101/gad.2.9.1144.

Salzer, W L, M Devidas, W L Carroll, N Winick, J Pullen, S P Hunger, and B A Camitta. 2010. "Long-Term Results of the Pediatric Oncology Group Studies for Childhood Acute Lymphoblastic Leukemia 1984-2001: A Report from the Children's Oncology Group." *Leukemia* 24 (2): 355–70. doi:10.1038/leu.2009.261.

Sanjana, Neville E., Ophir Shalem, and Feng Zhang. 2014. "Improved Vectors and Genome-Wide Libraries for CRISPR Screening." *Nature Methods* 11 (8): 783–84. doi:10.1038/nmeth.3047.

Sanz, Eva, Norman Muñoz-A, Jorge Monserrat, Ana Van-Den-Rym, Pedro Escoll, Ismael Ranz, Melchor Alvarez-Mon, and Antonio de-la-Hera. 2010. "Ordering Human CD34+CD10-CD19+ Pre/pro-B-Cell and CD19- Common Lymphoid Progenitor Stages in Two pro-B-Cell Development Pathways." *Proceedings of the National Academy of Sciences of the United States of America* 107 (13): 5925–30. doi:10.1073/pnas.0907942107.

Sapolsky, Robert M, L Michael Romero, and Allan U Munck. 2000. "How Do Glucocorticoids Influence Stress Responses? Integrating Permissive, Suppressive, Stimulatory, and Preparative Actions." *Endocrine Reviews* 21 (1): 55–89. doi:10.1210/er.21.1.55.

- Sarkar, Gobinda, and Steve Sommer. 1990. "Shedding Light on PCR Contamination." *Nature*. doi:10.1038/347340b0.
- Sasaki, K, and Y Sonoda. 2000. "Histometrical and Three-Dimensional Analyses of Liver Hematopoiesis in the Mouse Embryo." *Archives of Histology and Cytology* 63 (2). JAPAN: 137–46.
- Sasson, Ravid, Kimihisa Tajima, and Abraham Amsterdam. 2001. "Glucocorticoids Protect against Apoptosis Induced by Monophosphate and p53 Activation in Immortalized Human Granulosa Cells : Involvement of Bcl-2 *." *Society* 142 (2): 802–11. doi:10.1210/endo.142.2.7942.
- Scheidereit, C, S Geisse, H M Westphal, and M Beato. 1983. "The Glucocorticoid Receptor Binds to Defined Nucleotide Sequences near the Promoter of Mouse Mammary Tumour Virus." *Nature* 304 (5928): 749–52. doi:10.1038/304749a0.
- Scherer, S. 2008. *A Short Guide to the Human Genome*. Cold Spring Harbor Laboratory Press.
- Schmidt, Stefan, Julie A E Irving, Lynne Minto, Elizabeth Matheson, Lindsay Nicholson, Andreas Ploner, Walther Parson, et al. 2006. "Glucocorticoid Resistance in Two Key Models of Acute Lymphoblastic Leukemia Occurs at the Level of the Glucocorticoid Receptor." *The FASEB Journal : Official Publication of the Federation of American Societies for Experimental Biology* 20 (14): 2600–2602. doi:10.1096/fj.06-6214fje.
- Schmidt, Stefan, Johannes Rainer, Stefan Riml, Christian Ploner, Simone Jesacher, Clemens Achmüller, Elisabeth Presul, et al. 2006. "Identification of Glucocorticoid-Response Genes in Children with Acute Lymphoblastic Leukemia." *Blood* 107 (5): 2061–69. doi:10.1182/blood-2005-07-2853.
- Schrappe, Martin, Stephen P Hunger, Ching-Hon Pui, Vaskar Saha, Paul S Gaynon, André Baruchel, Valentino Conter, et al. 2012. "Outcomes after Induction Failure in Childhood Acute Lymphoblastic Leukemia." *The New England Journal of Medicine* 366 (15): 1371–81. doi:10.1056/NEJMoa1110169.
- Schultz, Kirk R., D. Jeanette Pullen, Harland N. Sather, Jonathan J. Shuster, Meenakshi Devidas, Michael J. Borowitz, Andrew J. Carroll, et al. 2007. "Risk- and Response-Based Classification of Childhood B-Precursor Acute Lymphoblastic Leukemia: A Combined

Analysis of Prognostic Markers from the Pediatric Oncology Group (POG) and Children's Cancer Group (CCG)." *Blood* 109 (3): 926–35. doi:10.1182/blood-2006-01-024729.

Scott, Michelle S, and Motoharu Ono. 2011. "From snoRNA to miRNA: Dual Function Regulatory Non-Coding RNAs." *Biochimie* 93 (11): 1987–92.
doi:<http://dx.doi.org/10.1016/j.biochi.2011.05.026>.

Secker-Walker, L M, S D Lawler, and R M Hardisty. 1978. "Prognostic Implications of Chromosomal Findings in Acute Lymphoblastic Leukaemia at Diagnosis." *British Medical Journal* 2 (6151): 1529–30.
<http://www.pubmedcentral.nih.gov/articlerender.fcgi?artid=1608754&tool=pmcentrez&rendertype=abstract>.

Seet, C S, R L Brumbaugh, and B L Kee. 2004. "Early B Cell Factor Promotes B Lymphopoiesis with Reduced Interleukin 7 Responsiveness in the Absence of E2A." *J Exp Med* 199 (12): 1689–1700. doi:10.1084/jem.20032202.

Seibel, Nita L, Peter G Steinherz, Harland N Sather, James B Nachman, Cynthia DeLaat, Lawrence J Ettinger, David R Freyer, et al. 2008. "Early Postinduction Intensification Therapy Improves Survival for Children and Adolescents with High-Risk Acute Lymphoblastic Leukemia: A Report from the Children's Oncology Group. [Erratum to Document Cited in CA149:044425]." *Blood* 111 (10): 5262. doi:10.1182/blood-2008-03-144162.

Semerad, Craig L, Elinore M Mercer, Matthew A Inlay, Irving L Weissman, and Cornelis Murre. 2009. "E2A Proteins Maintain the Hematopoietic Stem Cell Pool and Promote the Maturation of Myelolymphoid and Myeloerythroid Progenitors." *Proceedings of the National Academy of Sciences of the United States of America* 106 (6): 1930–35.
doi:10.1073/pnas.0808866106.

Sethi, Jaswinder K. 2010. "Activatin' Human Adipose Progenitors in Obesity." *Diabetes* 59 (10). American Diabetes Association: 2354–57. doi:10.2337/db10-0923.

Shalem, O., N. E. Sanjana, E. Hartenian, X. Shi, D. A. Scott, T. S. Mikkelsen, D. Heckl, et al. 2014. "Genome-Scale CRISPR-Cas9 Knockout Screening in Human Cells." *Science* 343 (6166): 84–87. doi:10.1126/science.1247005.

- Shultz, Leonard D, Bonnie L Lyons, Lisa M Burzenski, Bruce Gott, Xiaohua Chen, Stanley Chaleff, Malak Kotb, et al. 2005. "Human Lymphoid and Myeloid Cell Development in NOD/LtSz-Scid IL2R Gamma Null Mice Engrafted with Mobilized Human Hemopoietic Stem Cells." *Journal of Immunology (Baltimore, Md. : 1950)* 174 (10). United States: 6477–89.
- Sigaux, François. 1994. "The V(D)J Recombination in Acute Lymphoid Leukemias: A Short Review." *Leukemia & Lymphoma* 13 (sup1). Taylor & Francis: 53–57. doi:10.3109/10428199409052675.
- Silva, Jose M, Mamie Z Li, Ken Chang, Wei Ge, Michael C Golding, Richard J Rickles, Despina Siolas, et al. 2005. "Second-Generation shRNA Libraries Covering the Mouse and Human Genomes." *Nat Genet* 37 (11): 1281–88. <http://dx.doi.org/10.1038/ng1650>.
- Silverman, L B, K E Stevenson, J E O'Brien, B L Asselin, R D Barr, L Clavell, P D Cole, et al. 2010. "Long-Term Results of Dana-Farber Cancer Institute ALL Consortium Protocols for Children with Newly Diagnosed Acute Lymphoblastic Leukemia (1985-2000)." *Leukemia* 24 (2): 320–34. doi:10.1038/leu.2009.253.
- Smith, P. K., R. I. Krohn, G. T. Hermanson, A. K. Mallia, F. H. Gartner, M. D. Provenzano, E. K. Fujimoto, N. M. Goeke, B. J. Olson, and D. C. Klenk. 1985. "Measurement of Protein Using Bicinchoninic Acid." *Analytical Biochemistry* 150 (1): 76–85. doi:10.1016/0003-2697(85)90442-7.
- Spijkers-Hagelstein, J A P, P Schneider, E Hulleman, J de Boer, O Williams, R Pieters, and R W Stam. 2012. "Elevated S100A8/S100A9 Expression Causes Glucocorticoid Resistance in MLL-Rearranged Infant Acute Lymphoblastic Leukemia." *Leukemia* 26 (6). England: 1255–65. doi:10.1038/leu.2011.388.
- Sreekumar, P G, R Karman, J Yaung, C K Spee, S J Ryan, and D R Hinton. 2005. "Protection from Oxidative Stress by Methionine Sulfoxide Reductases in RPE Cells." *Biochemical and Biophysical Research Communications* 334 (1): 245–53. doi:DOI 10.1016/j.bbrc.2005.06.081.
- Srinivasan, G, N T Patel, and E B Thompson. 1994. "Heat Shock Protein Is Tightly Associated with the Recombinant Human Glucocorticoid Receptor:glucocorticoid Response Element Complex." *Mol Endocrinol* 8 (2): 189–96. doi:10.1210/mend.8.2.8170475.

Staal, F J T, D de Ridder, T Szczepanski, T Schonewille, E C E van der Linden, E R van Wering, V H J van der Velden, and J J M van Dongen. 2010. "Genome-Wide Expression Analysis of Paired Diagnosis-Relapse Samples in ALL Indicates Involvement of Pathways Related to DNA Replication, Cell Cycle and DNA Repair, Independent of Immune Phenotype." *Leukemia : Official Journal of the Leukemia Society of America, Leukemia Research Fund, U.K* 24 (3): 491–99. doi:10.1038/leu.2009.286.

Stein, Wilfred D., Thomas Litman, Tito Fojo, and Susan E. Bates. 2004. "A Serial Analysis of Gene Expression (SAGE) Database Analysis of Chemosensitivity: Comparing Solid Tumors with Cell Lines and Comparing Solid Tumors from Different Tissue Origins." *Cancer Research* 64 (8): 2805–16. doi:10.1158/0008-5472.CAN-03-3383.

Steinbach, Daniel, Susann Wittig, Gunnar Cario, Susanne Viehmann, Angelika Mueller, Bernd Gruhn, Ralf Haefer, Felix Zintl, and Axel Sauerbrey. 2003. "The Multidrug Resistance-Associated Protein 3 (MRP3) Is Associated with a Poor Outcome in Childhood ALL and May Account for the Worse Prognosis in Male Patients and T-Cell Immunophenotype." *Blood* 102 (13): 4493–98. doi:10.1182/blood-2002-11-3461.

Stock, Wendy, Mei La, Ben Sanford, Clara D Bloomfield, James W Vardiman, Paul Gaynon, Richard A Larson, and James Nachman. 2008. "What Determines the Outcomes for Adolescents and Young Adults with Acute Lymphoblastic Leukemia Treated on Cooperative Group Protocols? A Comparison of Children's Cancer Group and Cancer and Leukemia Group B Studies." *Blood* 112 (5). United States: 1646–54. doi:10.1182/blood-2008-01-130237.

Stombaugh, Jesse, Abel Licon, Žaklina Strezoska, Joshua Stahl, Sarah Bael Anderson, Michael Banos, Anja van Brabant Smith, Amanda Birmingham, and Annaleen Vermeulen. 2015. "The Power Decoder Simulator for the Evaluation of Pooled shRNA Screen Performance." Edited by Marc Bickle, Hakim Djaballah, and Lorenz Martin Mayr. *Journal of Biomolecular Screening* 20 (8). Sage CA: Los Angeles, CA: SAGE Publications: 965–75. doi:10.1177/1087057115576715.

Strachan, D P. 1989. "Hay Fever, Hygiene, and Household Size." *BMJ (Clinical Research Ed.)* 299 (6710). England: 1259–60.

Strezoska, Saklina, Abel Licon, Josh Haimes, Katie Jansen Spayd, Kruti M. Patel, Kevin

Sullivan, Katarzyna Jastrzebski, et al. 2012. "Optimized PCR Conditions and Increased shRNA Fold Representation Improve Reproducibility of Pooled shRNA Screens." *PLoS ONE* 7 (8). doi:10.1371/journal.pone.0042341.

Styczynski, Jan, Beata Kurylo-Rafinska, Małgorzata Kubicka, Beata Kolodziej, Monika Pogorzala, Krzysztof Czyzowski, Robert Debski, et al. 2015. "Differential in Vitro Drug Resistance Profile Between First and Second Relapsed Acute Lymphoblastic Leukemia and Acute Myeloblastic Leukemia in Children." *Blood* 126 (23): 3696.
<http://www.bloodjournal.org/content/126/23/3696.abstract>.

Sultan, S M, Y Ioannou, and D A Isenberg. 2000. "Is There an Association of Malignancy with Systemic Lupus Erythematosus? An Analysis of 276 Patients under Long-Term Review." *Rheumatology (Oxford, England)* 39 (10). ENGLAND: 1147–52.

Surjit, Milan, Krishna Priya Ganti, Atish Mukherji, Tao Ye, Guoqiang Hua, Daniel Metzger, Mei Li, and Pierre Chambon. 2011. "Widespread Negative Response Elements Mediate Direct Repression by Agonist-Liganded Glucocorticoid Receptor." *Cell* 145 (2): 224–41. doi:10.1016/j.cell.2011.03.027.

Tavian, Manuela, and Bruno Péault. 2005. "Embryonic Development of the Human Hematopoietic System." *The International Journal of Developmental Biology* 49 (2–3): 243–50. doi:10.1387/ijdb.041957mt.

Taxman, Debra J, Chris B Moore, Elizabeth H Guthrie, and Max Tze-Han Huang. 2010. "Short Hairpin RNA (shRNA): Design, Delivery, and Assessment of Gene Knockdown ." *RNA Therapeutics . Methods in Molecular Biology* .
http://www.springerprotocols.com/Abstract/doi/10.1007/978-1-60761-657-3_10.

Tian, J, Y X Duan, C Y Bei, and J Chen. 2013. "Calycosin Induces Apoptosis by Upregulation of RASD1 in Human Breast Cancer Cells MCF-7." *Hormone and Metabolic Research = Hormon- Und Stoffwechselforschung = Hormones et Metabolisme* 45 (8). Germany: 593–98. doi:10.1055/s-0033-1341510.

Tobergte, David R., and Shirley Curtis. 2013. "No Title No Title." *Journal of Chemical Information and Modeling*. doi:10.1017/CBO9781107415324.004.

Tomkinson, Blake, Ray Bendele, Francis J. Giles, Eric Brown, Atherton Gray, Karen Hart,

Jeremy D. LeRay, Denny Meyer, Michelle Pelanne, and David L. Emerson. 2003. "OSI-211, a Novel Liposomal Topoisomerase I Inhibitor, Is Active in SCID Mouse Models of Human AML and ALL." *Leukemia Research* 27 (11): 1039–50. doi:10.1016/S0145-2126(03)00092-4.

Trageser, Daniel, Ilaria Iacobucci, Rahul Nahar, Cihangir Duy, Gregor von Levetzow, Lars Klemm, Eugene Park, et al. 2009. "Pre-B Cell Receptor-Mediated Cell Cycle Arrest in Philadelphia Chromosome-Positive Acute Lymphoblastic Leukemia Requires IKAROS Function." *The Journal of Experimental Medicine* 206 (8): 1739–53. doi:10.1084/jem.20090004.

Tsai, F Y, and S H Orkin. 1997. "Transcription Factor GATA-2 Is Required for Proliferation/survival of Early Hematopoietic Cells and Mast Cell Formation, but Not for Erythroid and Myeloid Terminal Differentiation." *Blood* 89 (10): 3636–43. <http://www.ncbi.nlm.nih.gov/pubmed/9160668> <http://www.bloodjournal.org/content/89/10/3636.abstract>.

Turner, Jonathan D., and Claude P. Muller. 2005. "Structure of the Glucocorticoid Receptor (NR3C1) Gene 5' Untranslated Region: Identification, and Tissue Distribution of Multiple New Human Exon 1." *Journal of Molecular Endocrinology* 35 (2): 283–92. doi:10.1677/jme.1.01822.

Turner, Jonathan D., Sara Vernocchi, Stephanie Schmitz, and Claude P. Muller. 2014. "Role of the 5'-untranslated Regions in Post-Transcriptional Regulation of the Human Glucocorticoid Receptor." *Biochimica et Biophysica Acta - Gene Regulatory Mechanisms* 1839 (11): 1051–61. doi:10.1016/j.bbagr.2014.08.010.

Udensi, Udensi K, and Paul B Tchounwou. 2014. "Dual Effect of Oxidative Stress on Leukemia Cancer Induction and Treatment." *Journal of Experimental & Clinical Cancer Research : CR* 33 (1): 106. doi:10.1186/s13046-014-0106-5.

Vago, Luca, Davide Cittaro, Cristina Toffalori, Dejan Lazarevic, Chiara Brambati, Giacomo Oliveira, Gabriele Bucci, Lara Crucitti, Nicoletta Cieri, and Lorenza Chiesa. 2014. "Backtracking Leukemia Clonal Evolution from Post-Transplantation Relapse to Initial Diagnosis to Identify Founder Mutations and Mechanisms of Immune Evasion." *Blood* 124 (21). Am Soc Hematology: 1185.

Vaidyanathan, Govindan, Mary J Cismowski, Guoshun Wang, Timothy S Vincent, Kevin D Brown, and Stephen M Lanier. 2004. "The Ras-Related Protein AGS1/RASD1 Suppresses Cell Growth." *Oncogene* 23 (34). England: 5858–63. doi:10.1038/sj.onc.1207774.

Van der Auwera, Geraldine A., Mauricio O. Carneiro, Christopher Hartl, Ryan Poplin, Guillermo del Angel, Ami Levy-Moonshine, Tadeusz Jordan, et al. 2013. "From fastQ Data to High-Confidence Variant Calls: The Genome Analysis Toolkit Best Practices Pipeline." *Current Protocols in Bioinformatics*, no. SUPL.43. doi:10.1002/0471250953.bi1110s43.

van Dijk, Fleur S, M Carola Zillikens, Dimitra Micha, Markus Riessland, Carlo L M Marcelis, Christine E de Die-Smulders, Janine Milbradt, et al. 2013. "PLS3 Mutations in X-Linked Osteoporosis with Fractures." *The New England Journal of Medicine* 369 (16): 1529–36. doi:10.1056/NEJMoa1308223.

van Dongen, Jacques J M, Vincent H J van der Velden, Monika Brüggemann, and Alberto Orfao. 2015. "Minimal Residual Disease (MRD) Diagnostics in Acute Lymphoblastic Leukemia (ALL): Need for Sensitive, Fast and Standardized Technologies." *Blood* 125 (26): blood-2015-03-580027. doi:10.1182/blood-2015-03-580027.

van Ewijk, W, G Holländer, C Terhorst, and B Wang. 2000. "Stepwise Development of Thymic Microenvironments in Vivo Is Regulated by Thymocyte Subsets." *Development* 127 (8): 1583–91. <http://www.ncbi.nlm.nih.gov/pubmed/10725235>.

Van Galen, Joost C., Roland P. Kuiper, Liesbeth Van Emst, Marloes Levers, Esther Tijchon, Blanca Scheijen, Esme Waanders, et al. 2010. "BTG1 Regulates Glucocorticoid Receptor Autoinduction in Acute Lymphoblastic Leukemia." *Blood* 115 (23): 4810–19. doi:10.1182/blood-2009-05-223081.

Waanders, Esme, Blanca Scheijen, Laurens T. van der Meer, Simon V. van Reijmersdal, Liesbeth van Emst, Yvet Kroeze, Edwin Sonneveld, et al. 2012. "The Origin and Nature of Tightly Clustered BTG1 Deletions in Precursor B-Cell Acute Lymphoblastic Leukemia Support a Model of Multiclonal Evolution." *PLoS Genetics* 8 (2): e1002533. doi:10.1371/journal.pgen.1002533.

Wallace, Jared, Ruozhen Hu, Timothy L Mosbruger, Timothy J Dahlem, W Zac Stephens, Dinesh S Rao, June L Round, and Ryan M O'Connell. 2016. "Genome-Wide CRISPR-Cas9

Screen Identifies MicroRNAs That Regulate Myeloid Leukemia Cell Growth." *PLoS One* 11 (4): e0153689. doi:10.1371/journal.pone.0153689.

Wang, Anyou, Mufadhal Al-Kuhlani, S Claiborne Johnston, David M Ojcius, Joyce Chou, and Deborah Dean. 2013. "Transcription Factor Complex AP-1 Mediates Inflammation Initiated by Chlamydia Pneumoniae Infection." *Cellular Microbiology* 15 (5). England: 779–94. doi:10.1111/cmi.12071.

Wang, Eric, Shinpei Kawaoka, Ming Yu, Junwei Shi, Ting Ni, Wenjing Yang, Jun Zhu, Robert G Roeder, and Christopher R Vakoc. 2013. "Histone H2B Ubiquitin Ligase RNF20 Is Required for MLL-Rearranged Leukemia." *Proceedings of the National Academy of Sciences of the United States of America* 110 (10): 3901–6. doi:10.1073/pnas.1301045110.

Wang, Weining, N Gopalakrishna Iyer, Hsien Ts'ung Tay, Yonghui Wu, Tony K H Lim, Lin Zheng, In Chin Song, et al. 2015. "Microarray Profiling Shows Distinct Differences between Primary Tumors and Commonly Used Preclinical Models in Hepatocellular Carcinoma." *BMC Cancer* 15. England: 828. doi:10.1186/s12885-015-1814-8.

Wang, Hidetoshi Indoh, Inoue, and Ikuo Horii. 2002. "ADVANTAGES OF IN VITRO CYTOTOXICITY TESTING BY USING PRIMARY RAT HEPATOCYTES IN COMPARISON WITH ESTABLISHED CELL LINES." *The Journal of Toxicological Sciences* 27 (3): 229–37. doi:10.2131/jts.27.229.

Waters, Katrina M, Ryan L Sontag, and Thomas J Weber. 2013. "Hepatic Leukemia Factor Promotes Resistance to Cell Death: Implications for Therapeutics and Chronotherapy." *Toxicology and Applied Pharmacology* 268 (2): 141–48. doi:<http://dx.doi.org/10.1016/j.taap.2013.01.031>.

Weishaupt, Holger, Mikael Sigvardsson, and Joanne L. Attema. 2010. "Epigenetic Chromatin States Uniquely Define the Developmental Plasticity of Murine Hematopoietic Stem Cells." *Blood* 115 (2): 247–56. doi:10.1182/blood-2009-07-235176.

Welner, R S, R Pelayo, and P W Kincade. 2008. "Evolving Views on the Genealogy of B Cells." *Nat Rev Immunol* 8 (2): 95–106. doi:10.1038/nri2234.

Wu, Jing, and Emery H Bresnick. 2007. "Glucocorticoid and Growth Factor Synergism

Requirement for Notch4 Chromatin Domain Activation." *Molecular and Cellular Biology* 27 (6). United States: 2411–22. doi:10.1128/MCB.02152-06.

Wu, Ning, Ming-Chao Zhong, Romain Roncagalli, Luis-Alberto Perez-Quintero, Huaijian Guo, Zhanqiang Zhang, Christelle Lenoir, Zhongjun Dong, Sylvain Latour, and Andre Veillette. 2016. "A Hematopoietic Cell-Driven Mechanism Involving SLAMF6 Receptor, SAP Adaptors and SHP-1 Phosphatase Regulates NK Cell Education." *Nat Immunol* 17 (4). Nature Publishing Group, a division of Macmillan Publishers Limited. All Rights Reserved.: 387–96. <http://dx.doi.org/10.1038/ni.3369>.

Yamada, Masateru, Akira Hirasawa, Satoshi Shiojima, and Gozoh Tsujimoto. 2003. "Granzyme A Mediates Glucocorticoid-Induced Apoptosis in Leukemia Cells." *FASEB Journal : Official Publication of the Federation of American Societies for Experimental Biology* 17 (12). United States: 1712–14. doi:10.1096/fj.02-1116fje.

Yamamoto, Tomoko, Mariko Isomura, Yinyan Xu, Juan Liang, Hiroshi Yagasaki, Yoshiro Kamachi, Kazuko Kudo, Hitoshi Kiyoi, Tomoki Naoe, and Seiji Kojima. 2006. "PTPN11, RAS and FLT3 Mutations in Childhood Acute Lymphoblastic Leukemia." *Leukemia Research* 30 (9): 1085–89. doi:10.1016/j.leukres.2006.02.004.

Yamashita, Yuka, Masashi Sanada, Kenichi Yoshida, Hiroo Ueno, Hiroko Tanaka, Yuichi Shiraishi, Kenichi Chiba, et al. 2015. "Clonal Evolution in Relapsed Pediatric Acute Lymphoblastic Leukemia." *Blood* 126 (23). American Society of Hematology: 1425. <http://www.bloodjournal.org/content/126/23/1425>.

Yang-Yen, Hsin Fang, Jean Claude Chambard, Yu Lin Sun, Tod Smeal, Thomas J. Schmidt, Jacques Drouin, and Michael Karin. 1990. "Transcriptional Interference between c-Jun and the Glucocorticoid Receptor: Mutual Inhibition of DNA Binding due to Direct Protein-Protein Interaction." *Cell* 62 (6): 1205–15. doi:10.1016/0092-8674(90)90396-V.

Ye, Min, Hong Zhang, Giovanni Amabile, Henry Yang, Philipp B Staber, Pu Zhang, Elena Levantini, et al. 2013. "C/EBPa Controls Acquisition and Maintenance of Adult Haematopoietic Stem Cell Quiescence." *Nature Cell Biology* 15 (4): 385–94. doi:10.1038/ncb2698.

Yeoh, Eng-Juh, Mary E Ross, Sheila A Shurtleff, W.Kent Williams, Divyen Patel, Rami Mahfouz, Fred G Behm, et al. 2002. "Classification, Subtype Discovery, and Prediction of

Outcome in Pediatric Acute Lymphoblastic Leukemia by Gene Expression Profiling.” *Cancer Cell* 1 (2): 133–43. doi:10.1016/S1535-6108(02)00032-6.

Yeung, Jenny, Helena Kempski, Michael Neat, Simon Bailey, Owen Smith, and Hugh J M Brady. 2006. “Characterization of the t(17;19) Translocation by Gene-Specific Fluorescent in Situ Hybridization-Based Cytogenetics and Detection of the E2A-HLF Fusion Transcript and Protein in Patients’ Cells.” *Haematologica* 91 (3): 422–24. <http://www.ncbi.nlm.nih.gov/pubmed/16531271>.

Yeung, Jenny, Elaine O’Sullivan, Mike Hubank, and Hugh J M Brady. 2004. “E4BP4 Expression Is Regulated by the t(17;19)-Associated Oncoprotein E2A-HLF in pro-B Cells.” *British Journal of Haematology* 125 (5): 560–67. doi:10.1111/j.1365-2141.2004.04953.x.

Zack, Travis I, Steven E Schumacher, Scott L Carter, Andrew D Cherniack, Gordon Saksena, Barbara Tabak, Michael S Lawrence, et al. 2013. “Pan-Cancer Patterns of Somatic Copy-Number Alterations.” *Nature Genetics* 45 (10). Nature Publishing Group, a division of Macmillan Publishers Limited. All Rights Reserved.: 1134–40. doi:10.1038/ja.2013.113.Venturicidin.

Zaman, Farasat, Dionisios Chrysis, Kirsten Huntjens, Andrei Chagin, Masaharu Takigawa, Bengt Fadeel, and Lars Sävendahl. 2014. “Dexamethasone Differentially Regulates Bcl-2 Family Proteins in Human Proliferative Chondrocytes: Role of pro-Apoptotic Bid.” *Toxicology Letters* 224 (2): 196–200. doi:<http://dx.doi.org/10.1016/j.toxlet.2013.10.020>.

Zhang, Huihua, Xiaojia Chen, Jiakang Wang, Wenhua Guang, Wei Han, Hang Zhang, Xuan Tan, and Yong Gu. 2014. “EGR1 Decreases the Malignancy of Human Non-Small Cell Lung Carcinoma by Regulating KRT18 Expression.” *Scientific Reports* 4 (July). The Author(s): 5416. <http://dx.doi.org/10.1038/srep05416>.

Zhang, Shimin, Jacqueline Jonklaas, and Mark Danielsen. 2007. “The Glucocorticoid Agonist Activities of Mifepristone (RU486) and Progesterone Are Dependent on Glucocorticoid Receptor Levels but Not on {EC50} Values.” *Steroids* 72 (6–7): 600–608. doi:<http://dx.doi.org/10.1016/j.steroids.2007.03.012>.

Zhong, Jiang F, Yi Zhao, Susan Sutton, Andrew Su, Yuxia Zhan, Lunjian Zhu, Chunli Yan, et al. 2005. “Gene Expression Profile of Murine Long-Term Reconstituting vs. Short-Term Reconstituting Hematopoietic Stem Cells.” *Proceedings of the National Academy of*

Sciences of the United States of America 102 (7): 2448–53.

doi:10.1073/pnas.0409459102.

Zhou, Junguo, and John A. Cidlowski. 2005. “The Human Glucocorticoid Receptor: One Gene,

Multiple Proteins and Diverse Responses.” *Steroids* 70 (5–7 SPEC. ISS.): 407–17.

doi:10.1016/j.steroids.2005.02.006.

Zhuang, Yuan, Philippe Soriano, and Harold Weintraub. 1994. “The Helix-Loop-Helix Gene

E2A Is Required for B Cell Formation.” *Cell* 79 (5): 875–84. doi:10.1016/0092-

8674(94)90076-0.

Zilfou, Jack T., and Scott W. Lowe. 2009. “Tumor Suppressive Functions of p53.” *Cold Spring*

Harbor Perspectives in Biology. doi:10.1101/cshperspect.a001883.